Assessment of the Effects of Extreme Heat Events on Buildings

Chang Shu

A Thesis

In the Department

of

Building, Civil and Environmental Engineering

Presented in Partial Fulfilment of the Requirements

for the Degree of

Doctor of Philosophy (Building Engineering) at

Concordia University

Montreal, Quebec, Canada

October 2021

CONCORDIA UNIVERSITY

SCHOOL OF GRADUATE STUDIES

This is to certify that the thesis prepared

By: Chang Shu

Entitled: Assessment of the Effects of Extreme Heat Events on Buildings

and submitted in partial fulfillment of the requirements for the degree of

Doctor Of Philosophy (Building Engineering)

complies with the regulations of the University and meets the accepted standards with respect to originality and quality.

Signed by the final examining committee:

_____ Chair
Dr. John Xiupu Zhang

_____ External Examiner
Dr. Ian Beausoleil-Morrison

_____ External to Program
Dr. Ursula Eicker

_____ Examiner
Dr. Hua Ge

_____ Examiner
Dr. Radu Grigore Zmeureanu

_____ Thesis Supervisor
Dr. Liangzhu Wang

_____ Thesis Co-Supervisor
Dr. Abhishek Gaur

Approved by   _____
Dr. Mazdak Nik-Bakht, Graduate Program Director

12/2/2021   _____
Dr. Mourad Debbabi, Dean
Gina Cody School of Engineering and Computer Science

Abstract

Assessment of the Effects of Extreme Heat Events on Buildings

Chang Shu, Ph.D.

Concordia University, 2021

Due to urbanization and global warming, extreme heat events, e.g., heat waves, in the urban area tend to occur much more intensively and frequently, imposing a great threat to the health and safety of urban dwellers. The warming temperature also leads to a deteriorating of the indoor thermal conditions. Studies on indoor overheating should be conducted to figure out the interactions between the outdoor environment and indoor conditions and estimate possible approaches to optimize the design and operation of the building system adapting to the changing climate. Considering the building and construction assets are typically designed for a long period over several decades or even centuries. The resiliency of the buildings to extreme conditions should be reconsidered under the future climate conditions, therefore the future weather inputs should be critical for the building overheating study, and any possible mitigation intervenes should be re-evaluated under different future scenarios to evaluate the robustness of the decision and detect the potential risks. The study includes a procedure to select buildings from Montreal city for the field monitoring study, followed by the outcome of building information surveys and site visits. After an overall evaluation of these buildings, 6 school buildings, 6 hospital buildings and 3 residential social housings have been selected for further studies. The measured data are used for the overheating assessment of these buildings and the calibration of these real building models. The measured data exhibited strong evidence of overheating in existing building stocks in Montreal, showing the necessity for further investigation to mitigate the overheating. To consider the spatial impact of urban climate, the study developed a high-resolution regional climate model for the Montreal and Ottawa region and elaborated the importance of preserving the urban effect in weather files for building studies. The generated climate dataset can be used as the input of EnergyPlus building simulations to evaluate the spatial-temporal pattern of indoor overheating. The validated climate model can also be extended for the future projection of urban scale overheating studies. In the future, overheating mitigation strategies can be applied to the baseline model to evaluate their effectiveness on both historical and future climate in the long run with the proposed workflow and the climate dataset generated by this study.

Acknowledgments

Along with my journey to a Ph.D., so many people generously provided their help and support to me. I would like to first thank my supervisor, Dr. Liangzhu (Leon) Wang, who is gracious enough to provide me opportunities to work on multiple different projects. During the over four years of doctoral study, Dr. Wang encouraged me to continuously move forward and overcome any challenges in my way. His passion for research and endeavors to innovate is contagious to everyone in the research group. The same acknowledgments to my co-supervisor, Dr. Abhishek Gaur at National Research Council Canada (NRCC), who led me to a new research field of climate data downscaling and weather file generation. His profound knowledge of climate data and statistical analysis is always a strong backup for me to explore new topics, and his humble and open mind to new concepts made our work efficient and enjoyable. Thank you, Dr. Wang, and Dr. Gaur, for your guidance and your dedication to making me excel in my research.

I would like to also thank Dr. Radu Zmeureanu and Dr. Hua Ge for their guidance and supervision on the project "Assessment and Mitigation of Summertime Overheating Conditions in Vulnerable Buildings of Urban Agglomerations", which is the core project during my Ph.D. to develop this thesis. The discussions with them on a weekly or bi-weekly basis helped me to extend my view to many other topics and inspired me to think more differently and learn the limitations of my work. I also hope to express my appreciation to Dr. Michael Lacasse, the respectful team leader in the Façade System and Products (FSP) group, who always provides me with every support, affection, and care. I enjoy the two years working, meeting, and chatting with him and all the other colleagues in the FSP group, which is a memorable time for me.

Furthermore, I would like to also acknowledge the collaborators in the building overheating project, Dr. Abdelaziz Lauoadi and Dr. Michal Bartko at NRCC, Dr. Sylvie Leroyer, and Dr. Stéphane Bélair at Environment and Climate Change Canada (ECCC), who provided their precious supports and help at the different stages of the project and my Ph.D. study. I also appreciate the days with my colleagues and friends, Lili Ji, Cheng Zhang, Senwen Yang, Danlin Hou, Dr. Dahai Qi, Dr. Lin Wang, Dr. Xuechen Bai, Weigang Li, and Zhe Xiao, who accompanied me over the hard and joyful days.

Since the start of the building overheating project, I have managed to connect with collaborators from multiple institutes, including Ministère de la santé et des services sociaux (MSSS), Ministère de l'Éducation et de l'Enseignement supérieur (MEES), Société d'habitation du Québec (SHQ),

Table of Contents

List of Figures

List of Tables

Chapter 1 Introduction

According to the United Nations, about 50% of the global population lived in cities in 2018 and it is expected that by 2050 this figure will increase to 68% of the world's total population (United Nations, Department of Economic and Social Affairs, Population Division, 2019). Urban areas are also home to infrastructure systems and buildings upon which the safety and comfort of the people critically rely. Several studies have highlighted that in the future, urban environments will experience the most drastic shifts in climate due to the combined effects of global warming and urbanization. It is estimated that the human activities after the industrial revolution have caused approximately 0.8 °C to 1.2 °C, and it is projected that shortly the temperature increase will be 1.5 °C between 2030 and 2052. The fifth assessment of the Intergovernmental Panel on Climate Change (IPCC) (IPCC, 2018) suggests that there will be an increased risk of injury, disease, and death due to more intensive heatwaves (IPCC, 2014a).

In recent years, the frequency and intensity of extreme heat events released more risks to human life (Meehl and Tebaldi, 2004). In 2003, the mega heatwave strokes Europe. Although the number of the death toll caused by the heatwave is different among the literature (Robine et al., 2008), it was estimated that the excess deaths are at least more than 22,000 due to the hot spell (Schär and Jendritzky, 2004). In 2010, more than 50,000 people died under the extreme heat stress of the heatwave in Russia (Otto et al., 2012). In 2018, extreme heat spell events in Canada between 30 June - 6 July contributed to about 100 deaths in the region (ECCC, 2019).

However, there is still no universal definition of the heatwave (Souch and Grimmond, 2004). Robinson specified the heatwave should be described by its frequency, severity, duration, and areal extent, and the definition of heat wave should vary for different locations (Robinson, 2011). WMO has defined heatwave as "A marked unusual hot weather (Max, Min, and daily average) over a region persisting at least two consecutive days during the hot period of the year based on local climatological conditions, with thermal conditions recorded above-given thresholds." (World Meteorological Organization, 2016).

Existing epidemiological studies focus on the extreme heat impact on public health. For such studies, the local effect of a heatwave is related to the increase of the relative risks of the health events during the heatwave period, for example, the mortality and morbidity change, the number of ambulance call-outs (ACOs), ambulance services uses (ASUs), emergency department

admission (EDA), emergency department presentations (EDPs), emergency department visits (EDVs), hospital admissions (HAs) and hospitalization (Xu et al., 2018). Although most of the heat-related deaths happen in buildings, the current heat-health-related studies are more focused on the outdoor climate pattern, but not the indoor overheating conditions. The indoor overheating analysis should be more related to the thermal feelings around the occupancy, which may also involve some stochastic factors, for example, the occupancy of the building (Mavrogianni et al., 2017, 2014), the types of the building, the location of the building, and the performance variation of the building construction situation and operations along with the changing climate (Figure 1-1). To build climate-resilient communities, it is essential to further enhance our current understanding of the interaction between the external surrounding environment of buildings and the indoor thermal conditions (Lomas and Porritt, 2017; Mylona, 2019).
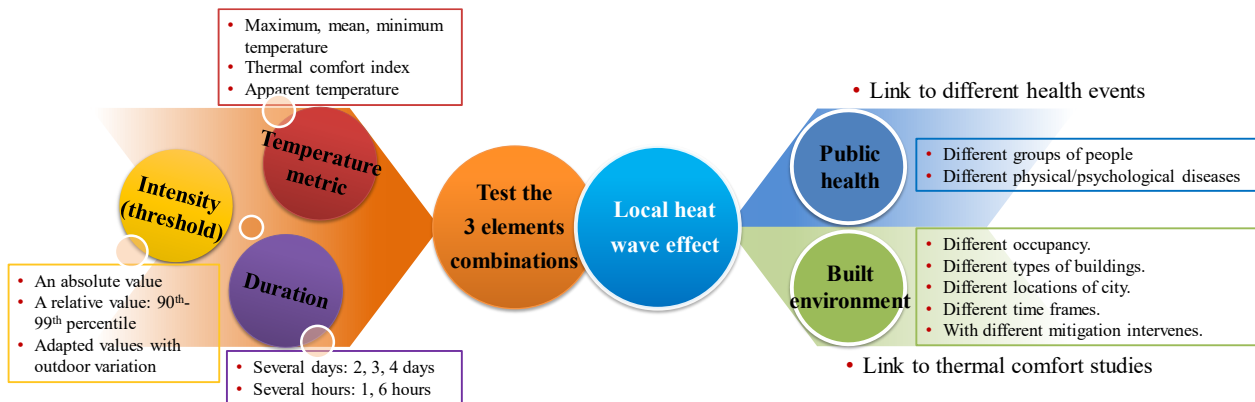
Figure 1-1 Investigation of the local effect of heatwaves and the definition method

1.1. Problem statement

It is unequivocal that the global climate has been consistently warming over the past decades and is projected to worsen in the future (IPCC, 2014b). Furthermore, extreme climate events such as heatwaves are projected to increase in frequency and intensity (IPCC, 2013). Overheating of building interior spaces as may arise from such climate change and extreme heat events have been identified as a major concern to the comfort and health of building occupants particularly of the vulnerable people such as the homeless, elderly, children, socially disadvantaged people, the physically challenged or the sick. Urban area centers that are subject to the urban heat island (UHI) effects may exacerbate the risk of overheating events in that indoor thermal conditions can reach excessive values over a prolonged period. In a recent heatwave of June 30 – July 7, 2018, up to 66 deaths were reported in Montreal with most of them being older residents, such as those people

who suffered from mental or chronic illness and addiction more easily than the others, as they were left without access to air conditioning in vulnerable communities of the city center (Laframboise, 2018).
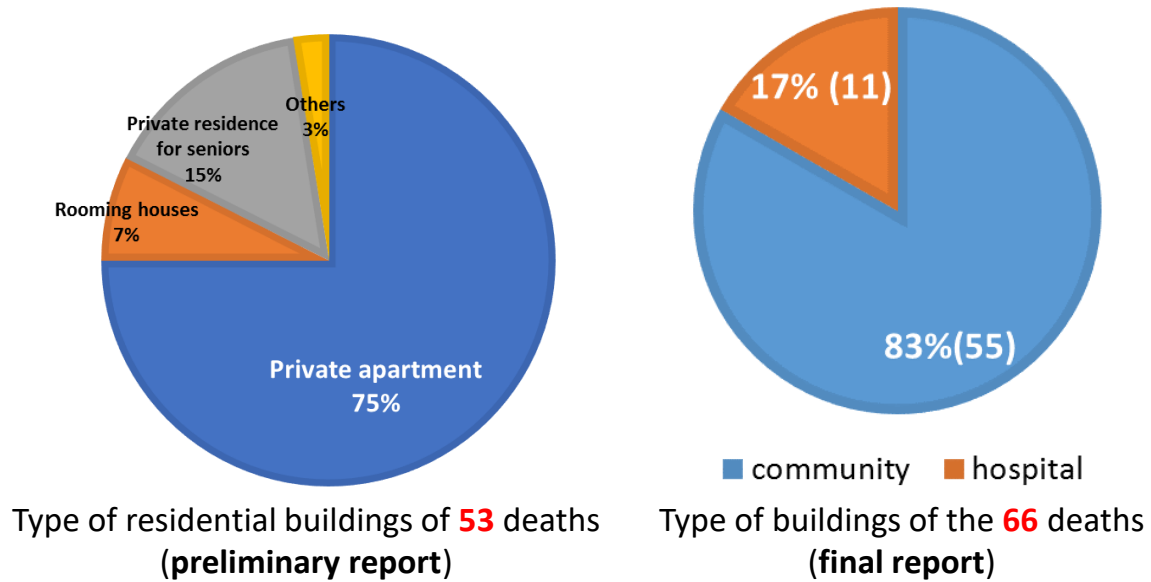
Figure 1-2 Location of heat-related-death archived in the report of the heat wave in 2018
(Direction régionale de santé publique de Montréal, 2018; Lamothe et al., 2019)

Buildings play a major role in limiting the risk of overheating events (Loughnan et al., 2015). Buildings influence the indoor thermal conditions to which occupants are exposed most of the time, given the fact that Canadian spend approximately 80% to 90% of their time indoors (IOM, 2011). Buildings that house vulnerable people and/or with poor management of indoor thermal conditions will suffer the most from the effects of overheating. It was found that most of the heat-related death (55/66) during the 2018 extreme heat event in Montreal happens in the community, and still, around 11 happened in the hospital (Figure 1-2). The resilience of hospitals against EHEs may help to reduce the mortality and morbidity of vulnerable groups of people, e.g., the elderly, the sick, and those having mental illnesses (Xu et al., 2018). The high indoor temperature in schools may also violate the academic performance of the children students aged between 8-14 (Barrett et al., 2015). The risk of overheating in mild climate area has been quantified by simulation studies, and more field monitoring are needed to cope with the future overheating problem due to the increase of IT equipment usage in classrooms and global warming trend (Jenkins et al., 2009). The severity of the indoor conditions depends on many factors of buildings: types (houses,

retirement homes, apartment buildings, schools, hospitals, etc.), internal space usage (occupant density, internal heat gains), construction characteristics (insulation levels, window proportions, solar shading, orientation of facades), and building operation (air-conditioning use, natural ventilation, etc.) (Quinn et al., 2014).

However, studies on building indoor thermal conditions as relating to the outdoor conditions are still very limited in Canada to enable the health care and building code organizations to establish threshold exposure limit of temperature and relative humidity to protect the health of the vulnerable population, which could be attributed to the following limitations and challenges: 1). There is a major lack of field monitoring data of indoor thermal environments for different building types in Canada. As a result, no reliable benchmarking data are available to support the assessment of the resilience level of the existing building stocks against overheating, and the establishment of threshold overheating exposure limit criteria. 2). There are limited simulation studies for establishing correlations between indoor and outdoor conditions, and the development of climate-adaptive mitigation strategies for developing associated guidelines against overheating. Accurate whole building performance simulations require adequate validations against field monitoring data. In the previous simulation study by Symonds et al. (Symonds et al., 2017), the simulation results were not in good agreement with the measurements due to the lack of dwelling data. In this study passive building mitigation strategies, including shading and natural ventilation, will be tested on the developed simulation models. 3). The whole building simulations also require accurate and detailed inputs of surrounding ambient conditions, which were often based on global/regional-scale weather and climate change data in the previous studies without considering the impacts from local microclimate environment down to building scales (Gracik et al., 2015). A scientific challenge remains to derive reliable climate change information at a spatial resolution that is relevant for building-scale impact assessments (e.g., < 1 m) as opposed to the resolution at which they are generated at a global scale (e.g.,>100 km) and downscaled to regional level also considering the uncertainty in projections as contributed due to the existence of multiple Global Climate Models (GCMs) and greenhouse gas emission scenarios. To tackle the challenges, we conduct a showcase study for the Ottawa and Montreal cities to assess the overheating risks in buildings.

1.2. Thesis objective

To solve the problems mentioned above, this thesis aims at two of the most critical elements in the study of building overheating, one is to collect the first-hand on-site measured indoor thermal condition data in the real buildings, and the second one is to build a reliable climate database that can be used to evaluate the urban scale overheating for both historical and future scenarios over a long-time frame.

There are still limited studies on city-scale field monitoring for building overheating in Canada, therefore the status of the current buildings during the summertime is still a question. How would the indoor overheating variate in the buildings at the different locations in a city? What are the common problems that may lead to overheating for the different types of buildings? How would the different occupants in the buildings overcome the overheating problem during the summer? How significant is the difference of overheating between the different rooms of the same building? How would the air conditioners variate the indoor thermal patterns in a building? All these questions are still not clear, and they cannot be easily answered without an in-depth field study. This study attempts to provide a peephole to these questions through a systematic building survey, site-visiting, and field monitoring.

The first practical difficulty to overcome for the large-scale study is how to efficiently sample the buildings that can be representative of the vulnerable or typical buildings in the city. The previous heat-related death, urban-scale climate patterns during the past heatwaves are investigated and a hierarchical procedure for building selection has been developed to help reduce the scope of the building selection. Building information surveys and on-site visits are then conducted to help collect first-hand information in the real buildings. All this information is consolidated for the selection of buildings for the field monitoring studies. The indoor air temperature and humidity are collected from the rooms of different conditions in these buildings and these data can quantitatively identify the current overheating conditions in these buildings. Since the definition and the assessment methods of overheating always change for different regions and areas, it is also necessary to clarify the difference in the different overheating methods when applied to the real building data in Montreal. Another purpose of the field monitoring is to provide the real building data for the calibration of the building models which can be used for the study of overheating assessment under various climate conditions or future scenarios and examine the effectiveness of the different overheating mitigation strategies. A high-quality field monitoring dataset can always

enable a series of studies as mentioned and this thesis intends to make this first step solid and in the correct and reasonable direction.

Another goal of this study is to figure out an efficient approach to generate a high-quality climate dataset for the building studies. For the overheating assessment during the summertime, it should cover a timeframe that is at least one summer (5 months from May to the end of September) to capture every possible indoor overheating during the year because of the existing overheating criteria are normally developed for the evaluation on an annual basis. The climate dataset should also incorporate the effect of the urban area, since the urban heat island effect has significantly changed the climate patterns in the city, and the urban microclimate always plays a non-neglectable role in the local building thermal performance. Existing building studies normally rely on a statistical or stochastic weather generator because it does not need expertise on climate modelling, while the reliability of these models should be questioned since the physical process in the climate is not solved. With this regard, this study develops a regional climate model for the Ottawa and Montreal area at a high-spatial-resolution to explore its potential for building overheating studies. The selection of the urban canopy models and the importance of the input information of the land cover has been first examined by the validation with the near-field climate observations. Then the added benefits of using the high-resolution climate model at a convection-permitting scale for overheating study have been first demonstrated in this study. To examine the effect of the urban area on building indoor overheating, the indoor conditions of the buildings at different locations have been compared by using the weather files extracted from the different locations of the simulated urban climate dataset. The contribution of this part of the work would identify the benefits of using an urban effect preserved climate dataset for overheating analysis and also develop a climate model that is ready for the study of the future projected scenarios.

Furthermore, to investigate the impact of climate change, the climate dataset should cover a time that is long enough to capture the long-term changes in the regional climate. Since the infrastructures like the buildings in the cities may normally stand for several decades, it is suggested in the existing studies that the weather files for buildings should cover 20-30 years. Existing studies have various discussions on how to select the typical or extreme weather files over a long time, while these data normally come from the observed dataset or a coarse resolution gridded dataset, which would not be enough for the urban scale analysis. An efficient framework to generate the long-term dataset should be developed based on the climate model developed in

this study but avoid the tremendous simulation workload and simulation time. The methodology of this part of the work would be mentioned in the discussion of future work since it still needs time to be completed.

1.3. Summary and the layout of the thesis

To outline the research gaps been solved by this study for the field of building overheating under extreme heat events. The thesis has been organized in the seven chapters following the current chapter.

Chapter 2 presents a systematic review on the current research status to help distinguish the current trend on building overheating study and the global distribution of the related studies. This also helps to further identify the most critical resources for the building overheating study: field monitoring dataset and historical/future climate dataset. The current field monitoring study and the methods to obtain the climate data have been reviewed critically. Since the literature review shows that a high-resolution dynamical downscaling approach is the most robust and reasonable way to generate the climate data with urban effect permitted. The application of using this type of high-resolution climate model (Convection-Permitting Model) for the simulation of urban heatwaves and the analysis of urban-scale overheating has been reviewed.

Chapter 3 established a systematic and reasonable procedure for the selection of buildings to do the field monitoring study in a Canadian metropolitan city Montreal, which can also help to extend the work for the other Canadian cities. Unlike the numerical simulation or experiments in the lab, field monitoring is more costly in terms of labour work, time, social and human resources, and economics. There are also concerns about the safety of instrument installation and data collection, permission to access the building, and reducing the disturbance and interruption of the actions of site visits on different purposes to the regular operation and work/life of the occupants in the measured buildings. This chapter introduced an efficient and effective procedure to obtain the building information for the building selection, summarized from the practical work with the different buildings and negotiation with the building managers.

Chapter 4 analyzes the field monitoring data for the selected school and hospital buildings, which is strong evidence to benchmark the current indoor thermal conditions of the various buildings in Montreal. Furthermore, the existing overheating assessment criteria and the widely used thermal indices that can be used to evaluate overheating have been reviewed and compared to identify the

discrepancy between the different criteria. The instruments used in this study and the installation methods have been described in detail to elaborate on how the measured data are collected. The field monitoring data has been used to compare the overheating of the different buildings and rooms to analyze the impact of the different room characteristics and operating conditions. The different overheating indices and criteria are compared through a correlation clustering analysis to help detect the potential connections in between and their general patterns associated with the collected measured dataset.

Chapter 5 describes the climate model been used in this study for the generation of the high-resolution climate dataset for urban overheating assessment. The Weather Research and Forecast (WRF) model has been used in this study for the simulation of the two cities, Ottawa and Montreal, at a spatial resolution of 1 km resolution. This study has compared the two most used urban canopy models for the urban climate simulation, including one simple bulk urban parameterization scheme (BULK), a multiple-layer urban canopy model -the building effect parameterization scheme (BEP), and two types of urban land cover has been used as the input for the simulation to help identify the impact of the land cover input on the accuracy of the urban climate simulation. The WRF simulation results are compared with the near-surface observation from the weather gauges in the domain, and the four most important climate variables, air temperature, relative humidity, wind speed and wind direction and the accumulated precipitation, are used to validate and compare the models.

Chapter 6 is dedicated to demonstrating the added value of using such a high-resolution climate model for the urban overheating analysis. Different from the regular Regional Climate Models (RCMs), the regional climate models (RCMs) conducted with a spatial resolution of less than 4 km are normally referred to as the Convection permitting models (CPMs). It can offer more reliable climatic information for the regional to local scale applications than the normal RCMs because they do not require convection parameterization, which is identified as a major source of errors and uncertainties in the RCMs. The current studies on building overheating only use the climate data from the coarse resolution RCMs, normally simulated with a grid spacing of more than 20 km. The added benefit of modelling climate at convection-permitting spatial resolutions (grid spacing < 4 km) was considered for a set of exterior climate and interior building simulations during EHEs in the urban areas of Ottawa and Montreal, Canada over the summer of 2018. The climate was modelled at two spatial resolutions: i) 25 km – typically considered for regional-scale

climate modelling, and ii) 1 km. The results derived from modelling at each of these resolutions were compared concerning their adequacy in predicting different measures of overheating outdoors as well as those within a typical single-detached home.

Chapter 7 focuses on using the high-resolution climate data for quantitative analysis of the effect of urban effect on building indoor overheating. In this chapter, the current methods to calculate the urban heat island effect using a Regional Climate Model is first reviewed for a critical selection of the urban heat island calculation in this study, which also helps to identify the urban area and rural area through the layout of the urban land cover. Then a limited number of locations throughout the urban area and rural area in the two cities, Ottawa and Montreal, are selected based on the simulated thermal conditions to represent the external climate conditions that a building may expose to at the different locations in the urban and rural areas. Building simulations are performed thereafter using the climate extracted from the selected locations to help identify their impact on the variation of indoor overheating.

Finally, in Chapter 8, the major conclusions are summarized, and the future work is proposed, which, most importantly, includes the usage of the field monitoring data for the real building model calibration and validation, and the procedures to extend the climate model in this study to efficiently generate the long-term high-resolution climate data.

Chapter 2 Literature review

2.1. Current research status on building overheating

A heatwave can have a great impact on so many aspects of people's life and society, particularly a rise in mortality and morbidity (Bassil and Cole, 2010; Campbell et al., 2018). However, there have been other reviews discussing the relationship between extreme heat and physical health risks. In this thesis, I only focus on the impact on buildings. Therefore, the literature searching rule (Figure 2-1) has been designed to consider the two groups of topic keywords for both extreme heat events and buildings. The topic words in the same group are connected by the "OR" relationship, while the two groups of words are connected by "AND" to limit the searching results with literature considering both topics. To avoid the repeating of the article contents in the searching outcomes, the types of the publication are limited to only articles, reviews, and editorials. And in this study, only the literature in the English language is considered for further review.
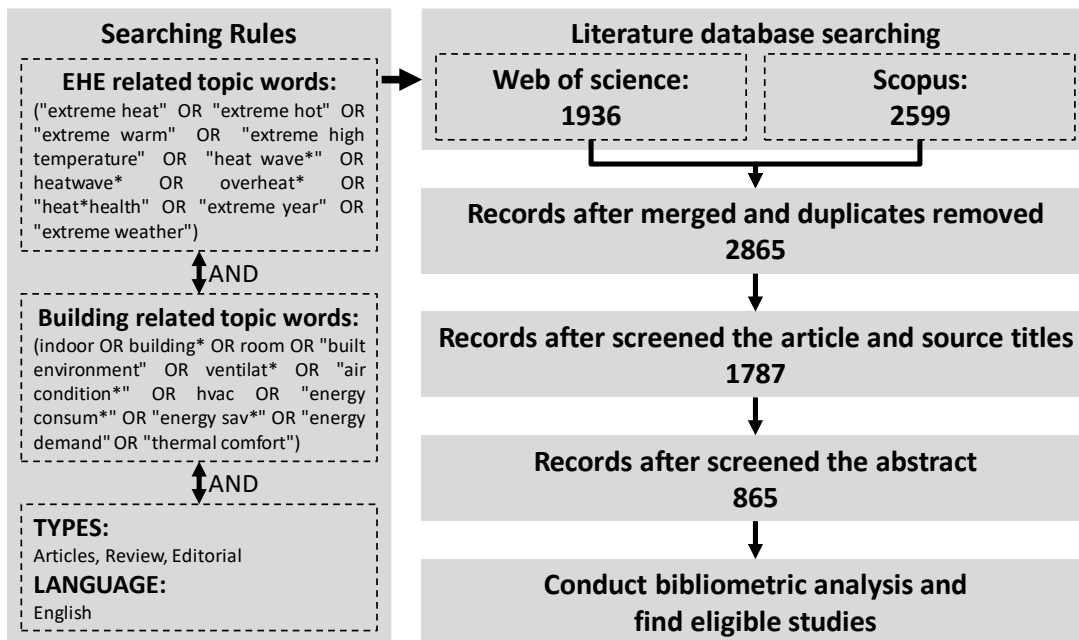
Figure 2-1 Searching rules and the number of papers after each screening step.

The words for the searching have covered a wide range of topics to ensure that any related articles can be captured into the initial literature database, which also consequently included a great number of papers not related to our interested field. With the above-mentioned searching rules, a literature database can be obtained through the search result of two of the most mainstream citation

databases and searching engines, Web of Science and Scopus. There are 1,936 items and 2599 items that met the searching rule in Web of Science and Scopus, respectively. Then the literature records from these two databases are merged and the duplicated items are removed, with 2,865 records left in total. These searching records are then filtered by reviewing the article and source titles to remove the research not related to the topic, i.e., ecological studies, nuclear engineering, transportation, and chemical studies. After this round of screening, 1,787 records are left in the database related to the urban and building research. To further concentrate the topic of articles onto the building scale overheating problems, another round of screening is conducted by reading the abstract of these records. Those studies only consider the urban scale or the outdoor thermal comfort without discussions on the effect of buildings that are therefore removed from the database. At last, 865 records are left in total which is related to the building performance under extreme heat conditions and the indoor overheating risks.

There is a comprehensive summary of the historical extreme heat events labelled by heatwave on Wikipedia ("List of heat waves," 2020) which is reviewed and summarized in Figure 2-2a for the heatwave that occurred in each continent. It can be observed that the frequency of heatwave events has increased in the 21st century, and after 2010, heat waves may happen on at least two continents each year, and sometimes might be more than once on the same continent or the events may affect multiple countries.

From the screened 865 articles after the abstracts are filtered, the locations of the authors can be plotted as bubbles on a world map (Figure 2-3), and the size of the bubbles indicates the number of publications of the specific country. The percentage of publications for each country is plotted in the pie chart. It can be noticed that the UK has the most publications with more than 200 articles published already, followed by the USA, Italy, China, and Germany. etc. Most of the studies happen in the temperate zone in Europe, North America, while relatively fewer studies can be found in the tropical zone. There is increasing research and policy interest in building overheating studies in heating-dominated climates (Zero Carbon Hub, 2015a). The death record during the 2003 and 2010 heat waves in Europe and Russia may also indicate a higher vulnerability in the group of people who have been used to temperate climate conditions (Armstrong et al., 2010). There is no study marked from Russia, which might be because the language of the literature for this review is limited to English only. This distribution of extreme heat and building overheating studies is similar to the result of the global review of the health impact of heatwave conducted by

S. Campbell et al. (Campbell et al., 2018). The co-authorship between the authors from different countries is also analyzed and plotted as connected curves on the map. Unlike the large-scale metrological or climatological studies which may have very intensive international collaborations, there are relatively fewer collaborations between countries to study the overheating in buildings. It can be found that the European countries have more frequent collaborations because of their close adjacency relationship, and China also has an intense collaboration with the UK, and Germany.
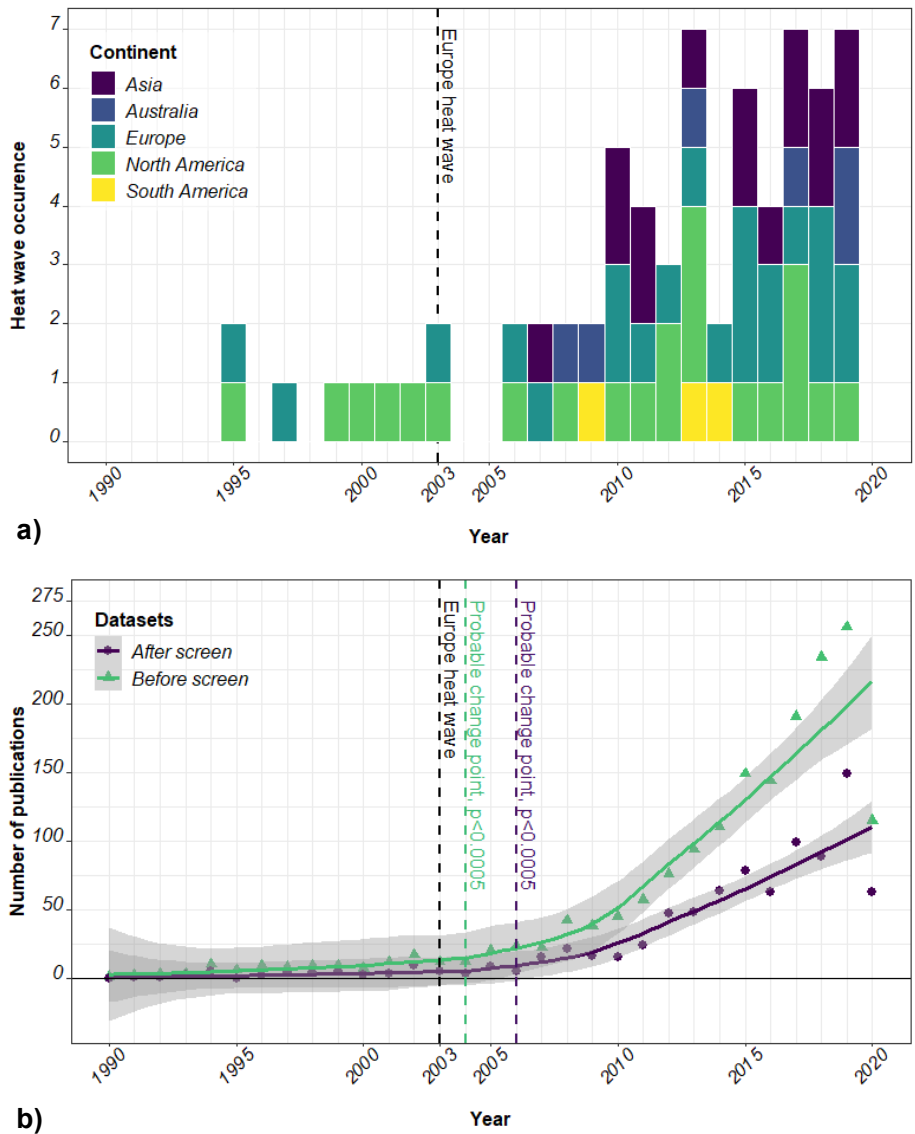
Figure 2-2 Heatwave occurrence in the different continent ("List of heat waves," 2020) (a) and the yearly publication trends (b)

Although at a similar latitude with the UK, the number of research in Canada is still far from compatible with the UK. The 2018 heatwave with almost 100 deaths in Quebec, which was mostly happened indoors, has attracted the attention of the government, society, the medical system, and other research institutes to launch studies on the impact of heatwaves on indoor overheating problems.
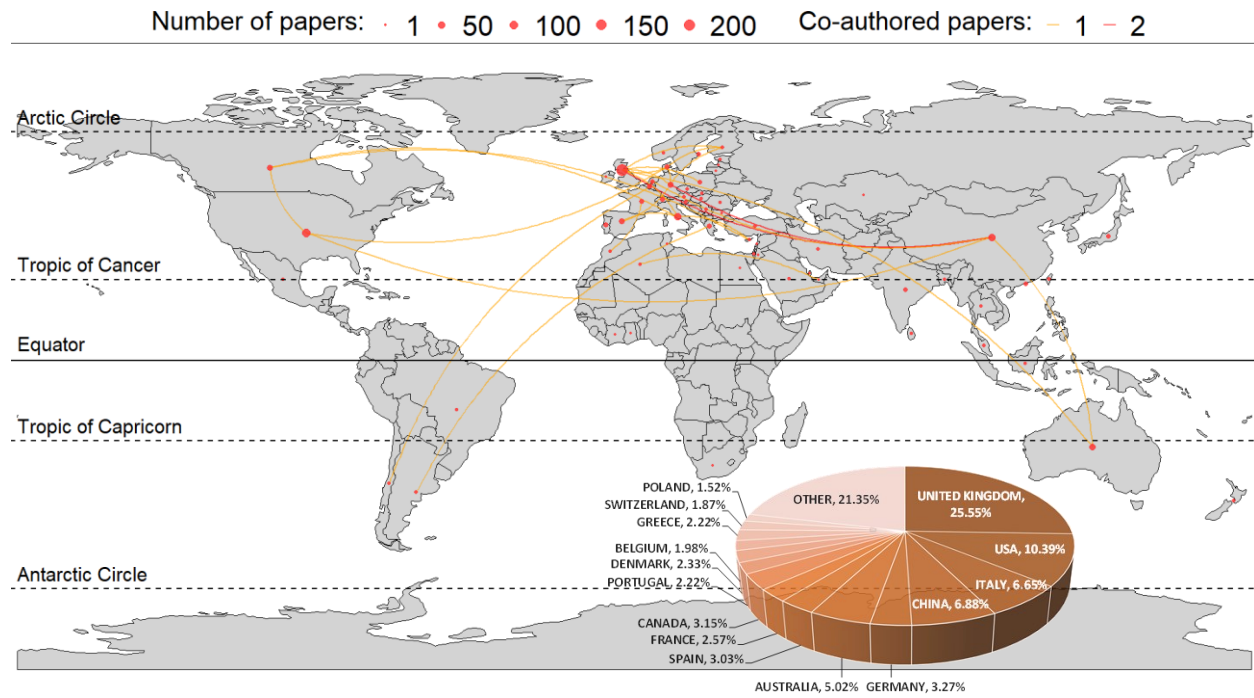
Figure 2-3 Global distribution of research on the impact of extreme heat events on buildings

2.2. Field monitoring of building overheating

The building overheating studies from the UK has contributed the most field monitoring studies as well, while there is a very limited number of field studies from other regions or countries, including Canada. Many researchers from Europe have conducted urban-scale or national-scale field monitoring studies on building overheating (Chen, 2019). Mavrogianni et al. (2010) monitored 36 dwellings for space overheating in the UHI of London (UK) during the mild summer of 2009, which found that 42% of the monitored dwellings failed to achieve the overheating criteria. Montazami and Nicol (2013) conducted a field measurement study for 140 classrooms in 18 naturally ventilated primary schools in London (UK) during the summer months of June and July of 2005, 2007, and 2008. It was found that students were more sensitive to thermal discomfort, and as such, the exceedance time ought to be 1%. Beizaee et al. (2013) conducted a national scale

study for 207 homes across England during the cool summer of 2007, and found around 21% of the monitored bedrooms have more than 5% of the nighttime hours is overheated even for a cool summer. Symonds et al. (2017) collected large-scale field monitoring data of 823 dwellings across the whole of England over the summer of 2011 and compared the measured data against the predictions from EnergyPlus simulations. The study found the simulations can be struggled to predict the maximum temperatures and not perform well during high temperatures, which therefore indicated the necessity to collect real-life data through field monitoring for the overheating assessment. McGill et al. (2017) collected the indoor temperature record for 60 buildings, and 57% of the bedrooms and 75% of the living rooms were identified to be overheating. van Loenhout et al. (2016) conducted field measurements in 113 homes for the elderly in the Netherlands in the summer of 2012, which found that the indoor temperature varied among the homes and was strongly related to the reported heat-related health problems for the group of the elderly. Since older people are particularly vulnerable to the health impact of overheating, Gupta et al. (2017) conducted case studies to monitor four care homes in England and found severe overheating problems in the monitored buildings. Recent studies by Mohamed et al. (2021) have focused on eight typical newly-built classrooms in two school buildings in UK's Midlands to study their overheating risks with around 4 days of data in the summer, and over 60% of the occupied times of these classrooms were found to be overheated. In their study, the occupancy levels and window opening schedules are also well recorded to explain the variation of the indoor thermal conditions. Touchie et al. (2016) conducted field measurements to evaluate overheating in post-war multi-unit residential buildings in Toronto, Canada. The overheating was evaluated in terms of temperature exceedance over the thermal comfort thresholds of 24°C, 26°C and 28°C. The measurements indicated that chronic overheating was present in all buildings during the summer months: all suites of all buildings exceeded 24°C and 26°C for 100% and 50% of the summertime, respectively, and some buildings exceeded 28°C up to 80% of the time. During the heat alert for the city, about 80% of suites surpassed 30°C. However, more field study is needed in Canada to collect the data for the assessment of the current building overheating conditions. Since most of the existing studies did not clarify how the monitored buildings and rooms are selected and some of the studies also pointed out that a survey is needed before the field monitoring, a building selection workflow for the field studies in the future should be established to disseminate the experience for such large-scale field monitoring practices. And urban-scale field monitoring

campaigns should be conducted to quantify the current building overheating conditions in Canadian cities.

2.3. Climate data for overheating assessment

2.3.1 Climate data selection and weather file generation

As a consequence of global warming, the increased occurrence of extreme heat events leads to higher morbidity and mortality (Meehl and Tebaldi, 2004; World Meteorological Organization (WMO) and World Health Organization (WHO), 2015). Overheating in buildings comes to be a major problem during the heatwaves which can impose fatal threats to the occupants' health (CIBSE, 2013; Quinn et al., 2014; Santamouris and Kolokotsa, 2015). The external climate is a significant driver of indoor building conditions. Taylor et al. (2014) conducted multiple building simulations for six cities from different climate regions across the UK to justify the importance of the weather files in the assessment of building indoor overheating conditions. Amoako-Attah and B-Jahromi, (2016) examined the variation of the simulated indoor operative temperature of detached residential buildings in London by using different weather files, which also affirmed the importance of selecting weather files for building-related studies. Cumulative efforts have been invested in finding the most representative weather file from a long-term climate series for building simulations (Berardi and Jafarpur, 2020; Guan, 2009; Herrera et al., 2017). As a result of climate change, typical hot conditions need to be considered in the weather files to help evaluate the building performance under the more frequent extreme weather events (Moazami et al., 2019). The Chartered Institution of Building Services Engineers (CIBSE) (CIBSE, 2002) first defined a method to select the third hottest year as the Design Summer Year (DSY) from a 21-year climate dataset for the sizing of mechanical cooling systems, which can also be used for building overheating analysis (CIBSE, 2014). Thereafter, the probabilistic DSY (pDSY) (Eames, 2016), the Summer Reference Year (SRY) (Jentsch et al., 2015), and the near extreme Design Reference Year (DRY)(Du et al., 2012) has been developed to consider the warmer than average conditions for building overheating analysis based on the DSY method. However, the DSY based methods do not include extreme values for the analysis of extreme heat events (Jentsch et al., 2014). To overcome this problem, several other weather data generation methods have been developed to include the extreme conditions from the long-term climate data. Extreme Meteorological Year (XMY) (Crawley and Lawrie, 2015; Ferrari and Lee, 2008), Untypical Meteorological Year

(UMY) (Narowski et al., 2013), Hot Summer Year (HSY) (Liu et al., 2016), and Extreme Warm Year (EWY) (Nik, 2016), are developed to select the climate data with the maximum values of their evaluated thermal metrics to construct the weather file. Guo et al. (Guo et al., 2019) proposed a new procedure of selecting the Typical Hot-Year (THY) for different cities of different climate conditions by analyzing the simulated indoor conditions of the typical residential building models instead of only the outdoor air temperature. Laouadi et al. (Laouadi et al., 2020b) developed the Reference Summer Weather Years (RSWY) to evaluate the transient Standard Effective Temperature (t-SET) using the two-node bio-heat model to consider the effect of not only air temperature but also other variables, e.g. humidity, airflow, radiation and also the status of the occupancy. RSWY can also be selected by evaluating three different features of the extreme heat conditions, including the intensity, duration and severity of the extreme heat event. This helps to describe the detailed properties of the hot conditions, which enables a precise estimation of the overheating risk.

The traditional representative weather year data are normally selected from multiple years which cannot reflect the spatial variation of the climate conditions, while buildings may expose to very different overheating risks even in the same city due to the various surrounding conditions(Klein Rosenthal et al., 2014; Taylor et al., 2015; Uejio et al., 2011). In 1999, a field monitoring campaign in London constructed a network of fixed temperature stations along eight transects of the city covering the whole urban and suburban areas, which provided the air temperature data to be strong evidence of urban heat island phenomenon (Kolokotroni et al., 2006; Kolokotroni and Giridharan, 2008; Watkins et al., 2002). The monitored data have been adopted by Kolokotroni et al. (Kolokotroni et al., 2009) to develop the London Site-Specific Air Temperature (LSSAT) model using an artificial neural network (ANN), which provides the localized weather data for a series of studies to discuss the urban heat island effect on buildings (Demanuele et al., 2012; Kolokotroni et al., 2012, 2010; Oikonomou et al., 2012). These studies used the climate data at the measured location across the Greater London Area, and a clear trend can be found that with the increase of the distance from urban center the indoor temperature and cooling energy can be lower (Demanuele et al., 2012; Kolokotroni et al., 2012) in summer while the heating energy consumption in winter can be higher (Kolokotroni et al., 2012, 2010). The study by Pyrgou et al. (2017) statistically compared the data collected from two different urban weather stations with the typical year data, highlighting the necessity of updating the building simulation weather files

frequently to include the microclimate phenomena for the evaluation of extreme conditions. These studies compare the overheating in buildings using the climate conditions at limited locations with measuring stations, which can be hard to reflect the overall pattern for the whole city.

To enable the neighborhood and individual building level design and decision making, high-resolution climate data are required to detect the smaller-scale climate difference (Macintyre et al., 2018; Murage et al., 2020; Taylor et al., 2018, 2015). A downscaling process is needed to enhance the resolution of data from a larger-scale parent climate dataset which can be Global Climate Models (GCMs) with the spatial resolution in the range of 100-300km, or some coarse resolution Regional Climate Models (RCMs) with the spatial resolution in the range of 10-75km (Giorgi, 2019). The application of the various downscaling procedures, including statistical downscaling, dynamical downscaling and a hybrid of both, for building simulations have been reviewed in several studies (Berardi and Jafarpur, 2020; Guan, 2009; Herrera et al., 2017; Moazami et al., 2019). More than 50% of the 111 building performance studies reviewed by Moazami et al. (2019) implemented the statistical approach to obtain the weather data due to the high level of expertise is required for the dynamical downscaling using the numerical weather models. The UK Climate Projections (UKCP09) dataset (Mylona, 2012) has been widely used for overheating studies in the UK, which is available at 25km grid scale originally provided by the UK Meteorological Office using the Hadley Centre Climate Model (HadCM3) (McCarthy et al., 2012). To further downscale the UKCP09 data, a stochastic weather generator (Jones et al., 2009) is available to reproduce the data on a 5km grid scale. This dataset incorporated the 5km×5km gridded rainfall dataset created by Perry and Hollis (2005a, 2005b), which was interpolated from the data of a dense observation network. Eames et al. (2012) have used the 5km grid climate dataset to investigate the temperature variation along the transect of two cities, Devon and Norfolk, in the UK, and found for both indoor and outdoor temperature, the temperature variation will be greater under future scenarios. Liu et al. (2017) also used the 5km×5km grid data to establish a new workflow of mapping the indoor overheating risks over the Sherfield city with the data from the seventeen grids covering the city. The statistical methods can also be extended to existing typical weather files or observation data to obtain a spatial distribution of climate variables. Hwang et al. (2020) have applied the "morphing' method (Belcher et al., 2005) to generate the location-specific weather files which integrated the urban heat island effect into typical year weather data. These weather files are used for a series of building simulations to obtain a high-resolution mapping of the building overheating

risk in 200m grid resolution. In their study, only two climate variables, air temperature and relative humidity, are customized independently without considering the inter-variable relationships for the localized weather files, whereas the other variables are not changed from the original baseline weather file. Even though some of the studies have already compared the climate information between different resolutions (Eames et al., 2012), the added value of using high-resolution dynamical downscaling models for building overheating analysis is still unclear. The reason is that comparing to the dynamical downscaling using the physical resolved numerical models, the statistical downscaling and the various weather generators may have the problems of: a) lower reproducibility, b) lack of different climate information, and c) lack of the persistence of the inter-variable patterns (Guan, 2009; Mylona, 2012).

2.3.2 Urban climate simulation using Regional Climate Models

According to the United Nations, about 50% of the global population lived in cities in 2018 and it is expected that by 2050 this figure will increase to 68% of the world's total population (United Nations, 2019). Urban areas are also home to infrastructure systems and buildings upon which the safety and comfort of the people critically rely. Several studies have highlighted that in the future, urban environments will experience the most drastic shifts in climate due to the combined effects of global warming and urbanization. To build climate-resilient communities, it is essential to further enhance our current understanding of urban climate systems and our ability to model them. The Weather Research and Forecasting (WRF) climate modelling system (Skamarock et al., 2019) has been used extensively in several previous studies to simulate urban climate in cities across the globe. Georgescu et al. (2013) for instance used the WRF model to investigate the potential effects of urban expansion of USA-Arizona's Sun Corridor on regional temperatures. It was found that urban expansion in the region could contribute up to a 4 ºC rise in temperatures under the most drastic urban expansion scenario. Using WRF, Salamanca et al. (2011) simulated planetary boundary layer processes over the city of Houston, Texas under four sets of urban parameterization schemes: a bulk scheme, a single-layer urban canopy model (UCM) with a fixed anthropogenic heat diurnal profile, a multilayer UCM, and finally a multilayer UCM with an integrated building energy model (BEM). From this study, it was concluded that to quantify anthropogenic heat effects on urban meteorology, the use of UCMs combined with BEMs is necessary, however for applications such as real-time weather prediction, a bulk scheme can simulate reliable estimates of

the urban climate and other data-intensive UCMs are not necessary. Similarly, Salamanca et al. (2018) conducted six numerical WRF-experiments using two different land surface models in combination with three urban parameterization schemes to evaluate their relative importance on the performance of WRF in simulating near-surface air temperature, wind speed, and water content profiles over Arizona, USA. It was concluded that the multilayer UCM Building Effect Parameterization (BEP) developed by Martilli et al. (2002) in combination with the BEM developed by Salamanca et al. (2010) and Salamanca and Martilli (2010), and the Noah-MP land surface model (Barlage et al., 2015; Niu et al., 2011; Yang et al., 2011) performed best in simulating urban climate at this semiarid urban environment.

Krayenhoff et al. (2018) used the WRF model to investigate the future increase in temperature as a result of potential future greenhouse gas emissions and urban expansion across the contiguous USA. It was found that the temperature response to urban expansion was different in the historical and future climates suggesting that the two forces dynamically interact to produce temperatures that are less than the simple sum of individual responses. Furthermore, it was concluded that infrastructure-related adaptation measures can only partially offset the temperature increases caused by future greenhouse gas emissions, and a reduction in the latter is essential to fully adapt to climate change. Argüeso et al. (2014) evaluated potential future increases in temperature due to projected climate change and urban expansion in the Sydney area (Australia) using the WRF model. They found that urban expansion will have major impacts on the nighttime temperature, which could potentially double the temperature increase in the city projected as a result of climate change alone. Paul et al. (2018) evaluated the accuracy of the WRF model towards simulating extreme precipitation over Mumbai city of India and found that WRF with a multi-layer UCM can capture averaged precipitation characteristics across the city on extreme precipitation days, especially when modelled values are evaluated regarding weather stations located within the urban areas of the city.

On the other hand, Hahmann et al. (2015) evaluated the performance of the WRF model towards simulating wind speeds over the North and Baltic seas and found that modelled annual mean wind speed differed from observations by only 3.2%. Additionally, the sensitivity of the model's performance to the number of vertical levels, the horizontal spatial resolution of the sea surface temperature, strength and form of nudging, planetary boundary layer parameterization, and length of the spin-up period were also investigated. The WRF model's performance was found to be

critically linked to the planetary boundary layer scheme and spin-up period. Jandaghian et al. (2018) evaluated the sensitivity of the WRF model to different physics parameterizations related to microphysics, cumulus, planetary boundary layer, radiation, and land surface models. The best set of physics schemes were used to drive the model and it was found that an increase of albedo of roofs, walls, and roads reduces the absorption of solar radiation and leads to a decrease in relative humidity, convective cloud formation, and precipitation in the Montreal metropolitan area. Potential future changes in precipitation extreme events over the western Canada region were evaluated in Erler and Peltier (2016) by performing 10-km spatial resolution WRF-simulations of climate over current and future periods. Results from this study indicated that global warming can result in increased wintertime precipitation extremes in the region. In addition to the WRF-urban modelling system (Chen et al., 2011), other models such as the Canadian-urban modelling system have been used to simulate urban environments in Canadian cities such as Vancouver (Leroyer et al., 2014), Montréal (Leroyer et al., 2011), and Toronto (Leroyer et al., 2018). To the best of our knowledge, no study has been performed to simulate the urban climate of Ottawa city.

2.3.3 Application of Convection-Permitting climate models

As a consequence of global warming and urban expansion, the frequency and intensity of extreme heat events (EHEs) in cities around the globe is increasing, resulting in both high morbidity and mortality (CIBSE, 2013; Meehl and Tebaldi, 2004; Santamouris et al., 2015; World Meteorological Organization (WMO) and World Health Organization (WHO), 2015). Urban areas are typically warmer, wetter, and less windy than the areas surrounding them due to their distinct morphology (Oke, 1982). This urban-rural climate contrast cannot be properly simulated by global climate models (GCMs) operating at a spatial resolution of 100-300 km, and typically a downscaling step is required to complete a useful simulation.

A limited-area regional climate model (RCM) performs dynamic downscaling of GCMs and produces regional-scale climate estimates at 10-50 km spatial resolution (Giorgi, 2019). State-of-the-art reanalysis datasets such as ERA-Interim (Dee et al., 2011), North American Regional Reanalysis (Mesinger et al., 2006) and the Climate Forecast System Reanalysis (Saha et al., 2010), also provide regional-scale estimates of historical climate at aforementioned spatial resolutions. The RCMs add value over the GCMs for three reasons: i) the finer resolution allows a more realistic representation of surface forcing such as orography, lakes, rivers, and coastal regions; ii)

the finer resolution allows a more accurate discretization of equations, and thus, a better simulation of the atmospheric circulation and gradients; and iii) with finer resolution, a broader range of fine-spatial scale processes can be explicitly resolved, which includes mesoscale weather phenomena such as sea breezes, lake-effect snowstorms, local winds, tropical cyclones and mesoscale convective systems (Giorgi and Gutowski Jr, 2015).

Several studies have investigated the benefit or "added value" (Di Luca et al., 2015) of modelling climate at finer regional scales. Lucas-Picher et al. (2017) compared climate across North America over 1979-2014 as simulated by the Canadian Regional Climate Model version 5 (CRCM5) (Martynov et al., 2013; Šeparović et al., 2013) at 0.44°, 0.22°, and 0.11° spatial resolutions. They concluded that higher spatial resolution simulations showed a more realistic description of complex climate phenomena as orographic precipitation, precipitation extremes, sea-breeze formulation, and similar climate phenomena. Similarly, Qiu et al. (2020) compared climate simulations performed at 20 km and 5 km over South Korea over a 20-year historical period and concluded that both sets of climate simulations captured the spatially and temporally averaged climate characteristics. Meanwhile, finer scale simulations better simulated the intensity and frequency of extreme events and spatio-temporal variations in climate variables. Mayer et al. (2015) discussed the importance of performing high-resolution climate simulations for assessing the impacts of extreme events on infrastructure by comparing 8 km resolution simulation results with lower resolution simulations conducted at about 70 km over Scandinavia. On the other hand, (Curry et al. (2016) identified limited added value of 15 km resolution simulations over 45 km resolution simulations from the Canadian Regional Climate Model version 4 (Caya and Laprise, 1999) in terms of predicted temperature and precipitation. It was concluded that the added value by RCMs depends on the variable to be evaluated and the problem to be addressed.

Convection permitting models (CPMs) are a type of regional climate model (RCMs) in which climate simulations are conducted at a spatial resolution of less than 4 km. CPMs offer more accurate climatic information for regional to local scale applications than RCMs because they do not require convection parameterization, which is identified as a major source of errors and uncertainties in the RCMs. At the same time, they allow for an even more accurate representation of surface and orographic fields in the simulations (Prein et al., 2015). Several studies have used CPMs to obtain local scale climate using boundary conditions from GCMs (Mahoney et al., 2013, 2012) or RCMs (A F Prein et al., 2013; Andreas F Prein et al., 2013; Rasmussen et al., 2014). The

CPMs have been found to add value over RCMs in simulating mean precipitation (Ban et al., 2014; Fosser et al., 2015; Langhans et al., 2013), their spatial patterns(A F Prein et al., 2013; Andreas F Prein et al., 2013), and extremes (Ban et al., 2014; Chan et al., 2013; Rasmussen et al., 2014). Similar improvements in the modelling of temperature and its extremes have been obtained (Hohenegger et al., 2008; A F Prein et al., 2013). Meanwhile, their added value has also been demonstrated in local-scale impact assessments, for instance, in the simulations of the energy and mass balance of glaciers (Mölg and Kaser, 2011), river runoff, and flood forecasting (Bartholmes and Todini, 2005; Cloke and Pappenberger, 2009), and renewable energy production (Foley et al., 2012; Kleissl, 2013; Tölle et al., 2014).

CPMs have been used to model urban climate, assess the effects of urbanization and climate change in urban areas, and evaluate the effectiveness of various heat-stress mitigation strategies. Van Weverberg et al. (2008) isolated the contribution of urban heat island (UHI) on temperatures recorded in Uccle, Belgium, by conducting 1 km resolution simulations using the Weather Research and Forecasting (WRF) model (Skamarock et al., 2019) and comparing them with the observational records. The role of urban growth in forming four historical EHEs in the Phoenix, Arizona metropolitan area was evaluated by Grossman-Clarke et al. (Grossman-Clarke et al., 2010). It was found that new urban developments around the city caused an intensification and expansion of the area experiencing extreme temperatures during EHE. Wouters et al. (Wouters et al., 2013) simulated the UHI over Paris by conducting 1 km resolution urban climate simulations using an Advanced Regional Prediction System (Xue et al., 2001, 2000). Taha (Taha, 2008) demonstrated that UHI could be mitigated by up to 3ºC in Sacramento by increasing the city's albedo and urban vegetation cover. Schubert and Grossman-Clarke (2013) demonstrated the effectiveness of increasing green urban infrastructure, high-reflective surfaces, and judicious selection of building materials in effectively reducing the heat stress in Berlin, Germany, during EHE.

The external climate is a significant driver of a building's indoor conditions. A few recent studies have used climate simulated by CPMs in simulating the indoor environment in buildings. Ciancio et al. (2018) simulated the climate of the metropolitan area of Rome by performing a 4 km resolution WRF simulation. The simulated outdoor conditions were used to undertake building energy simulations in EnergyPlus (U.S. Department of Energy's and Building Technologies Office, 2020). The results were compared with another two simulations using the weather data

recorded at airports. The study concluded that using the weather data from airports might result in an underestimation of cooling energy consumption and an overestimation of heating energy consumption in the city as urban effects are not accounted for. Similar conclusions were drawn by Jain et al. (2020), who emphasized the importance of using climate data with urban effects incorporated, which can be simulated in a WRF simulation, for the prediction of building energy in Chicago. Luo et al. (2020) evaluated the spatial variation of the building waste heat emission in Los Angeles, California, by conducting WRF simulations at 500m spatial resolution and building energy simulations using EnergyPlus. It was concluded that heat emission from the buildings during EHEs exacerbates the outdoor heat stress, especially in densely populated urban districts in the city.

Chapter 3 Field Monitoring - Building Survey, Site Visiting, and Selection

The study established the procedures for urban-scale multiple building overheating measurements, which can be an example for other cities to conduct similar studies in Canada. This chapter presents the enormous practical challenges to connect with the local building managers and to make access to the buildings happen even during the pandemic, which ensures the success of the instrument installation and data collection. The procedure of building selection as described in sections 3.1 and 3.2 can be summarized as a practice guideline. The building survey and site visits in sections 3.3 and 3.4 also collected first-hand information to help people understand the real operation conditions, occupancy, and construction details of different types of buildings. The final building selection results are presented in section 3.5.

3.1. Building selection procedure

In this study, the field monitoring will be carried out for a limited number of school and hospital buildings for three years. Therefore, determining the best combination of buildings as regards the most vulnerable to EHEs, can be a significant challenge to ensure capturing both the EHE and indoor overheating problems during the long-term monitoring program.
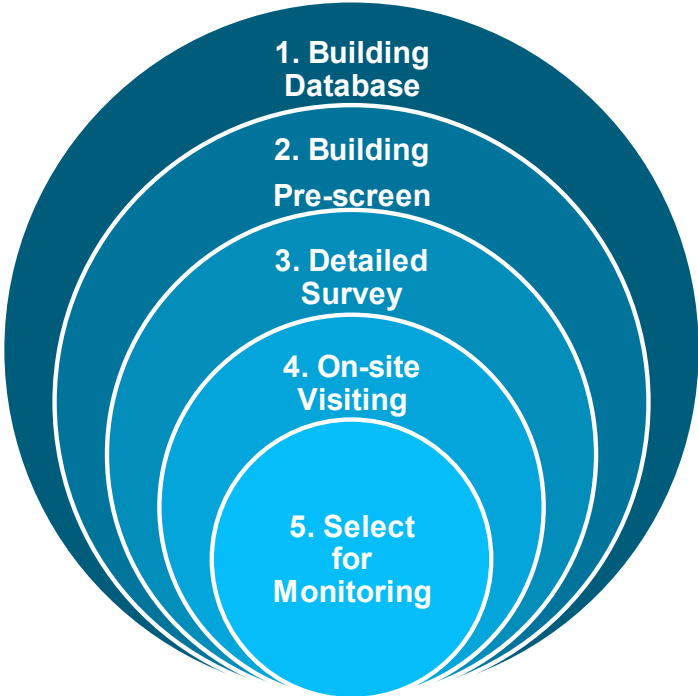
Figure 3-1 Procedure for screening and selection of buildings for field monitoring.

A 5-step guideline for the screening and selection of buildings for field monitoring is given in Figure 3-1. A vast database for all the hospital buildings in Montreal was obtained from the: (i) Ministère de la santé et des services sociaux (MSSS), (ii) 5 different Centre intégré universitaire de santé et de services sociaux (CIUSSSs) in Montreal. As well, for selection of school buildings, the Ministère de l'Éducation et de l'Enseignement supérieur (MEES) provided information on 5 different Montreal school boards. Typically, the building database should have a significant number of buildings to permit covering more possibilities for potential cases.

To further reduce the scope for building selection, a pre-screening of the building database was conducted. An investigation on previous heat-related deaths during EHEs showed the location and distribution of emergency calls and the heat-related deaths attributed to EHEs; these are highly related to the urban heat island intensity as given in Figure 3-2. As well, most of the health events (i.e., heat-related deaths and emergency calls) happened in areas with intensive heat island problems (Figure 3-2), indicating those dwelling in these areas may have had a higher exposure during the EHE, and the buildings in these areas may be more vulnerable to overheating issues. Thus, the location of the buildings becomes an essential criterion for the selection of appropriate buildings to study. Google maps and Google Street views were found to be useful tools to inspect the location, orientation, and surrounding environment of the buildings. A graphic set of each of the buildings was created from the southern view on Google Street maps, and the buildings were filtered using the following criteria:

1. Schools mainly with children aged 8 – 14.
2. Hospitals with long-term residents.
3. The building location is close to those sites where deaths had been previously noted.
4. Buildings with a longer façade facing the north-south direction
5. Buildings that were not close to green areas or parks

Buildings located in a high-density neighborhood and close to major streets or parking lots have large areas of impervious land cover without any shading

For that reduced set of candidate buildings, a building information survey was prepared to permit gathering detailed information about this set of buildings. A building information survey form was distributed to the building owners and their material service managers to obtain information on construction details, building equipment, and related information. The survey sheet also contained information in which the study objectives were provided and that to explain the possibility for

building managers to support the study. The building information survey form is organized into 5 sections:

1. General information of buildings: building name construction year, number of floors, number of occupants, etc.

2. Building performance and occupant behaviour: thermal comfort and historical heat-related health events, building activities, overheating complaints, and relevant measures to mitigate impacts of overheating.

3. HVAC system: type of system, fresh air system, cooling system, ventilation, etc.

4. Building envelope: type of envelope construction, materials, window type, window-wall-ratio, etc.

5. Building plans.
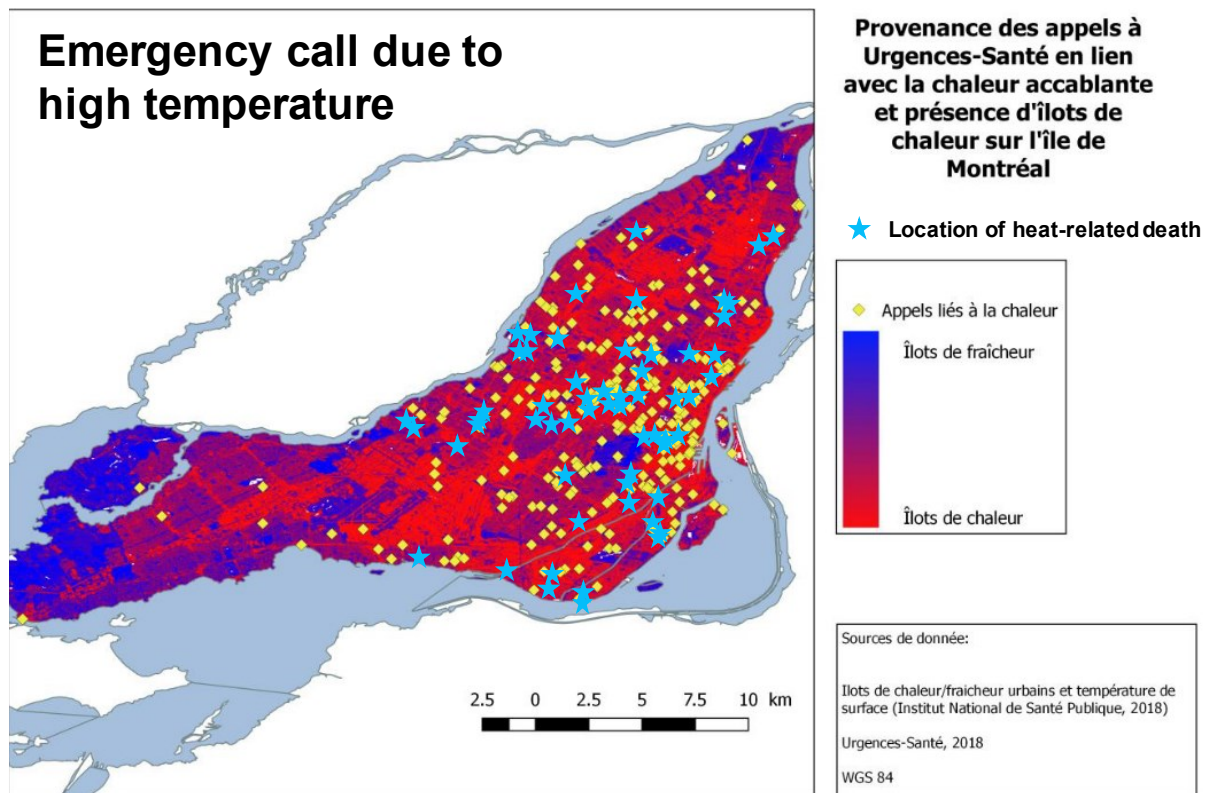
Figure 3-2 Distribution of emergency calls due to EHEs in 2018 and death-related EHEs as provided in a heat island intensity map (Lamothe et al., 2019; The Institut national de santé publique du Québec, 2018)

After we received the survey forms, it was important to conduct on-site visits to gather more firsthand information about the building. The visits to hospital sites were conducted in July

whereas this occurred in September for schools. Usually, it is optimal to have a team comprised of four members, each member assigned a corresponding task; these were:

1. Communicate with the building manager to know the function of the rooms, building system, and equipment, confirm important questions on the previous building information survey forms.

2. Communicate with people in the building, i.e., students and teachers in schools, patients, and doctors in the hospital, to know the general level of comfort in the building.

3. Take photos to keep a good record of the site; undertake thermal images of building surfaces for quantitative comparisons later.

4. Take notes of the communications and use a checklist for process control to ensure all tasks have been completed.

Along with the practice of visits to many different buildings, a team approach using assigned tasks provided a most effective and efficient way to collaborate with building managers and users. Too many personnel for a visit may disturb the building occupants of which may be undesirable.

Decisions for the selection of buildings were made after completing the site visit. The overall distribution of selected buildings, the real condition of the building, and the attitude and intention for collaboration of the building owners should be considered comprehensively. The results of these major steps during the site studies are discussed in the next section.

3.2. Building prescreening result

In the first step, a list of 200 hospitals and 396 schools was obtained for the Montreal area. The locations of the buildings were marked on Google maps, as in Figure 3-3, so that the locations could be compared with those of the previous heat-related deaths (red stars). After that, the large database of buildings was filtered to 64 schools and 53 hospitals over the entire island.

Some of the locations would not be able to participate in this project, given that for some, either they had no overheating problems evident in their buildings or, retrofitting activities were to take place shortly. To determine these instances, the building survey form was used to investigate these candidate buildings and communicate with the respective building managers. Several completed survey forms were received at the end of step 4: 12 hospitals and 15 schools. On-site visits are the most critical step for final decisions on selecting buildings. As examples, only one hospital building, and one school building are each described.
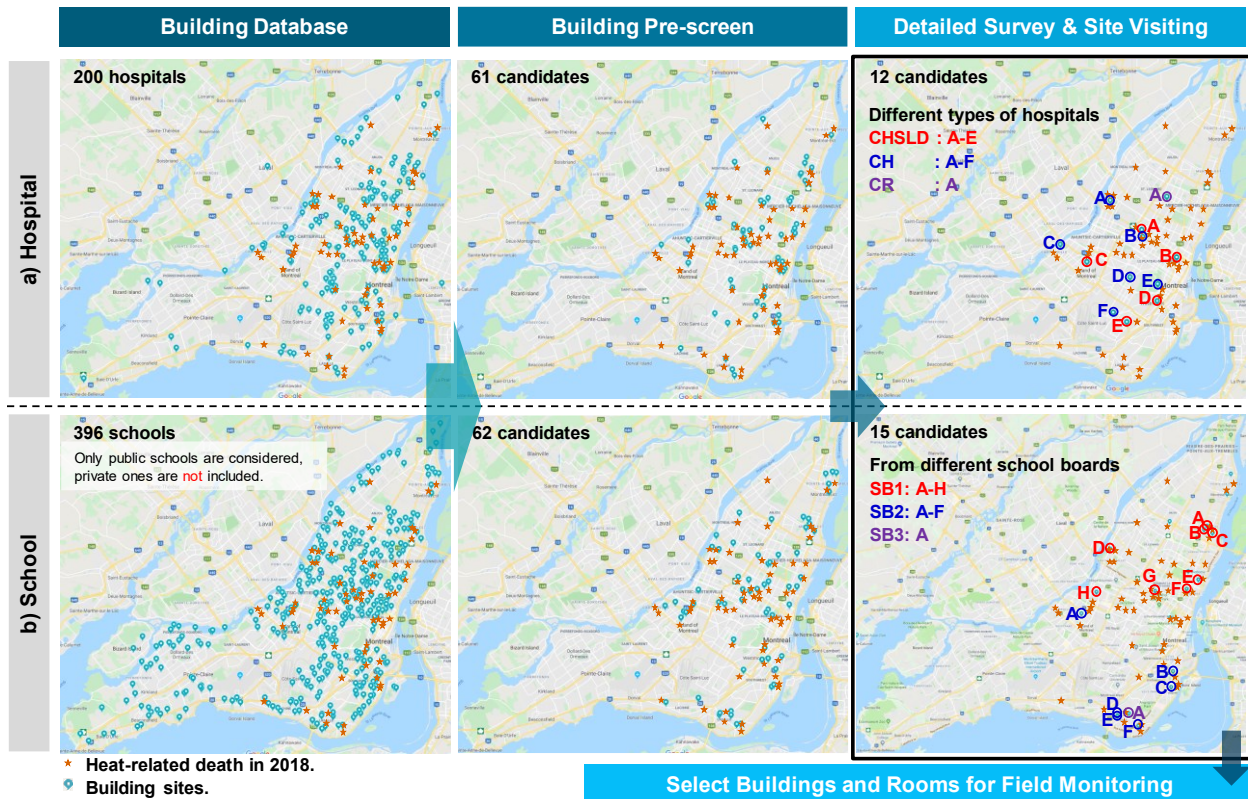
Figure 3-3 Distribution of a) hospital buildings and b) primary school buildings on Montreal Island and locations of heat-related death in 2018. (CHSLD-Residential and long-term care centre, CH-Hospital centre, CR-Rehabilitation centre, SB-School board)

3.3. Site-visiting study

3.3.1 Site visits to hospital buildings

Site visits to CH-D

This hospital has seven floors in total with a building envelope composed of ceramic, brick and plaster without insulation. The window- wall-ratio is 40%-50%, and curtain and blinds are installed inside for shading. The plant coverage in proximity to the building is low, whereas building density is high in the surroundings.

Although there exists a centralized air conditioning system, it does not cover the whole building. To deal with the overheating problem in summer, a temporary air conditioning system is temporarily installed in the corridor during the summertime (round air ducts; Figure 3-5). In some rooms without centralized AC, window units are used. There is no AC system on the top floor (7th floor). The rooms facing south, including a family room, a clinic room, and a therapy room, have

higher indoor temperatures than that of the corridor. There are also overheating problems on the 5th floor. On that floor it was found that apparent high temperature occurs in a waiting room without operable windows; this room is often fully occupied. As such, these rooms, having obvious overheating complaints and problems, are potential candidates for monitoring later in the study.
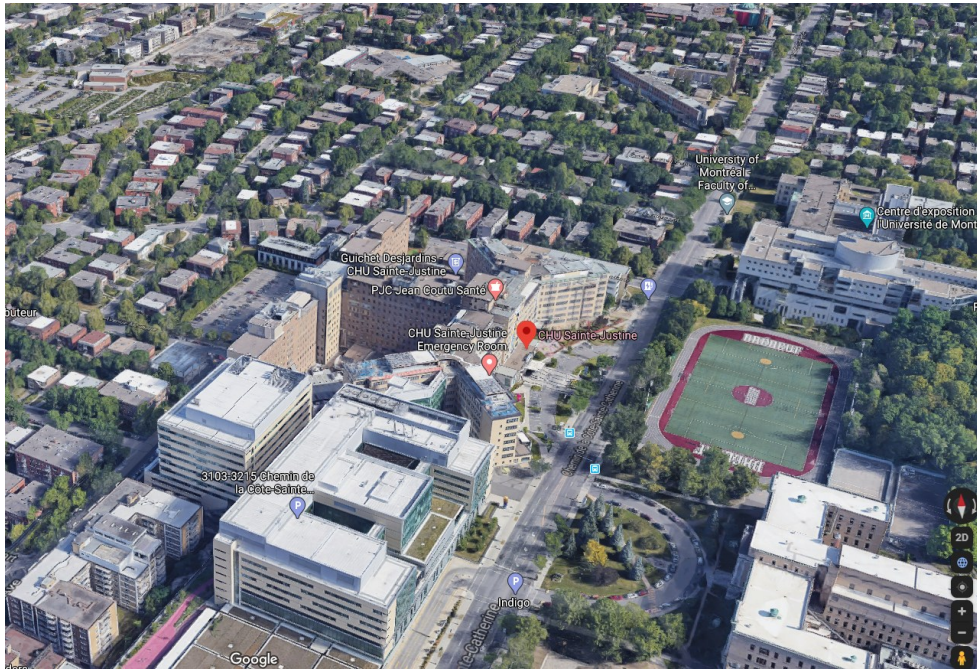
Figure 3-4 Site view of CH-D from the south view
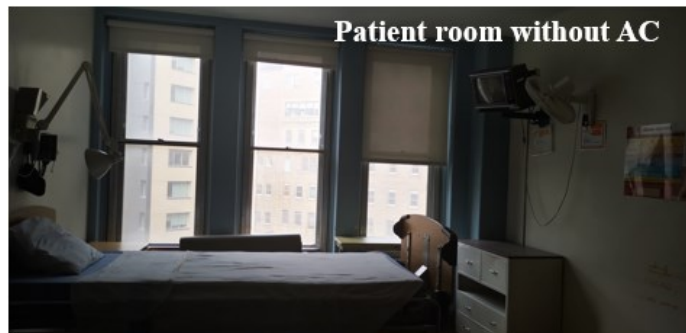
Figure 3-5 On-site visiting of CH-D

Site visits to CHSLD-A

Site visitings can be a confirmation of the building information survey and an effective way to find more detailed information.

Figure 3-6 Site view of CHSLD-A from the south view

Figure 3-7 HVAC system rooftop units of CHSLD-A

CHSLD-A is a long-term care center of 6 floors for senior people with severe overheating problems built in 1984. It is located in an area with a large number of previous heat-related deaths. From the google street view in Figure 3-6, it can be easily observed that the building have a longer side façade facing the south, and there are no open area, parks and few plants in the adjacent area, the surrounding buildings are low-rise. Other surrounding information from building surveys can also be confirmed. The window wall ratio is around 30-40%, and the façade colour is red-brown, but the roof colour on the google view was dark grey, which is different from the on-site observed colour (Figure 3-7) which should be white.

During the site visit, checking the building equipment on the roof and in the mechanical room should be a major task to inspect the layout of the HVAC system (Figure 3-8). There are several outdoor units of the air conditioners for the office rooms, a centralized VRV system for the activity rooms on each floor and a fresh air intake on the roof for corridors.

However, there is normally no air-conditioning in the patient rooms and the indoor thermal conditions are not desirable. The elder people in the building felt hot and stuffy in the corridors and the patient rooms. We have visited a patient room on the top floor and the patient inside complained the room is too hot and has added even two portable fans to ventilate and cool down the room (Figure 3-8). The staff of the hospital informed us that they may suggest the patients stay in the activity rooms till the night during hot summer days, because there is cooling in the activity room, and it was found that a curtain is used between the activity room and the corridor to separate the spaces and preserve the cooled air in the activity room (Figure 3-8). Although there are fresh air diffusers in the corridor and diffusers, they are not working well. As we have confirmed the fresh air units were working when we visited the roofs, there was still no air supply from the fresh air diffusers indoors. There is no cooling in the dining rooms and ceiling fans are used to improve thermal comfort.

Figure 3-8 Indoor conditions of different types of rooms in CHSLD-A

3.3.2 Site visits to school buildings

Site visits to SB2-D

This selected school has two floors and one basement, was built in 1951, and in the 1990s, a gym and two classrooms were added. There is a fresh air system in the gym, but no cooling for the entire building and no fresh air system for the rest of the building.

Four typical classrooms were selected to be monitored. Two large classrooms next to the gym on the 1st floor are south facing and have received complaints of overheating. However, the thermal image in these two classrooms exhibited a noticeable difference because, in one of them, a portable air conditioner had been added, whereas the other room is cooled passively through the operation of the windows. These two classrooms can be used for completing comparisons and thus are an ideal pair for undertaking case studies.
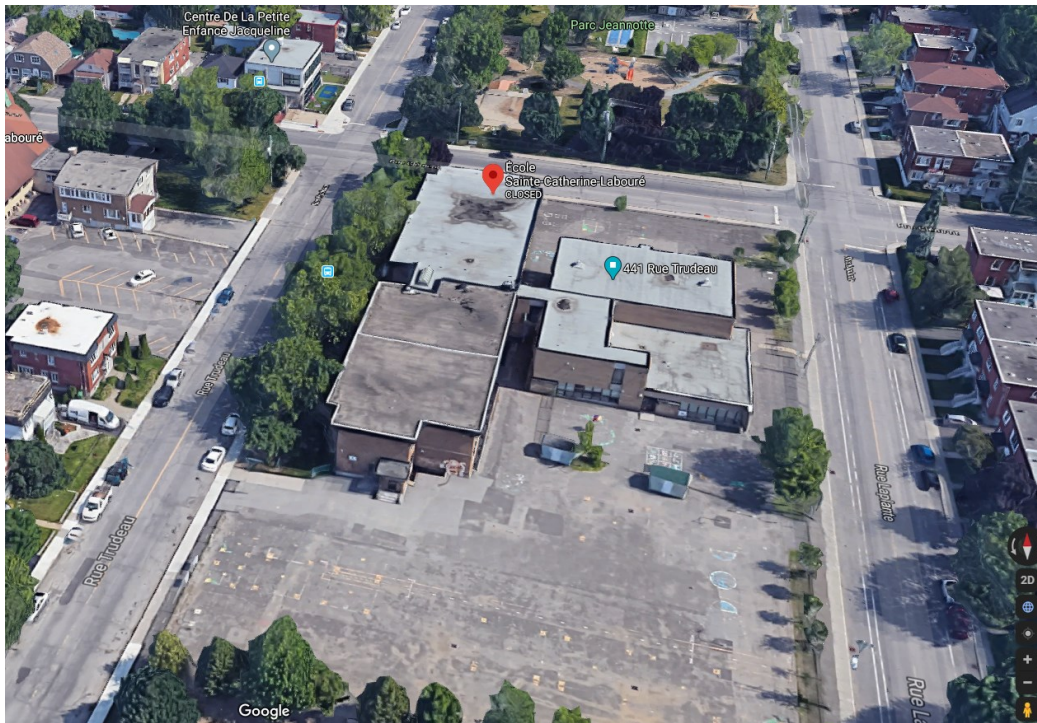
Figure 3-9 Site view of SB2-D from the south view

For those classrooms located on the 2nd floor (top), the temperature in the morning could reach 47 ℃ in the southwest-facing rooms in June and August, whereas the classroom on the opposite side (facing Northeast) is much cooler. Therefore, these two classrooms have also been selected for comparative studies.
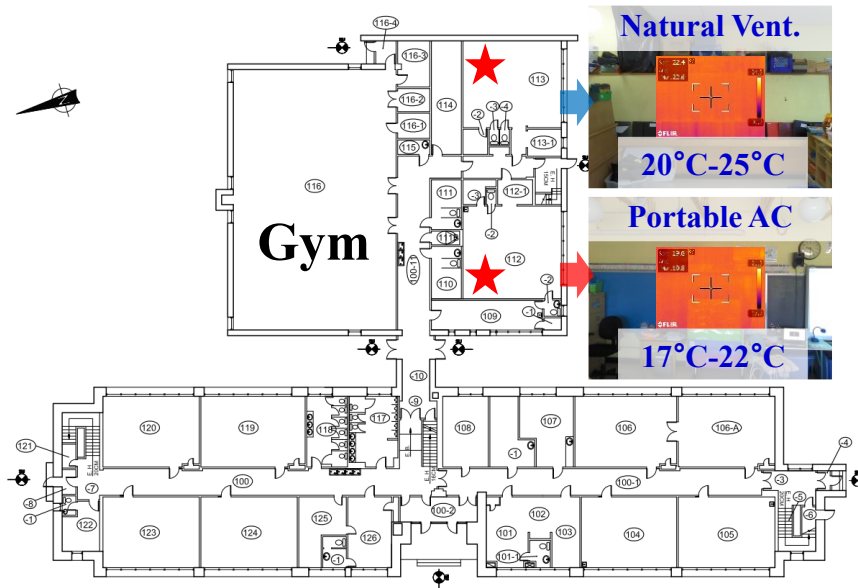
Figure 3-10 Building plan, thermal images, and photos of 1st floor of SB2-D

Site visits to SB1-D

SB1-D is a 2-story school built in 1954 surrounded by a park on the north and large areas of the impervious playground on the south and east side of the buildings, as in Figure 3-11. It is identified to be vulnerable to overheating as it has a long side façade facing the south and its large window-wall ratio between 40% and 50% (Figure 3-11). There are also no trees close to the building to provide shades for the building envelope. The building structure is concrete, and the cladding is a brick veneer. The roof colour is grey, and the building façade is red-brown.
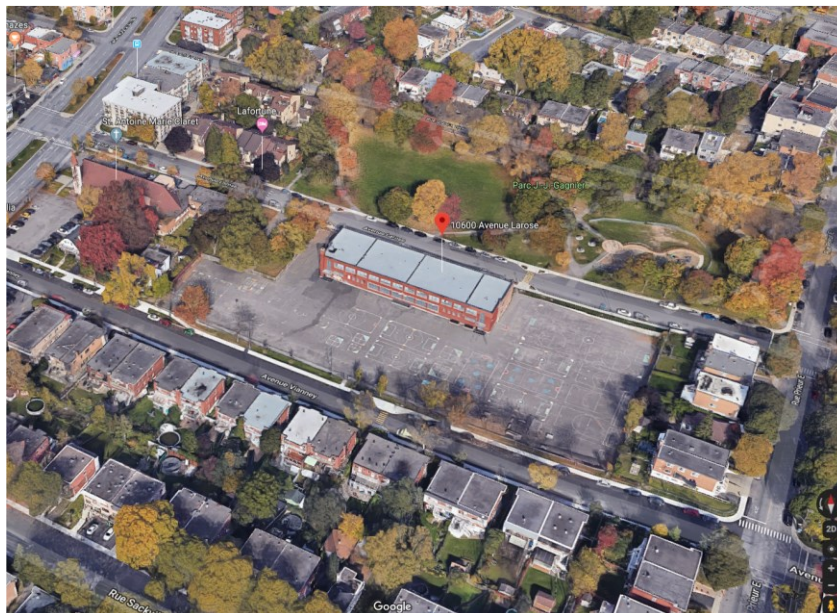
Figure 3-11 Site view of SB1-D from the south view

Figure 3-12 Indoor conditions of the school SB1-D

There is no cooling and no fresh air system in this building, and the building is cooled down by natural ventilation. There is a window above the door for each classroom for natural ventilation and portable fans are used during the summer to improve indoor thermal comfort.

There are complaints in the southwest facing classrooms on the top floor. 2 classrooms on different orientations were visited and the interior wall surface temperatures were measured using infra-red thermal images. A noticeable temperature difference of 2 to 3 degrees can be detected between these 2 classrooms. After the site-visiting, some more comprehensive information on the buildings can be confirmed and collected. The building overheating attributes are analyzed for the final selection.
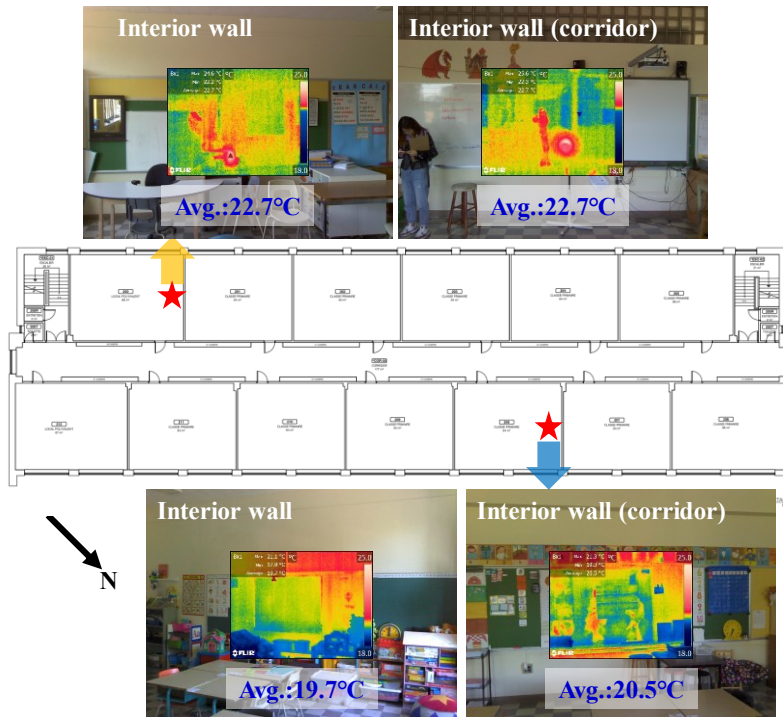
Figure 3-13 Thermal images of different classrooms and the building plan of SB1-D

3.4. Summary of the building information

As is mentioned in the previous section, the building information survey consists of 5 parts covering very comprehensive aspects of the building. But it was found that it is hard to know the real performance of the buildings and hard to conclude the occupants' behaviour and the HVAC system with the concise answers to the survey sheet. Although the building information survey is conducted before the site visit, it seems much efficient to analyze and extract useful information from the survey forms after the site visitings.

We therefore first classified the buildings into 2 groups of categories according to the site investigations: (i) buildings with overheating complaints and (ii) without complaints (Table 3-1). Then the potential factors considered in the survey forms, as summarized in Appendix D, are analyzed to find out the most valuable cases to study the overheating problems in the summer.

Table 3-1 Overheating complaints in the visited buildings

Bldg. Types	With complaints	Few complaints
Hospitals	CHSLD-A,B CH-A,B,D,F	CHSLD-C,D,E CH-B,C,E CR-A
Schools	SB1-A,B,D,G SB2-A,B,D,E	SB1-C,E,F,H SB2-C,F SB3-A

After the survey and site visiting, it was found that the cooling system is seldom used in schools. Among the 15 buildings visited, only SB1-H has a cooling system in a newly built part. Most of the school buildings only have fresh air supply to the corridor, gym, and basement. The buildings are usually cooled through cross-ventilation (SB1-F, SB2-B, C) and night ventilation (SB3-A). The thermal comfort of the building is highly related to the surrounding environment. The orientation of the rooms and the distribution of adjacent plants are the most important factors affecting indoor conditions. The overheating complaints that happened in school buildings are majorly on the top floor of the buildings. The vulnerable rooms are majorly facing the south (SB1-B, SB2-A), southwest (SB1-D), southeast (SB2-B, D, E), and west (SB1-A, G). Most of the overheating complaints happen in buildings with large window-wall-ratios, e.g. 40-50% (SB1-A, D, G; SB2-A, D, E) and >50% (SB1-B).

SB2-D and E seem to have the most severe overheating complaints and are therefore selected, the teachers and students use words like "melting" to describe their feelings in the southeast facing classrooms in the morning of July and September. These two buildings are next to each other, with

large impervious playgrounds on the southeast side of the building but tall trees on the west or south side of the building providing external shadings to the building envelope. Another 2 schools (SB1-A, D) from SB1 have a similar problem and are also selected. SB3-A is selected because it is a typical building in SB3 with the Building Automation System (BAS) installed to monitor the air temperature in the fresh air system. SB2- D is selected because this building is built in 3 distinctive construction year periods. For the new part built-in 2014, they have temperature sensors in each room and well managed fresh air system, while for the old part, there are no plants close to the building and there are major complaints in the south and west-facing rooms due to its large windows.

On the other hand, for the hospital buildings, the HVAC system is much more complicated, and most of them have cooled down the corridor and the rooms are cooled down by open doors. Window air conditioning units are often used for individual offices or patient rooms. Therefore, unlike the schools, most of the thermal comforts in hospital buildings are highly related to the design and operation of the HVAC system. Some of the hospitals (CHSLD -A, B; CH-A, D) reported there is insufficient fresh air supply in the corridor.

The selection of hospital buildings does not restrict to the building with severe overheating problems: CHSLD-A, B, and CH-D are selected because they have the most severe overheating complaints. The thermal feeling in CH-D is very different in different areas of the building, and the occupants in CHSLD-A are complaining it is "hot and stuffy" in both public areas and patient rooms. CHSLD-B has a fresh air supply only for the halls but not in the corridors. CH-C is a historical building with few central systems for cooling but there is surprisingly good thermal comfort. This might be related to its spacious corridors, efficient natural ventilation and terracotta claddings. It is, therefore, be selected for further study. CHSLD- C is selected as a positive case study because it has a well-managed air conditioning system and an ideal indoor thermal feeling. At last, to cover more overheating vulnerable groups of patients, CR-A is selected since it is for kids with mental illness.

3.5. Building selection result

A careful and comprehensive review of overheating problems in the selected buildings their distribution helps identify six schools and six hospitals for further field studies. Most of the selected buildings are well distributed over all the central and eastern parts of Montreal thus

capturing the city scale climate pattern; a few of the building locations are close to one another and the plan for these buildings is to share one weather station for the local weather conditions.
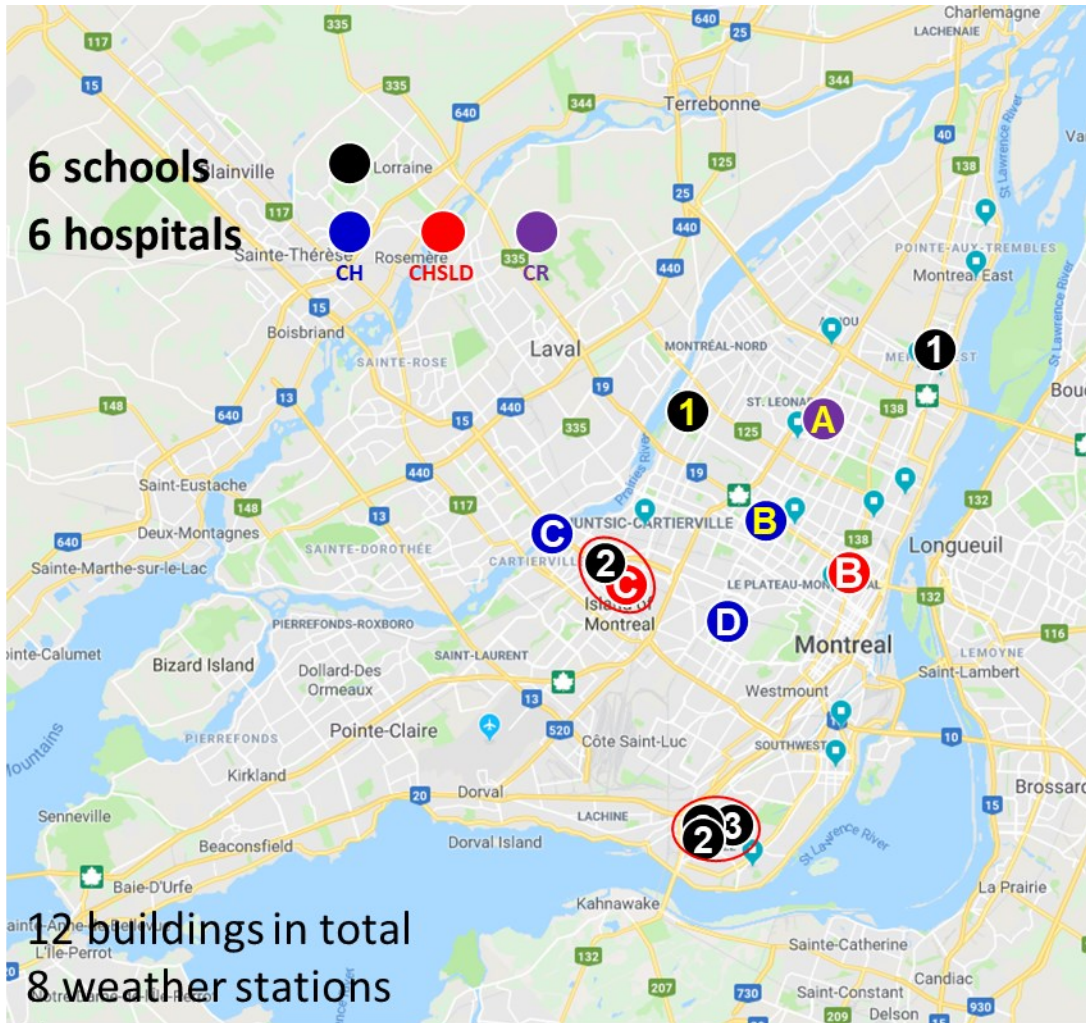
Figure 3-14 Distribution of selected school and hospital buildings.

3.6. Summary

A systematic guideline for the selection of buildings to complete field monitoring of overheating events and interior building conditions has been postulated in this chapter. The methods in this guideline can be implemented for large-scale field monitoring studies with limited site options, and where both local weather data and indoor conditions need to be captured. The study reached the following major conclusions and contributions:

- A five-step building prescreens, and selection framework has been established to help locate the vulnerable and typical buildings over the city scale.

- The building prescreen has been performed by an investigation on the heat-related death in the past heatwave, the urban heat island pattern of the city, and the general building outlook and its surrounding environment.

- The building information survey form has been designed (Appendix A) and distributed to the building managers to collect the current conditions in the buildings, covering the general conditions of the building, the indoor thermal performance during the past summers, occupant activities in the building, building envelope information and the building drawings.

- Site visits have been organized for 16 school buildings, 12 hospitals buildings over Montreal. The checklist and list of actions of the site visits can be found in Appendix B. The residential buildings have been selected by the social housing office based on the selection criteria listed in Appendix C. After the site visit, 6 hospital buildings and 5 school buildings are selected for field monitoring.

- For the school buildings, it was found that most of the buildings from the school board SB1 and SB2 have large window-wall ratios, and are without mechanical ventilation systems and cooling for the classrooms built before the 1990s. Classrooms on the top floors, facing the south, east, and west, and without any external shading from the adjacent trees tend to be more vulnerable to overheating because of the great portion of the heat gain from the solar radiation. The selected school from SB3 have small windows in the classrooms and they also have the mechanical ventilation operated for night ventilation, which significantly reduced their risk of overheating compared to the other two school boards.

- For the hospital buildings, the situation would be quite different in the different hospitals and the situation is more complicated than in the schools since the functions of the rooms are more diverse. The buildings with overheating complaints normally have few accesses to air conditioners in each room, and only rely on the ventilation and cooling in the corridors or halls, while the cool air or fresh air supply may not be sufficient to cool down and ventilate the rooms.

After the buildings are selected as described in this chapter, the temperature and humidity (and CO_2) sensors are installed on-site, and the data can be collected for quantitative analysis of the overheating conditions in these buildings.

Chapter 4 Field Monitoring – Data Analysis for Overheating Assessment

In this chapter, the instruments used for the measurement of the building's local weather and indoor thermal conditions are first presented in section 4.1. The characteristics of the monitored rooms and the available data are summarized in section 4.2 to provide an overview of the scope for analysis. Multiple overheating assessment metrics and the thermal indices are elaborated in section 4.3, and the method for comparison between them is in section 4.4. Section 4.5 provided case studies on a school building and hospital building, and the overheating in all selected rooms is compared in section 4.6. Finally, the different assessment metrics are compared through a correlation study and clustering analysis in section 4.7.

4.1. Field monitoring instruments

4.1.1 Weather stations

The weather stations use the RX3004 logger from HOBO Onset, with LCD and GSM/HSPA cellular communications. The selected weather station (Figure 4-1) is composed of temperature & humidity sensor (S-THB-M002), pyrometer (S-LIB-M003), wind speed (RM Young Wind Monitor Sensor) and direction (RM Young Wind Monitor Sensor) sensors, rainfall sensor (S-RGB-M002). The specification of the sensors is listed in Table 4-1.

Before the installation of the weather stations, a site visit to the rooftop of the building is performed with the building manager to confirm the weather station installation location and grounding point. The installation location should be an open area away from obstructions, HVAC equipment and exhaust fans to avoid their impact on the sensors. For the safety of the installation, the tripod should be away from the edge of the building. This also helps to reduce the impact of the turbulence bubble from the edge of the roof on the wind speed and wind direction sensors. The feet of the weather station tripod are attached to 12kg concrete blocks with concrete anchor bolts, and the legs of the tripods should spread as wide as possible while keeping the feet and blocks level with the roof. Three guy wires of 4 m length are used to fasten the tripods with connection to 20 kg concrete blocks and 30 kg weatherproof sandbags. All the concrete blocks are placed on rubber mats to protect the roofing. The mast of the tripod is levelled vertically with bidirectional post level and the wind monitor on the mast is 3 m high above the roof.
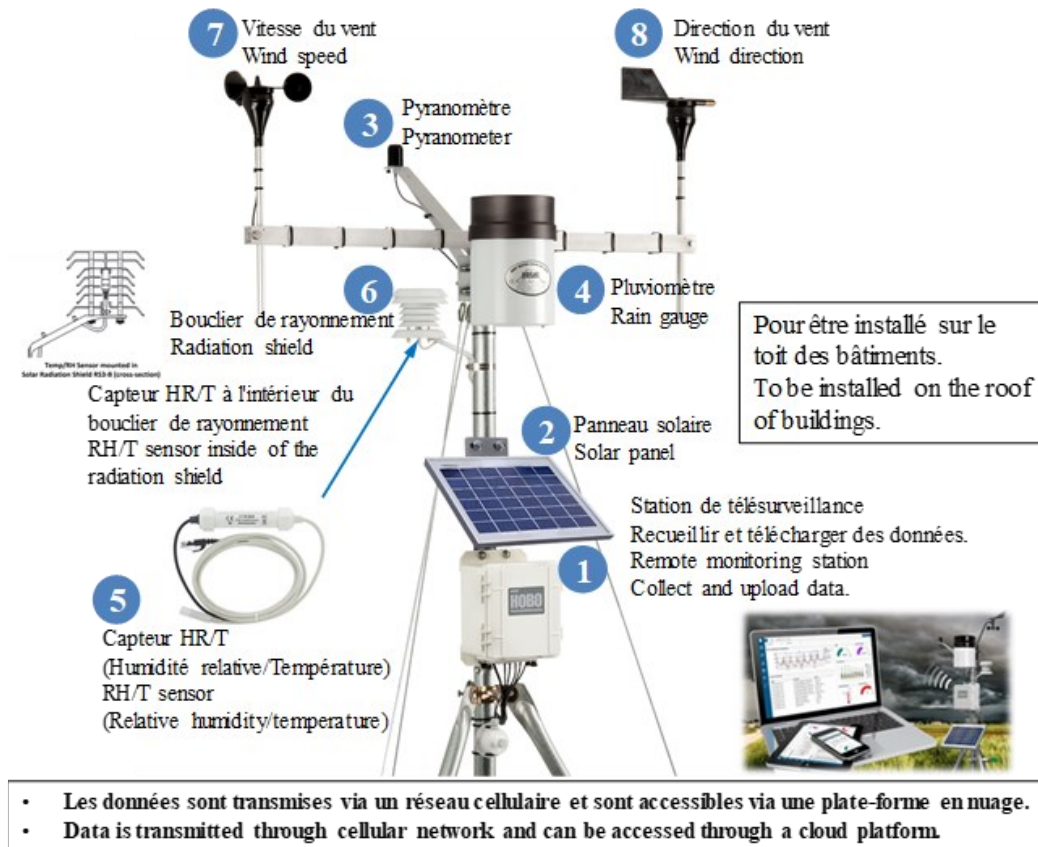
Figure 4-1 Schematic sketch of the weather station.

Table 4-1 Sensor specification of the rooftop weather station

Type	Temperature sensor	RH sensor	Pyrometer	Wind speed sensor	Wind direction sensor	Rainfall sensor
Model	S-THB-M002	S-THB-M002	S-LIB-M003	RM Young Wind Monitor Sensor	RM Young Wind Monitor Sensor	S-RGB-M002
Range	-40°C - 75°C	0-100% -40°-75°C	0-1280 W/m²	0-76 m/s	0- 355°, 5° dead band	0-12.7 cm
Accuracy	±0.21°C 0° - 50°C	±2.5% 10% - 90%	±10 W/m² or ±5%	±1.1 m/sec or ±4%	±5 °	±1.0%
Resolution	0.02°C at 25°C	0.1%	1.25 W/m²	0.2 m/s	1.4 °	±0.2 mm
Operation Condition	-40°C-75°C	-40°C-75°C	-40°-75°C	-40°-75°C	-40°C-70°C	0° - 50°C
Response Time	5 min	5 min	N/a	N/a	N/a	N/a

The wind monitor has been aligned to the true south and fastened on the mast to have accurate wind direction. The weather station is powered the solar energy, so the solar panel should be aligned facing the south and tilted to around 70 degrees to prevent snow accumulation during the winter months. The RH/T sensors are placed in the solar radiation shield to avoid the effect of direct solar irradiation on the sensor. The pyrometer is levelled horizontally to capture the global horizontal irradiation intensity and on the south side of the tripod to avoid the shading from the mast or the wind monitor. Later the measured global horizontal irradiation can be split into the direct horizontal irradiance, direct normal irradiance, and diffused horizontal irradiance. The rain gauge is attached to a 12 kg concrete block on a rubber mat around a 4 m distance from the mast to avoid rain shielding from the weather station. The data logger is placed in a tight weatherproof box, and it can transfer the data from all sensors to a cloud platform through 4G internet. Finally, the weather stations are grounded with a ground cable attached to the mast of the weather station by professional electricians. An example of the installed weather stations can be found in Figure 4-2.

Figure 4-2 Photo of one of the installed weather stations.

4.1.2 Indoor sensors

There are two models of the indoor sensors in use for this study: MX1101 (RH-T sensor) and MX1102 (RH-T-CO_2 sensor), made by Onset (Figure 4-3). These loggers are small-powered, self-contained sensors with LCD screens and onboard memory. They use Bluetooth to modify settings and download data, and the communication range is within 100 m. The specification of the indoor sensors is listed in Table 4-2.
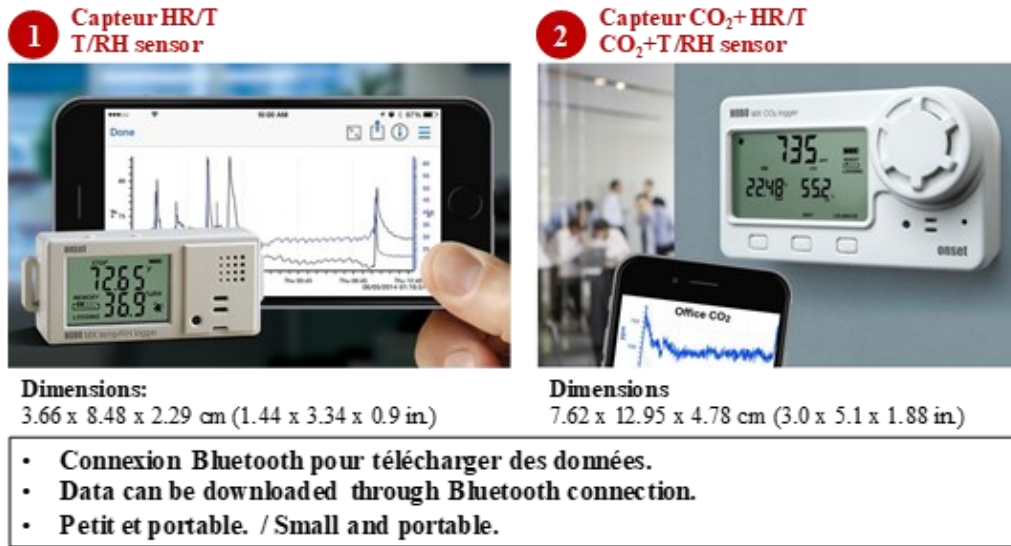
Figure 4-3 Schematic sketch of the indoor sensors.

Table 4-2 Sensor specification of the indoor sensors

Model	MX1101 (RH-T sensor)		MX1102 (RH-T-CO2 sensor)		
Model	Temperature sensor	RH sensor	Temperature sensor	RH sensor	CO2 sensor
Range	-20°- 70°C	1% - 90%	0° - 50°C	1%-70%	0 - 5,000 ppm
Accuracy	$\pm$0.21°C 0° - 50°C	$\pm$2.0% 20% - 80%	$\pm$0.21°C 0° - 50°C	$\pm$2% 20% - 80%	$\pm$50 ppm $\pm$5% of reading at 25°C
Resolution	0.024°C at 25°C	0.01% RH	0.024°C at 25°C	0.01%	1.4 °C
Operation Condition	-20° to 70°C	-20° to 70°C	0° - 50°C 0 - 95%	0° - 50°C 0 - 95%	0° - 50°C 0- 95%
Response Time	7:30 minutes in air moving 1 m/s	20 seconds to 90% in airflow of 1 m/s	12 minutes to 90% in airflow of 1 m/s	1 minute to 90% in airflow of 1 m/s	1 minute to 90% in airflow of 1 m/s
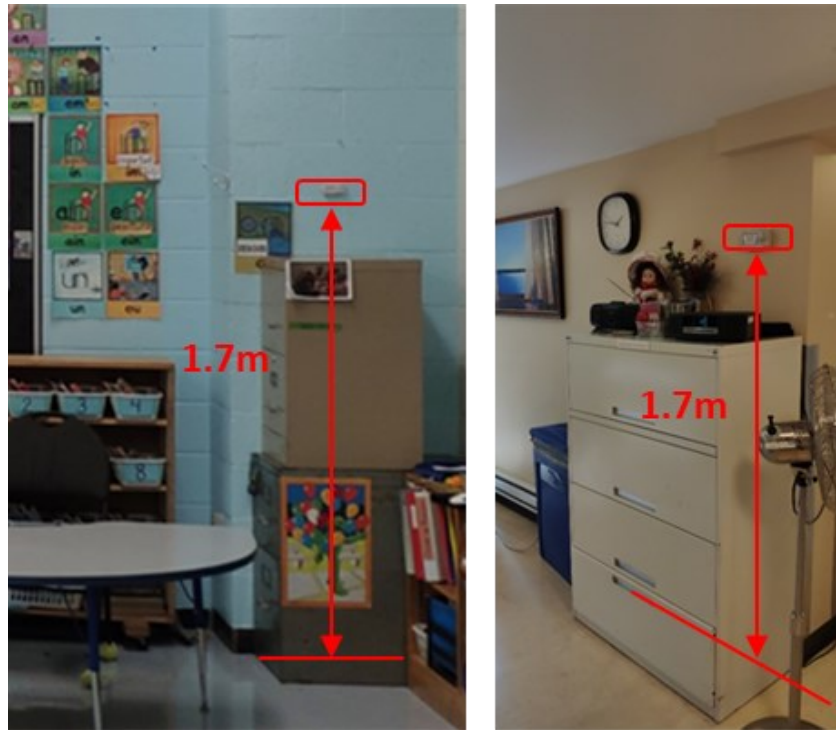
Figure 4-4 Photo of the installed indoor sensors.

The indoor sensors are installed 1.7 m above the floor which is considered as the height of an adult. The sensors are attached to the internal walls on the corridor side of the room to avoid direct solar irradiation on the sensors. The sensor should be away from the electrical utilities, e.g., televisions, refrigerators, to avoid the thermal interaction with the heat from this equipment. The sensors with CO_2 (MX1102) are installed in some large rooms with unpredictable occupation schedules in the selected buildings, e.g., activity room or dining rooms of long-term care buildings, the waiting room of the hospitals, and the gyms of the schools, to help keep track of the occupation in these spaces. Examples of the installed sensors are shown in Figure 4-4. The data logger of the sensor has been configured with an interval of 10 min for the data collection, and the data have been averaged for each hour to conduct the hourly analysis.

4.2. Monitored rooms and data

Due to the COVID pandemic in 2020, the installation of the field monitoring devices could not be completed as expected, and by the end of the summer in 2020, we gained the access to six school buildings and three hospital buildings. In at least two typical rooms of each building temperature and humidity sensors were installed, the selected rooms are facing different orientations and

located on different floors. Since some of the rooms in these buildings are renovating, the sensors in some of the rooms did not capture the regular thermal condition as normal days and some of the sensors were damaged. After an analysis of the cleaned dataset, the available data logged in these 9 buildings are summarized in Table 4-3. It was found the data in 33 rooms of 8 buildings have covered the same timeframe from 2020-07-18 00:00:00 to 2020-08-07 00:00:00 (TF-5, 20 days in total). Therefore, in this study, only these 20 days' data are analyzed for the comparison of overheating in different buildings and rooms.

Table 4-3 Monitored timeframes for each building in 2020.

Time frame index TF	Monitored Time Frames		Duration (Days)	Duration (Hours)	Case studies	Comparison analysis
	Start	End				
TF-1	2020-05-23 00:00:00	2020-10-01 00:00:00	131	3144	SB1-A, SB1-D	
TF-2	2020-06-24 00:00:00	2020-10-01 00:00:00	99	2376	SB2-A, SB2-D, SB2-E	
TF-3	2020-07-10 00:00:00	2020-10-01 00:00:00	83	1992	SB3-A	
TF-4	2020-07-15 00:00:00	2020-08-13 00:00:00	29	696	CH-B	
TF-5	2020-07-18 00:00:00	2020-08-07 00:00:00	20	480	CR-A	All schools and CR-A, CH-B
TF-6	2020-05-01 00:00:00	2020-07-16 00:00:00	76	1824	CH-D	

The outlook of the selected buildings and rooms and their surrounding environment obtained from the site visits and the google street view are shown in Appendix E. The characteristics of the monitored rooms are shown in Figure 4-5. Among the evaluated 33 rooms, 39 % of the rooms come from the hospital buildings and the rest are from the schools. From the on-site visit to these buildings, most of the overheated rooms were found on the top floor of the buildings, receiving more heat gain through the roof, we, therefore, selected more rooms (79%) from the top floor than those on the lower floors (21%). The orientation of the rooms is calculated by the direction of the vector normal to their exterior walls, and if the room has more than one exterior wall facing different orientations, the orientation of the room is calculated by the weighted sum of the vectors using the wall areas. Most of the selected rooms are facing southeast (SE) and southwest (SW), which are expected to be more vulnerable to overheating as well as the rooms facing the south (S), whereas the rooms facing the other direction are also covered in this study. From the field survey of the studies buildings, we also found that there was little cooling in the school buildings, though

some of the building managers told us they may use portable air conditioners when it is necessary. Since it was hard to keep track of the usage of air conditioning, we only roughly summarized the rooms with a window air conditioner installed and those rooms that may have a portable air conditioner, but still, 76% of the rooms have no access to air conditioning. For the mechanical ventilation, the third school board (SB3) is having night cooling in the building and some of the hospital buildings only have mechanical ventilation to the activity room or waiting rooms.
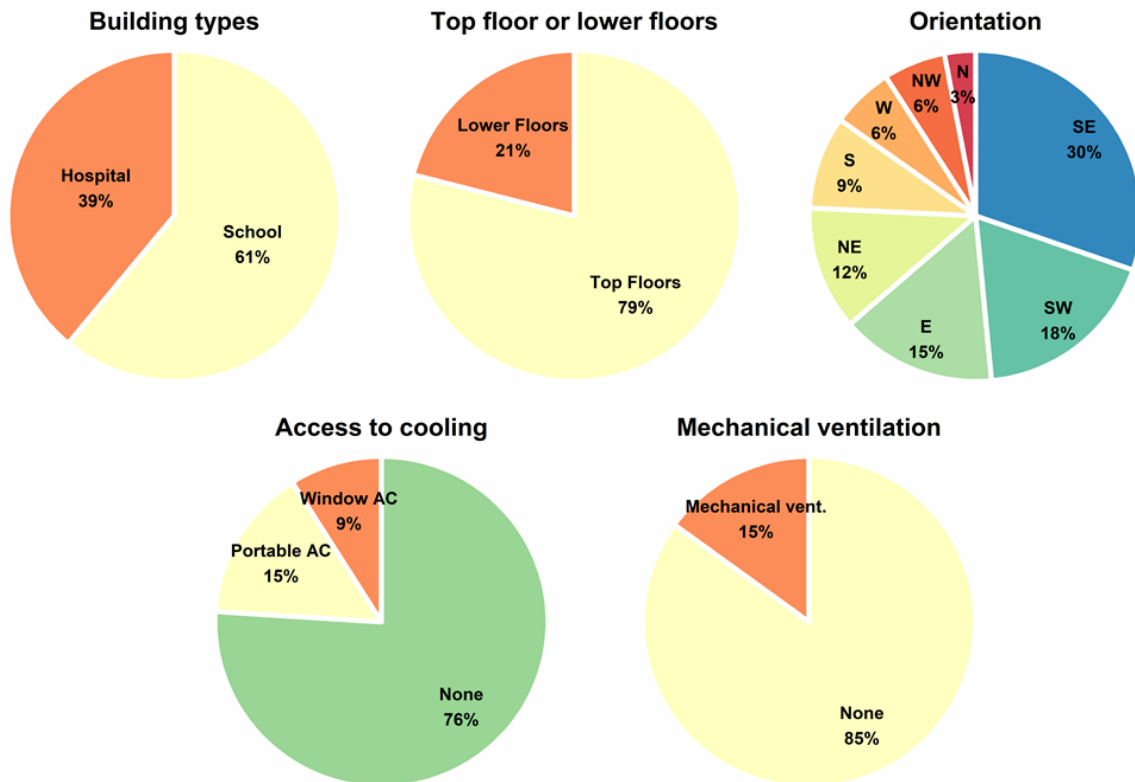
Figure 4-5 Summary of the characteristics of the investigated rooms in the field monitoring.

The dimensions of these rooms are measured during the several site visits, the room areas, window area and the operable window area of the 33 rooms are summarized in descending order in Figure 4-6. The office and patient rooms in the hospital buildings are normally smaller than 25 m², and the activity rooms are much larger than the regular rooms in the hospital. Most of the windows in the hospitals are having a smaller size than those in the schools, this might be because the classrooms may need more glazing on the wall for the natural lighting. And since the classrooms in the school buildings have more windows than the rooms in hospital buildings, the operable window area in most of the classrooms is also larger than the rooms in hospitals. Among all the

field monitored rooms, the school building SB3-A has exceptional smaller windows than the schools from other school boards (SB1 and SB2).
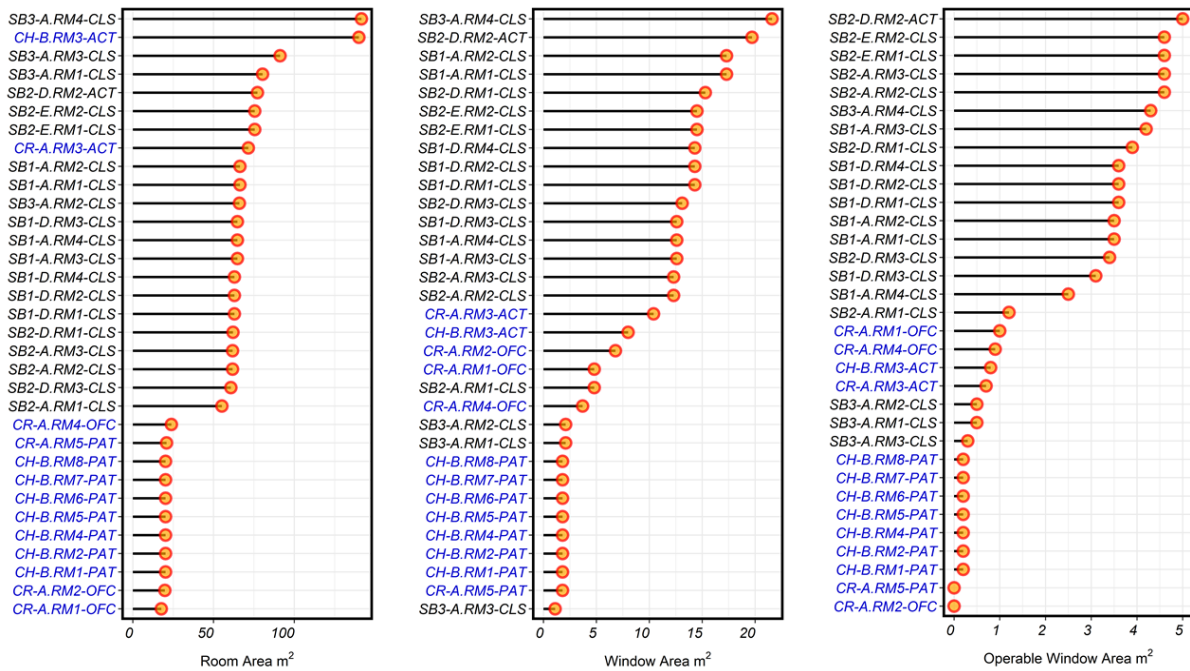
Figure 4-6 The room area, window area and operable window area of the field monitored rooms

4.3. Overheating assessment criteria and thermal indices

There exist many approaches for the evaluation of overheating in buildings, in which different threshold values are provided, beyond which overheating is thereafter considered. These threshold values have been based on static or adaptive thermal comfort, heat stress level, or heat-related health outcomes of the building occupants. One common approach to assessing overheating is using the number of hours above the chosen threshold value over an entire summer period. This threshold can be a fixed value or a function of different variables of the external environment. Most of the current criteria are using air temperature as the only indicator of the building's indoor thermal or overheating condition, while studies show that the thermal sensation of the occupants might also be affected by other environmental variables, for example, the humidity, wind speed and solar radiation. Many studies have summarized the most used thermal metrics (Holmes et al., 2016). However, it is still unclear how results from the different thermal metrics and overheating assessment methods may change when using different approaches.

In this study, a comparison is made of overheating in multiple field-monitored buildings using several different overheating indices, including dry-bulb temperature, the heat index (HI), humidex

(H), standard effective temperature (SET), wet-bulb globe temperature (WBGT), summer simmer index (SSI), and discomfort index (DI).

4.3.1 Fixed temperature criteria

For the fixed temperature criteria used in this study, three (3) temperatures thresholds were considered based on different existing overheating assessment criteria: 25 °C, 28 °C, and 32 °C. The temperature threshold of 25 °C is obtained from the Passive House Institute (PHI) (PHI, 2016). The fixed operative temperatures of 28 °C were also widely used for defining multiple overheating criteria. In CIBSE Guide A (CIBSE, 2011), CIBSE TM52 and TM59 (CIBSE, 2017, 2013), the indoor temperature should not exceed 26 °C and 28 °C for 1% of the annual occupied hours for bedrooms and living rooms in residential buildings. And this fixed temperature of 28 °C is also used for school and office buildings (CIBSE, 2011; Zero Carbon Hub, 2015b). Building Bulletin 101 (Department for Education Schools and Families (DfES), 2006) indicated that the temperature in the classrooms above 28 °C should not exceed 120 hours and the air temperature in classrooms during occupied hours should not exceed 32°C. The Healthcare Technical Memorandum HTM03 (Department of Health, 2007a) suggested that indoor dry-bulb temperatures should not exceed 28°C for more than 50 hours a year.

4.3.2 Adaptive temperature criteria

For adaptive comfort criteria, the temperature limit is usually a function of the outdoor running mean temperature. The CIBSE (CIBSE, 2013) employed the adaptive thermal comfort levels defined by the European Standard EN 16798-2019 (BS EN 16798, 2019), in which three (3) categories of comfort level are identified based on the predicted comfort temperature:

$$T_{comf} = 0.33T_{rm} + 18.8 \qquad (4-1)$$

where, T_{rm}, is the running mean daily average temperature, estimated by:

$$T_{rm} = \frac{T_{ed-1} + 0.8T_{ed-2} + 0.6T_{ed-3} + 0.5T_{ed-4} + 0.4T_{ed-5} + 0.3T_{ed-6} + 0.2T_{ed-7}}{3.8} \qquad (4-2)$$

and where T_{ed-1} is the daily mean external temperature for the previous day, T_{ed-2} is the daily mean external temperature for the day before, and so on.

The upper limits of the three (3) categories of thermal comfort (Eqs. (4-3)~(4-5)) are used for the evaluation of overheating in this study:

$$\text{Cat 1: } T_{cat1_{upper}} = 0.33T_{rm} + 18.8 + 2 \qquad (4-3)$$

$$\text{Cat 2: } T_{cat2_{upper}} = 0.33T_{rm} + 18.8 + 3 \qquad (4-4)$$

$$\text{Cat 3: } T_{cat3_{upper}} = 0.33T_{rm} + 18.8 + 4 \qquad (4-5)$$

The ASHRAE standard 55 (ASHRAE-55, 2017) has also similarly defined an adaptive thermal comfort, with the upper operative temperature limit defined as

$$T_{ASHARE_{upper}} = 0.31T_{rm} + 21.3 \qquad (4-6)$$

It can be noted that the ASHRAE thermal comfort upper limit is very close to the upper limit definition for Category 1 thermal comfort given in BS EN 16798, so in this study, only the upper limit of the three categories of thermal comfort defined in BS EN 16798 is evaluated.

4.3.3 Humidex

The Humidex (humidity index, H) (Environment and Climate Change Canada, 2021) is an index developed by the Canadian meteorologists Masterson and Richardson (Masterton and Richardson, 1979) to describe how the climate feels to the average person considering the effect of both temperature and humidity and it has been widely used by the Canadian weather forecast services for the heat alert system. The Humidex (H) is a dimensionless quantity while it is normally interpreted equivalent to degree Celsius. It can be calculated by

$$H = T_{air} + \frac{5}{9}\left[6.11 \times e^{5417.7530\left(\frac{1}{273.16} - \frac{1}{273.15+T_{dew}}\right)} - 10\right] \qquad (4-7)$$

The Environment Canada has adopted the scales for the Humidex (H) with four levels: from 20 - 29 as comfortable, 30-39 as some discomfort, 40-45 as great discomfort and dangerous when it is above 45. In this study, we use an extended version of the Humidex scale in Table 4-4 to have a more detailed description of indoor overheating.

Table 4-4 Assessment scale of Humidex H *(Havenith and Fiala, 2016)*

Humidex	Scale of comfort
20-29	Little to no discomfort
30-35	Slight discomfort sensation
35-40	Strong discomfort. Caution: limit the heaviest physical activities.
40-45	Strong indisposition sensation. Danger: avoid efforts.
45-54	Danger: stop all physical activities.
> 54	Death danger: imminent heat stroke.

4.3.4 Heat Index

The heat index is an index to describe the heat perception derived by multiple regression analysis with the combined consideration of the air temperature T_{air} and relative humidity RH (Rothfusz and Headquarters, 1990). It is widely used in the United States and other counties (Flores-Larsen and Filippín, 2021; Sun et al., 2020) and it has been adopted by the Occupational Safety and Health Administration (OSHA) to assess heat stress (Administration, 2014).

$$HI = -8.78469475556 + 1.61139411T_{air} + 2.338549RH - 0.14611605T_{air}RH$$
$$- 0.012308094T_{air}^2 - 0.0164248277778RH^2 + 0.002211732T_{air}^2RH$$
$$+0.00072546T_{air}RH^2 - 0.000003582T_{air}^2RH^2 \quad (4-8)$$

Note that, the Rothfusz regression is conducted under a condition when the temperature and humidity can ensure a HI value higher than 26.7°C. If the above calculated HI is smaller than 26.7°C, another simpler regression formula should be used which is

$$HI = 1.1T_{air} + 0.0261RH - 3.94 \quad (4-9)$$

In addition, to better evaluate the heat stress under extreme dry or humid conditions, two adjustments should be added to the HI calculation for correction.

$$AJ_{dry} = -\left(\frac{13-RH}{7.2}\right)\sqrt{1 - \frac{|5/9\,T_{air}-63|}{17}} \quad if\ RH < 13\%\ and\ 26.7 < T_{air} < 44.4°C (4-10)$$

$$AJ_{humid} = \left(\frac{RH-85}{10}\right)\left(\frac{30.56-T_{air}}{5}\right) - 17.8 \quad if\ RH > 85\%\ and\ 26.7 < T_{air} < 30.6°C (4-11)$$

The scale of HI used in this study is the version from NOAA (Table 4-5).

Table 4-5 Assessment scale of Heat Index HI *(National Weather Service, 2021)*

Heat Index °C	Category	Effect on the body
26.7-32.2	Caution	Fatigue is possible with prolonged exposure and activity. Continuing activity could result in heat cramps.
32.2-41.6	Extreme Caution	Heat Cramps and heat exhaustion are possible. Continuing activity could result in heatstroke.
41.6-54.4	Danger	Heat cramps and heat exhaustion are likely; Heatstroke probable with continued activity.
>54.4	Extreme Danger	Heatstroke is imminent.

4.3.5 Wet-Bulb Globe Temperature

The wet-bulb globe temperature (WBGT) is a type of apparent temperature to estimate the effect of the external environment, including temperature, humidity, wind, and radiation, on humans. It is normally measured with a device with three different types of thermometers, the dry bulb temperature T_d, the wet-bulb temperature T_w and the globe temperature T_g, which is sensitive to the radiant heat and WBGT is calculated by a weighted sum of these three components Eq. (4-12). For the indoor application of WBGT, a variant of the definition is provided without dry bulb temperature T_d in Eq. (4-13)

$$WBGT = 0.7T_w + 0.2T_g + 0.1T_d \qquad (4-12)$$

$$WBGT = 0.7T_w + 0.3T_g \qquad (4-13)$$

Since we have only measured the air temperature T_{air} and relative humidity RH in the rooms, the WBGT is calculated through an estimating equation of air temperature T_{air} and the water vapour pressure V_p. The water vapour pressure V_p can be estimated by the air temperature and relative humidity (American College of Sports Medicine, 1984). This estimation method has been adopted by the Australian Bureau of Meteorology (Australian Bureau of Meteorology, 2021).

$$WBGT = 0.567T_{air} + 0.393V_p + 3.94 \qquad (4-14)$$

$$V_p = \frac{RH}{100}\left(6.105e^{\frac{17.27T_{air}}{237.7+T_{air}}}\right) \qquad (4-15)$$

WBGT has been adopted by several different institutes for their standard and code, for example, the National Institute for Occupational Safety and Health (NIOSH) (Brenda Jacklitsch et al., 2016), the American Conference of Governmental Industrial Hygienists (ACGIH) (ACGIH, 2010), Occupational Safety and Health Administration (OSHA) (Occupational Safety and Health Administration, 2011), American Industrial Hygiene Association (AIHA) (DiNardi, 2003), American College of Sports and Medicine (ACSM) (Armstrong et al., 2007), the Armed Services (DOD, 2003) and the International Standard Organization (ISO) (ISO 7243, 2017). However, the assessment scales of the WBGT are quite different in these regulations, which have been reviewed and compared by (B. Jacklitsch et al., 2016). In this study, the WBGT reference limit values from ISO 7243 (ISO 7243, 2017) have been used since it is widely recognized as an international standard and it also covered a wider range of WBGT values from 22 to 32 °C to describe the different thermal condition levels.

Table 4-6 Assessment scale of WBGT *(ISO 7243, 2017)*

Metabolic rate M (W/m2)	The reference value of WBGT			
	Person acclimatized to heat (°C)		Person not acclimatized to heat (°C)	
Resting M<65	33		32	
65< M <130	30		29	
130< M <200	28		26	
With sensible air movement or not	No	Yes	No	Yes
200< M <260	25	26	22	23
M>260	23	25	18	20

4.3.6 Summer Simmer Index

The Summer Simmer Index (SSI) is developed by Pepi (1987) as an equivalent temperature quantity to relate both temperature and humidity to describe how hot it feels by a normal person during the summer months. It has been updated in 2000 by Pepi and Maynard (2000), and the calculation formula of the new Summer Simmer Index (SSI) can be derived in degree Celsius as,

$$SSI = 1.98 T_{air} - 1.1(0.55 - 0.0055 RH)(9 T_a/5 - 26) - 14.15 \qquad (4-16)$$

The Summer Simmer Index (SSI) has been widely used in the urban climate and also indoor spaces for the evaluation of heat stress during the summer months (Cannistraro et al., 2014; Lazurca et al., 2016; Patania et al., 2015). The assessment of the SSI in different comfort scales can be found in Table 4-7.

Table 4-7 Assessment scale of SSI *(Patania et al., 2015)*

SSI °C	Scale of comfort
28.3-32.8	Moderately warm
32.8-37.8	Warm
37.8-44.4	Very warm
44.4-51.7	Extremely warm
51.7-65.6	Dangerously warm
>65.6	Life-threatening

4.3.7 Discomfort index

The original discomfort index is developed by Thom (Thom, 1959) in 1959 to approach the effective temperature by simple linear adjustment applied to the dry-bulb T_d and web-bulb temperature T_w in °F.

$$DI = 0.4(T_d + T_w) + 15 \qquad (4-17)$$

An alternative version of the discomfort index is proposed by (Giles et al., 1990) so that it can be calculated directly by the dry-bulb air temperature and the relative humidity.

$$DI = T_d - 0.55(1 - 0.11RH)(T_d - 14.5) \qquad (4-18)$$

Here the T_d is in °C and RH is the relative humidity in %. It has been widely used for the urban heat risk alert system and the assessment of indoor hot and humid environments (Giles et al., 1990; Matzarakis and Mayer, 1991; Musco et al., 2016; Poupkou et al., 2011; Siami and Ramadhani, 2019) and the assessment scales of DI can be found in Table 4-8.

Table 4-8 Assessment scale of DI *(Giles et al., 1990; Matzarakis and Mayer, 1991; Musco et al., 2016; Poupkou et al., 2011; Siami and Ramadhani, 2019)*

DI °C	Discomfort conditions
<21	No discomfort
21-27	Less than 50% of people feel discomfort
24-27	More than 50% of people feel discomfort.
27-29	Most of the population feels discomfort.
29-32	Everyone feels severe stress
>32	Medical emergency.

4.3.8 Standard Effective Temperature

The Standard Effective Temperature (SET) is developed based on the two-node bioheat model (Gagge et al., 1986) and has been adopted by the ASHRAE 55(ASHRAE-55, 2017; Doherty and Arens, 1988). Compared to the other thermal index used in this study, SET is a more advanced rational thermal comfort model. It can be applied to dynamic conditions and it can provide the thermal quantities of the human body, for example, the skin temperature and wittedness (Zhang and Lin, 2020). SET has been widely used for the evaluation of thermal comfort of indoor space and development based on the two-node model of SET has been performed to extend its usage under more scenarios (Ji et al., 2021; Nazarian et al., 2017; Zhang and Lin, 2020). Some recent studies have adopted SET for the assessment of building overheating (Ji et al., 2021; Laouadi et al., 2020b) to provide a more detailed description of the status of the human body under hot or warm conditions.

The concept of SET is defined as the air temperature of a standard environment with the relative humidity of 50%, air velocity of 0.1m/s and radiant temperature identical to the air temperature, and in this standard environment, the heat loss from the skin of a typical adult occupant at the activity level of 1.0 met and clothing level of 0.6 clo should be kept equivalent to the actual

environment (ASHRAE-55, 2017). The heat balance of the human body is solved by dividing the body into the core node and skin node. Therefore, SET cannot be calculated by a simple equation, but an iterative procedure is needed. Although there are already new studies proposing new versions of the SET (Ji et al., 2021), the original SET calculation program described in ASHRAE 55(ASHRAE-55, 2017) has been used in this study. SET considered not only the environmental parameters, including the air temperature, relative humidity, airflow velocity, radiant temperature, but also the characteristics of the individual occupants, which includes the metabolic rate and clothing insulation. Since only the air temperature and relative humidity can be obtained from the field study, the other parameters are estimated by reasonable assumptions. The airflow velocity is assumed to be 0.1 m/s which is regarded as non-sensible air movement in most of the studies and the suggestions in ASHRAE 55. The radiant temperature is assumed to be the same as the dry-bulb air temperature, which is also suggested for the indoor environment (Laouadi et al., 2020b). The metabolic rate and clothing insulation are assumed to be a standard scenario in summer of which are 1.0 met and 0.6 clo. Note that these assumed values are also consistent with the assumptions for the assessment using WBGT in ISO 7243 (ISO 7243, 2017).

Table 4-9 Assessment scale of Standard Effective Temperature SET *(Parsons, 2007)*

SET °C	Thermal sensation	Physiological state
>37.5	Very hot, very uncomfortable	Failure of thermoregulation
34.5-37.5	Hot, very unacceptable	Profuse sweating
30.0-34.5	Warm, uncomfortable, unacceptable	Sweating
25.6-30.0	Slightly warm, slightly unacceptable	Slight sweating, vasodilation
22.2-25.6	Comfortable and acceptable	Neutrality
17.5-22.2	Slightly cool, slightly unacceptable	Vasoconstriction
14.5-17.5	Cool and unacceptable	Slow body cooling
10.0-14.5	Cold, very unacceptable	Shivering

4.4. Method for assessment metrics and criteria comparison

The definitions of the thermal index are very different, and the assessment scales using these thermal indices can be different, and even the descriptions of the different levels of thermal index assessment scales are also quite different. It would be a problem of how to compare them. In this study, a correlation analysis is proposed to help cluster the different thermal indices and the

overheating criteria and then conduct a rank correlation (Kendall, 1948; Kruskal, 1958) to evaluate the degree of concordance between the thermal index and criteria. The purpose of the analysis is to evaluate how the rankings of the overheating in different buildings and rooms may vary when using the different thermal index and overheating criteria. After the different thermal indices are calculated using the measured air temperature and humidity, the mean value of these quantities is first calculated for the different rooms to indicate the general thermal condition when evaluated using this specific thermal index. Then the percentage of overheating hours is calculated by evaluating the number of hours above the given threshold values in the assessment tables listed in Section 4.3. The Pearson correlation analysis can be first conducted among these mean values of the thermal index and the percentage of overheating hours using the different criteria to show their potential linear dependencies and help to cluster the different criteria into groups for detailed comparison. Then Kendall's correlation analysis among the percentage of overheating hours using different thermal indices can help identify how the different criteria agree with each other. The Pearson correlation coefficient is defined as,

$$\rho_{X,Y} = \frac{Cov(X,Y)}{\sigma_X \sigma_Y} \qquad (4-19)$$

where $Cov(X,Y)$ is the covariance of the two rank variables, and σ_X and σ_Y are the standard deviations of the rank variables.

The rank correlation of Spearman's correlation and Kendall's correlation is therefore considered and explained in the following discussion. Spearman's rho r_s correlation coefficient (Spearman, 1904) is defined as the Pearson correlation coefficient (Bravais, 1844) between the rank values of the two variables, which therefore evaluates the linear correlation of the rank value between the two sets of data. It can be calculated by simply covert the original data X and Y into rank values R_X and R_Y and then calculate their Pearson correlation coefficient.

$$r_s = \rho_{R_X,R_Y} = \frac{Cov(R_X,R_Y)}{\sigma_{R_X} \sigma_{R_Y}} \qquad (4-20)$$

Where ρ denotes the Pearson correlation coefficient which should be applied to the two rank variables R_X and R_Y, $Cov(R_X,R_Y)$ is the covariance of the two rank variables, and σ_{R_X} and σ_{R_Y} are the standard deviations of the rank variables. When there are no ties in the two sets of data, the above equation can be derived into a simple equation,

$$r_s = 1 - \frac{6 \sum d_i^2}{n(n^2 - 1)} \tag{4 - 21}$$

where $d_i = R(X_i) - R(Y_i)$ is the difference between the ranks of the ith sample. Compared to Pearson's correlation, Spearman's correlation is non-parametric, so no assumption of the normal distribution is required (Friedman, 1937). The Spearman's rho evaluates if one variable can be described by another variable through a monotonic function, and when the Spearman is +1 or -1, each of the variables is changing monotonically with the other.

The Kendall' tau correlation coefficient (Abdi, 2008; Kendall, 1938) is defined as the portion of the total number of concordant pairs minus the total number of discordant pairs in the total number of pair combinations in the observation.

$$\tau_a = \frac{C - D}{N} \tag{4 - 22}$$

Where N=C+D, and it can be estimated by a total number of pair combinations in the n observations.

$$N = \frac{n(n - 1)}{2} \tag{4 - 23}$$

To account for the ties in the data, Kendall's tau-a should be adjusted to Kendall's tau-b, which is defined as

$$\tau_b = \frac{C - D}{\sqrt{(N - T_1)(N - T_2)}} \tag{4 - 24}$$

$$T_1 = \sum_i \frac{u_i(u_i - 1)}{2} \tag{4 - 25}$$

$$T_2 = \sum_j \frac{v_j(v_j - 1)}{2} \tag{4 - 26}$$

Where u_i is the number of tied values in the i-th group of ties for the first variable, and v_j is the number of tied values in the jth group of ties for the second variable. This would be essential for calculating Kendall's correlation between the percentage of overheating hours using different metrics because there would exist ties between the evaluation of different rooms. In this study, Kendall's tau-a and Kendall's tau-b are both expressed as Kendall's tau by default. Compared to Spearman's test, Kendall's tau is more complicated for calculation, while it is more intuitive to evaluate the degree of concordance. On the other hand, Spearman's rho can detect extreme rank deviations between the two variables. In addition, Kendall's tau can achieve a significant level

with a smaller sample size because its p-value follows the z-statistics, while Spearman's rho follows the t-statistics. This property in Kendall's tau is important since a sample size of 33 rooms is used in this study. In the following discussions, the comparison of the different thermal indices and overheating criteria is evaluated by Kendall's tau. Kendall's tau correlation has also been used in the previous studies on building overheating. Mavrogianni et al., (Mavrogianni et al., 2014) calculated Kendall's tau between the overheating in buildings of different occupancy and behaviour scenarios through a large scale of building simulations to evaluate the impact of the occupancy pattern on overheating. Similarly, Taylor et al., (Taylor et al., 2014) also used Kendall's correlation analysis to investigate the concordance of the overheating assessment when using the different weather files for the simulation of a large number of different building configurations.

4.5. Case studies

The case studies in this section elaborate on the overheating evaluation using temperature-based fixed criteria and adaptive criteria. The weather condition monitored at the building SB2-D can be found in Appendix F. This study assumes that the weather condition in the whole city follows a similar trend as that measured at one of the buildings, and it can be noticed that during the 20 days of TF-5, the outdoor air temperature decreased during July 20-23 due to the reduction of solar radiation, and at the end of this period (August 2-5), the temperature is also at a lower level which can also be related to the reduced solar radiation and the associated rainy days. The evaluation using the other thermal index is evaluated in a similar way to the fixed temperature criteria and the results are collected in Appendix H.

4.5.1 Field monitoring of a school building

The building SB1-D is a two-storey school built in 1954 and a new part built-in 2019 is next to the building. The outlook of the building and its surroundings are shown in Figure 4-7. The longer side of the building is along the street in the NW-SE direction. On the north side of the building are sparse trees between the building and the street, while on the other side the building on the south is a playground with impervious ground cover.

The four selected rooms are on the top floor of the building, two of them facing the street on the north and the other two facing the playground on the south (Figure 4-7). The four rooms are having a similar layout of the room size, window size and operable window size in general. The RM3-CLS has a slightly smaller room area and window size compared to the other three rooms.

Figure 4-7 The surroundings and outlook of the building SB1-D and the monitored rooms

The hourly temperature of the room during TF-5 can be found in Figure 4-8, and the whole available data including the hourly temperature and indoor relative humidity for this building during TF-1 can be found in Appendix G. It is obvious that the indoor temperature of these monitored rooms has lower temperatures during TF-5 than that around the middle of July and August, but it still maintained a relatively high temperature of around 31 °C. Compared to the outdoor environment, the variation of the indoor temperature and humidity are much smaller. The relative humidity of the four rooms is only fluctuating between 45 to 50 %. In Figure 4-8, the fixed temperature thresholds (25°C, 28°C and 32 °C) are shown with horizontal lines and the adaptive temperature threshold of the BS EN criteria are also shown with step curves. The large portion of window area of these rooms (window-wall-ratio: 40-50%) made the solar gain from the windows a major contributor to the overheating of the indoor space. The indoor temperature of these rooms is therefore quite sensitive to their orientations: RM1 and RM2 facing the north side have a much higher temperature than RM3 and RM4 facing the south, and the trees on the RM1 and RM2 side help to alleviate the heat gain of these two rooms, while the large area of the impervious playground outside of RM3 and RM4 somehow enhanced the reflection of solar irradiation and increased the surrounding air temperature of RM3 and RM4 because of the increase of the thermal capacity of the ground.

In general, the building SB1-D is subject to the severe overheating problem: all the 4 measured rooms have indoor temperature always above 28 °C which does not achieve the requirement in Building Bulletin 101 (Department for Education Schools and Families (DfES), 2006) that only 120 hours is allowed to be higher than 28 °C for classrooms. Furthermore, the temperature in the room RM1 and RM2 have even exceeded 32 °C which is the upper limit of the temperature in Building Bulletin 101 (Department for Education Schools and Families (DfES), 2006). Compared to the adaptive temperature thresholds in EN 16798-2019 (BS EN 16798, 2019), the indoor temperature of RM3 and RM4 is fluctuating around the Cat III threshold, and RM1 and RM2 are having their lowest temperature of most of the days falling close to the Cat III threshold. There were only 3 days the indoor air temperature of RM3 and RM4 fell below the Cat II threshold during TF-5, while for only 2 days the indoor temperature of RM1 and RM2 got lower than the Cat II threshold. These observations conclude that this building SB1-D cannot achieve the temperature-based criteria outlined in the existing standards/code.
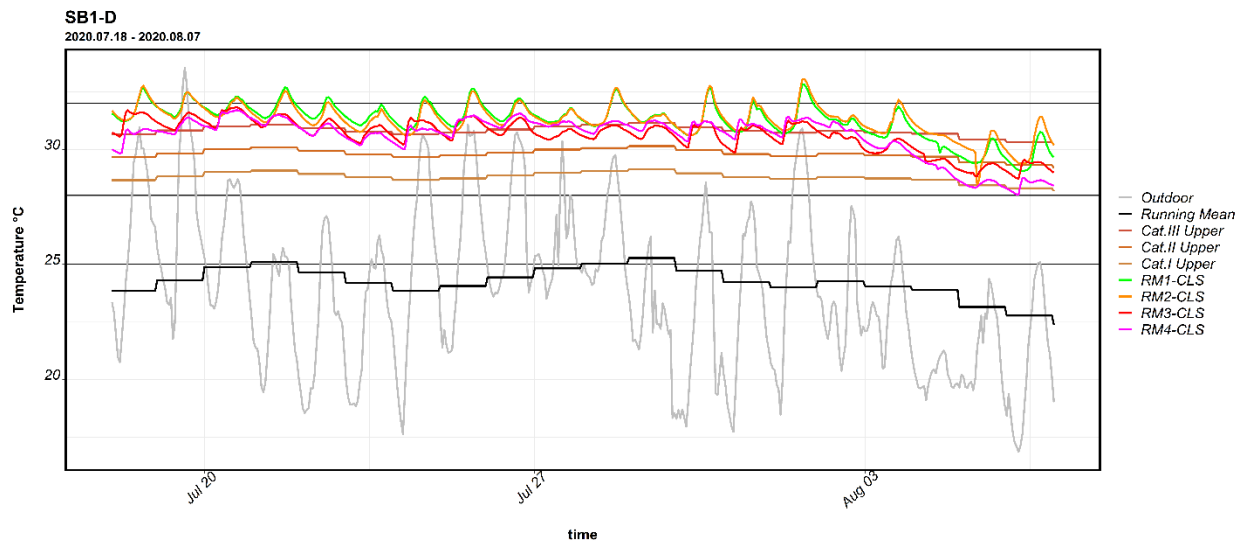
Figure 4-8 Hourly indoor and outdoor temperature monitored at building SB1-D

4.5.2 Field monitoring of a hospital building

The building CH-B is an L-shaped five-storey hospital building built in 1959, and there is another building of a similar height lay on the Southeast of it. Tall and dense trees can be found along the Northwest side of the building and sparse trees can be found along the Northeast side of the building. A major street is on the southwest side of the building and no trees are standing between the building and the street.

Figure 4-9 The surroundings and outlook of the building CH-B and the monitored rooms

Eight rooms in this building have been selected for the field monitoring study which is marked in Figure 4-9. Six of the rooms (RM3-8) are on the top floor of the building and two of them (RM1-2) are on the second floor. Five of the rooms (RM2-3, RM5, RM7-8) are facing the south side (SE or SW) of the building, and there are few shades from the external objects on this side of the building. While the other three of them (RM 1, RM4 and RM6) are facing the northwest of the building where the tall trees on this side may block some of the external sunlight for the room on the second floor. Among the 8 buildings in CH-B, 4 of them have access to cooling: RM5 and RM8 have a window AC unit installed, and RM1 and RM3 may have a chance to use a portable AC unit to cool down the space. Seven of the selected rooms are small patient rooms (around 20-25 m^2) with only one patient in the room and these rooms have small windows of around 2 m^2 for each of them. The window wall ratio (WWR) of RM1, RM4-6 is around 14% and only 6 for RM2, and RM7-8. And only the activity room RM3 has a very large area of 140 m^2 with a very unpredictable occupancy pattern in the space.

CH-B
2020.07.18 - 2020.08.07

Legend:
- Outdoor
- Running Mean
- Cat.III Upper
- Cat.II Upper
- Cat.I Upper
- RM1-PAT
- RM2-PAT
- RM3-ACT
- RM4-PAT
- RM5-PAT
- RM6-PAT
- RM7-PAT
- RM8-PAT
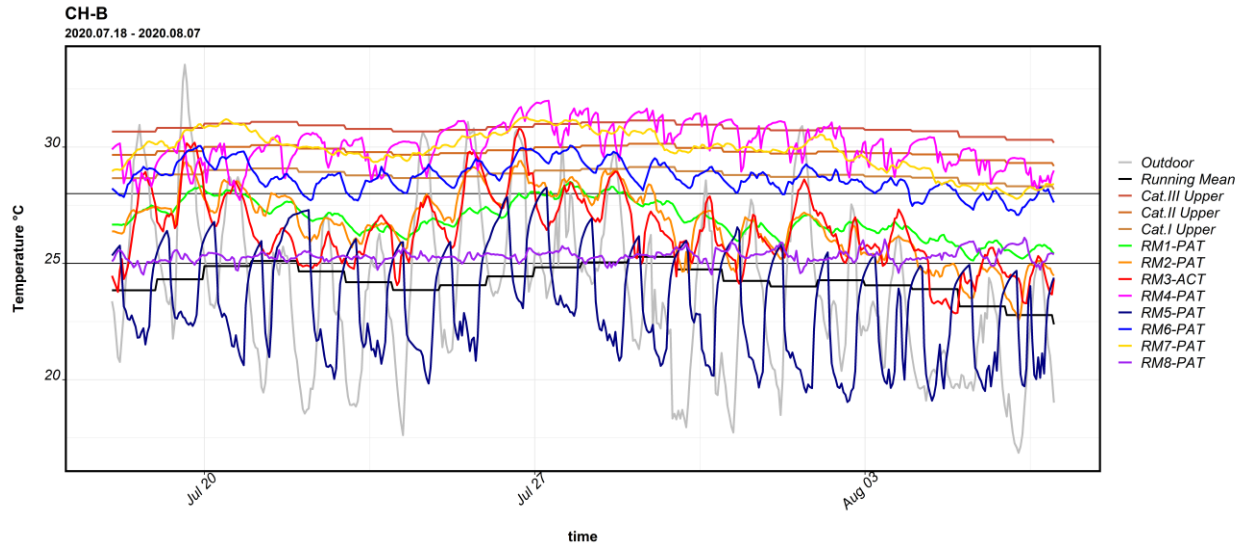
Figure 4-10 Hourly indoor and outdoor temperature monitored at building CH-B

The hourly temperature of the room during TF-5 can be found in Figure 4-10, and the whole available data including the hourly temperature and indoor relative humidity for this building during TF-4 can be found in Appendix G. The orientation of the room may still affect the indoor air temperature using the heat transfer through the external wall of the building, for example, RM6 and RM7 are both on the top floor without air conditioning in the room, while the temperature in RM7 seems to always have a higher temperature than RM6, and for most of the time during TF4, the temperature difference can be around 1-2 °C between these two rooms. The rooms on the top floor of the building may still have a higher chance to get overheated, for example, the temperature in RM2 on a lower floor, is lower than that of the room RM7, which has the same orientation but on the top floor. Meanwhile, unlike the situation in the school building SB1-D, building CH-B has small windows and the exposure of the room to solar radiation would not be the only dominant factor to the indoor overheating. For example, the rooms RM4 and RM6 have the same orientation, both without access to cooling, and very similar layout of the room, while the temperature in the RM4 has a higher temperature than RM6 in most of the days during TF-5. This might be affected by the behaviour patterns of the occupants in the room, for example, the usage of electric utilities, natural ventilation by open windows, and the operation of the shading curtains. Another interesting observation of RM4 is that its indoor air temperature may drop around midday when the outdoor condition normally reaches the highest temperature in the day. This might be because the occupant in RM4 may move to the dining region in RM3 to have lunch and part of the utilities in this room

60

will be turned off, and another reason might be the cooling in its adjacent rooms during the hottest hours may help cool down RM4.

The air conditioners in the building can effectively mitigate the overheating in the room, but the situation may vary significantly if the operation of the AC units is different. The four rooms (RM1, RM3, RM5, and RM8) with air conditioners installed have significantly different patterns. The room RM8 has a very stable air temperature at around 25 °C during the evaluated 20 days (TF-5), which indicates that the air conditioner in this room is always open and the setpoint has been configured to be a constant value of around 25 °C. The situation in RM1 is quite different from RM8, which has maintained an indoor air temperature at a low level (<28 °C) and the diurnal variation of the air temperature in these rooms is also smaller than the other rooms without air conditioners, but its variation still follows the trend of the outdoor air temperature. This indicates that the cooling air supply in this room is not sufficient to fully resist the outdoor environment, but it is good enough to avoid the extremely high temperature in the room. An interesting situation can be found in RM5, which seems to have the largest diurnal variation in the air temperature and the monitored air temperature in the room varies from 20 °C to 28 °C during the 20 days observations. And unlike the other rooms to have a daytime temperature higher than the nighttime temperature, RM5 is having most of the nighttime temperature much higher than that during the daytime (Figure 4-11). From the hourly temperature variation (Figure 4-10), it can be noticed that the temperature in RM5 normally reaches the peak value during the morning around the sunrise hours, then there may have a significant drop to a temperature level below 22 °C during the daytime and rebound very soon in the late afternoon around the sunset hours. The daily peak temperature in RM5 is at a similar level to the daily lowest temperature in RM2 and RM3. This indicates that the air conditioner is turned off in this room during the night time, and the setpoint of the air conditioner has been set to a very low value during the daytime for most of the days in the monitored period. Another interesting observation can be found in the activity and dining room RM3, which may have an even higher temperature than that in a room without the air conditioner, for example, RM2, and the highest temperature in this room normally happen during noon. This might be because room RM3 has a very high occupant volume during lunchtime, and it is a large open space connected to the corridor, so the only portable air conditioner in this room is not enough to fully control the indoor temperature in this room.
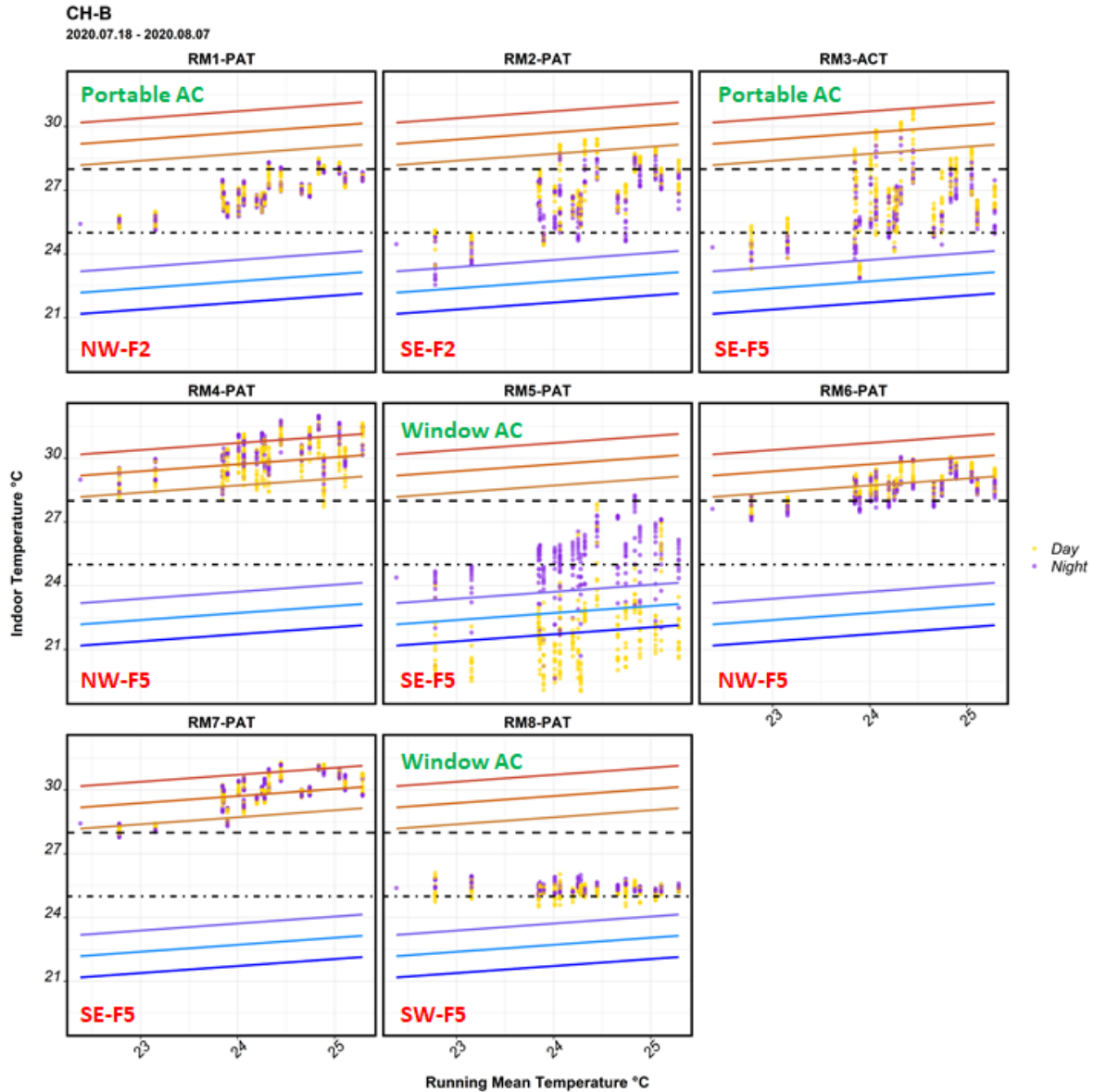
Figure 4-11 Scatter of indoor air temperature with the running mean temperature

In general, the situation in the hospital building can be more complicated than that in a school building, and the multiple factors may tangle together to formulate the current overheating status in the hospital. For the 4 rooms with AC installed, RM1, RM5 and RM8 have most of the time with the air temperature below 28 °C and below the threshold of the BS EN Cat I and they would be very promising to achieve the requirement in EN 16798-2019 (BS EN 16798, 2019) and HTM03 (Department of Health, 2007a). While the cooling in room RM3 is not sufficient to serve for the occupants during lunchtime, and it may have a higher chance to have a temperature higher than 28 °C and the BS EN Cat II. The temperature in the three rooms RM4, RM6 and RM7 on the

top floor but without air conditioner have most of the observed times higher than 28 °C, and they are reluctant to achieve the requirements in EN 16798-2019 (BS EN 16798, 2019) and HTM03 (Department of Health, 2007a).

4.6. Compare the overheating of different rooms

The two case studies in Section 4.5 provided a basic understanding of how the measured data relates to the characteristics of the building and the room, the surrounding environment, and the occupant pattern. An overall comparison of measured data and the overheating condition in the eight-building can help understand the problems in common and the difference between the rooms. The measured indoor air temperature and relative humidity have been shown in Figure 4-12, and the evaluated percentage of overheating hours are in Figure 4-13. The boxplot of the air temperature and relative humidity exhibited the general value ranges of these two environmental variables in the rooms. It can be found that most of the rooms with higher air temperature may have lower relative humidity in these observed results.
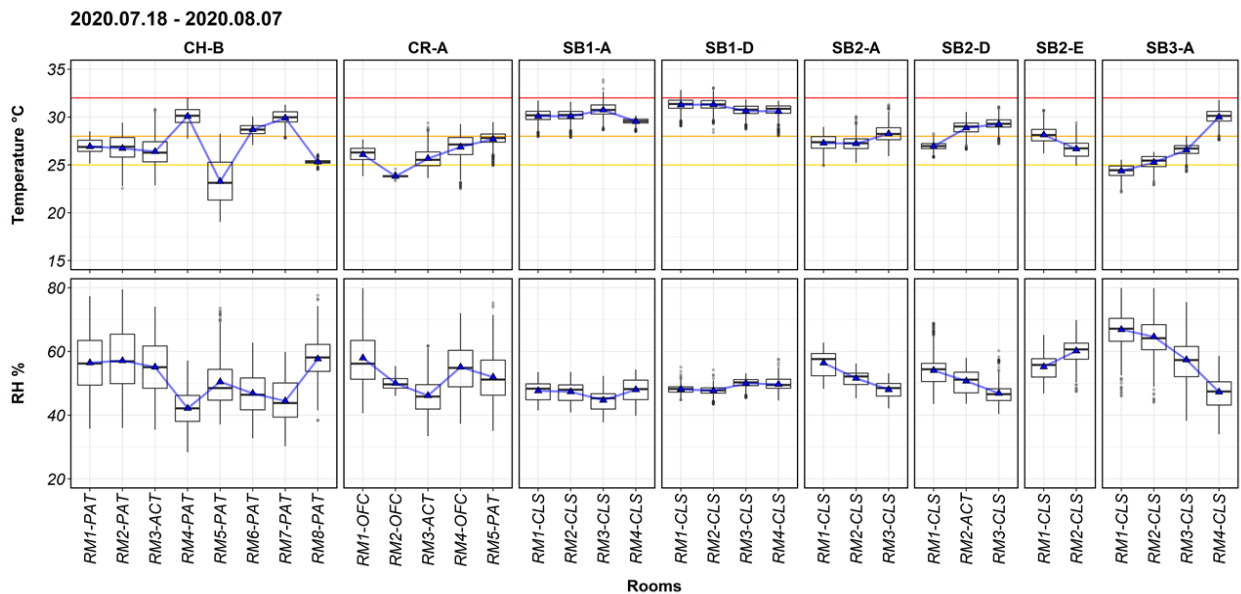
Figure 4-12 Boxplot of the monitored indoor air temperature and relative humidity for the eight buildings during TF-5

For the school buildings, the overheating conditions of the schools from the three different school boards (SB1, SB2 and SB3) are quite different. All the rooms at the two schools SB1-A and SB1-D from the first school board SB1 have almost 100% of the hours with a temperature higher than 28 °C, and some of the rooms even have a temperature higher than 32 °C (SB1-A [RM3-CLS],

SB1-D [RM1-CLS, RM2-CLS]) (Figure 4-13). Since all the field monitored rooms are on the top floor of the buildings, the temperature ranges in these rooms are similar which also show an overall very severe overheating in the two buildings.

Because of the large-scale renovations in the school board SB2 during the summer of 2020, some of the selected rooms could not be accessed for the field monitoring study, and some of the installed sensors were damaged due to the renovation activity in the building. Most of the rooms have a large window-wall ratio of over 30%, therefore the orientation and floor of the room (on the top floor or lower floor) come to be a significant factor affecting the indoor condition as discussed for SB1-D. The available data collected from these three buildings exhibited quite different overheating conditions in the different rooms. The room RM3 of SB2-D is facing a large impervious playground on its east side and it has a large window-wall ratio of over 40%, which leads to overheating with around 60% of hours above 28 °C and over 25% of hours above the Cat. I threshold of BS EN criteria. In comparison, room RM1 has a much smaller window-wall ratio of 20% and its orientation is facing the north, which leads to lower exposure to overheating. For the building SB2-D, the two rooms RM2 and RM3 on the top floor have more than 80% of hours above 28 °C, while the room RM1 on the first floor with trees outside its window has few chances to exceed the 28 °C and BS EN adaptive thresholds. For building SB2-E, the two rooms RM1 and RM2 have a similar layout, while the measured data exhibited that RM1 has a higher mean temperature and more overheating hours than RM2 which is different from the site visiting in 2019 that RM1 has a lower temperature than RM2. This might be because the two rooms were sharing one portable air conditioner, which was used in RM1 during the site visit in 2019, while in the summer of 2020 the portable air conditioner might be turned off or even moved to RM2.

SB3-A is the only school selected from the school board SB3 for this field study because it was acknowledged during the survey and site visiting stage that this school board has few overheating problems, and most of the buildings in this school board have mechanical ventilation systems operated for a night cooling. SB3-A has been selected as a typical building from SB3 to show how does the ventilation system in the school building help to alleviate the overheating problem. It can be noticed that the temperature in the rooms RM1, RM2 and RM3 of this building kept at a low level all the time, with 0% of hours to exceed the 28 °C and BS EN adaptive thresholds. While the room RM4 still has a very severe overheating, with more than 95% of hours above 28 °C and more than 60% of hours above the Cat II threshold of the BS EN criteria. By comparing the layout of

the room RM4 with the other 3 rooms in Appendix E, it can be noticed that the room RM4 is a much larger classroom than the other 3 rooms, and it has a large window-wall ratio of around 30% while the other rooms only have a small window with window wall ratio of no more than 5%. And it has both big windows facing the south and west with a large impervious parking area at its outside. Furthermore, due to the larger area of the room, the ventilation rate for this room might not be sufficient to purge the heat accumulated during the daytime.
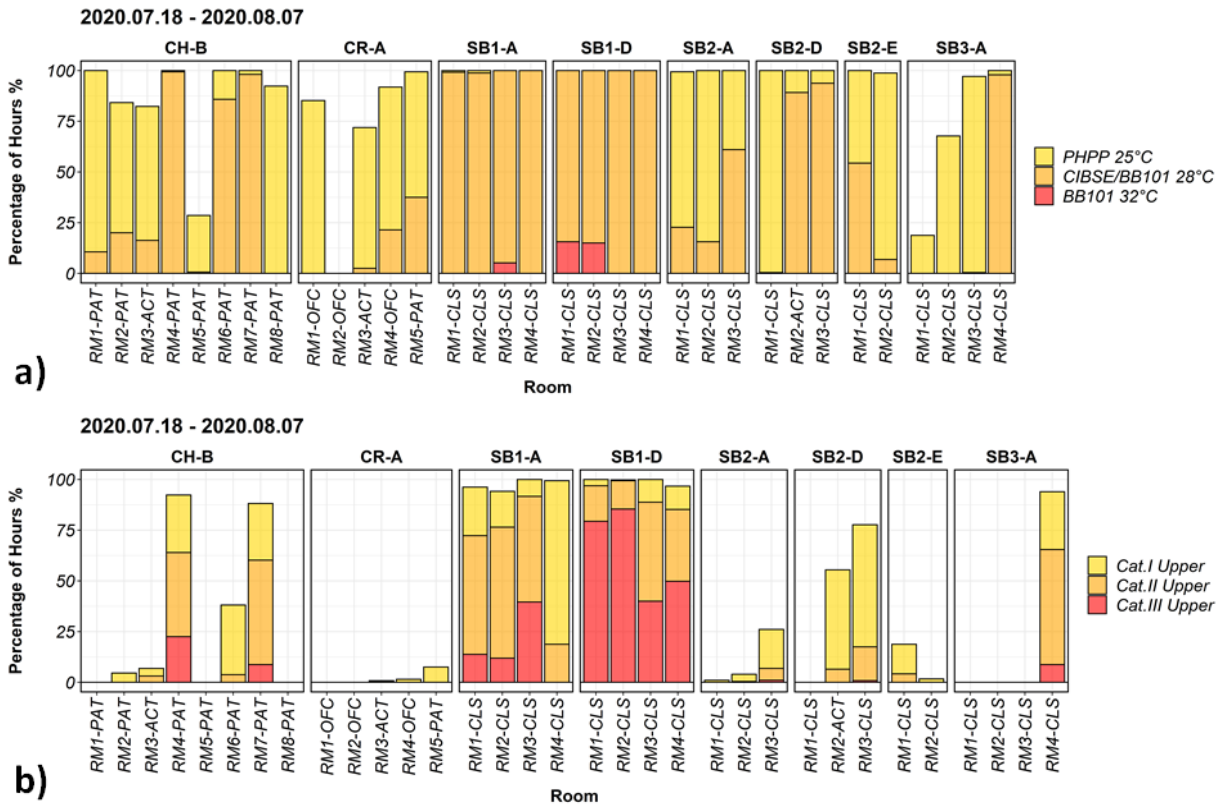
Figure 4-13 Percentage of overheating hours in different buildings and rooms evaluated by a) the fixed temperature criteria and b) the adaptive temperature criteria during TF-5

For the hospital building CH-B, rooms RM4, RM6 and RM7 are the most overheated ones with 80% of hours above 28°C, and the other rooms RM1, RM3, RM 5 and RM8 with air conditioner and RM2 on the second floor of the building have no more than 20% of hours above 28°C and no more than 10 % of hours above the adaptive temperature threshold of BS EN. Another hospital building CR-A has generally well condition and few overheating complaints during the survey and site-visiting, because they have fresh air and cooling supply to the hall and corridor area, and most of the rooms have a window AC installed. In this study, three of the rooms RM1, RM4, and RM5

without AC installed have been selected for the monitoring to compare with the other typical rooms with a window AC in the room, e.g., RM2 and RM3. It was found the patient room RM5 has the most severe overheating problem with more than 35% of hours above 28°C, while it has only no more than 10 % of an hour above the Cat I threshold of BS EN.

4.7. Compare the overheating metrics

The above analysis and the calculated overheating hours using the fixed temperature threshold and the adaptive temperature threshold shows that the overheating evaluation using the different criteria might have a significant discrepancy in between. Some recent studies also propose to use other thermal comfort indices for overheating evaluation (Laouadi et al., 2020a), which also might be quite different from the existing temperature-based overheating criteria. Therefore, a comparison of the different thermal indices and criteria should be conducted to clarify their difference.

4.7.1 Correlation analysis of the mean and maximum values of thermal indices

The thermal index of each room has been calculated using the equations given in Section 4.3. To examine the linear dependencies of the evaluated mean and maximum values between the different thermal indices, the Pearson's r correlation coefficient has been calculated and shown in Figure 4-14, being arranged into three categorical groups, one group for the mean and maximum relative humidity (C-RH), the other two groups for the mean and maximum values of the different thermal indices (C-Mean, C-Max). In general, the mean values of the different thermal indices are highly positively correlated to each other with a correlation coefficient of more than 0.95 between each of the variables, which shows that the average level of the indoor thermal condition evaluated by different thermal indices can agree well with each other with a linear model.

For the maximum values of the thermal indices, the correlation is not as strong as those between the mean values, while still, most of them have achieved a correlation coefficient higher than 0.90. Lower correlation coefficients in this group can be found between T_{max} and SSI_{max}, or DI_{max}, and that between T_{max} and H_{max}, or $WBGT_{max}$ is even lower to below 0.8. This suggests that, unlike the mean values, the extreme values evaluated by the different thermal indices can be less linearly dependent on each other. Checking the correlation coefficient between the thermal indices and the relative humidity, both C-Mean and C-Max can be divided into two subgroups, one is the variables T, SET and HI, which have a strong negative correlation with the mean and maximum values of

the relative humidity, and the other sub-group should be the four variables that are more affected by the relative humidity, SSI, DI, H and WBGT, which still have the negative correlation with the relative humidity values but gets weaker comparing the variables in the first sub-group. Among the second subgroups of the thermal indices, the negative linear dependency of H and WBGT can be very small, and the p-value of the correlation coefficient cannot achieve an ideal significant level, which indicates that these two thermal indices tend to be more independent from the relative humidity in the room. The strongest negative correlation can be found between T and RH, which means that for those rooms with higher indoor temperature T they may have lower RH. While for the other six variables, SET, HI, SSI, DI, H and WBGT, that are intrinsically affected by the relative humidity, these negative correlations have been alleviated. This can be explained by the range of the relative humidity in the studies rooms, that most of them have an indoor humidity to be between 30% and 70% which does not achieve a humidity level (e.g., > 80%) to affect their thermal stress.

The relative humidity and the mean and maximum values of the different thermal indices are shown in Figure 4-15, with the room names aligned in ascending order of their mean air temperatures. The temperature ranges of the different thermal indices are quite different from each other, which brought about the original difficulty to compare their difference in overheating assessment, for example, the SSI and H tend to occupy the higher value range in the scale of the air temperature, while the DI tend to be much lower than that, and the other three thermal index, HI, SET and WBGT air having values close to the air temperature. The RH of the rooms shows a descending trend in general, which explained the negative correlation coefficient between RH and T. Only three out of the 33 rooms have the mean RH close to or higher than 60% and 12 of them have their maximum RH higher than 70%. The mean values of the thermal index tend to grow monotonically along with the increasing mean air temperature, and the rooms with lower mean air temperatures may have their thermal index values more affected by the RH. The maximum thermal index values are less concordant to the mean values, but also follow the trend of the maximum air temperature.
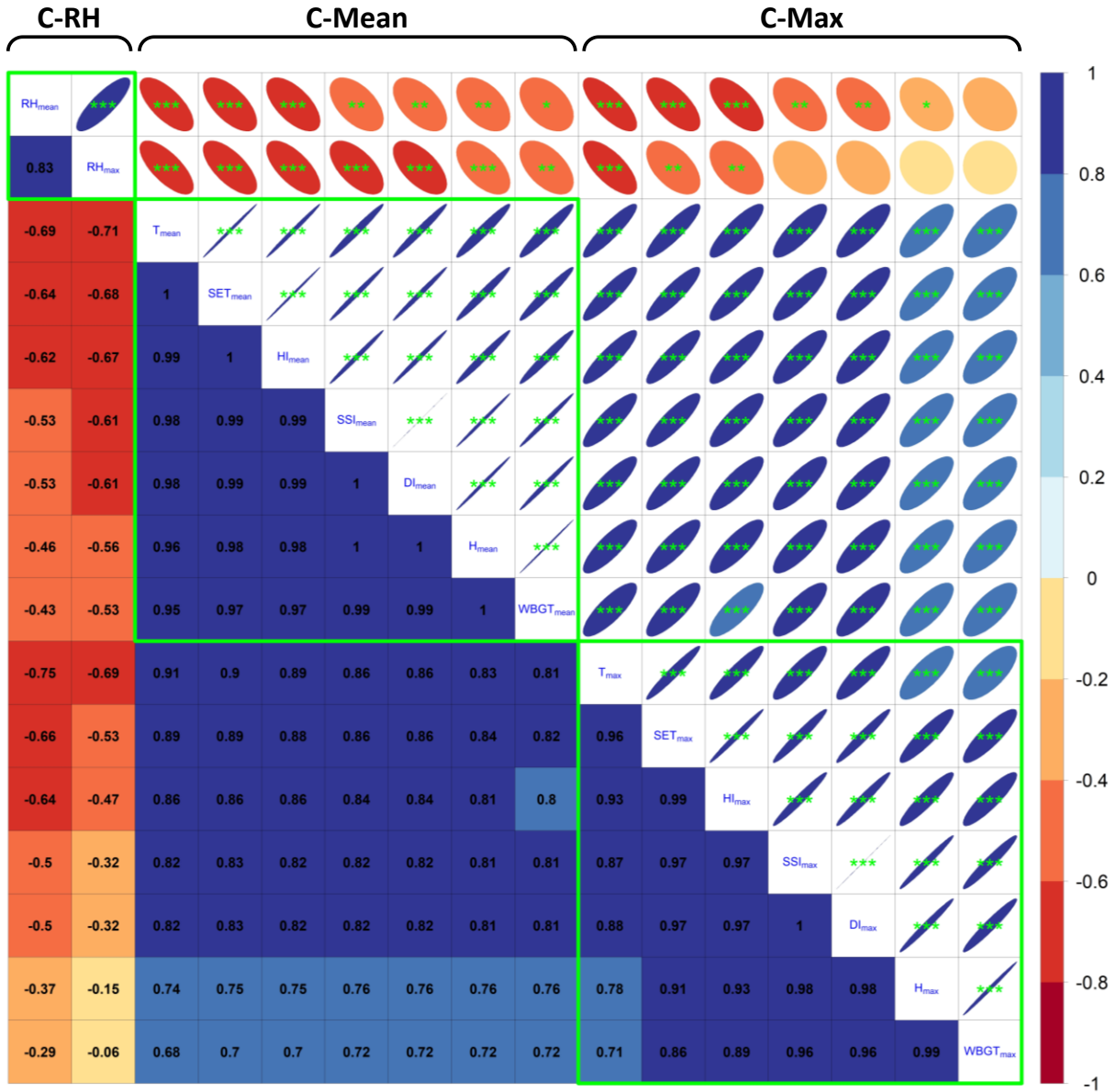
Figure 4-14 Pearson's r correlation coefficient between the mean value of different variables, the
* signs indicate the significant levels: ***-p-value < 0.001, **-p-value < 0.01, * p-value < 0.5.

To quantitatively evaluate the concordance between the different thermal indices, Kendall's tau
has been calculated and shown in Figure 4-16. The mean values of the thermal indices still
achieved a high degree of concordance, while less concordance for the maximum values and
Kendall's tau between the C-Mean and C-Max is even lower. This indicates that the evaluation of
the extremes can be quite different from the means.
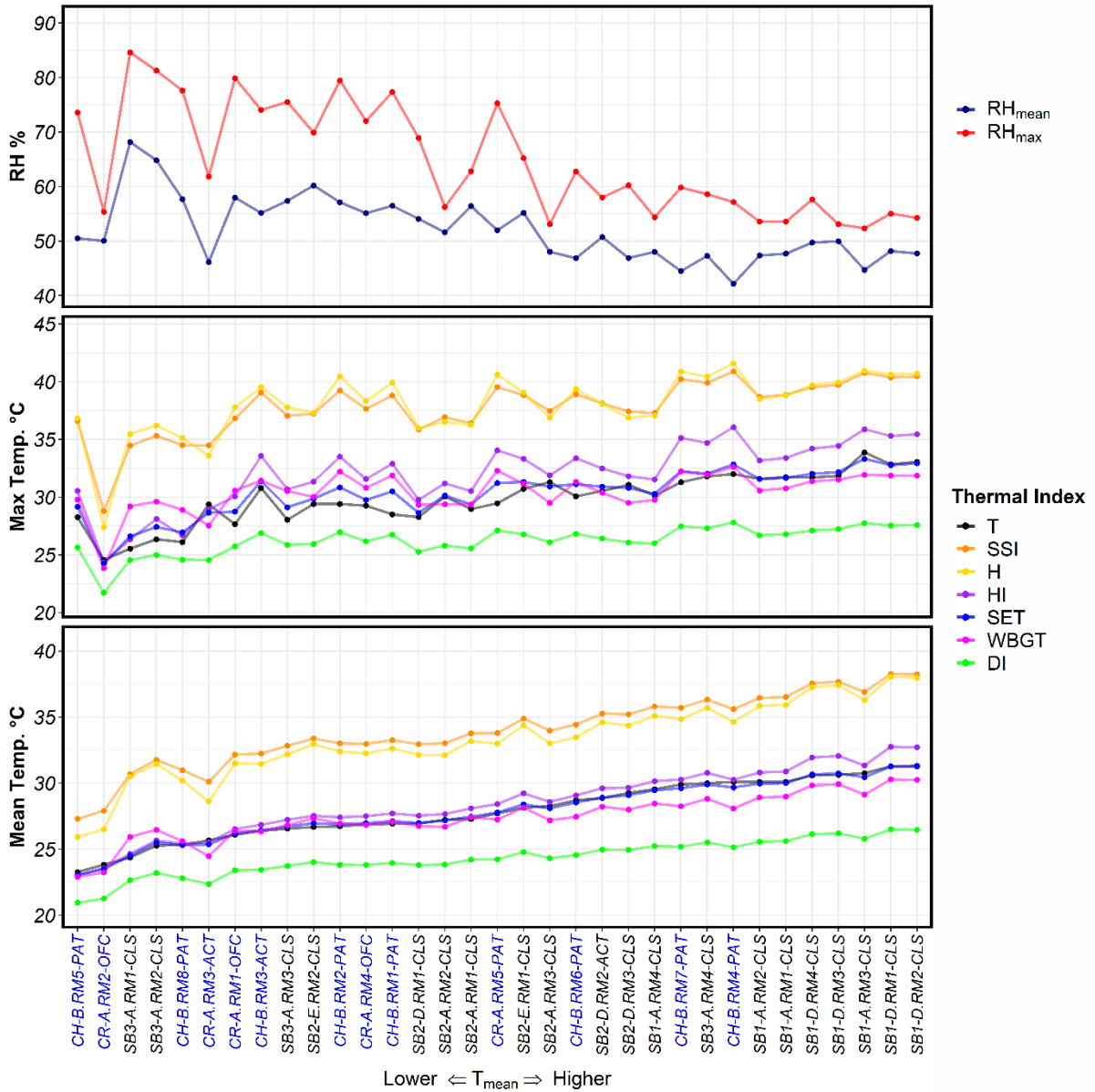
Figure 4-15 Mean and maximum values of the thermal stress metrics in the monitored rooms ordered by the rank of their mean temperature
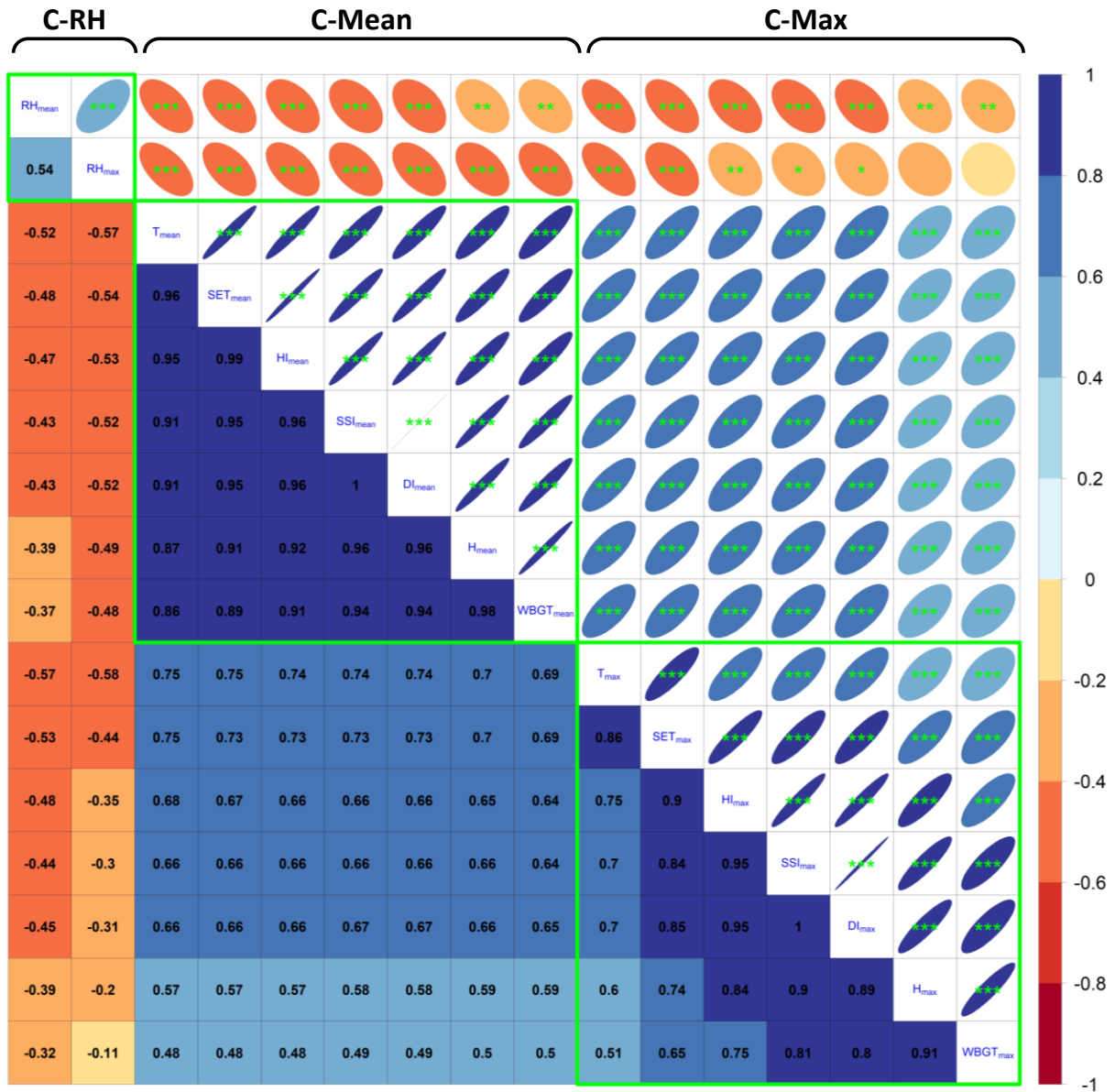
Figure 4-16 Kendall's tau correlation coefficient between the mean value of different variables, the * signs indicate the significant levels: ***-p-value < 0.001, **-p-value < 0.01, * p-value < 0.5.

4.7.2 Correlation analysis of the overheating hours identified by different criteria

To further explore the concordance of the different thermal indices using their thermal limit thresholds or the assessment scales described in Section 4.3, the percentage of overheating hours in the evaluated 33 rooms is calculated using the different thermal stress thresholds. Figure 4-17 shows the distribution of the percentage of overheating hours evaluated by the different thresholds

of the thermal indices. A significant difference can be noticed when the thresholds of the thermal indices are not too high. If the thresholds are selected to out of the range, the percentage of overheating hours would be all 0 for the 33 rooms, for example, 40.6 °C or above for HI, 45°C or above for H, 44.4°C or above for SSI, 29°C or above for DI, and 34.5°C or above for SET. These thresholds are therefore excluded from the discussion in the following study.
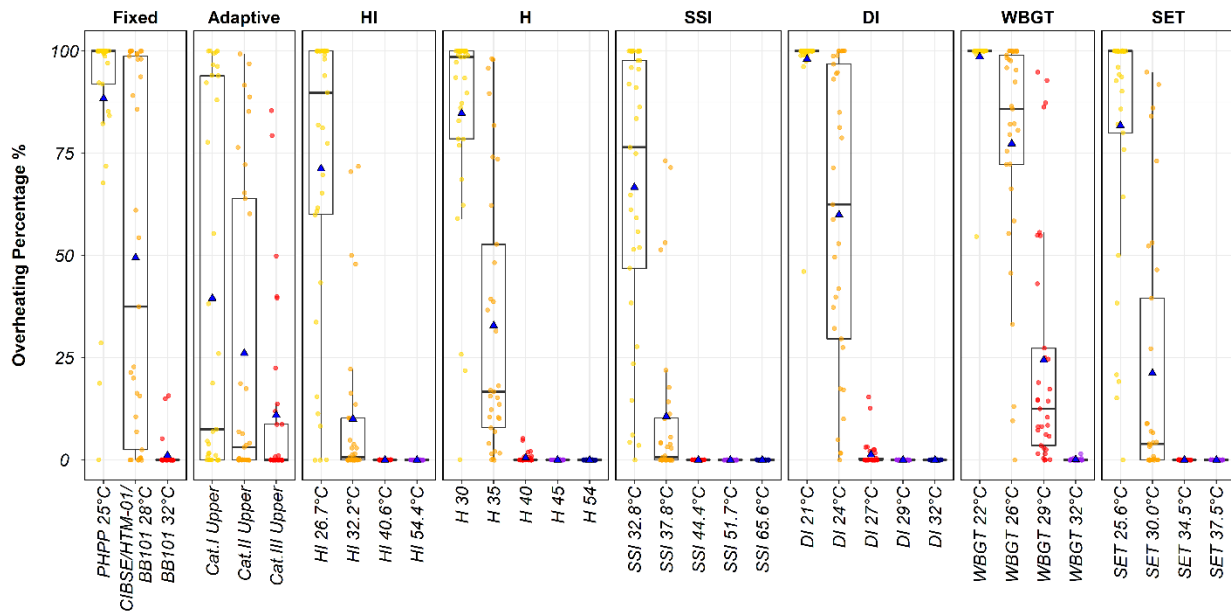
Figure 4-17 Comparison of the overall ranges of the overheating evaluated by different assessment methods, jitter points show the value for each room.

To explore the potential connections between the thresholds of the different thermal indices, a hierarchical clustering analysis has been conducted by taking the Pearson's correlation coefficients as the Euclidean coordinates, and it successfully clustered the similar criteria of different thermal index threshold values into 6 groups with different levels of the overheating. The calculated Pearson's r correlation coefficient is plotted in Figure 4-18, and the correlation between the different criteria and the mean air temperature is also provided in the first column as a reference to help understand the relationship of the different clusters with the mean air temperature. The correlation coefficients inside of each of the clusters are positively strong, while the coefficients between the groups would be relatively weak.

Figure 4-18 (correlation matrix). Lower-triangular Pearson's r values by criterion:

	T mean	DI 21°C	WBGT 22°C	Temp. 25°C	H 30	HI 26.7°C	WBGT 26°C	SET 25.6°C	Temp. 28°C	Cat.I	SSI 32.8°C	DI 24°C	Cat.II	SSI 37.8°C	H 35	HI 32.2°C	WBGT 29°C	SET 30.0°C	Cat.III	Temp. 32°C	H 40	DI 27°C	WBGT 32°C
DI 21°C	0.41																						
WBGT 22°C	0.38	1																					
Temp. 25°C	0.72	0.47	0.43																				
H 30	0.78	0.49	0.46	0.87																			
HI 26.7°C	0.9	0.36	0.32	0.79	0.86																		
WBGT 26°C	0.85	0.45	0.42	0.81	0.97	0.92																	
SET 25.6°C	0.82	0.42	0.38	0.89	0.92	0.95	0.93																
Temp. 28°C	0.93	0.23	0.2	0.51	0.62	0.82	0.73	0.66															
Cat.I	0.9	0.19	0.16	0.42	0.53	0.71	0.65	0.55	0.96														
SSI 32.8°C	0.94	0.36	0.32	0.73	0.86	0.97	0.94	0.9	0.89	0.8													
DI 24°C	0.95	0.31	0.28	0.65	0.78	0.93	0.88	0.82	0.95	0.88	0.98												
Cat.II	0.83	0.15	0.13	0.33	0.43	0.57	0.53	0.44	0.8	0.9	0.66	0.74											
SSI 37.8°C	0.65	0.11	0.09	0.24	0.31	0.41	0.39	0.31	0.57	0.65	0.48	0.53	0.82										
H 35	0.88	0.2	0.17	0.43	0.53	0.67	0.65	0.55	0.85	0.91	0.77	0.83	0.94	0.82									
HI 32.2°C	0.65	0.11	0.09	0.24	0.3	0.4	0.39	0.31	0.56	0.65	0.47	0.53	0.82	1	0.82								
WBGT 29°C	0.79	0.16	0.14	0.35	0.44	0.56	0.55	0.46	0.73	0.8	0.65	0.71	0.93	0.92	0.96	0.92							
SET 30.0°C	0.79	0.14	0.12	0.31	0.4	0.53	0.5	0.41	0.74	0.83	0.62	0.69	0.97	0.91	0.95	0.91	0.98						
Cat.III	0.66	0.1	0.09	0.23	0.3	0.4	0.38	0.31	0.57	0.66	0.47	0.53	0.84	0.97	0.83	0.97	0.9	0.92					
Temp. 32°C	0.44	0.06	0.05	0.14	0.18	0.24	0.24	0.18	0.34	0.4	0.28	0.32	0.57	0.78	0.56	0.8	0.64	0.64	0.86				
H 40	0.51	0.08	0.07	0.18	0.23	0.31	0.27	0.24	0.42	0.48	0.34	0.38	0.61	0.76	0.55	0.77	0.61	0.63	0.81	0.91			
DI 27°C	0.54	0.08	0.07	0.18	0.23	0.31	0.29	0.24	0.44	0.52	0.36	0.41	0.67	0.88	0.65	0.9	0.74	0.73	0.91	0.94	0.95		
WBGT 32°C	0.16	0.05	0.05	0.1	0.1	0.16	0.07	0.14	0.17	0.15	0.12	0.11	0.13	-0.03	0.03	-0.04	-0.02	0.05	0.04	-0.08	0.24	0.07	

Figure 4-18 Pearson's r correlation coefficient of the evaluated overheating percentages between different criteria, the * signs indicate the significant levels: ***-p-value < 0.001, **-p-value < 0.01, * p-value < 0.5.

The first cluster is the criteria with extra-low-level thresholds (C-XL), which includes the DI 21 °C and WBGT 22°C and their correlation with mean air temperature is also not that strong, showing that these criteria can hardly represent the thermal conditions in the measured rooms.

The second cluster is the criteria with the low-level threshold (C-L), including the fixed temperature threshold of 25 °C, H 30, HI 26.7°C, WBGT 26°C, SET 25.6 °C. In this cluster of

criteria, the fixed temperature threshold of 25°C and H 30 still have a lower correlation to the mean temperature levels of the measured rooms than the other indices in the group.

The third cluster is the criteria with the medium level thresholds (C-M), including the fixed air temperature threshold of 28 °C, adaptive temperature threshold of BS EN Cat I, SSI 32.8 °C, and DI 24°C. This cluster of criteria has the highest correlation with the mean air temperature, which indicates they can properly reflect the contrast of the general indoor thermal condition in the different rooms.
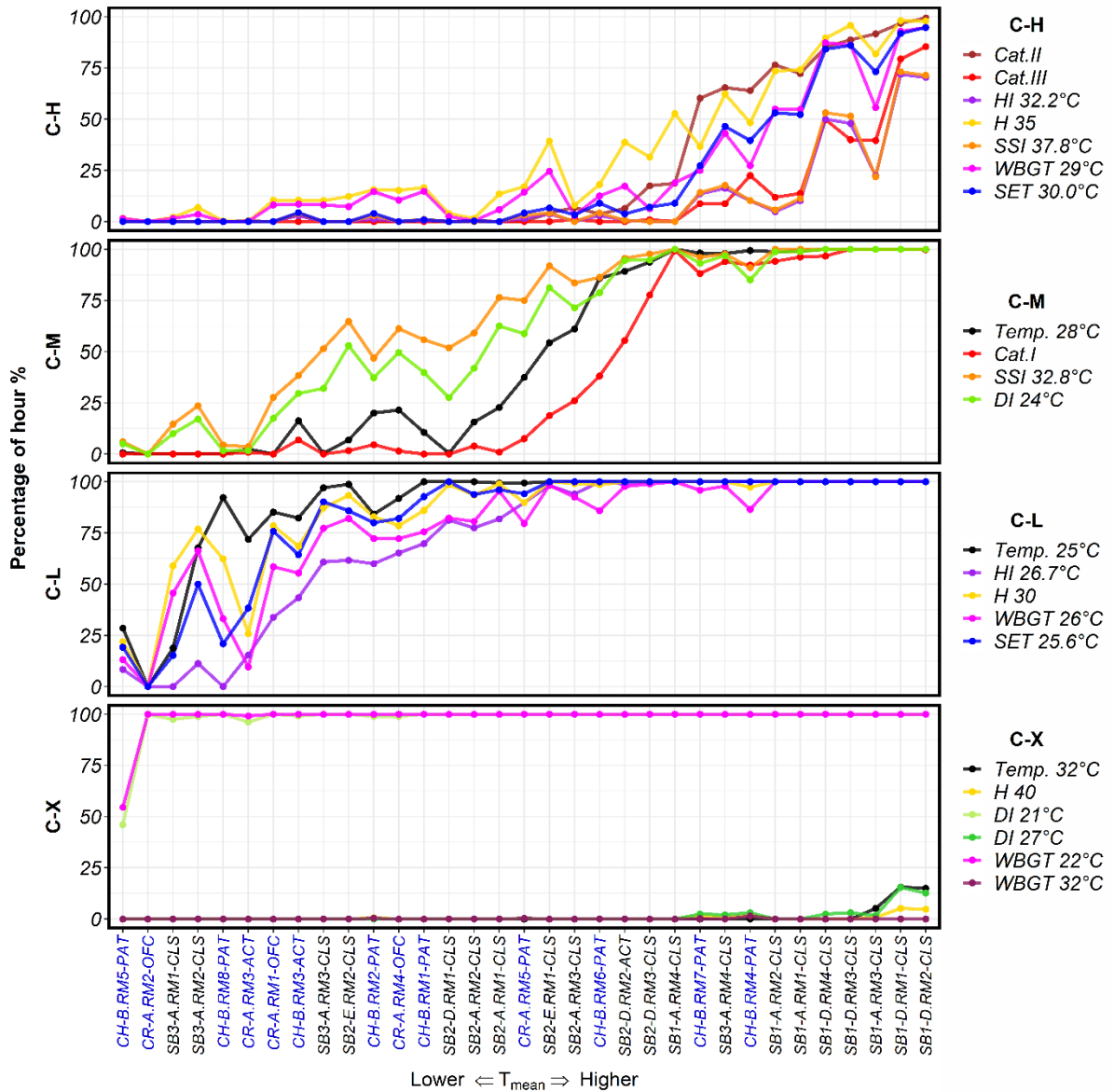
Figure 4-19 The percentage of overheating hours evaluated by the different clusters of criteria.

The fourth cluster is the criteria with the high-level thresholds (C-H) which is the greatest number of criteria in comparison to the other clusters, which includes the adaptive temperature threshold of BS EN Cat. II and Cat. III, SSI 37.8 °C, H 35, HI 32.2 °C, WBGT 29 °C, SET 30.0°C. The correlation of this group of criteria with the mean air temperature is smaller than that for the C-M, showing the difference between the evaluations of overheating can be different from the evaluation of the mean conditions. The Cat. II and Cat. III is in this same cluster, showing that both the adaptive thresholds follow well with the daily variation of the indoor air temperature.

The fifth cluster and the sixth cluster are combined to be the cluster of criteria with extra-high-level thresholds (C-XH), including the fixed air temperature threshold of 32 °C, H 40, DI 27 °C and WBGT 32 °C. The criteria of WBGT 32 °C is already exceeded the WBGT range of almost all the rooms in this study, therefor with only one room has the percentage of overheating hours above 0. That is why it has been a singular group in the hierarchical clustering process. The other criteria in this cluster also have over 80% of the rooms been evaluated to be with 0 percentage of hours above the thresholds, which is inconsistent with the information collected from the building survey and site visiting.

In Figure 4-19, the evaluated percentage of overheating hours have been shown for the clusters of different threshold levels, the C-XL and C-XH are combined as C-X because these criteria evaluated almost all the rooms with either 0% or 100% of hours above the thresholds. The criteria in C-L also shows 50 % of the rooms exceeding the thresholds, while it also misinterpreted some of the non-overheating rooms to have more than 50% of hours being overheating., for example, CH-B[RM8-PAT], SB3-A[RM2-CLS], and the rooms in CR-A. Comparing the C-X and C-L, the two clusters C-H and C-M seem to be able to capture proper overheating for both the rooms with and without the overheating complaints gathered from the survey and site-visiting studies, while there still exists a non-neglectable difference between the different criteria. For example, the adaptive temperature threshold of BS EN Cat I in cluster C-M provides a lower percentage of overheating than the fixed temperature threshold of 28 °C because the threshold also grows when the outdoor temperatures increase, while SSI 32.8 °C and DI 24 °C provided a higher percentage of overheating than the fixed temperature threshold 28 °C for those rooms with a mean indoor relative humidity of around 60% or maximum RH of 70% or above. This reflected the effect of the humidity in changing the overheating assessment results.
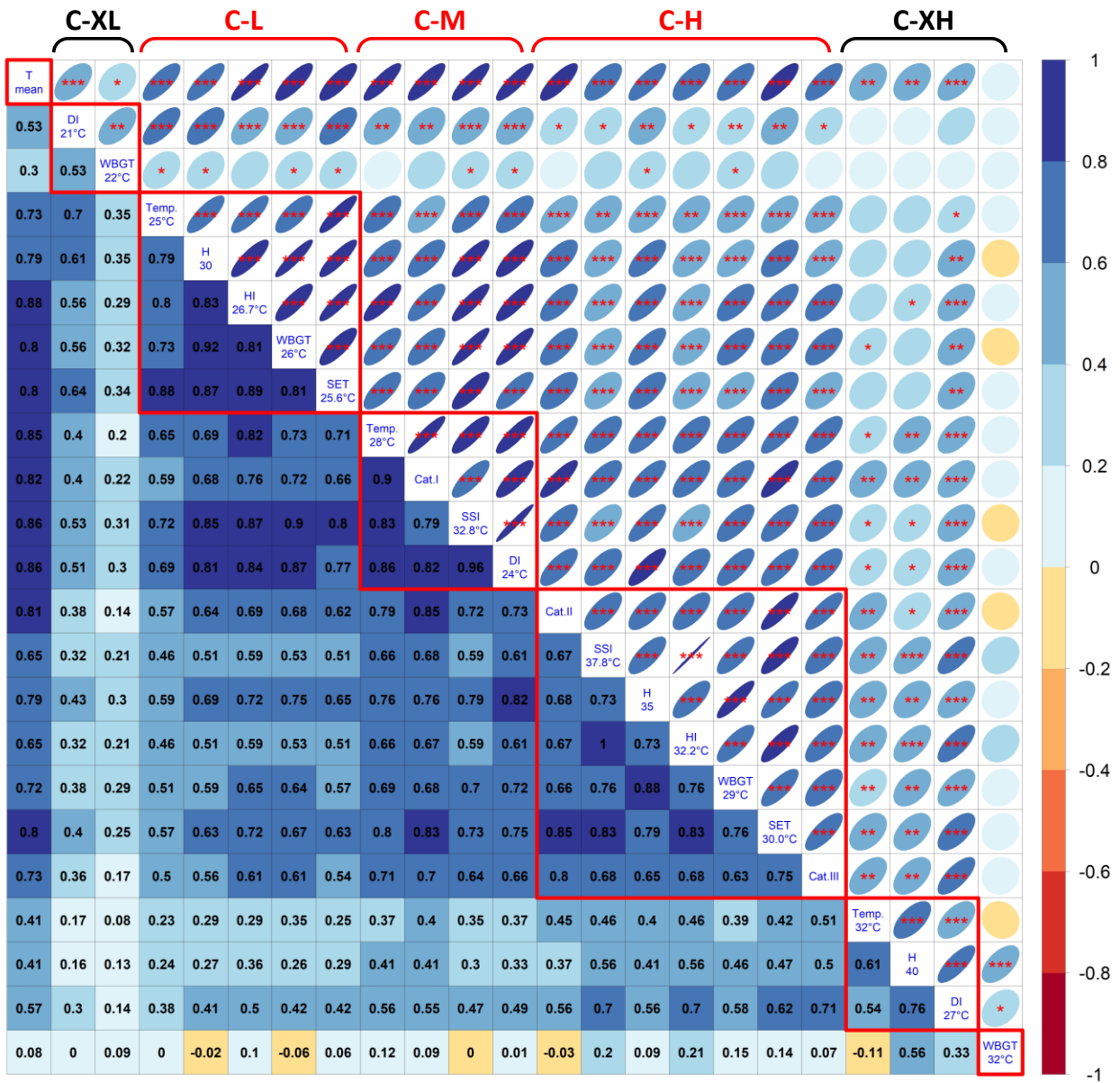
Figure 4-20 Kendall's tau correlation coefficient of the evaluated overheating percentages between different criteria, the * signs indicate the significant levels: ***-p-value < 0.001, **-p-value < 0.01, * p-value < 0.5.

For the results in the cluster of C-H, the curves of BS EN Cat II and Cat III sandwiches most of the other criteria in the cluster. While the criteria of H 35 and WBGT 29 °C exhibits to be higher than the Cat II for the rooms with lower mean air temperature and higher RH, this is can be explained by the weaker negative correlation between H, WBGT and RH – they are more affected by the RH. The results of criteria SSI 37.8 °C and HI 32.2 °C are both very close to that of Cat III,

75

and the criteria of SET 30.0 °C have evaluated a percentage of overheating in between Cat II and Cat III but closer to Cat II for most of the rooms. Therefore, the C-H can be further divided into two sub-clusters (C-H1, and C-H2) to be consistent with the two different levels of overheating evaluated by Cat II and Cat III.

The degree of concordance between the different criteria is also evaluated quantitatively using Kendall's tau correlation coefficient, as shown in Figure 4-20. Stronger concordance can be found in clusters C-L and C-M, while lower in cluster C-H. This shows that the diversity in overheating assessment using the higher thresholds of the different thermal indices. Note that, the two criteria, SSI 32.8 °C and DI 24 °C in C-M also have a high Kendall's correlation with the criteria in the cluster of C-L, this observation is also consistent with Figure 4-19 that for the rooms with medium mean temperature but high RH, the percentage of overheating evaluated by these two criteria will be close to the results in C-L. C-M is therefore further divided into two subclusters (C-M1 and C-M2). Similarly, in cluster C-L, the fixed temperature threshold of 25°C also has a lower correlation coefficient with the other criteria in the cluster, and the overheating hours evaluated by the temperature threshold of 25°C are also at a higher level in comparison to the other criteria in this cluster. C-L is therefore further divided into two subclusters (C-L1 and C-L2). A general equivalency between the different criteria can be summarized in Figure 4-21.

Group	Fixed °C	Adaptive Category	HI °C	H (°C)	SSI °C	DI °C	WBGT °C	SET °C
C-XL						21	22	
C-L1	25							
C-L2			26.7	30			26	25.6
C-M1					32.8	24		
C-M2	28	Cat I						
C-H1		Cat II		35			29	30.0
C-H2		Cat III	32.2		37.8			
C-XH	32			40		27	32	
Excluded Thresholds					44.4			
			40.6	45	51.7	29		34.5
			54.4	54	65.6	32		37.5

Figure 4-21 Map of the equivalency between the different criteria.

4.8. Summary

In this chapter, the instruments and their installation methods in the field monitoring have been elaborated which can be a guideline for future works. The considerations for the room selection and the currently available data adopted in this study are also explained. Two case studies, one for a school building and one for a hospital building, are provided by using the well-established temperature-based overheating criteria to help identify the general overheating conditions in these buildings. The findings from these two cases studies are generalized to the others by comparing the degree of overheating in the different buildings and rooms. The collected data have been analyzed through the different overheating assessment methods of various thermal indices for the comparison between the different assessment criteria. Major findings and conclusions can be summarized as follows:

- The measured data from the eight buildings confirmed some findings from the site visiting as discussed in Chapter 3. The school buildings from the two school boards SB1 and SB2 have a severe overheating problem and they cannot achieve the overheating criteria in Building Bulletin 101 and European Standard EN 16798-2019. The school building SB3-A has much better condition than the building from the other two school boards because of the application of mechanical ventilation in the classrooms, while there is still one classroom with large windows facing the west and south have the risk of overheating.

- For hospital buildings, the difference of the overheating between the different rooms of the same building can be even greater than that between the different buildings. Three rooms in CH-B on the top floor without air conditioning are found to have the severe overheating problem that can hardly achieve the criteria in HTM03, and the indoor temperature may exceed the Cat II or even Cat III temperature threshold in EN 16798-2019, while there are also three rooms in CH-B with few overheating problems because the air conditioners in the room can maintain the indoor temperature at a low level. CR-A has a generally well condition which is consistent with the findings during the survey and site-visiting because they have fresh air and cooling supply to the hall and corridor area, and most of the rooms have a window AC installed.

- The measured data exhibited strong evidence of overheating in existing building stocks in Montreal, showing the necessity for further investigation to mitigate the overheating.

- The mean and maximum values of the calculated thermal indices in the 33 monitored rooms are compared through a correlation analysis. It was found that all the evaluated thermal indices have a negative correlation with relative humidity, which indicates that for rooms with high thermal index levels, the relative humidity in the room would be at a lower level. This suggests that, for these observed 20 days periods, the conditions of the humidity in the rooms would not affect the thermal comfort significantly for the rooms with extremely hot conditions.

- The general overheating evaluated through the different types of the thermal index are compared and clustered with the criteria at a similar level through a correlation clustering process. Even though the scales of the different thermal indices are quite different, the different thermal index thresholds of the similar levels can still achieve strong concordance in evaluation for the different rooms. Furthermore, The measured data exhibited strong evidence of overheating in existing building stocks in Montreal, showing the necessity for further investigation to mitigate the overheating.

Chapter 5 Overheating Assessment by Climate Modelling - Weather Research and Forecast (WRF) Validation

The objective of this chapter is to evaluate the performance of the WRF model over the Ottawa metropolitan area, Canada, and investigate the sensitivity of the model towards the use of different urban land use-land cover datasets and urban parametrization schemes. The outline of this chapter is as follows: data for WRF model evaluation and numerical experiments are described in section 5.1. The discussion of the results is presented in section 5.2, and finally, the conclusions of this chapter are summarized in section 5.3.

5.1. Methodology

The nonhydrostatic (V4.0) version of the WRF model coupled to the Noah land surface model (LSM; Chen and Dudhia 2001a, b; Ek et al. 2003) is used to model urban meteorology surrounding the Ottawa city from June 01 to August 31, 2018. These three months were selected because the city, its surrounding areas, and Canada, in general, experienced unusually high temperatures during the summer of 2018. This period also included an extreme heat spell event between 30 June-6 July that contributed to about 100 deaths in the region (ECCC, 2019).

5.1.1 WRF experiments

Three high spatial resolution WRF model experiments were conducted, each one covering the same three-month summertime period from 01 June to 31 August 2018, to evaluate the WRF model's ability to reproduce the diurnal cycle of near-surface meteorology and accumulated precipitation under present-day weather conditions. All WRF-experiments share the same numerical domain that is composed of three two-way nested domains with 276 × 296, 250 × 283, and 391 × 364 grid points, distanced 9, 3, and 1 km, respectively. The innermost domain includes the metropolitan areas of Ottawa and Montreal (see Figure 5-1 for more details). The vertical dimension is split into 40 eta levels, with 14 within the lowest 1.5 km to better characterize planetary boundary layer processes. National Centers for Environmental Prediction (NCEP) North American Regional Reanalysis products (number ds608.0), which are available every 3 h with a spatial resolution of 32 km, are used to provide the initial and boundary conditions needed to conduct the WRF model experiments.

Weather Stations in the domain
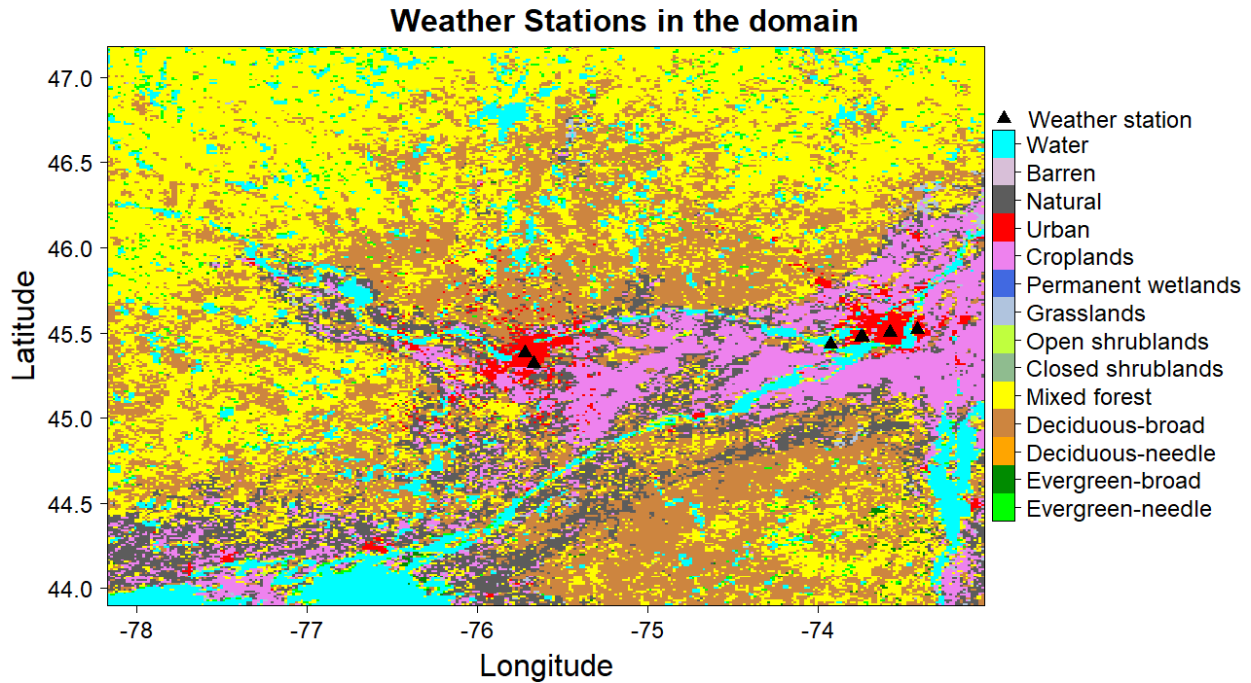
Figure 5-1 The innermost domain, the layout of land use and land cover, and the weather stations

The planetary boundary layer is parameterized with the two-order closure Mellor-Yamada-Janjic (Janjić, 1994) turbulent parameterization. Radiative processes are parameterized with the (Dudhia, 1989) scheme for the shortwave radiation and with the Rapid Radiative Transfer Model (Mlawer et al., 1997) for the longwave radiation. The bulk urban parameterization (Liu et al., 2006) included in the Noah LSM is used with the first WRF-experiment (hereafter denoted as Noah-bulk WRF-experiment) to represent zero-order effects of urban surfaces. This urban physics option assumes common values for the entire urban domain and presupposes an urban fraction of one in each urban grid cell. Despite its simplicity, the bulk urban parameterization has been successfully employed in real-time weather forecasts (e.g., Liu et al., 2006). The second WRF-experiment is performed with the multilayer UCM building effect parameterization (BEP; developed by Martilli et al. (2002) that is coupled to the Noah LSM to characterize the impacts of urban surfaces (henceforth denoted as Noah-BEP WRF-experiment). Unlike the bulk urban parameterization, the multilayer UCM BEP represents the urban geometry using infinitely long street canyons and recognizes three different urban surfaces in the urban canopy layer, namely, roofs, roads, and vertical walls. Urban surfaces interact directly with WRF through the whole urban canopy layer and buildings (vertically distributed) are considered sources and sinks of heat and momentum from the ground surface up

to the highest building present in the urban domain. Finally, the third WRF-simulation (henceforth denoted as Noah-BEP-MOD WRF-experiment) is also performed with the multilayer UCM BEP but this time the urban domain for Ottawa metropolitan area is obtained from the 2010 Land Cover of Canada Data Set (https://open.canada.ca/data/en/dataset/c688b87f-e85f-4842-b0e1-a8f79ebf1133), which is available at a spatial resolution of 30 m but considering just one urban class.

Urban fraction and building parameters needed with the multilayer UCM BEP are detailed in Table 5-1. Thermal properties for roofs, roads, and vertical walls are extracted from (Clarke et al. 1991) and correspond to standard building materials. These thermal properties are also described in Table 5-1. Moderate Resolution Imaging Spectroradiometer (MODIS) land cover classification is used to characterize the nonurban land use categories in all WRF-experiments and the urban domain for Noah-BULK and Noah-BEP WRF-experiments.

Table 5-1 Urban parameters and thermal properties used within the Noah-BEP and Noah-BEP-MOD WRF-experiments.

Urban fraction	0.70		
Building plan area fraction	0.333		
Percent of buildings 5 m high	15		
Percent of buildings 10 m high	70		
Percent of buildings 15 m high	15		
Thermal properties of building materials	Roof	Wall	Road
Thermal conductivity (W m^{-1} K^{-1})	0.67	0.67	0.74
Specific heat ($\times 10^6$ J m^{-3} K^{-1})	1.32	1.32	1.40
Surface's emissivity	0.90	0.90	0.95
Surface's albedo	0.20	0.20	0.125
Urban vegetation	Croplands		

5.1.2 Update urban land cover

The default land cover dataset in WRF used in this study is the Moderate Resolution Imaging Spectroradiometer (MODIS) land cover classification. To update the land cover, a binary file for the land cover information should be extracted from the 2010 Land Cover of Canada Data, and a corresponding index file need to be prepared for the geogrid.exe program. A comparison of the

land cover used in WRF has been plotted in Figure 5-2, the area of the urban pixels in red color has an obvious increase which indicates the expansion of the urban area. Note that in this chapter, only the urban land cover of the Ottawa city at the center area of the computational domain is updated for demonstration, and the urban land cover of Montreal is the same with default, so as to highlight the difference in the improvement of the results affected by the updates of the urban land cover.
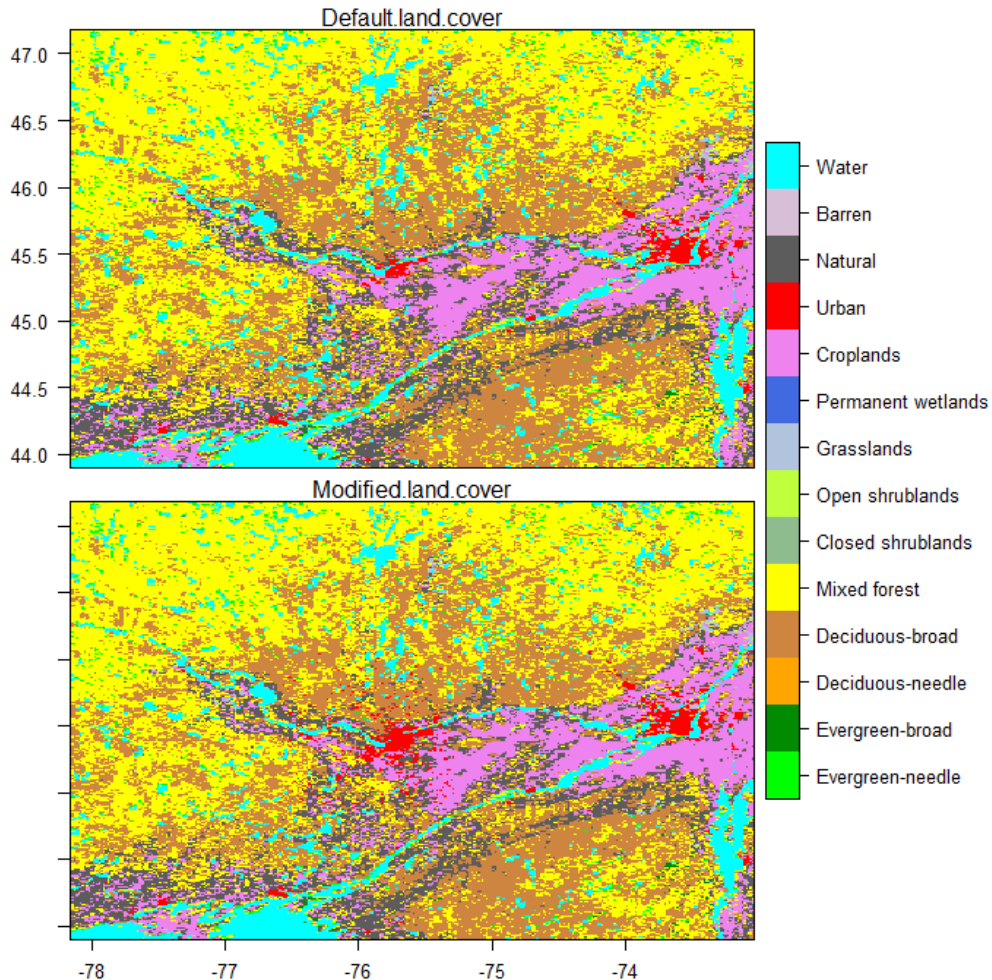
Figure 5-2 The land cover types distributions in the third domain before and after the urban land cover modification.

5.1.3 Validation setup

The 1 km resolution simulation results are validated with the time series observed data from the weather stations in the domain, which covers the area of both Ottawa and Montreal. The weather

data from two weather stations in Ottawa, one in the urban area and the other in the airport, and five weather stations in Montreal, distributed at Mc-Tavish, International Airport, Pierre Elliott Trudeau Airport, St-Hubert, and Ste-anne-de-bellevue, are used for the validation of the WRF results (Figure 5-1). As the weather stations at the International Airport and the Pierre Elliott Trudeau Airport are close to each other, the weather stations are plotted in a zoomed view in Figure 5-3. The observations of near-surface air temperature, wind speed, relative humidity, and precipitation recorded at this climate gauging station are collected from Environment and Climate Change Canada (ECCC) and used for assessing the performance of the WRF model experiments around both cities.

The performance of the WRF simulation compared to the observation data is evaluated by the two metrics, root-mean-square error (RMSE) and mean absolute error (MAE). Smaller values of these two metrics indicate a better model performance in reproducing the weather variable. Four weather variables, air temperature, relative humidity, wind speed and wind direction, accumulated precipitation, are extracted and compared with the historical data from the weather stations.

The procedures to do the validation are in three steps: i) identify the grid cell index close to the weather stations. ii) extract the variables from these grid cells and align the data in a time series, note that a five-hour time difference should be considered because the simulation in WRF is in UTC and the observed data is in the local EST time zone. iii) plot the time series data simulated by different models together with the observed data and calculate the RMSE and MAE values for the quantitative comparison of the models.

The results of the validation are discussed in Section 5.2 with the data from the Ottawa-Urban weather station as an example.
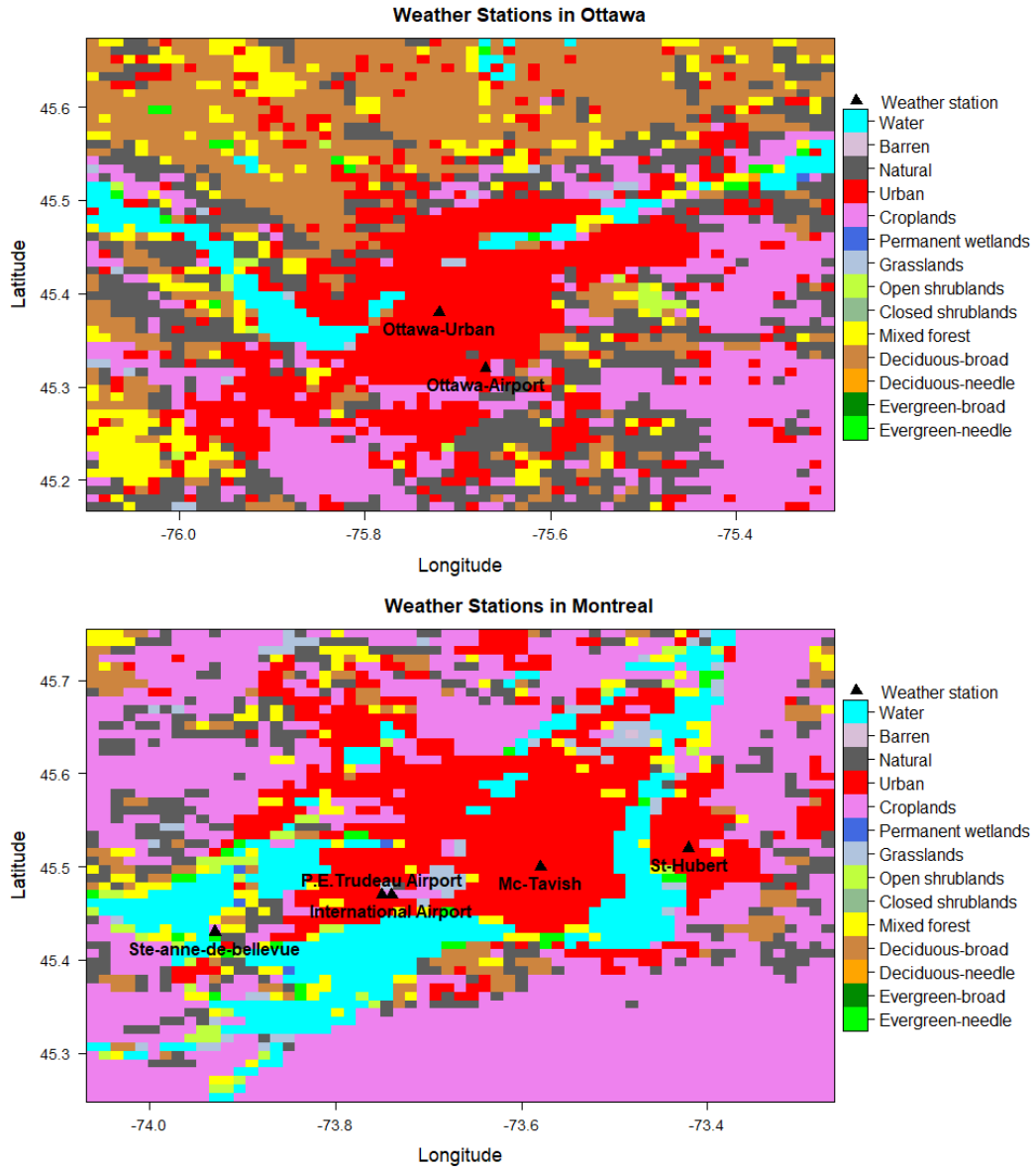
Figure 5-3 The weather stations in Ottawa and Montreal.

5.2. Validation results

5.2.1 Air temperature
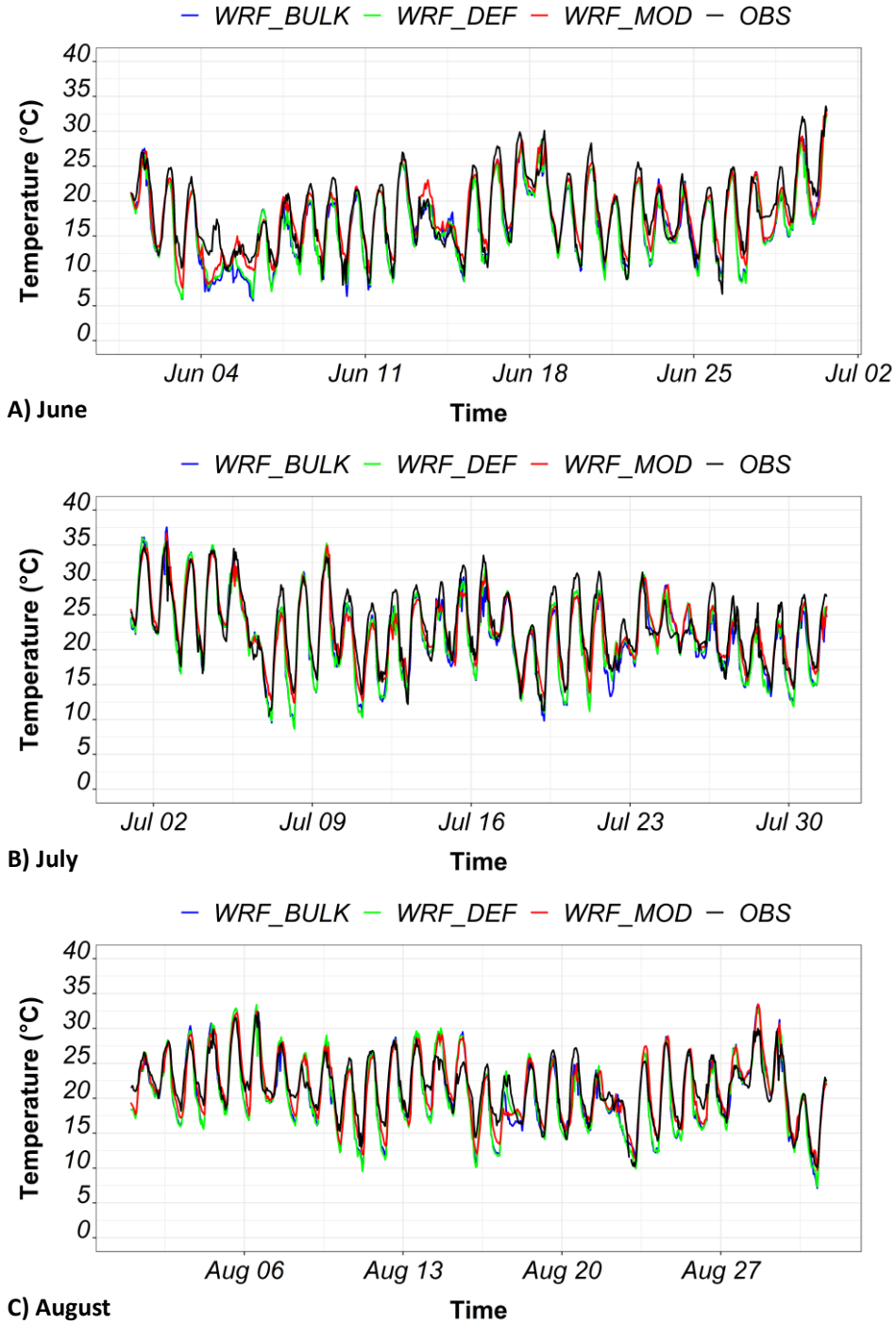
Figure 5-4 Time series of observed (black) and WRF modeled 2-m air temperature at the Ottawa-Urban weather station in A) June, B) July, and C) August

In Figure 5-4, the simulation results of the 3 WRF models, the default land cover with the BULK urban model (DEF-BULK), the default land cover with the BEP urban model (DEF-BEP), and the modified land cover with the BEP urban model (MOD-BEP), at the Ottawa-Urban weather station are plotted together with the historical observed data. The three models can well capture the diurnal variation of the air temperature in the three months. The RMSE and MAE of the models compared to the data from 7 weather stations are within 3 °C as summarized in Table 5-2 and in general, the MOD-BEP performs the best among the 3.

Table 5-2 RMSE and MAE of the 3 months 2-m air temperature results at 7 weather stations in Montreal and Ottawa

Months		June			July			August		
Models		DEF-BULK	DEF-BEP	MOD-BEP	DEF-BULK	DEF-BEP	MOD-BEP	DEF-BULK	DEF-BEP	MOD-BEP
RMSE °C	Mc-Tavish	2.1	2.2	2.1	1.8	2.3	2.3	1.9	2.2	2.2
	International Airport	2.5	2.5	2.4	2.5	2.6	2.6	2.2	2.5	2.5
	Pierre Elliott Trudeau	2.6	2.7	2.6	2.6	2.7	2.7	2.3	2.7	2.7
	St-Hubert	2.2	2.2	2.1	1.7	2.1	2.0	1.9	2.1	2.1
	Ste-anne-de-bellevue	2.5	2.5	2.5	2.6	2.5	2.5	2.3	2.4	2.3
	Ottawa-Urban	2.1	1.9	1.8	1.9	2.0	1.9	2.0	1.9	1.9
	Ottawa-Airport	2.7	2.6	2.0	2.5	2.4	2.0	2.3	2.4	1.9
MAE °C	Mc-Tavish	1.6	1.7	1.7	1.5	1.9	1.9	1.4	1.8	1.8
	International Airport	2.0	2.0	2.0	2.1	2.2	2.2	1.7	2.1	2.1
	Pierre Elliott Trudeau	2.1	2.2	2.1	2.2	2.3	2.3	1.8	2.2	2.2
	St-Hubert	1.7	1.7	1.6	1.4	1.7	1.6	1.5	1.7	1.7
	Ste-anne-de-bellevue	2.1	2.1	2.0	2.1	2.0	2.0	1.8	1.9	1.9
	Ottawa-Urban	1.6	1.5	1.4	1.5	1.5	1.5	1.6	1.5	1.5
	Ottawa-Airport	2.1	2.1	1.5	2.0	1.9	1.6	1.9	1.9	1.5

5.2.2 Relative humidity
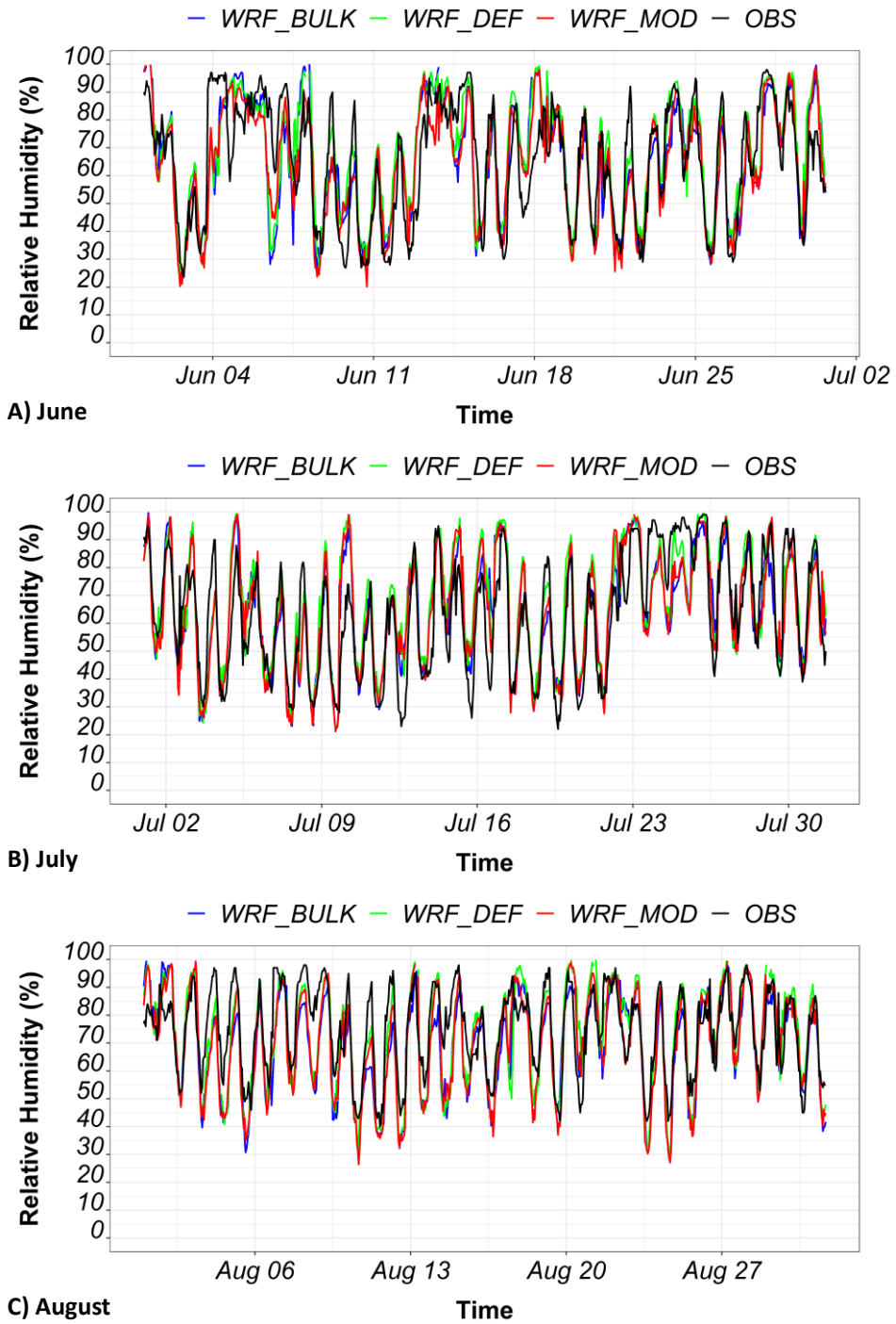
Figure 5-5 Time series of observed (black) and WRF modeled at the Ottawa-Urban weather station in A) June, B) July, and C) August

The simulation of relative humidity from the three models can also capture the time series pattern observed by the weather station as plotted in Figure 5-5. However, a relatively larger deviation between the simulation and the measured data can be observed. In Table 5-3, the RMSE and MAE are summarized. It can be noticed that the MOD-BEP does not always perform the best in comparison to the other two models for the Montreal weather stations, while it performs much better for those in Ottawa. That might be because the urban pixels are only modified for the Ottawa city but not for Montreal.

Table 5-3 RMSE and MAE of the 3 months relative humidity at 7 weather stations in Montreal and Ottawa

Months		June			July			August		
Models		**DEF-BULK**	**DEF-BEP**	**MOD-BEP**	**DEF-BULK**	**DEF-BEP**	**MOD-BEP**	**DEF-BULK**	**DEF-BEP**	**MOD-BEP**
RMSE %	Mc-Tavish	14.8	15.5	15.1	12.5	14.9	15.0	11.5	13.0	12.2
	International Airport	16.1	17.1	16.5	16.0	17.0	16.9	12.6	13.6	13.2
	Pierre Elliott Trudeau	17.4	18.4	17.9	17.5	18.5	18.3	13.0	14.2	13.8
	St-Hubert	13.6	13.4	13.2	10.7	11.8	11.9	12.2	11.9	11.2
	Ste-anne-de-bellevue	17.0	17.3	17.0	16.5	16.2	16.5	13.5	13.5	12.8
	Ottawa-Urban	13.9	13.5	12.3	11.9	12.7	12.2	11.9	10.8	11.1
	Ottawa-Airport	15.6	16.1	12.4	15.6	14.7	12.6	11.6	12.1	11.6
MAE %	Mc-Tavish	11.5	12.3	12.0	9.8	11.8	11.9	8.9	10.1	9.6
	International Airport	12.9	13.8	13.2	13.3	14.1	13.9	9.9	10.9	10.6
	Pierre Elliott Trudeau	14.2	15.1	14.5	14.8	15.7	15.5	10.2	11.3	11.1
	St-Hubert	10.7	10.2	10.0	8.3	9.4	9.4	9.3	9.1	8.7
	Ste-anne-de-bellevue	13.7	13.8	13.6	13.3	12.9	13.2	10.4	10.4	9.9
	Ottawa-Urban	10.8	10.5	9.6	9.2	9.8	9.4	9.6	8.5	8.8
	Ottawa-Airport	12.8	13.1	9.7	12.2	11.5	9.7	9.2	9.5	9.0

5.2.3 Wind speed and wind direction
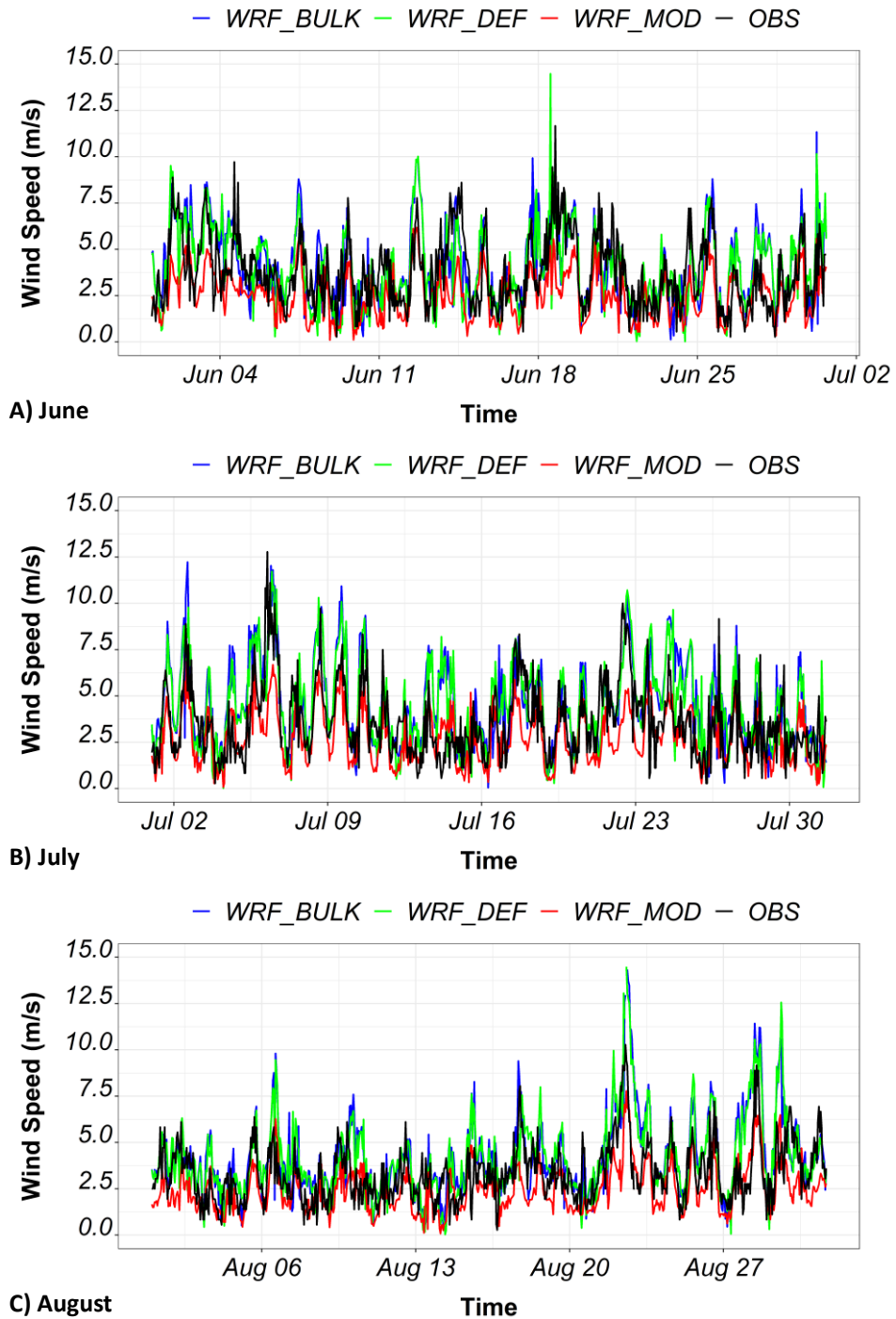
Figure 5-6 Time series of observed (black) and WRF modeled 10-m wind speed at the Ottawa-Urban weather station in A) June, B) July, and C) August

The simulated wind speed time series curves are still close to the observations at the Ottawa-Urban weather station as in Figure 5-6. However, as the figures in Appendix K, we can see an obvious deviation exists between the result of the DEF-BULK model and the other curves at the St-Hubert and Mc-Tavish weather stations. There might be two reasons: i) there are great land cover changes at those two locations while it is not considered in this test, and ii) the BULK model is not able to capture the wind speed characters at those two locations. The RMSE and MAE are summarized in Table 5-4, and the MOD-BEP, in general, performs better than the others.

Table 5-4 RMSE and MAE of the 3 months wind speed at 7 weather stations in Montreal and Ottawa

Months		June			July			August		
Models		DEF-BULK	DEF-BEP	MOD-BEP	DEF-BULK	DEF-BEP	MOD-BEP	DEF-BULK	DEF-BEP	MOD-BEP
RMSE m/s	Mc-Tavish	3.7	1.7	1.7	3.8	1.8	1.7	3.6	1.7	1.6
	International Airport	1.9	1.9	2.0	1.9	1.8	1.8	2.0	2.0	2.0
	Pierre Elliott Trudeau	1.8	1.8	1.8	1.8	1.7	1.7	2.0	2.0	1.9
	St-Hubert	2.0	2.1	2.1	2.0	2.0	2.0	2.1	1.9	1.9
	Ste-anne-de-bellevue	2.2	2.0	2.1	2.2	2.0	2.0	2.2	2.1	2.0
	Ottawa-Urban	2.0	1.4	1.4	2.2	1.3	1.4	2.2	1.3	1.2
	Ottawa-Airport	1.8	1.9	1.9	2.2	2.1	1.8	2.0	1.9	1.5
MAE m/s	Mc-Tavish	3.2	1.4	1.4	3.3	1.4	1.4	3.0	1.3	1.2
	International Airport	1.5	1.5	1.5	1.4	1.4	1.4	1.5	1.5	1.4
	Pierre Elliott Trudeau	1.4	1.4	1.4	1.4	1.3	1.3	1.5	1.5	1.4
	St-Hubert	1.5	1.7	1.6	1.5	1.6	1.6	1.6	1.5	1.5
	Ste-anne-de-bellevue	1.7	1.6	1.6	1.7	1.6	1.6	1.6	1.6	1.5
	Ottawa-Urban	1.6	1.1	1.1	1.8	1.0	1.1	1.7	1.0	1.0
	Ottawa-Airport	1.4	1.4	1.5	1.7	1.6	1.3	1.4	1.4	1.2
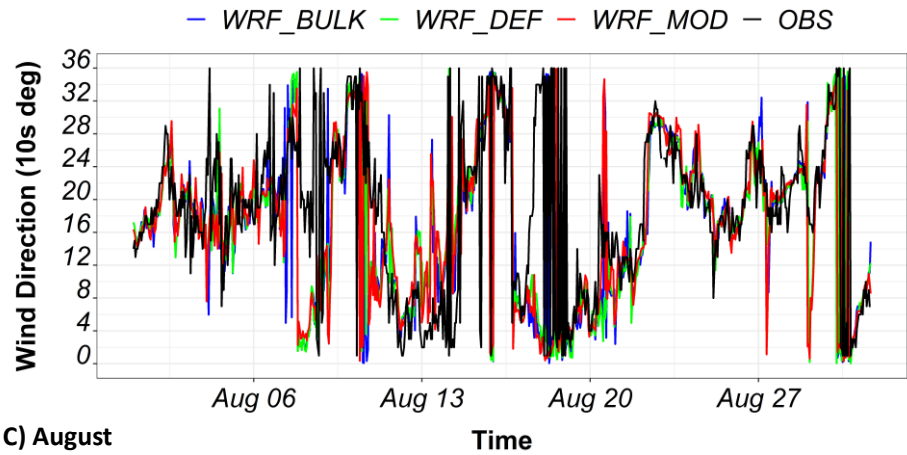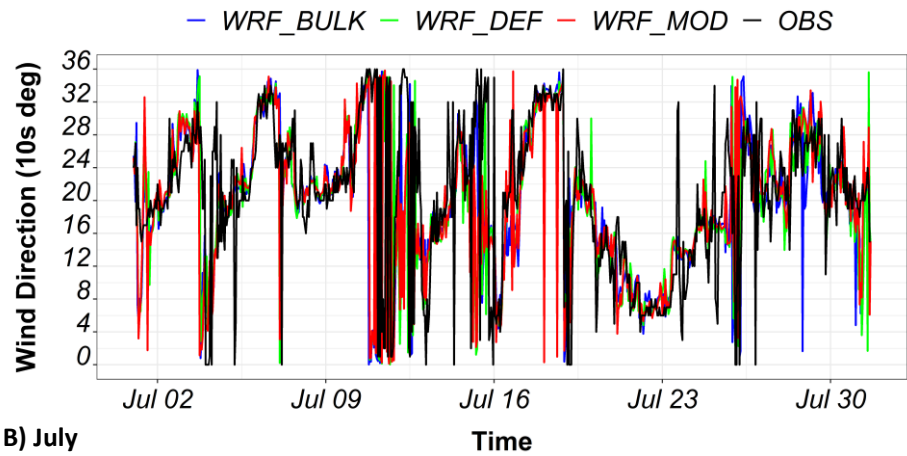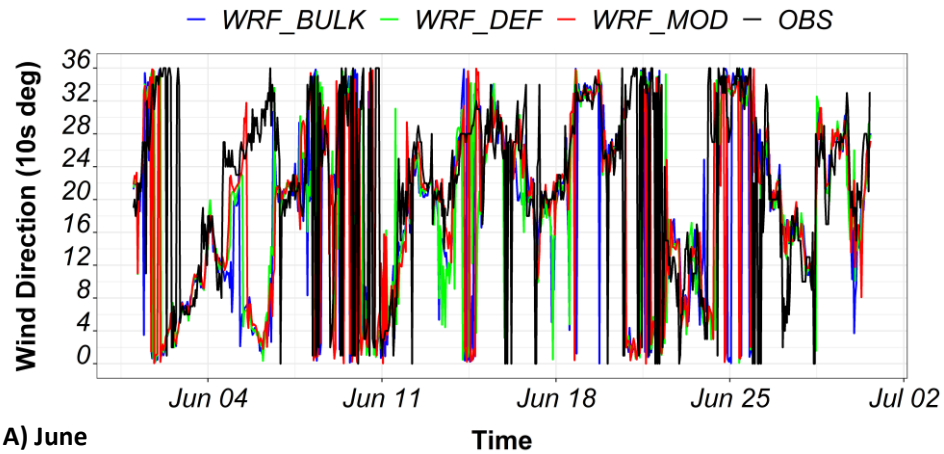
Figure 5-7 Time series of observed (black) and WRF modeled 10-m wind direction at the
Ottawa-Urban weather station in A) June, B) July, and C) August

The wind direction is always fluctuating with time, which is not easy to capture even in the measurements. In Figure 5-7, the wind direction results are plotted with the historical observations, and some large deviations can be observed between the simulation and the measurements. However, the simulation, in general, follows the variation in the observation. From the values of RMSE and MAE in Table 5-5, the MOD-BEP model still exhibits an obvious advantage in reproducing the wind-related variables.

Table 5-5 RMSE and MAE of the 3 months wind direction at 7 weather stations in Montreal and Ottawa

Months		June			July			August		
Models		DEF-BULK	DEF-BEP	MOD-BEP	DEF-BULK	DEF-BEP	MOD-BEP	DEF-BULK	DEF-BEP	MOD-BEP
RMSE °	Mc-Tavish	11.2	10.8	10.6	8.5	8.5	8.7	11.5	11.0	11.2
	International Airport	10.9	10.3	10.6	7.4	7.7	7.6	10.1	10.0	9.8
	Pierre Elliott Trudeau	9.7	9.8	9.9	6.7	6.3	6.5	8.5	8.8	9.2
	St-Hubert	10.1	10.2	9.6	6.3	6.8	6.8	9.9	9.2	9.5
	Ste-anne-de-bellevue	10.4	10.2	10.0	7.3	7.6	7.5	11.3	11.1	11.2
	Ottawa-Urban	13.9	12.8	13.3	8.1	8.2	8.8	11.8	11.6	11.6
	Ottawa-Airport	12.8	12.2	12.2	8.1	7.7	8.3	9.6	9.4	9.9
MAE °	Mc-Tavish	6.9	6.7	6.4	5.3	5.3	5.3	7.5	7.1	7.3
	International Airport	6.6	6.2	6.4	4.2	4.4	4.3	6.2	6.1	6.0
	Pierre Elliott Trudeau	5.8	5.8	5.8	3.8	3.8	3.8	5.3	5.4	5.6
	St-Hubert	5.8	5.8	5.4	3.6	3.9	3.8	5.8	5.4	5.7
	Ste-anne-de-bellevue	6.3	6.2	6.1	4.3	4.4	4.3	7.2	6.9	6.9
	Ottawa-Urban	8.8	8.0	8.1	5.1	5.1	5.3	7.5	7.2	7.3
	Ottawa-Airport	7.8	7.4	7.1	4.8	4.5	4.9	5.7	5.5	5.8

5.2.4 Accumulated precipitation

The precipitation data obtained from the weather stations in Montreal are daily data, while the data from the Ottawa weather stations are hourly data. The number of missing data in the historical weather data files is summarized in Table 5-6. For the weather stations in Montreal, there at least one day's missing data, and those missing data were filled with 0 mm precipitation by assuming no rain on those days.

Table 5-6 Number of missing data found in the weather station data files

Location	Time interval	June	July	August
Mc-Tavish	1 day	0	3	0
International Airport	1 day	0	1	0
Pierre Elliott Trudeau	1 day	1	0	1
St-Hubert	1 day	6	4	4
Ste-anne-de-bellevue	1 day	1	1	4
Ottawa-Urban	1 hour	1	0	0
Ottawa-Airport	1 hour	0	0	0

The accumulated precipitation is plotted in Figure 5-8, and through the time series curves in the plot, it is hard to figure out which model performs the best, because the models are performing quite differently at different times. For example, in June, the DEF-BULK curve is much closer to the observation curve than the other two models, while in July, the DEF-BEP and MOD-BEP models are much better than DEF-BULK. So, it seems the precipitation variable is quite sensitive to the models and the times to compare.

In Table 5-7, the total rain depths of different models at different weather stations are summarized. It can be noticed that sometimes the DEF-BULK and DEF-BEP model can be even better than the MOD-BEP model. But for the two weather stations in Ottawa, the MOD-BEP model performs the best in comparison to the other two models. That might be because only the land use land cover inputs around the Ottawa city are updated with the 2010 Canada land cover database. This also proves the importance to use the new land cover information to improve accuracy.
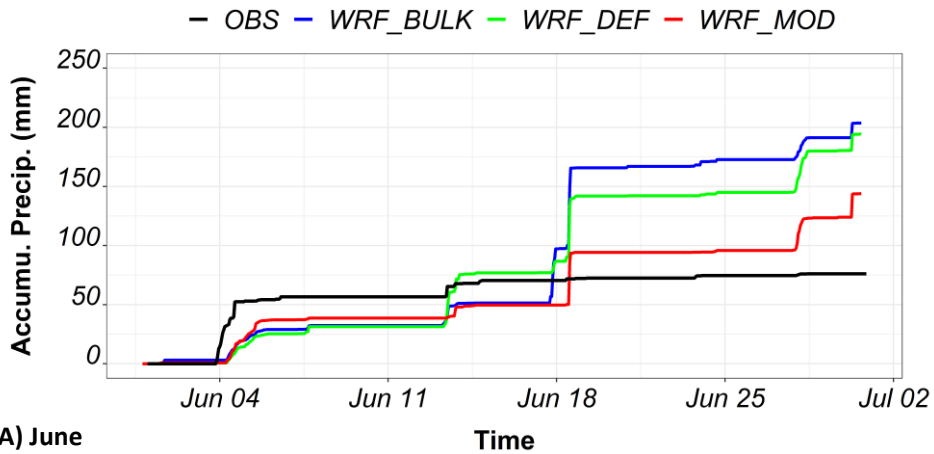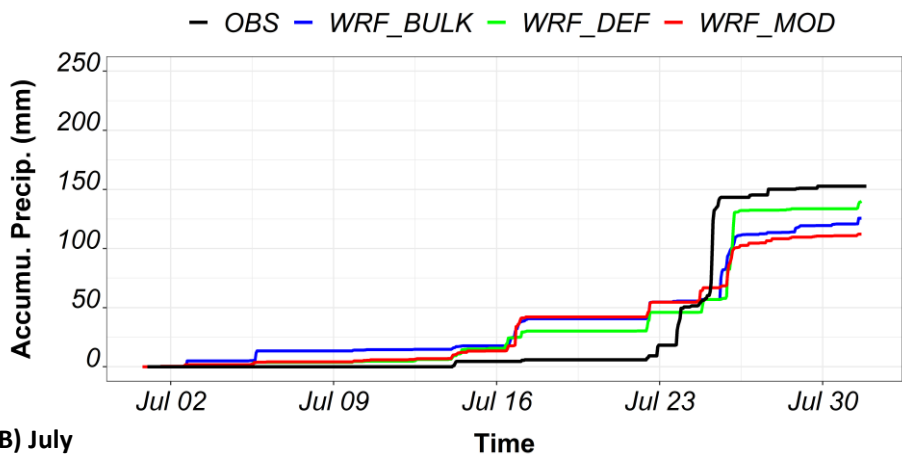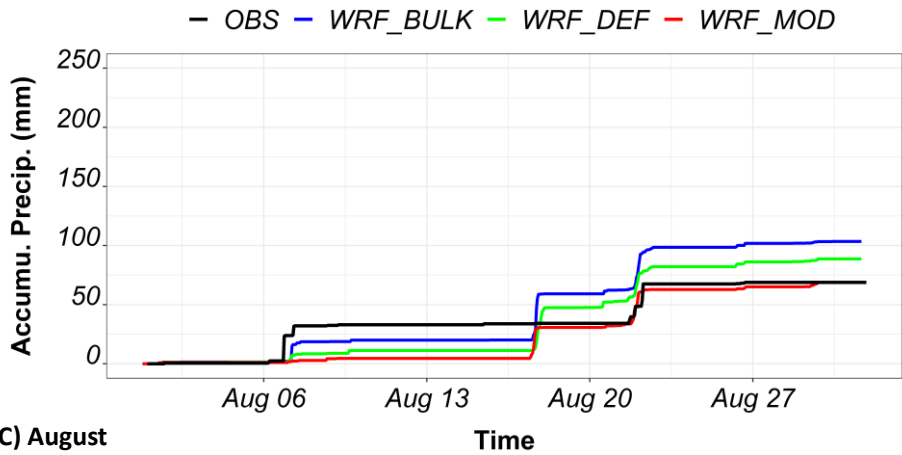
Figure 5-8 Time series of observed (black) and WRF modeled accumulated precipitation at the Ottawa-Urban weather station in A) June, B) July, and C) August

Table 5-7 Monthly accumulated precipitation at the 7-weather station in Montreal and Ottawa

Location	Data source	Accumulated precipitation mm		
		June	July	August
Mc-Tavish	Observation	86	80	54
	DEF-BULK	148	170	93
	DEF-BEP	124	110	92
	MOD-BEP	193	110	127
International Airport	Observation	82	98	66
	DEF-BULK	127	142	78
	DEF-BEP	159	116	87
	MOD-BEP	150	85	87
Pierre Elliott Trudeau	Observation	75	93	59
	DEF-BULK	126	135	80
	DEF-BEP	161	109	90
	MOD-BEP	143	89	91
St-Hubert	Observation	80	37	40
	DEF-BULK	148	144	87
	DEF-BEP	118	122	89
	MOD-BEP	161	106	82
Ste-anne-de-bellevue	Observation	71	60	53
	DEF-BULK	125	166	86
	DEF-BEP	141	65	106
	MOD-BEP	167	77	112
Ottawa-Urban	Observation	76	153	69
	DEF-BULK	191	121	103
	DEF-BEP	180	134	89
	MOD-BEP	124	111	69
Ottawa-Airport	Observation	70	171	98
	DEF-BULK	192	160	102
	DEF-BEP	175	112	91
	MOD-BEP	154	117	89

5.3. Summary

The WRF model (coupled to the Noah LSM) has been evaluated by performing three high spatial resolution numerical experiments (i.e., at 1 km horizontal grid spacing) during a three-month summertime period in 2018 over the city of Ottawa and surrounding rural areas. Results demonstrate that WRF can realistically reproduce the daily evolution of near-surface air temperature, wind speed, and relative humidity, but it was not able to reproduce properly the accumulated precipitation during June (i.e., it was considerably overestimated). The smallest

WRF-modeled mean absolute errors (MAEs) for 2-m air temperature were 1.4 °C, 1.5 °C, and 1.5 °C during June, July, and August, respectively (see Table 5-2 for more details). Concerning near-surface wind speed, the smallest WRF-modeled MAE was 1.1 m/s during both June and July, and 1 m/s during August, respectively (see Table 5-4 for more details). Regarding near-surface relative humidity, the smallest WRF-modeled MAEs were 9.6 %, 9.4 %, and 8.7 % during June, July, and August, respectively (see Table 5-3 for more details).

Some of the novel aspects of this study are as follows:

- WRF model is evaluated over a longer timeframe (June-August 2018) than the previous studies where the model is evaluated over one or two weeks. The evaluation period also covers the duration of an extreme heat spell event lasting June 30 - July 6, 2018, because of which over 100 people died in this region. The evaluation is also more rigorously performed by comparing the weather observations at multiple locations (7 in total) and by considering climate parameters such as precipitation, relative humidity and wind speed that have not been commonly included in previous WRF model validation studies.

- The use of two different urban parameterization schemes on WRF model accuracy in modelling urban climate in this region has been evaluated and it is found that the use of an advanced urban parameterization scheme i.e., multilayer UCM in the WRF model results in a more accurate description of near-surface wind speed, precipitation, and relative humidity.

- The impact of the use of a more accurate description of urban land cover in the WRF model on its accuracy has been evaluated and found that it results in more accurate modelling of near-surface temperature, wind speed, precipitation, and relative humidity in the region.

- One of the important findings of this study is that precipitation is found to be very sensitive to the use of advanced urban parameterization schemes, and more accurate depiction of urban areas in the model, which is also an important finding for more accurate modelling of precipitation and its extremes in this region.

Chapter 6 Overheating Assessment by Climate Modelling - Added Value of High-resolution Climate Models

Previous studies have used high-resolution climate datasets for building simulations, while they only focused on studying the building's impact on the outdoor environment and/or evaluating the building energy consumptions. This study proposes to use the high-resolution climate simulation completed with a convection permitting model (CPM) for building overheating studies. The major difference between the CPMs and traditional coarse-resolution regional climate models (RCMs) have been elaborated in section 2.3.3, while the added value of CPMs over RCMs has not yet been quantified in a building overheating context. The study in this chapter fills this research gap by comparing two sets of simulations of an extreme summer season recorded in the Ottawa and Montreal region of Canada. The first set of simulations is conducted at a typical RCM spatial scale (25 km), and the second at a CPM scale (1 km). The results from this study provide evidence and novel information that help confirm the importance of using CPMs when assessing overheating in buildings located in urban areas. The rest of the chapter is organized as follows: the details of the study area, data, and methods are provided in section 6.1, followed by results and discussion in section 6.2, and conclusions in section 6.3.

6.1. Methodology

6.1.1 Study area and evaluation period

The study area comprises two Canadian cities: Ottawa, in the province of Ontario, and Montreal in the province of Quebec (Figure 6-1). The region encompassing these cities experienced an extreme heat event (EHE) from June 30 – July 05, 2018, resulting in around 70-100 heat-related deaths in both provinces (ECCC, 2019). During this EHE, parts of Ottawa reached an all-time highest humidex (Environment and Climate Change Canada, 2021) value of 47, and the city of Montreal's public health office recorded 66 heat-related deaths in the city (Lamothe et al., 2019). The city-scale overheating of the two cities is evaluated over the five months of Summer 2018 (May 01 – September 30), encompassing the EHE.

The layout of the two cities used in the WRF simulations can be seen from Figure 6-2, which shows the distribution of the land use and land cover (LULC) surrounding the two cities from the 2015 North American Land Change Monitoring System (NALCMS) dataset ("North American

Land Change Monitoring System (NALCMS) dataset, 2015," 2015). The urban areas are represented in the WRF model by the means of a single urban class because our previous work showed that using more than one category of urban land cover in the cities didn't add any value in the WRF model in terms of its accuracy in modelling urban climate parameters in these cities. The Ottawa River passes through the north of the city. On the other hand, the layout of the urban area in Montreal is quite different. The center of the city is located on Montreal Island, which is surrounded by rivers. There are also several small agglomerations of urban areas outside the island. Both cities are surrounded by croplands and forested areas. The study area normally experiences a semi-continental climate, with warm, humid summers and cold winters.
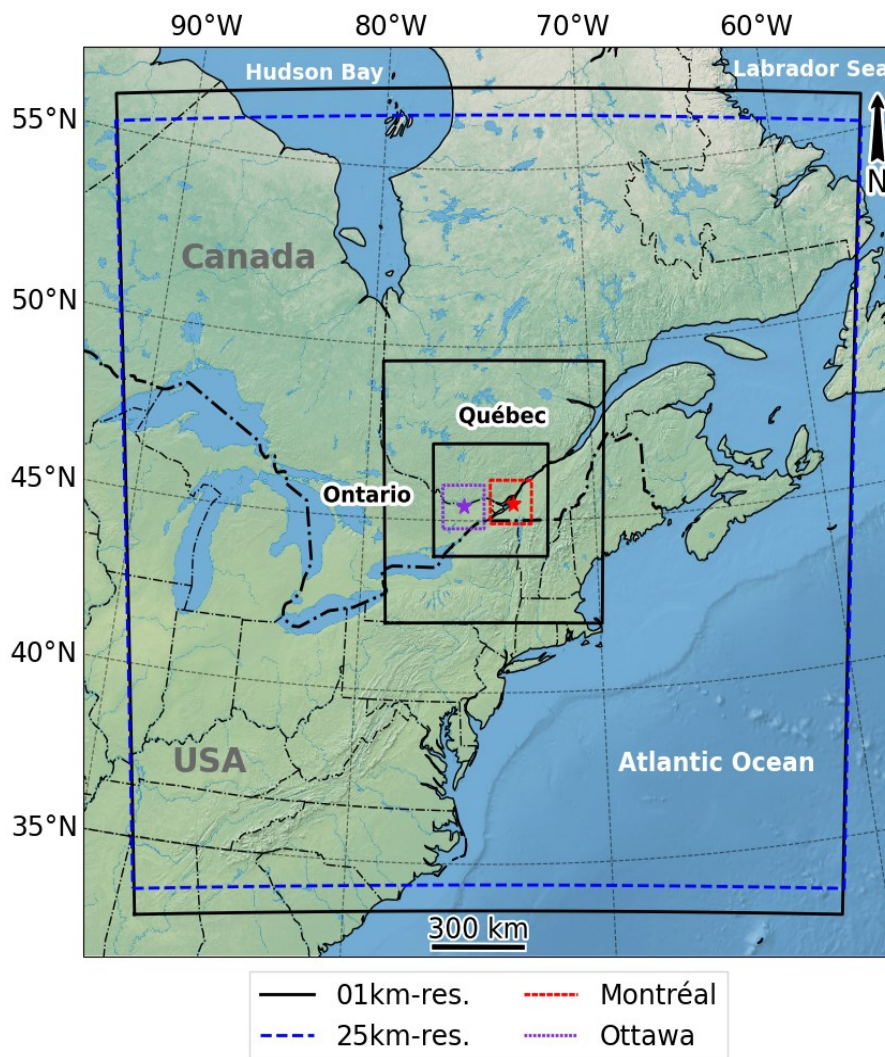
Figure 6-1 The numerical domain in WRF simulation surrounding the geographical location of the study area and the two cities, Ottawa and Montreal.
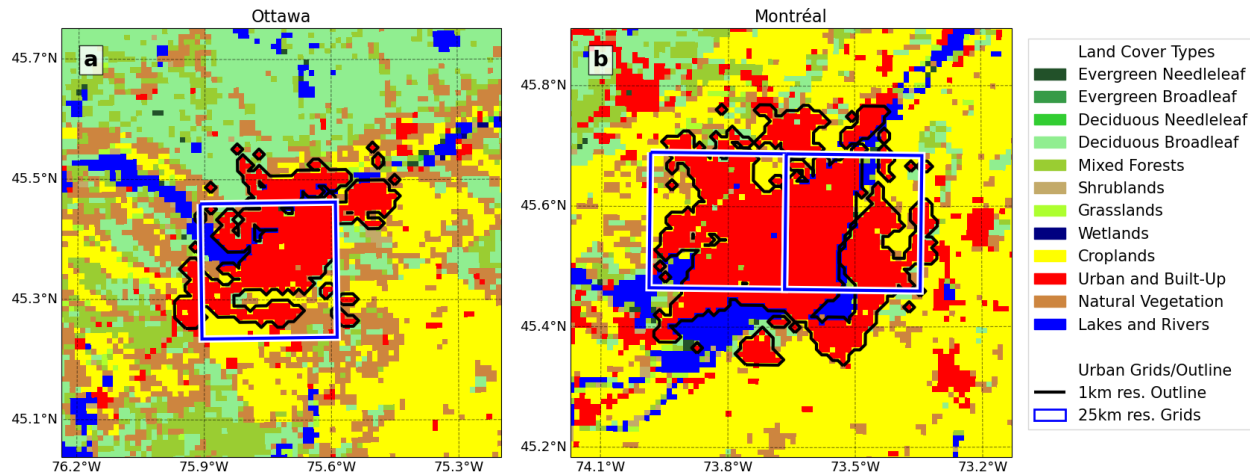
Figure 6-2 Land use and land cover (LULC) around a) Ottawa and b) Montreal cities and the outlines of the urban area considered in 1 and 25 km resolution climate simulations.

6.1.2 Weather Research and Forecasting (WRF) configurations

The regional climate model used in this study is the Weather Research and Forecasting (WRF) model (Skamarock et al., 2019). The National Centers for Environmental Prediction (NCEP) North American Regional Reanalysis (NARR) product # ds608.0 (National Centers for Environmental Prediction, National Weather Service, NOAA, U.S. Department of Commerce, 2005) are used as the initial and boundary conditions for the WRF simulations. The setup of the simulations completed at a 1 km-resolution consists of three two-way nested domains with 276×296, 250×283, and 391×364 grid points at a grid distance of 9, 3, and 1 km, respectively. For simulations completed at the 25 km-resolution, only one non-nested domain is used with 100×100 grid points, covering a similar area (shown as the dotted blue line in Figure 6-1) as the first parent domain in the simulation completed at a 1 km-resolution (shown as the solid black line in Figure 6-1). The two-way nested simulation can exchange the simulation results between the parent domains and subdomains, so there exists great difference in the time costs between the simulations of the two different resolutions: the 1 km resolution simulation can take around 50 times of the computer time for the 25 km resolution simulation. The domains for both set of simulations are centered in the middle of the Ottawa and Montreal cities (74.63°W, 45.47°N).

A series of WRF simulations were conducted in our previous study to evaluate the performances of using different urban parametrizations and LULC datasets and identify optimum settings for the modelling of urban climate in the two cities (Gaur et al., 2021). The model configuration listed in Table 6-1 simulated urban climate in the cities with the best accuracy is therefore adopted in this

study as well. Note that the cumulus parameterization is only activated for simulations completed at the 25 km resolution and the first domain with a grid spacing of 9 km in the simulation completed at the 1 km resolution. In comparison, the model of the second and third domains with a grid spacing of 3 km and 1 km can resolve the deep convection as the grids are smaller than 4 km.

Table 6-1 Physical parameterization schemes in WRF simulations.

Category	Physical parameterization scheme
Microphysics	WRF Single-Moment 3-class scheme (WSM3) (Hong et al., 2004)
Land Surface model	NOAH (Chen and Dudhia, 2001a)
Planetary boundary layer	Two-order closure Mellor-Yamada-Janjic (Janjić, 1994)
Shortwave radiation	Dudhia scheme (Dudhia, 1989)
Longwave radiation	Rapid Radiative Transfer Model (RRTM) (Mlawer et al., 1997)
Cumulus parameterization	Kain-Fritsch scheme (Kain, 2004) for domains of grid size > 4 km
Advection scheme	Runge-Kutta 3rd order
Land cover classification	MODIS 21-category
Number of vertical layers	40
Urban canopy model	Multilayer UCM building effect parametrization (BEP) (Martilli et al., 2002)

6.1.3 Climate observations

Table 6-2 Details of climate gauging stations for WRF model evaluation.

Short Name	Full Name (Province)	Latitude (°N)	Longitude (°E)	Local LULC type
GATI	Ottawa Gatineau A (Québec)	45.52	-75.56	Croplands
OTUB	Ottawa Cda Rcs (Ontario)	45.38	-75.72	Urban and Built-up
OTAP	Ottawa Intl A (Ontario)	45.32	-75.67	Urban and Built-up
MIRA	Montreal Mirabel Intl A (Québec)	45.68	-74.04	Urban and Built-up
SHUB	Montreal/St-Hubert (Québec)	45.52	-73.42	Urban and Built-up
MCTA	McTavish (Québec)	45.50	-73.58	Urban and Built-up
PETR	Montreal/Pierre Elliott Trudeau Intl (Québec)	45.47	-73.75	Croplands
INTL	Montreal Intl A (Québec)	45.47	-73.74	Urban and Built-up
ANNE	Ste-Anne-De-Bellevue 1(Québec)	45.43	-73.93	Croplands

The WRF model is validated over the time of analysis, i.e., May-September 2018 with regards to its performance in simulating observed values of climate variables: air temperature, and wind speed, as recorded at Environment and Climate Change Canada (ECCC) operated climate gauging stations surrounding the cities of Ottawa and Montreal. The observations of hourly climate are collected from ECCC historical climate database (ECCC, 2021). Nine climate gauging stations are

located around the two cities and contain the hourly observations of the variables that are used for analysis. These ECCC stations and their local LULC types are listed in Table 6-2.

6.1.4 Building simulation model

Previous studies have found that most of the heat-related deaths in the 2018 EHE happened in residential buildings (Lamothe et al., 2019). In this study, a typical residential building type: a single-detached home, was selected for the assessment. A building model of the archetype single-detached home (Parekh, 2012), shown in Figure 6-3, was prepared in EnergyPlus (U.S. Department of Energy's and Building Technologies Office, 2020). The building model has comprised of four thermal zones: the underground basement, living room on the first floor, bedroom on the second floor, and an attic on the top of the building. The total footprint area of the building was 80.20 m^2. In Table 6-3, the building envelope configurations are listed, following the current construction practice (National Research Council of Canada, 2015) for homes. The internal heat gains and schedules also follow recommendations taken from the National Building Code of Canada (National Research Council of Canada, 2015), with 5 W/m^2 for lighting, 5 W/m^2 for equipment, and 500 $W/person$ for the servicing of hot water. The occupancy of the building was considered for a typical family of three people. The building model was naturally ventilated for the evaluation of the potential overheating under a free-running condition following the requirements of the overheating guidelines (CIBSE, 2011). Natural ventilation (open window) was available when the outdoor air temperature was lower than the indoor air temperature, and the indoor air temperature was higher than 26°C (National Research Council of Canada, 2015). The natural ventilation of the building is simulated using the Airflow Network model, and the infiltration of the building envelop is also estimated by the same model with the crack air flow equation. The occupant schedules for the living room were defined as 7:00 to 21:00 hours and 22:00 to 6:00 hours for the bedroom according to the most recent version of the National Energy Code of Canada for Buildings (NECB) (National Research Council of Canada, 2017).

The climate inputs for EnergyPlus simulations are prepared from WRF outputs from (1 or 25 km resolution) grids closest to the locations of interest. The climate variables considered from WRF simulations are dry-bulb air temperature, dew point temperature, relative humidity, atmospheric station pressure, global horizontal radiation, wind speed and wind direction, cloud fraction, rainfall and snow depth. In addition, the global horizontal radiation is used to estimate direct horizontal

irradiance, direct normal irradiance, and diffused horizontal irradiance using widely used methods (Gaur et al., 2019).

Table 6-3 Envelope components for building model of archetype single-detached home

Component	Material and properties
Window	Double clear with Low-E (U = 1.58; VT = 73%; SHGC = 0.67, WWR =15%)
Roof	Asphalt shingles with attic insulation (RSI 8.2)
Walls	Wood stud with Vinyl cladding (RSI 4.5)
Basement Wall	Insulated concrete (RSI 1.7)
Basement Slab	Insulated concrete (RSI 1.6)
Blinds	Internal blinds
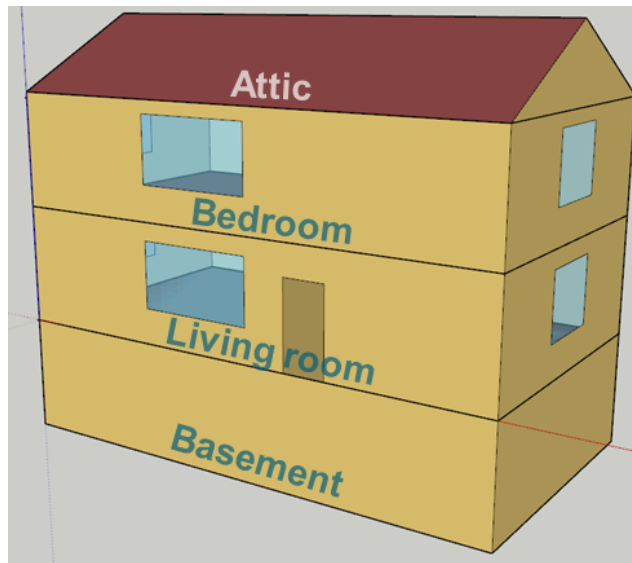
Figure 6-3 Archetype single-detached home building model used for indoor overheating analysis using EnergyPlus.

6.1.5 Overheating assessment

There is no universal definition and criteria for defining EHE for overheating assessments (Laouadi et al., 2020a). A literature review of previous studies has shown that a fixed or adaptive temperature threshold value can be chosen to identify overheating events (Laouadi et al., 2020a; Lomas and Giridharan, 2012; Lomas and Porritt, 2017). In this study, a fixed temperature threshold was used for overheating assessment since it has been widely used in previous overheating studies, standards, and codes, and is more suitable for our application, i.e., to compare climate simulations at multiple spatial resolutions. Following the practical guidelines of extreme weather file selection (CIBSE, 2014) and indoor overheating evaluation (CIBSE, 2011), the threshold value for outdoor

overheating was chosen as 28°C, and for indoor overheating, the used temperature thresholds were 28°C for the living room, and 26°C for the bedroom. Furthermore, operative temperature (T_{opt}), which better reflects the thermal sensation of occupants, was used for indoor overheating evaluation. These values have also been adopted by other standards, codes and guidelines (Department of Health, 2007b; Zero Carbon Hub, 2015c, 2015b).

The hours with air temperature or an indoor operative temperature higher than the above thresholds were defined as overheating hours (OH) and were used to calculate the percentage of overheating (POH) durations using the total number of hours over the evaluation period (e.g., 3672 h in total for May-September 2018). To segregate indoor overheating in different building spaces, the percentage of overheating hours was calculated for the daytime and nighttime, assuming occupancy of the living room in the daytime (7 AM to 9 PM) and bedrooms in the nighttime (10 PM to 6 AM). The mean air/operative temperature and maximum air/operative temperature were also calculated to quantify overheating.

6.2. Results and discussions

6.2.1 Accuracy of simulations completed at 25 and 1 km grid resolution

The accuracy of the modelled near-surface climate variables from simulations completed at 25 and 1 km resolution was quantified by comparing the simulated data with the hourly measurements from nine weather stations surrounding the Ottawa and Montreal cities. The root means square error (RMSE), mean absolute error (MAE) and mean bias error (MBE) associated with the simulation results were calculated using Eqs. (6-1) ~ (6-3).

$$RMSE = \sqrt{\frac{\sum_{i=1}^{N}(x_{m,i} - x_{o,i})^2}{N}} \qquad (6-1)$$

$$MAE = \frac{\sum_{i=1}^{N}|x_{m,i} - x_{o,i}|}{N} \qquad (6-2)$$

$$MBE = \frac{\sum_{i=1}^{N}(x_{m,i} - x_{o,i})}{N} \qquad (6-3)$$

where i corresponds to each time step in the evaluation, N is the total number of hours, and $x_{m,i}$ and $x_{o,i}$ are the simulated and measured values, respectively.

From the results summarized in Table 6-4, RMSE and MAE associated with simulations completed at a 1 km resolution are lower than those at a 25 km resolution for both air temperature

and wind speed. The MBE of air temperature from simulations completed at a 1 km and 25 km resolution are negative, indicating that air temperatures are underestimated for both simulations. The MBE ranged from -0.4 ºC to -2.0 ºC for temperatures derived from simulations of 1 km resolution and -1.4 ºC to -2.6 ºC for those at a 25 km resolution, showing the magnitude of underestimation is lower for simulations completed in at the 1 km resolution than those at the 25 km resolution. The MBE of wind speed varies between negative and positive values for different weather stations, reflecting the complex and highly variable nature of the wind speed variable. The MBE of wind speed from the 1 km resolution model varies between -1.4 m/s to 1 m/s, whereas MBE from the 25 km resolution model varies from -1.3 m/s to 1.5 m/s, indicating higher accuracy of simulations completed at 1 km as compared to 25 km resolution.

Table 6-4 Root Mean Square Error (RMSE), Mean Absolute Error (MAE), and Mean Bias Error (MBE) of the simulated near-surface variables: air temperature and wind speed.

Criteria	Variables	Resolution	GATI	OTUB	OTAP	MIRA	SHUB	MCTA	PETR	INTL	ANNE	Avg.
RMSE	Air Temperature (°C)	1 km	2.6	2.5	2.4	2.5	2.4	2.6	3.3	3.0	3.2	2.7
		25 km	3.1	3.0	2.9	2.7	2.8	3.4	3.5	3.4	2.9	3.1
	Wind Speed (m/s)	1 km	1.7	1.5	1.6	1.3	1.9	1.6	1.7	2.2	1.7	1.7
		25 km	2.1	1.4	1.7	2.3	1.9	1.9	1.7	2.1	2.4	2.0
MAE	Air Temperature (°C)	1 km	2.0	2.0	1.9	1.9	1.9	2.1	2.6	2.4	2.6	2.2
		25 km	2.5	2.4	2.3	2.2	2.3	2.8	2.9	2.8	2.4	2.5
	Wind Speed (m/s)	1 km	1.3	1.1	1.2	1.0	1.4	1.3	1.3	1.8	1.3	1.3
		25 km	1.6	1.1	1.3	1.8	1.5	1.5	1.3	1.7	1.9	1.5
MBE	Air Temperature (°C)	1 km	-0.4	-0.8	-0.8	-0.6	-0.8	-1.3	-2.0	-1.8	-1.9	-1.1
		25 km	-1.9	-1.9	-1.8	-1.4	-1.6	-2.4	-2.6	-2.5	-1.7	-2.0
	Wind Speed (m/s)	1 km	0.6	0.3	-0.6	0.3	-0.8	1.0	-0.4	-1.4	0.7	0.0
		25 km	1.1	-0.1	-0.7	1.5	-1.0	1.2	-0.8	-1.3	1.5	0.2

The observed hourly temperatures were also compared with simulation results completed at 1 and 25 km resolution using scatterplots and linear regression analysis. The results are presented for all nine climate gauging stations in Table 6-2. The simulation results for the 1 km resolution and trend line (in red) are found to be better aligned with the observations than the temperatures from simulations completed at a 25 km resolution for eight out of nine stations. For one station (ANNE), the results are similar. The distribution of the scatter points illustrates that hourly temperatures from simulations completed at a 25 km resolution are lower than those from 1 km resolution,

especially at higher temperatures. This can be seen from a comparison of the linear regression lines of simulations completed at a 25 km resolution with a greater deviation from observations at higher temperatures than lower temperatures. On the other hand, simulations completed at a 1 km resolution demonstrate a lower level of errors under extreme temperatures showing their higher utility for overheating assessments.

The regression coefficients of both sets of simulations are summarized in Table 6-5. The simulations completed at 1 km have a higher coefficient of determination (R^2) on average of 0.78 then the 25 km resolution with R^2 of 0.73, showing the 1 km resolution model has a stronger capability for simulating the variance in air temperature. The simulations completed at a 1 km resolution show a stronger positive correlation with the observations (0.97), which is significantly better than those at a 25 km resolution (0.93). Also, the simulations completed at 1 km resolution exhibit a lower level of underestimation in air temperature with the averaged intercept of -0.5 compared to the value of -0.64 from the simulations completed at 25 km resolution.

Table 6-5 Linear regression coefficients between observations and simulations at nine climate gauging stations.

Linear regression coefficients	Station	GATI	OTUB	OTAP	MIRA	SHUB	MCTA	PETR	INTL	ANNE	Average
Slope	1 km res.	0.96	1.03	0.97	0.98	0.94	0.98	0.96	0.93	0.96	0.97
	25 km res.	0.87	0.93	0.91	0.93	0.91	0.98	0.96	0.95	0.96	0.93
Intercept	1 km res.	0.28	-1.32	-0.11	-0.23	0.34	-0.84	-1.16	-0.33	-1.16	-0.50
	25 km res.	0.48	-0.52	0.00	-0.07	0.22	-1.94	-1.68	-1.38	-0.88	-0.64
R-squared	1 km res.	0.84	0.82	0.85	0.83	0.85	0.67	0.78	0.72	0.70	0.78
	25 km res.	0.76	0.75	0.78	0.79	0.78	0.62	0.64	0.66	0.75	0.73
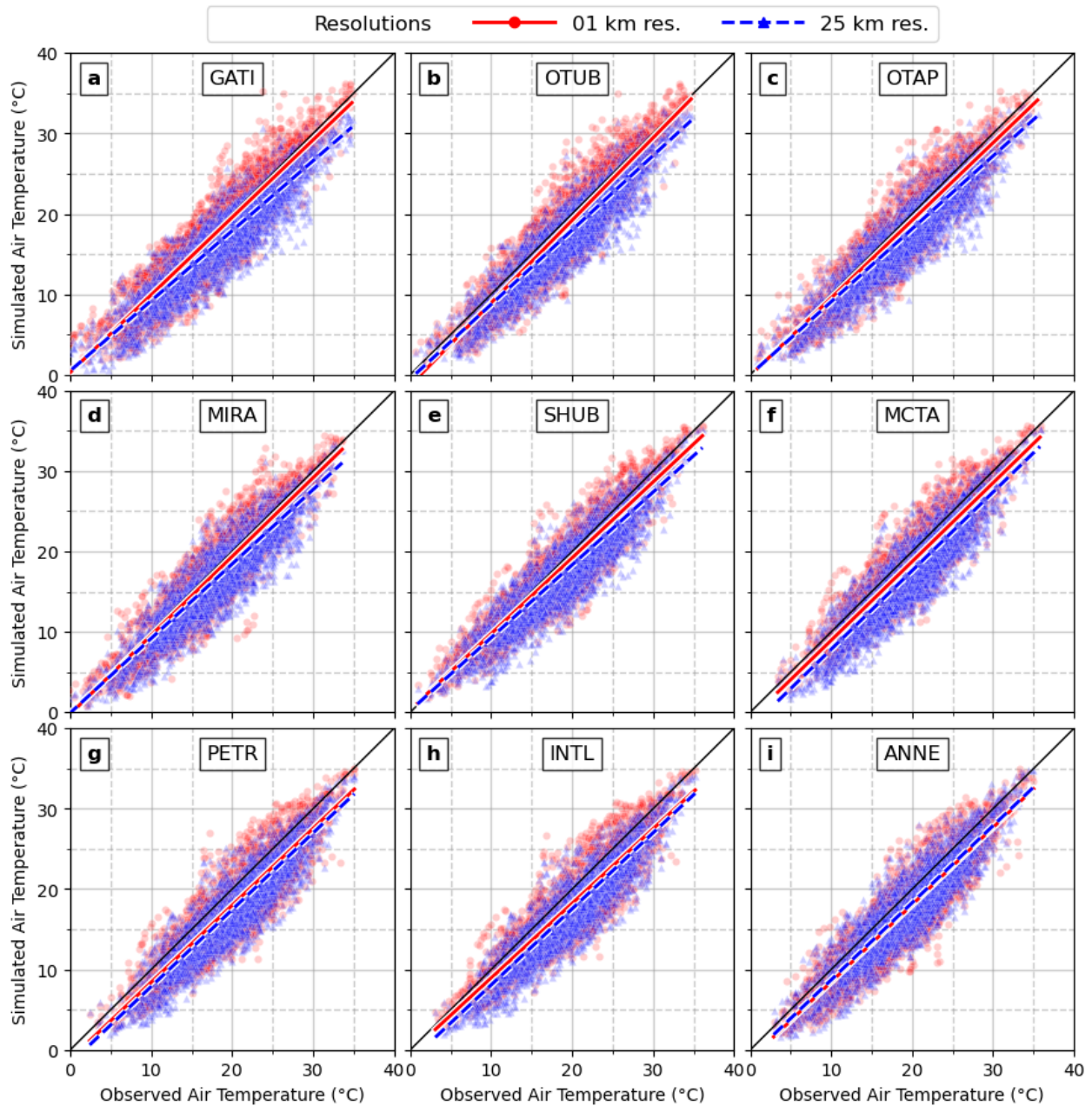
Figure 6-4 Comparison of the simulated and measured air temperatures from the nine weather stations during the five months (May 01 - September 30) in the summer of 2018. The red solid lines show the correlation between the observation and the WRF simulations completed at 1 km resolution, and the blue dashed lines show the correlation between the observation and the WRF simulations completed at 25 km resolution.

6.2.2 Outdoor overheating from simulations completed at 1 and 25 km grid resolution

In addition to being more accurate, the simulations completed at 1 km resolution can capture the spatial distribution of temperature extremes and overheating better within and around the two cities than those at 25 km resolution. This is clear from Table 6-5, which shows the distribution of mean air temperature over May-September 2018 obtained from simulations completed at 1 and 25 km resolution. The spatial variation of temperature is better represented in the simulations completed at 1 km resolution, whereas the urban extents of the Ottawa (Montreal) city are encompassed by one (two) simulation completed at 25 km resolution grids. Therefore, urban temperatures, and resulting overheating, are not properly captured by the simulations completed at 25 km resolution. Moreover, the urban-rural differences in climate are not well captured. For example, the lower temperatures over water bodies are not well captured in simulations completed at 25 km resolution, whereas they are better captured in simulations completed at 1 km resolution.

The temperatures, their extremes, and resulting overheating are generally underpredicted in simulations completed at 25 km resolution over the land areas compared to simulations completed at 1 km resolution. The difference in mean air temperature ($T_{air,mean}$), maximum air temperature ($T_{air,max}$) and overheating hours above 28°C ($OH_{28°C}$) between simulations completed at 1 and 25 km resolution are shown in Figure 6-6. For the $T_{air,mean}$ (Figure 6-6 a, d) over May-September 2018, the magnitude of underprediction can be up to 2°C. The underprediction in the case of $T_{air,max}$ can be up to 3°C. Finally, the total number of overheating hours are also severely underpredicted (up to 200 hours over five months) in the simulations completed at 25 km resolution as compared to the results simulations completed at 1 km resolution. These results demonstrate that simulations completed at 1 km resolution are more suited to capture the variations in extreme temperatures and the associated overheating conditions than those at 25 km resolution.
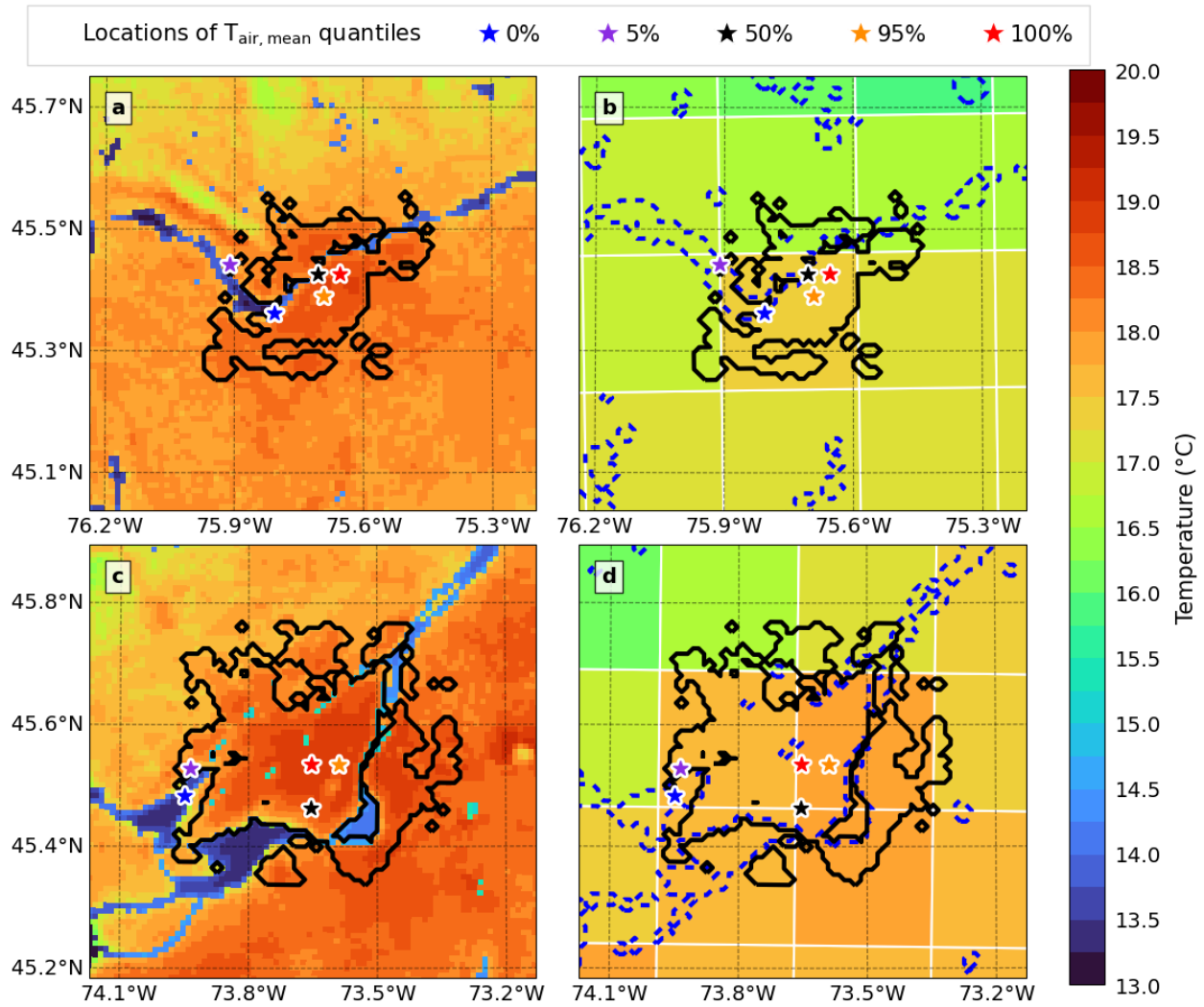
Figure 6-5 Modelled air temperature distribution averaged over the five months (May - September 2018) around the two cities: Ottawa (a,b) and Montreal (c,d) from simulations completed at 1 km resolution (a,c), and 25 km resolution (b,d).

To further investigate the differences in simulated overheating over urban areas from the two simulation groups, five grids from simulations completed at a 1 km resolution were selected in each city for assessment. These grids correspond to 0, 5, 50, 95, and 100th quantiles of simulated mean air temperature over the Summer of 2018 from simulations completed at a 1 km resolution. Hereafter, these grids are referred to the city names (Ottawa or Montreal), data source (fine or coarse resolution results), and quantile values associated with the grid. For example, OF_0 denotes the Ottawa Fine resolution grid with the 0th quantile value in terms of mean temperature. Similarly, the 25 km grid associated with these 1 km grids is referred to the city names (Ottawa or Montreal)

and data source (fine or coarse resolution results). For example, OC refers to the Ottawa Coarse grid case. In the case of Montreal, the two grids are named as MC_W (Montreal Coarse grid located on the West) and MC_E (Montreal Coarse grid located on the East). The locations of these representative grids are shown in Figure 6-5 (1 km simulation grids) and Figure 6-2 (25 km simulation grids). In the case of Ottawa, all selected 1 km grids fall within one 25 km grid, whereas in the case of Montreal, two 1 km grids are located within MC_W and three 1 km grids are in MC_E.
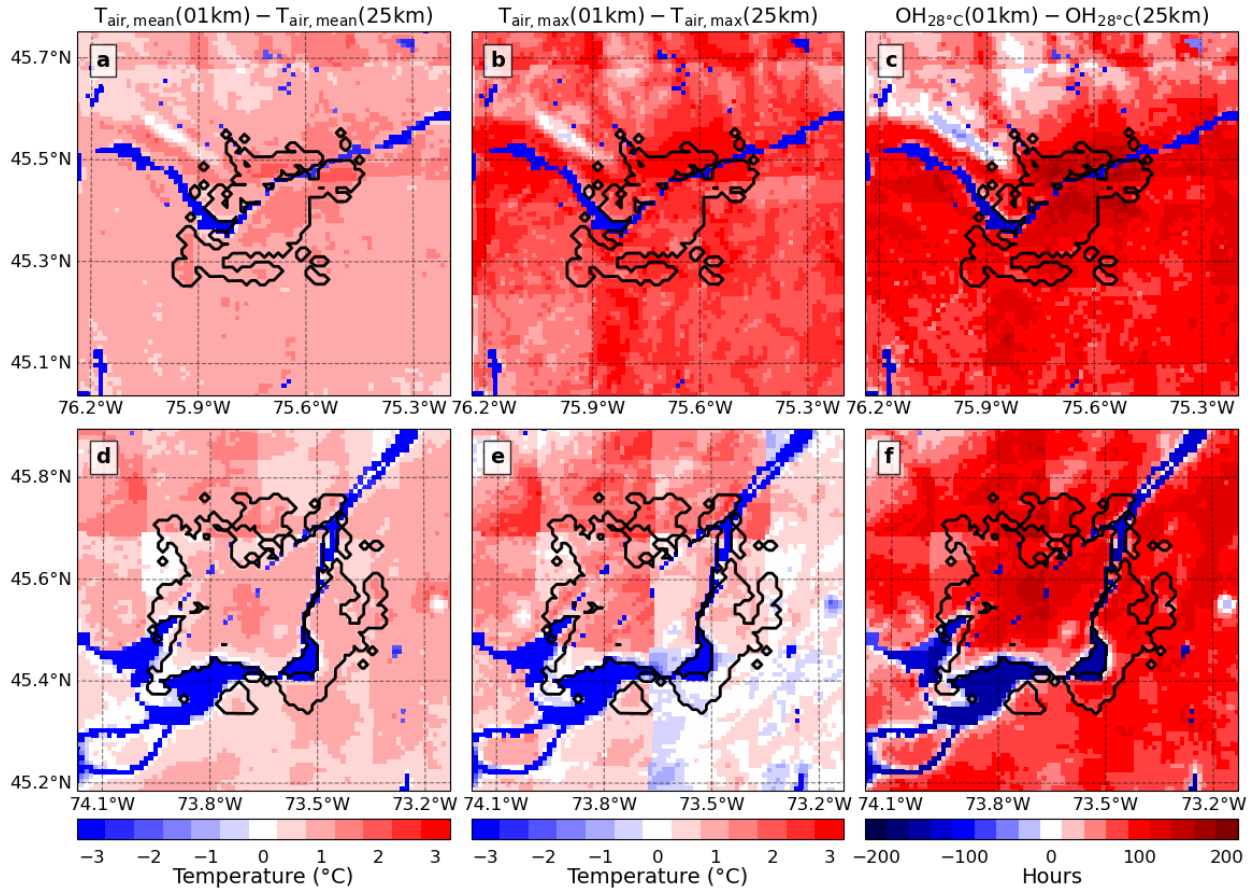
Figure 6-6 The difference in simulation results completed at 1 km and 25 km grid resolutions over Ottawa (a, b, c) and Montreal (d, e, f) in terms of mean air temperature (a, d), maximum air temperature (b, e) and the number of overheating hours (c, f).

The mean ($T_{air,mean}$) and maximum air temperatures ($T_{air,max}$), percentage of overheating hours over 28ºC ($POH_{28° C}$), and mean wind speed (WS_{mean}) for the representative grids are summarized in Figure 6-6. The results show that the mean and extremes of temperature and overheating conditions are highly underestimated in simulations completed at a 25 km resolution. The number of the overheating hours at the 50th percentile 1 km simulation grid is almost twice

the value of that at the 25 km simulation grid. In fact, for both cities, the mean and extremes temperatures and overheating hours from simulations completed at a 25 km resolution are always lower than the values associated with the 5th percentile 1 km simulation grid, which means that only 5% of 1 km simulation grids have lower mean and extremes temperatures, and overheating hours than the 25 km simulation grids. This is also true for the wind speeds where none of the 1 km grids in Ottawa and less than 5% of 1 km simulation grids in Montreal are found to have lower wind speeds than simulations completed at a 25 km resolution.

Table 6-6 Summary of the outdoor thermal conditions at representative urban grids for simulations completed at 1 km and 25 km grid resolution.

Climate statistic	Ottawa grids						Montreal grids						
	OC	OF_0	OF_5	OF_{50}	OF_{95}	OF_{100}	MC_W	MC_E	MF_0	MF_5	MF_{50}	MF_{95}	MF_{100}
$T_{air,mean}$ ($°C$)	17.3	13.8	17.9	18.4	18.7	18.8	17.5	17.8	13.4	17.7	18.5	18.9	19.0
$T_{air,mean}^{day}$ ($°C$)	19.2	15.0	19.8	20.8	21.0	21.1	19.4	19.7	14.3	19.9	20.7	20.9	21.1
$T_{air,mean}^{night}$ ($°C$)	14.1	11.8	14.8	14.5	14.9	15.0	14.4	14.6	12.0	14.1	15.0	15.6	15.5
$T_{air,max}$ ($°C$)	33.6	25.1	34.9	36.3	36.1	36.1	34.0	35.3	23.8	35.0	35.2	35.9	35.9
$POH_{28°C}$ (%)	3.3	0.0	4.5	7.0	7.1	7.5	3.2	3.8	0.0	4.1	6.0	6.6	7.1
WS_{mean} (m/s)	2.9	2.6	2.6	2.3	2.3	2.2	2.8	2.9	3.4	2.2	2.6	2.7	2.4

The hourly distribution of temperatures from simulations completed at a 1 and 25 km resolution and their difference over the analysis time from May 1 to September 30, 2018, is presented in Figure 6-7 and Figure 6-8, respectively, for the 50th percentile location. Figure 6-7 illustrates that both simulations completed at 1 and 25 km resolutions can capture the much higher temperature that occurred during the EHE of June 30 – July 5, 2018, than other days during the evaluated 5 months.
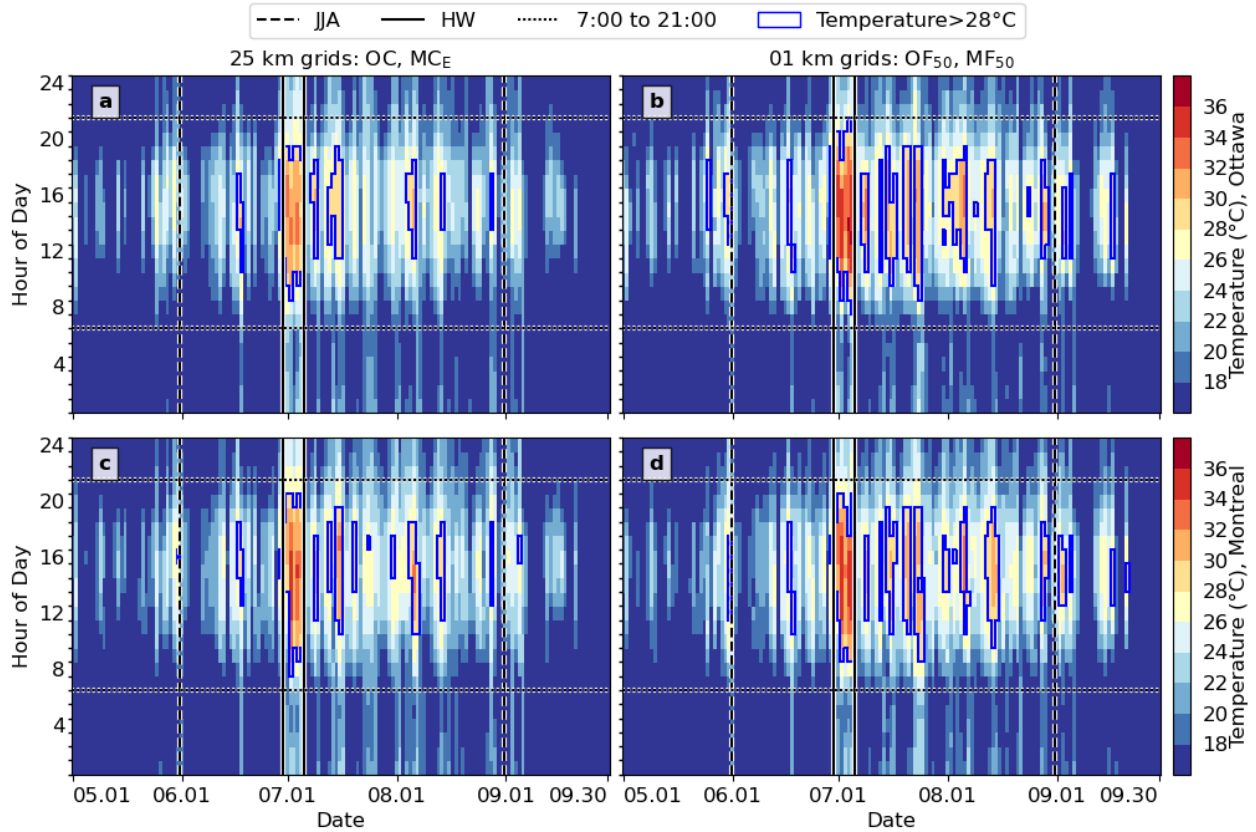
Figure 6-7 The hourly distribution of the outdoor air temperature of simulations completed at 1 and 25 km grid resolution at 50th percentile urban location in Ottawa and Montreal. (HW: heatwave period from June 30 to July 5, 2018, shown with vertical solid lines; JJA: June, July and August shown with vertical dashed lines)

However, Figure 6-8 makes it clear that the intensity of the extreme event is underestimated in the simulations completed at a 25 km resolution, as found in the previous results. For example, during the five months, 69% of hours in Ottawa and 75% of hours in Montreal have a higher temperature than the simulations completed at a 25 km resolution. Another important observation from Figure 8 is that the underprediction of temperatures in simulations completed at a 25 km resolution, which can be as high as 10ºC in some cases, is more prevalent in the daytime than the nighttime. A high overestimation of temperatures of up to 6 ºC is obtained in the simulations completed at a 25 km resolution during the nighttime.
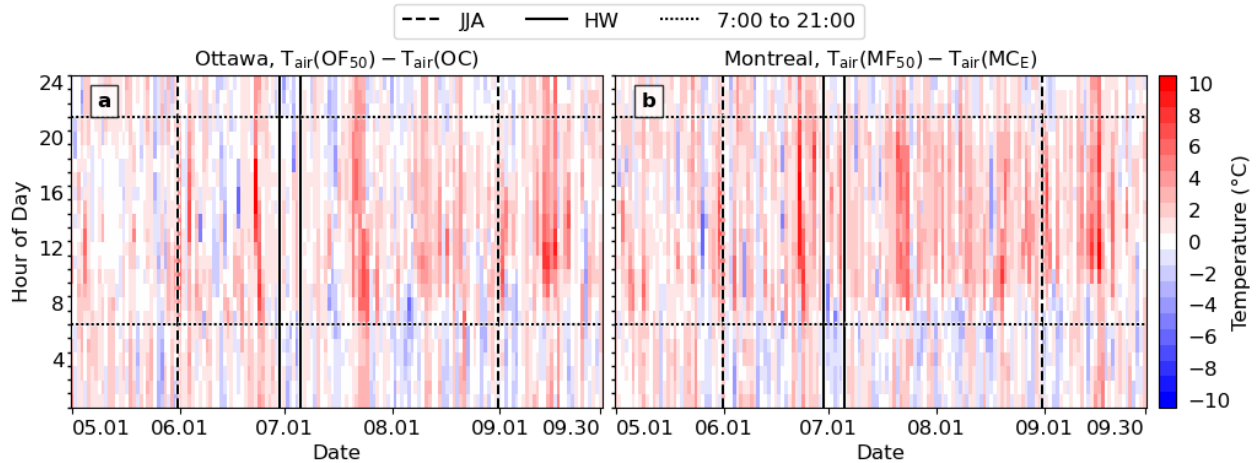
Figure 6-8 The hourly difference in outdoor air temperature from simulations completed at 1 and 25 km grid resolution at 50th percentile urban location in Ottawa and Montreal. (HW: heatwave period from June 30 to July 5, 2018, shown with vertical solid lines; JJA: June, July and August shown with vertical dashed lines)

6.2.3 Indoor overheating from simulations completed at 1 and 25 km grid resolution

The outdoor conditions at the selected representative grids from simulations completed at 1 and 25 km using the WRF model were used as inputs into the EnergyPlus program to simulate the indoor environment in the archetype single-detached home. As mentioned before, indoor overheating was calculated using operative temperatures instead of air temperatures for the outdoor overheating assessment. The results are shown in Table 6-7, Table 6-8 and Figure 6-9, Figure 6-10. The indoor operative temperatures were found to be higher than the outdoor air temperatures by about 8-10 ºC, and the percentage of overheating hours ($POH_{28° C}$) with temperatures more than 28ºC were found to be 2-3 times greater than those from the outdoor overheating analysis, so the building undergoes a much longer overheating period than that evident for the outdoors.

Between the different sections of the single-detached home, higher temperatures and overheating conditions were found in the bedroom (located on the 1st floor) than in the living room (located on the ground floor). This is likely because of the thermal stratification effect in buildings when warmer air circulates and moves from the lower to upper spaces. The comparison of Table 6-7 and 8 shows that the operative temperatures in the bedroom are up to 1ºC higher, which, together with a lower threshold (26 ºC) for the calculation of overheating in the bedroom, leads to about 45% more overheating hours than in the living room. Since occupants often spend more time in the

bedroom than the living room, this potentially creates high overheating risks. In addition, the temperature difference was found higher during the day than during the night.

Table 6-7 Summary of thermal conditions in the living room of the archetype single-detached house building simulated at representative grids from simulations completed at 1 and 25 km grid resolution

Climate statistic	Ottawa grids						Montreal grids						
	OC	OF_0	OF_5	OF_{50}	OF_{95}	OF_{100}	MC_W	MC_E	MF_0	MF_5	MF_{50}	MF_{95}	MF_{100}
$T_{opt,mean}$ (°C)	25.7	24.9	26.0	26.3	26.3	26.4	25.7	25.8	24.7	26.0	26.2	26.3	26.4
$T_{opt,mean}^{day}$ (°C)	26.2	25.3	26.6	27.0	27.0	27.1	26.3	26.4	25.2	26.7	26.9	27.0	27.1
$T_{opt,mean}^{night}$ (°C)	24.7	24.2	24.9	25.1	25.1	25.2	24.8	24.8	24.0	24.9	25.1	25.2	25.2
$T_{opt,max}$ (°C)	34.9	28.7	35.9	37.0	36.6	37.3	35.9	36.7	28.7	36.6	36.7	37.4	37.6
$POH_{28°C}$ (%)	9.2	0.2	12.8	16.2	16.9	17.6	8.6	9.4	0.1	12.6	15.7	16.3	17.5
$POH_{28°C}^{day}$ (%)	14.5	0.3	19.9	25.2	26.1	27.0	13.2	14.3	0.1	19.9	24.1	24.9	26.8
$POH_{28°C}^{night}$ (%)	0.4	0.0	1.1	1.2	1.7	1.8	0.9	1.2	0.0	0.3	1.5	2.0	2.1

Table 6-8 Summary of thermal conditions in the bedroom of the archetype single-detached house building simulated at representative grids from simulations completed at 1 and 25 km grid resolution.

Climate statistic	Ottawa grids						Montreal grids						
	OC	OF_0	OF_5	OF_{50}	OF_{95}	OF_{100}	MC_W	MC_E	MF_0	MF_5	MF_{50}	MF_{95}	MF_{100}
$T_{opt,mean}$ (°C)	26.2	25.4	26.6	26.8	26.9	27.0	26.2	26.3	25.2	26.6	26.8	26.9	27.0
$T_{opt,mean}^{day}$ (°C)	26.7	25.7	27.2	27.5	27.6	27.7	26.8	26.8	25.5	27.3	27.5	27.5	27.7
$T_{opt,mean}^{night}$ (°C)	25.3	24.8	25.5	25.7	25.7	25.8	25.4	25.4	24.7	25.5	25.7	25.8	25.8
$T_{opt,max}$ (°C)	35.9	29.8	37.0	38.1	37.7	38.3	37.0	37.7	30.8	37.9	37.8	38.6	38.7
$POH_{26°C}$ (%)	48.9	35.0	56.7	61.0	62.8	64.1	49.7	50.3	28.2	58.6	60.0	61.9	62.3
$POH_{26°C}^{day}$ (%)	60.0	46.3	67.6	71.9	73.4	74.3	60.7	61.6	37.2	69.8	70.4	71.8	72.5
$POH_{26°C}^{night}$ (%)	30.2	16.3	38.5	42.9	45.0	47.0	31.5	31.4	13.2	39.8	42.6	45.4	45.5
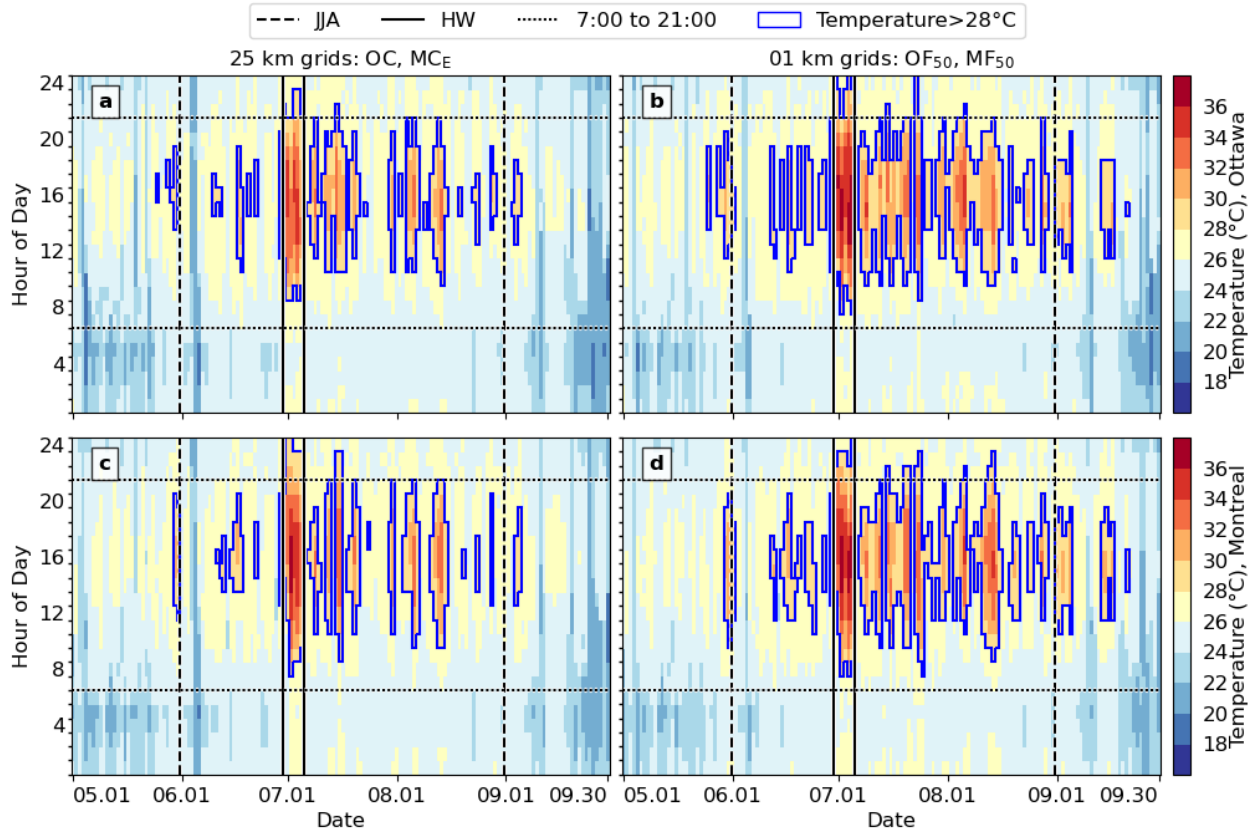
Figure 6-9 The hourly distribution of the indoor operative temperature in the living room from simulations completed at 1 and 25 km grid resolution at 50th percentile urban location in Ottawa and Montreal. (HW: heatwave period from June 30 to July 5, 2018, shown with vertical solid lines; JJA: June, July and August shown with vertical dashed lines)

Finally, indoor overheating was obtained from simulations completed at 1 and 25 km resolution, and their relative difference is investigated. The timing of the EHE during June 30-July 5, 2018, is well captured in the indoor temperatures from both simulations completed at 1 and 25 km resolution, as shown by Figure 6-9. It shows the indoor operative temperatures in the living room for the 50th percentile urban location however, its magnitude was underestimated in the results of simulations completed at 25 km simulation resolution. In line with the observations made from the outdoor overheating assessment, the operative temperatures and percentage of overheating hours from the simulations completed at 25 km resolution fall between the 0th and 5th quantile urban grids in both cities, again highlighting that indoor overheating at more than 95% of the urban grids is underpredicted if simulations completed at 25 km resolution are used for the assessment. This is also reflected from the difference in the number of overheating hours obtained at, for example,

the 50th percentile grid (Figure 6-10). Our results indicate that about 80% of hours in Ottawa and 73% of hours in Montreal over the time of analysis are simulated with higher temperatures from simulations completed at 1 km than the 25 km resolution. The difference in mean operative temperature between simulations completed at 1 and 25 km resolution is slightly lower than the difference obtained in terms of outdoor air temperatures; however, the percentage of overheating hours is comparable.
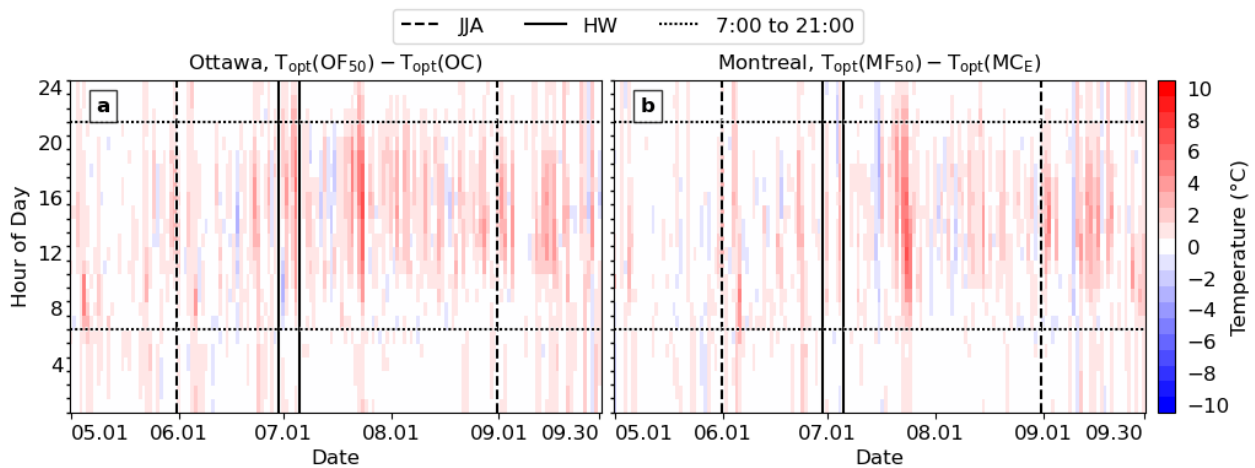
Figure 6-10 The hourly difference in indoor operative temperature in the living room from simulations completed at 1 and 25 km grid resolution at 50th percentile urban location in Ottawa and Montreal. (HW: heatwave period from June 30 to July 5, 2018, shown with vertical solid lines; JJA: June, July and August shown with vertical dashed lines)

6.3. Summary

This study highlights the added value of using high-resolution convection-permitting climate data over regional climate model (RCM) simulated data for the overheating assessment in cities. The study was conducted for two major Canadian cities: Ottawa and Montreal, over a period ranging between May and September 2018. Urban climate simulations were performed at a convection-permitting spatial resolution of 1 km, and a typical RCM spatial resolution of 25 km using a Weather Research and Forecasting (WRF) model. The magnitude of overheating as occurred outdoors and within a single-detached home was evaluated by using the two sets of climate data completed at either grid resolution. The conclusions of this chapter are as follows:

- The results demonstrate greater accuracy from simulations undertaken at a 1 km grid resolution when modelling the outdoor climate than that obtained at a 25 km resolution by

comparing with the observation at nine weather stations in the domain. The air temperature is underestimated in simulations for both 1 and 25 km resolution, whereas simulations completed at a 1 km resolution have smaller bias, mean absolute error, and root means squared error than those done at 25 km. The added accuracy of 1 km simulations in modelling extreme high temperatures is especially evident from the validation results.

- The temporal variation in air temperatures over the period of the analysis (i.e., June 30 – July 05, 2018) is well captured in simulations undertaken at both 1 km and 25 km grid resolution. However, the simulations done at a 25 km resolution are found to underpredict mean air temperatures by up to 2 ℃ over the entire study domain. The maximum air temperatures are underpredicted by up to 3 ℃, and the number of overheating hours could be underpredicted by up to 200 hours, which is half the number of overheating hours predicted from the simulation completed at a 1 km resolution.

- The indoor operative temperatures are found to be higher than the outdoor air temperatures by about 8-10 ℃, and the number of overheating hours with temperatures more than 28℃ is found to be 2-3 times greater than that obtained from the outdoor overheating analysis. The indoor overheating is also underestimated using the 25 km resolution climate data, at least 70% of hours over the time of analysis are predicted with lower temperatures from simulations completed at 25 km than the median level of the 1 km resolution results.

- The results from this study also permitted showing that, if simulations done at a 25 km grid resolution are used to assess outdoor and indoor overheating in the cities of Ottawa and Montreal, the extent of overheating in terms of modelled temperatures, their extremes, and the number of overheating hours can be underpredicted in about 95% of the urban area grids of both cities. These results highlight the importance of completing urban climate simulations using convection-permitting climate data as compared to regional climate models for outdoor and indoor overheating analysis in cities.

In the face of rapid urbanization and climate change, future projected overheating effects must be quantified in the urban centers of cities for different urban growth and climate change scenarios by conducting convection-permitting climate simulations from which heat-stress mitigation strategies can be developed in the future.

Chapter 7 Overheating Assessment by Climate Modelling – Spatial Impacts of Climate on Buildings

In this study, the spatial variation of the overheating conditions in a city is evaluated using the climate data generated at 1 km resolution by the Weather Research and Forecast (WRF) model (Skamarock et al., 2019). And the impact of climate distribution is evaluated by using the climate data for building simulation in EnergyPlus (U.S. Department of Energy's and Building Technologies Office, 2020). The details of both the climate model and the building model are described in section 6.1 from the previous chapter. In section 7.1, the proposed procedure of selecting climate representative locations from the spatial mapping of the city is elaborated. Thereafter, the results including the comparison of different climate data and a comparison of the indoor overheating conditions using the climate data from different locations in the city are discussed in section 7.2. Finally, this chapter is summarized in section 7.3.

7.1. Select representative locations for building simulation

7.1.1 Urban and rural areas for urban heat island calculation

Through systematic literature research of the existing studies, five commonly used methods of urban heat island calculation can be identified:

a. Comparing the climate data from where the existing weather stations are located inside and outside the city area (Bhati and Mohan, 2016; Chen et al., 2016; Miao et al., 2009; Morini et al., 2016; Zhang et al., 2011).

b. Selecting a square region from the urban center and picking another one (Cui and De Foy, 2012; Palou and Mahalov, 2019) or multiple (Han et al., 2020; Li et al., 2019) square regions with a specified distance to the boundary of the city to be the rural region.

c. Manually replace all the built-up urban land covers in the computational domain with natural land cover types for a reference case simulation, then compare the simulation results with and without these urban land covers (Bohnenstengel et al., 2011; Chen et al., 2014; Chew et al., 2021; Imran et al., 2018; Kang et al., 2014; Li and Norford, 2016; Vogel and Afshari, 2020).

d. Select a rectangular (Li et al., 2014; Li and Bou-Zeid, 2013; Sharma et al., 2016; Touchaei and Wang, 2015; Wang et al., 2016) or ellipse (Zhou et al., 2017) shaped area covering the

whole city and the surrounding rural area, then compare the climate data from the urban grids or the official administrative region of the city (Göndöcs et al., 2017) with that from the rural grids inside the domain area.

e. identify the polygon shape of the urban region based on the urban land cover (Li et al., 2019; Zhou et al., 2014) or the official administrative border of the city (Vogel and Afshari, 2020), then consider the rural area to be the area within a specified buffer distance from the edge of the polygon (Li et al., 2019; Zhou et al., 2014) or a ring area (Vogel and Afshari, 2020) surrounding the polygon urban area.

The first method is the most used approach for the calculation of urban heat island intensity, it is convenient to compare the simulated urban heat island with the observations from the weather stations (Oke, 1981). While the calculated urban heat island intensity can be very sensitive to the selection of the weather station locations (Li et al., 2018; Oke, 2006). Using high-resolution climate simulation data enables a more advanced approach to evaluating the urban heat island around the cities. The second method considers an average of the inside of the selected squared region from the urban and rural area, and the selected squared regions can be in different directions of the city to consider their relative locations to the city (Han et al., 2020; Li et al., 2019), this may somehow reduce the uncertainty of than only selecting a location at the weather station, but it is still hard to justify the representativeness of the selected area. The third method created a virtual rural reference case by replacing the urban area with other natural land cover types, for example, cropland, forest. etc., which do not need to select different locations for comparison. The main purpose of these studies is to discuss how the urban built-up region and anthropogenic behaviors may change the local climate on a physical basis, which is not consistent with the current study of evaluating the local climate effect on buildings overheating. The fourth and the fifth method considers the overall climate distribution across the city, and the urban and rural areas are identified by the practical areas of the cities. The urban heat island is calculated by an average of the values from all the urban grids and all the rural grids with different natural land cover types. The only difference between both methods is that the fourth method considers only a regular shaped area that reduced the repetitiveness for the selection of rural areas for different cities with various spatial shapes

In this study, the fifth method is identified for this study which outlines the polygon shape of the urban region based on the urban land cover (Giscience et al., 2021; Li et al., 2019; Moffett et al.,

2019; Rasul et al., 2016; Zhou et al., 2014) and then considers the rural area to be the area within a specified buffer distance from the edge of the polygon (Li et al., 2019; Zhou et al., 2014) surrounding the polygon urban area. To identify the rural area, Yao et al. (Yao et al., 2019) suggested keeping 10km to 30km distance between the rural boundaries and the urban boundaries to avoid introducing other uncertainties caused by different climate conditions of father geospatial regions. Through a series of sensitivity studies by increasing this distance from 10km to 30km, it was found the calculated urban heat island intensity does not change much with the increase of the distance for both cities in the study, so the buffer distance of 10km from the urban boundary is considered to be the rural area, which is also consistent with the implementation in the two papers (Moffett et al., 2019; Rasul et al., 2016). The regions within 3km distance to the urban boundary are excluded because they might still be highly affected by the urban region (Li et al., 2019; Yao et al., 2019; Zhou et al., 2014). We also excluded the water bodies and the terrains with 50m higher than the highest elevation of the urban area, which might have a significant impact on the local temperature for the urban heat island intensity calculation (Göndöcs et al., 2017; Li et al., 2019; Yao et al., 2019; Zhou et al., 2014).
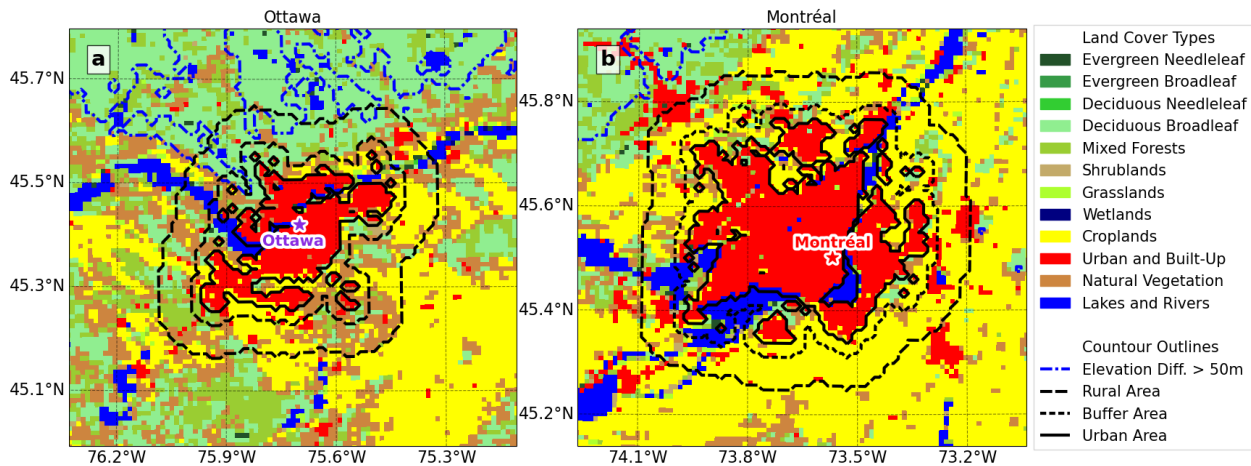
Figure 7-1 Land use and land cover with the outlines of urban and rural areas of a) Ottawa and b) Montreal cities

The distribution of the land cover types and the shapes of the urban boundary, rural boundary and the excluded buffer region in between is specified in Figure 7-1. The urban area of Montreal city is covered by 1184 1km grids which is double times the urban areas of Ottawa that are covered by 501 grids. The number of grids for the rural area of Montreal and Ottawa is 1316 and 1112. The main city area is on Montreal Island that is surrounded by rivers, and in its surrounding, there are

also several smaller suburban cities and a large area of cropland. While for Ottawa, although there is one river passing through the city center, the distribution of urban region tends to be clustered to the only single center of the city, and in its surrounding, there are cropland and more forest regions. To the north of the city area, there are mountains with elevated terrains stretched close to the edge of the urban region.

7.1.2 Select representative locations from urban and rural areas.

To specify the weather data to be used for the overheating assessment, multiple studies have been focused on developing a procedure of creating representative climate datasets from long-term climate datasets (Berardi and Jafarpur, 2020; Herrera et al., 2017; Laouadi et al., 2020b; Nik, 2016). CIBSE (2014) has developed a systematic approach to select the design summer year (DSY) by evaluations of several overheating metrics for the climate data from different years. A similar concept is adopted here in this study. Instead of selecting the climate data from multiple years, the evaluation of the climate data has been conducted over the different grids across the whole city to find the locations exposed to different levels of heat conditions.

For this study, the selection of the representative locations in the urban and rural areas adopted the temperature-based overheating assessment methods, which is the most straightforward for the comparisons of the indoor overheating conditions from different locations in the same city. The locations are selected by the evaluation of three different aspects, including a) the time-averaged air temperature over the evaluated five months, b) the overheating hours above the fixed temperature threshold, c) and the cooling degree hours (CDH) with the base temperature of the fixed temperature threshold. The fixed temperature threshold in this study is 28°C for both the outdoor and the indoor conditions since it is the most used value in the literature and standards for overheating assessment in residential buildings (CIBSE, 2011; Department of Health, 2007b; Zero Carbon Hub, 2015c, 2015b) and also the selection of extreme weather files (CIBSE, 2014). It is defined to be an extremely hot condition when the temperature is higher than 28°C, so the number of hours above 28°C reflects the occurrence of overheating within the evaluated period. The cooling degree hour is defined as the cumulative number of overheating hours weighted by the magnitude of exceedance above the threshold temperature values, which evaluates both the temperature levels and the occurrence of overheating, the equation to calculate it is:

$$CDH = \sum_{T_{air}>28} (T_{air} - 28) \qquad\qquad (7-1)$$

After the three metrics are calculated, the locations with the five (5) different quantiles, 0%, 5%, 50%, 95%, and 100%, of the three evaluated metrics are considered to represent the general conditions in the city. The quantiles of 0% and 100% are selected for the locations of the extreme cases with the maximum and minimum potential of overheating in the city, and the quantiles of 5%, 50% and 95% help to conclude the most possible range of the overheating conditions in the city. The selection of the five locations using each of the metrics is conducted separately for the urban and rural regions to show the general difference in the climate conditions between the urban and rural areas. Therefore, 10 locations would be selected using each of the metrics for each city, and it is expected to have 30 locations selected in total for each city with the 3 metrics considered. In Figure 7-2, the selected locations are summarized with the distribution of the three metrics. The selected locations are indexed by the metrics for the selection (T for mean temperature, H for overheating hours, C for cooling degree hours) followed by its level of percentile of the evaluated metric hereafter. For example, T100 indicates the location with the maximum value in the urban/rural area in the city, H00 for the location with the minimum overheating hours in the urban/rural area in the city, and C50 means the cooling degree hour of the location is the median value of the whole urban/rural area of the city. The distribution of the selected locations for Ottawa shows that the metrics with higher values are more clustered in the city center, while for Montreal the locations with higher values may not always be in the center of the city, for example, the C100 is even not on the Montreal Island but located at the east of the city, and C95 is at the south-east corner of the city. This exhibits the impact of the water area surrounding the center of the city. And it shows there might be not only one hottest center in the urban area, and it is critical to consider the spatial distribution of these thermal metrics over the city for the selection of representative locations for further studies.

Some existing studies (Taylor et al., 2014) have found the outdoor air temperature has the highest correlation to indoor temperature, other climate variables, e.g. wind speed, solar radiation, relative humidity .etc. may still not be neglected for building-related studies, that is why we only use the three selected temperature-based metrics for the overheating analysis. But it is worth mentioning that the proposed method of selecting representative locations in a city can also be implemented

for other variables to obtain some representative locations for consideration of the various climate conditions in the city for different purposes of studies.
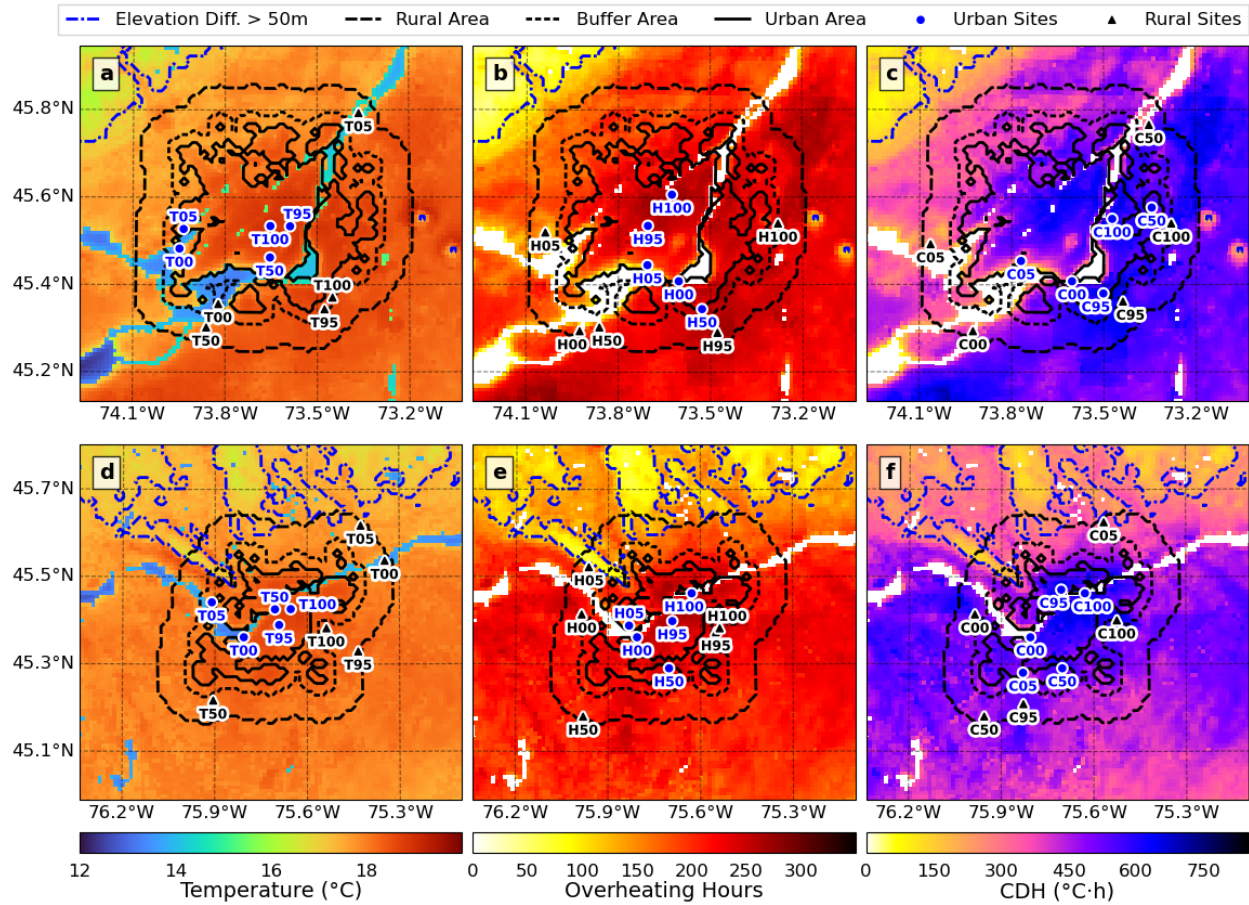
Figure 7-2 Site selection based on the three criteria of a, d) mean outdoor air temperature over the 5 months; b, e) the overheating hours above 28°C; and c, f) Cooling degree hours (CDH) with a base temperature of 28°C.

7.2. Building simulation results

The spatial distribution of climate data may help distinguish the difference of the building thermal evaluation at different locations over the city, while the difference between different locations and which one can better represent the general overheating condition in the city is still unclear. In this section, the indoor overheating assessment of the single building model using the climate data at the selected locations specified in Section 7.1 for the urban and rural areas is compared to help unveil the doubts.

7.2.1 Comparison of the indoor overheating at selected locations

The indoor overheating conditions of the bedrooms in the single house buildings at different locations in the WRF model are summarized in Figure 7-3 and Figure 7-4. The buildings in rural areas may have lower values in the overheating metrics than the urban area in general, this might be due to the cooler outdoor air temperature and higher wind speed in the rural area. For the locations with the 50 quantiles in Montreal, the mean temperature of those three buildings in the urban area is 0.26°C higher than that of those three in a rural area on average, and the overheating hours at the three locations in the urban area have an average of 104 hours higher than that of the three locations in a rural area. For Ottawa, this means the temperature difference and overheating hour difference between urban and rural are even larger, which is calculated to be 0.38°C and 123 hours.
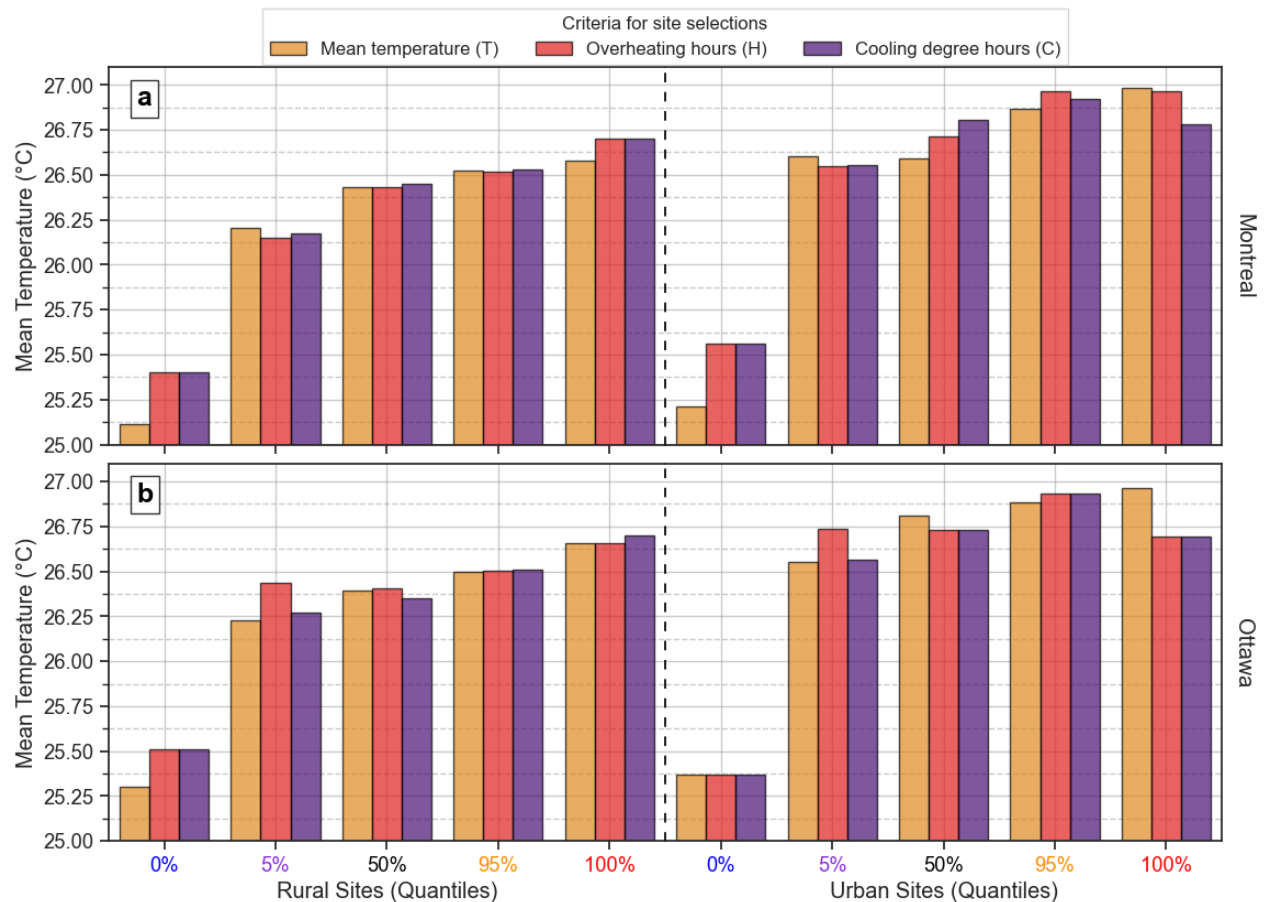
Figure 7-3 Comparison of the mean indoor operative temperature during the 5 months in summer (MJJAS) in the bedroom of single house buildings using the climate data from different selected locations in a) Montreal and b) Ottawa.
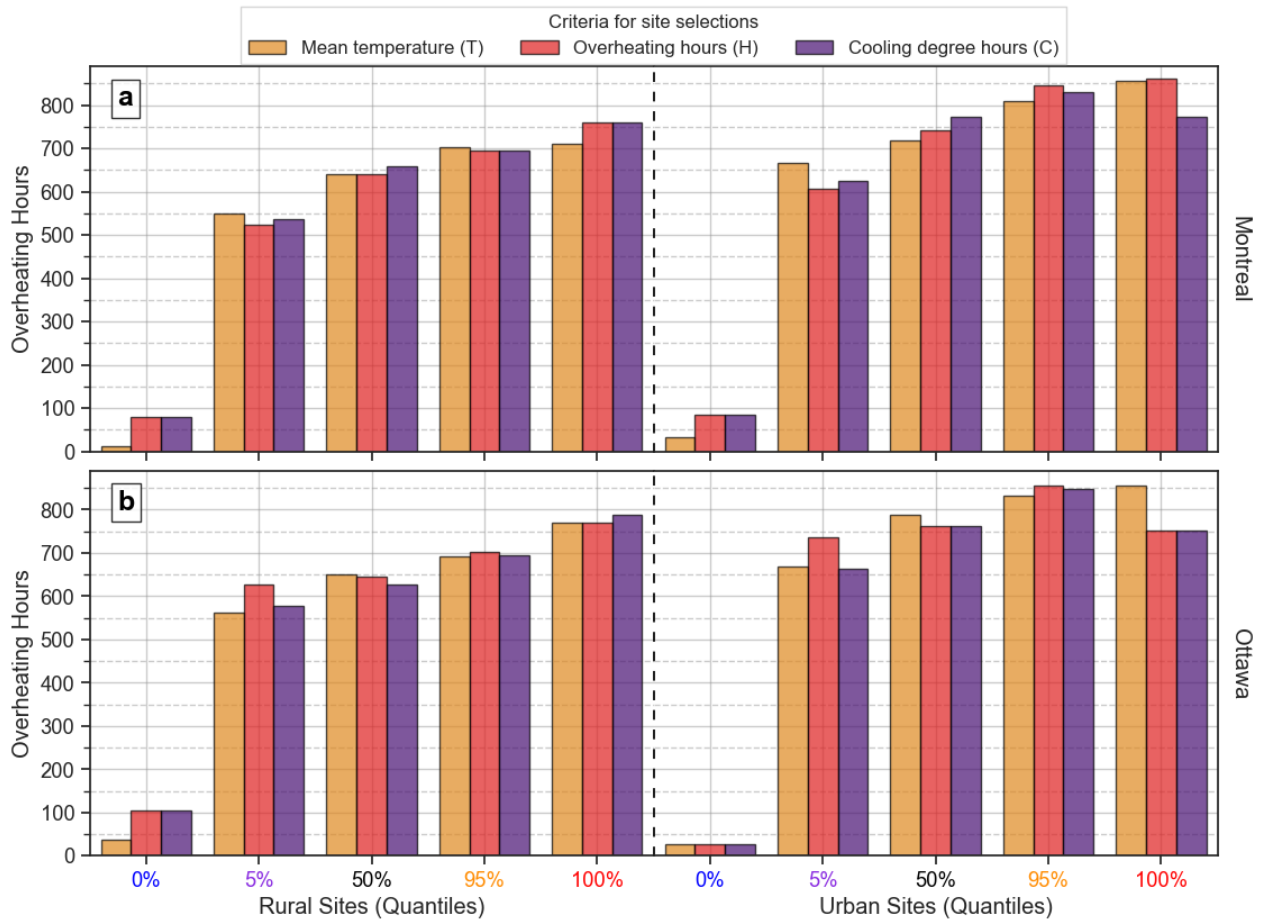
Figure 7-4 Comparison of the overheating hours above 28°C during the 5 months in summer (MJJAS) in the bedroom of single house buildings using the climate data from different selected locations in a) Montreal and b) Ottawa.

In Figure 7-3, a significant difference between locations of the intra-urban (and intra-rural) area can be observed. For the urban area of Montreal, the location T100 has the maximum mean indoor operative temperature of 27.0°C, and T00 has the minimum of 25.2°C, which identified a possible mean indoor operative temperature difference of 1.8°C. For the urban area of Ottawa, the maximum mean indoor operative temperature difference between the selected locations is (T100-T00) 1.6°C. A distance difference can also be found in Figure 7-4 for the comparison of overheating hours between locations. For the urban area of Montreal, location H100 has the maximum overheating hour of 862 hours, and T00 has the minimum of 33 hours, which identified a possible overheating hour difference of 829. For the urban area of Ottawa, the maximum evaluated overheating hour difference is also 829 hours which is observed between T100 and T00. However, there exists a significant difference between locations with 00 quantiles and 05 quantiles,

while the difference between locations with quantile 05 and quantile 100 is much smaller than that. This reminds us that only a small portion of the locations (grids) may fall into the evaluated range between locations with 00 quantiles and 05 quantiles, while most of the locations (grids) should be in the range of that between locations with quantile 05 and quantile 100. Therefore, when conducting the overheating analysis of the buildings in the city, people should avoid selecting these cool locations which cannot represent the overall overheating conditions in the city.
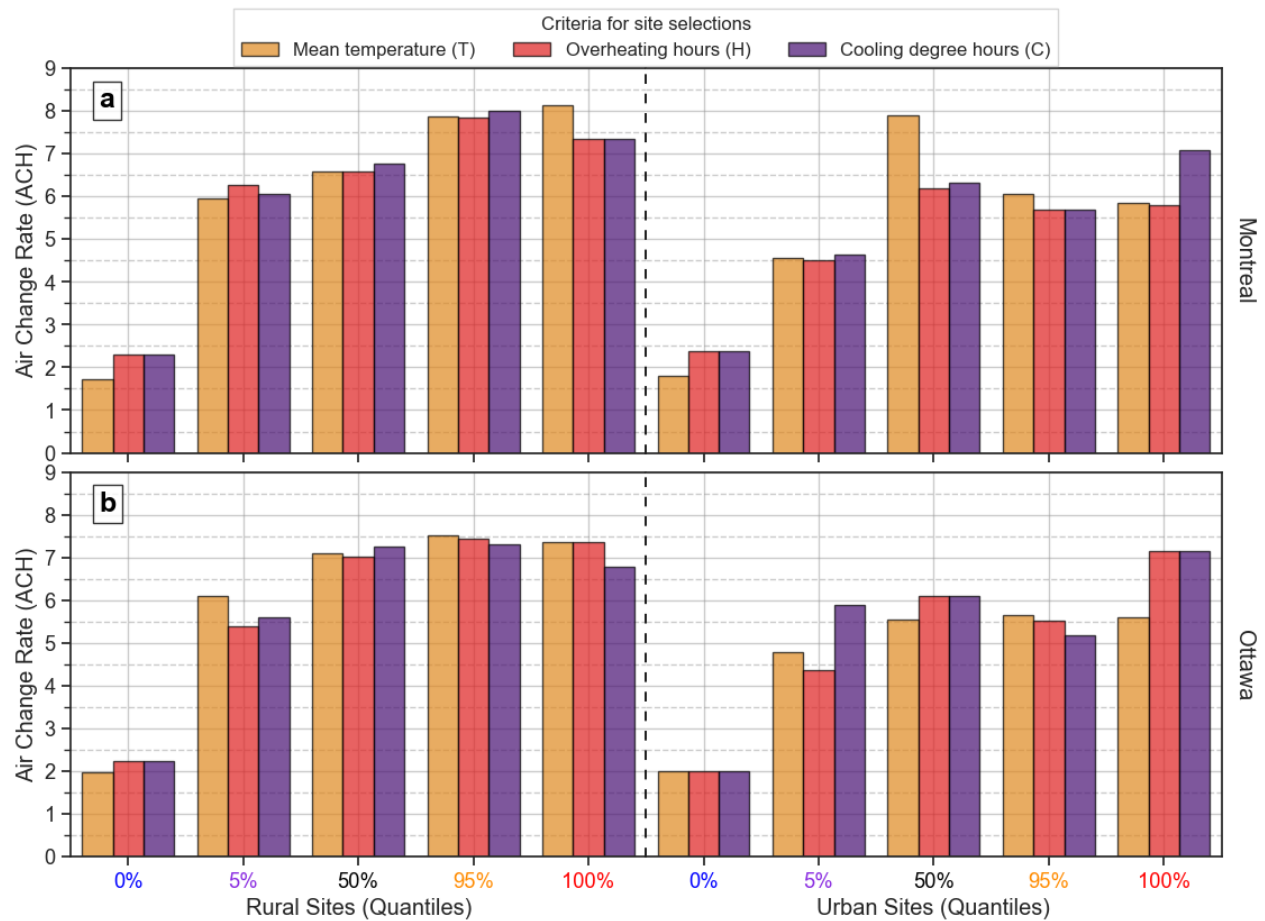
Figure 7-5 Comparison of the mean air change rate during the 5 months in summer (MJJAS) in the bedroom of single house buildings using the climate data from different selected locations in a) Montreal and b) Ottawa.

Figure 7-3 and Figure 7-4 also exhibited the trend that, no matter for urban or rural areas, locations selected with the higher quantile of the overheating metrics for outdoor climate may have correspondingly more severe overheating conditions indoors, while exceptions can still be found that locations with higher quantiles may have lower mean operative temperature or overheating hours. For example, in Montreal, the urban C100 has lower mean operative temperature and

overheating hours than those from T, H, C95, T50 still has higher overheating hours than the three locations with 05 quantiles, but it has a lower mean operative temperature than that at T05. A similar outcome also happens in the urban area of Ottawa, the location H, C100 has both the mean operative temperature and overheating hours even lower than the buildings at T, H, C50 and H05, and location H05 may have a higher mean operative temperature than H, C50 though its overheating hour is still smaller than H, C50. This can be explained by the difference in the local wind speed which may lead to the different natural ventilation conditions of the building. The average air change rate of the rooms over the 5 months is therefore provided in Figure 7-5. It can be found that, for the locations in Montreal urban area, C100 and T50 have much higher air change rates than the other sites, which indicates the natural ventilation at these two locations helped with the indoor temperature control. Among the locations in Ottawa, the air change rate in the buildings at H, C100 is much higher than the other sites, this significantly reduced the overheating in the buildings, while for H05, the air change rate is much lower than other sites apart from climate T, H, C00, which explains, why it may have comparable or even more severe overheating than locations with quantile 50. This suggests the importance to include the local wind condition for the whole building thermal simulation.

7.2.2 Comparison between H95 and H05 in Montreal urban area

The longer overheating exposure time can also impose a great threat to the health and safety of the occupants due to the cumulative water loss and the increased core temperature of the human body (International Standard Organization, 2004; Laouadi et al., 2020a; Ooka et al., 2010). This requires a better estimate of the duration of the overheating, while the summarized overheating metrics, mean operative temperature and overheating hours, cannot reflect the detailed overheating information in the time series. The H95 and H05 locations in the urban area of Montreal are selected for the comparison of the whole time series between different locations. The hourly data of outdoor air temperature and the indoor operative temperature have been shown in the heatmap plot in Figure 7-6. It clearly shows that the indoor operative temperature is higher than the outdoor air temperature in general, the temperatures indoors are elevated compared to that of the outdoors due to the indoor heat gain by the building utilities. For both the indoor and outdoor conditions, the simulation captured the higher temperature during the daytime than the night-time, and the significantly higher temperature during the heatwave period than the rest of the days in the

summer. The maximum indoor operative temperature at H95 during the heatwave can be 38.5°C, and 37.8°C at H05.
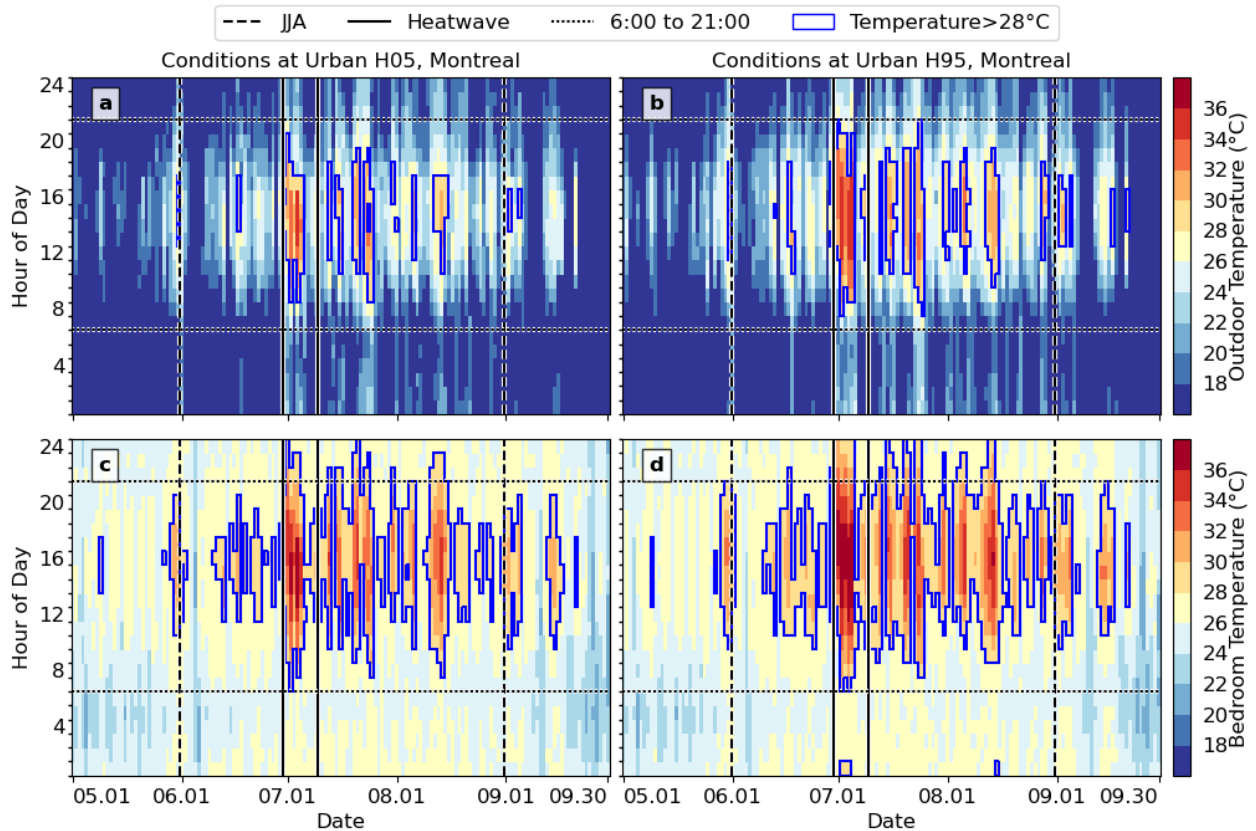
Figure 7-6 Time series heatmap of the a,b) outdoor air temperature, c,d) bedroom operative temperature at a,c,e) H05, and b,d,f) H95 locations in Montreal.

To better compare the difference in time series between the locations, the heatmap of the hourly temperature of H95 subtracted by that of H05 is plotted in Figure 7-7. A greater temperature difference between the sites happens in the outdoors than indoors between locations, while there still exists a great temperature difference for indoors. The indoor operative temperature at H95 is higher than that at H05 for 75% of the hours during the five months, and the difference can be even higher in the hot hours during the heatwave period, which can be as great as 5.8°C. The indoor condition at both locations exhibits a longer time to be higher than 28°C compared to the outdoors, and the overheating conditions at H95 may normally have one or two hours longer on each of the days than that at H05, no matter for indoors or outdoors. In general, the increased overheating hours at a hotter location are normally distributed next to the existing overheating hours that can be found from a cooler location in the same city, this helps to better quantify the

increased mortality risk at a location compared to another one in the city. And there are also exist several days that may have several hours of overheating above 28°C found in the building at H95, while none of such overheating can be observed in the building at H05. For example, there are 9 overheating hours at H95 on August 7, while no overheating hour is outlined at H05. A higher possibility is also observed for the building at H95 to have the condition of temperature above 28°C extends after 23:00, while for location H05, this overheating condition normally ends before 23:00. This means using the climate data at a cool location in the city, e.g., H05 may significantly underestimate the overheating during the night.
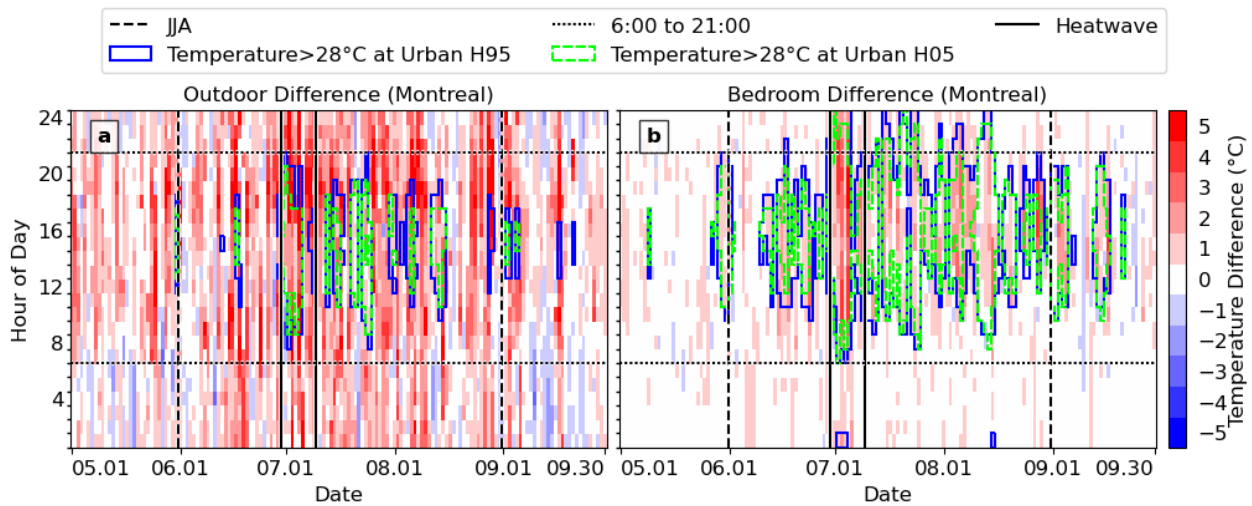
Figure 7-7 Comparison of the a) outdoor air temperature and b) operative temperature in bedroom at locations H95 and H05 in the urban area of Montreal.

7.2.3 Comparison between H50 and H05 in Ottawa urban area

As discussed in Section 7.2.1, the mean indoor operative temperature, and overheating hours in the building at H100 of the Ottawa urban area is much lower than expected, and it has an equivalent value with that at H05, so it is an ideal case to compare the overheating condition between different locations with similar overheating conditions (Figure 7-8). It is found that they may still have obvious differences along with the time series, 71% of the hours over the five months have the absolute temperature difference higher than 0.5°C (<-0.5°C, or >0.5°C), and 46% of the hours over the five months have the absolute temperature difference higher than 1°C. The difference of the outdoor air temperature between locations varies between -4.4°C to 8.1°C, and that of the indoor operative temperature varies between -4.4°C to 3.4°C.
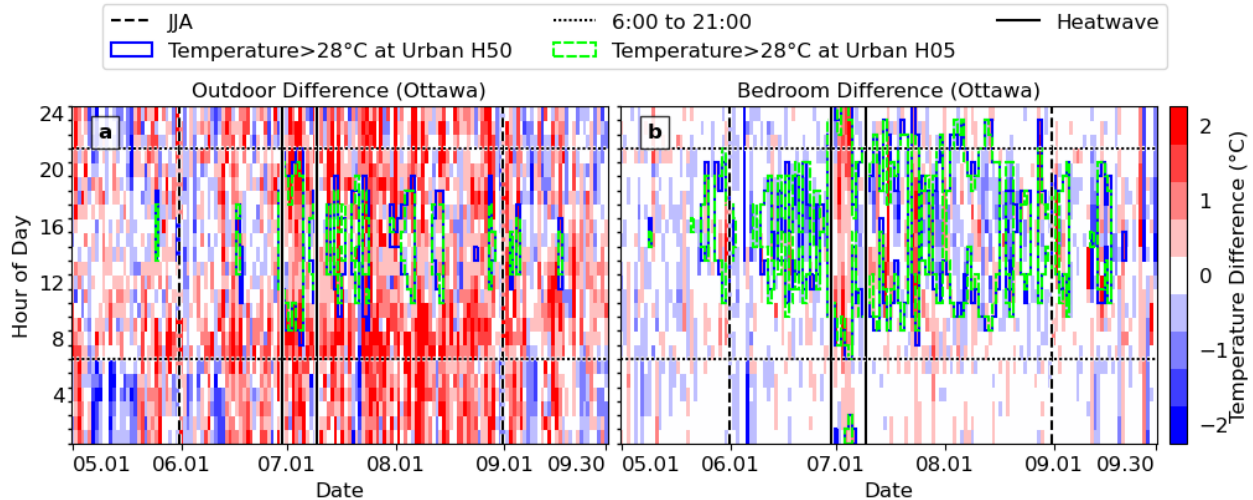
Figure 7-8 Comparison of the a) outdoor air temperature and b) operative temperature in bedroom at locations H50 and H05 in the urban area of Ottawa.

7.2.4 Comparison between urban and rural locations

The overall difference in overheating conditions between urban and rural areas has been shown in Figure 7-3 and Figure 7-4. To better show the difference between locations from the urban and rural areas along with the time series, the locations with 50 percentiles (median) of the overheating metric are compared between urban and rural areas. For example, the urban T50 of Ottawa and rural T50 of Ottawa has been compared and their difference has been plotted in Figure 7-9. Although the location from the urban area has a higher mean temperature than the rural location as observed, a distinct lower temperature can still be observed in the morning than the location from the rural area for the outdoor condition. It can be identified as the urban cool island, which is consistent with existing findings (Duan et al., 2019; Theeuwes et al., 2015; Yang et al., 2017). While for the comparison of the indoor operative temperature, the building at urban area does not show that many hours lower than the temperature in the building at rural area, and the hours with the lower indoor operative temperature at urban area occur slightly later than the cool hours in the outdoor. The absolute value of the temperature difference is also much smaller than that for the outdoor condition comparisons. For the example in Figure 7-9, the building at the urban area has been exposed to the outdoor temperature with 40% of the hours lower than that in the rural area, and the greatest difference can be -7.2°C found during the heatwave, while for the indoor condition, the building in the urban area has 22% of the hours lower than that in the rural area, and the greatest difference can be -4.5°C. This exhibits that urban cool island in the buildings is

normally postponed for each of the days and with attenuated intensity due to the higher thermal capacity and the internal heat gain in the building enclosures, and the indoor overheating in an urban area is more severe than that in a rural area.
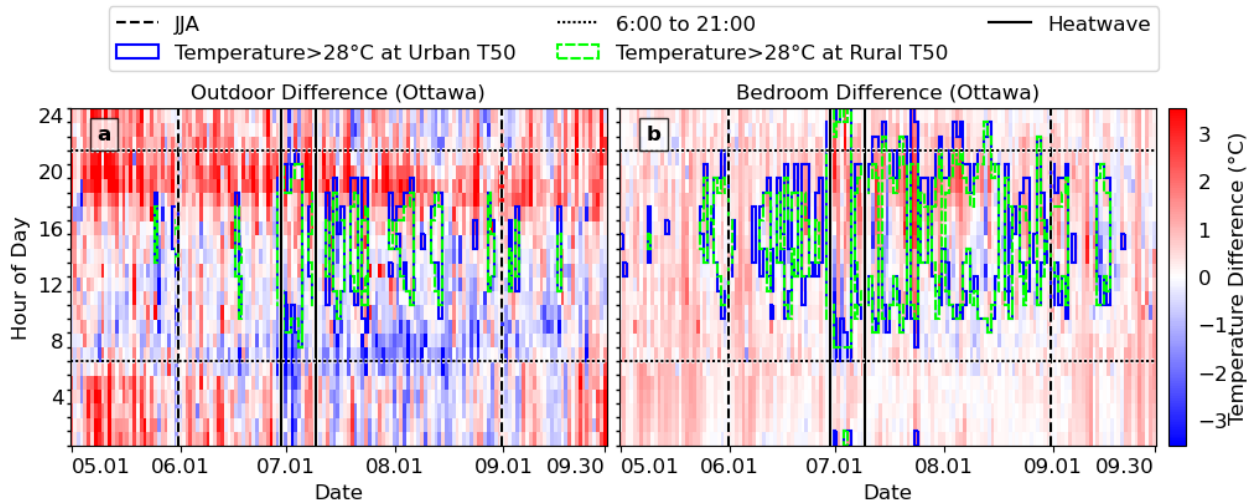
Figure 7-9 Comparison of the a) outdoor air temperature and b) operative temperature in bedroom at location T50 in the urban and rural areas of Ottawa.

7.3. Summary

This study has been devoted to quantifying the effect of the spatial distribution of climate data at different locations for the building thermal analysis. A complete procedure of evaluating the overheating conditions of different locations in the city from the high-resolution climate data has been demonstrated by evaluating the distribution of the overheating metrics across the whole city followed by selecting the locations with different quantiles of the overheating metrics. The indoor simulation results of using the different climate data from different locations in the high-resolution are compared together with their local outdoor climate conditions to show the importance of using the climate data at a proper location even for the same city. Conclusions can be summarized in the following points:

- Great intra-urban overheating condition difference has been detected through a comparison of the locations with overheating metrics of the quantile of 00 and 100. The difference in the mean indoor operative temperature over the five months between the locations can be 1.8°C in Montreal and 1.6°C in Ottawa, and the difference in the overheating hours between the locations can be 829 hours in both cities.

- The duration of the overheating may normally have 2 hours' difference between locations with overheating metrics of 95 and 05 quantiles. And even for different locations with similar mean indoor operative temperature and overheating hour values, the period of overheating occurrence can be quite different.

- Locations with higher temperature-based overheating metrics may have a more severe overheating condition in the buildings in general, while other climate variables may also affect indoor overheating conditions. In this study, it is found that the local wind speed is very important for the overheating evaluation of the buildings with operable windows for natural ventilation in which the wind speed can markedly change the indoor overheating condition by variating the overall air change rate of the building.

Chapter 8 Conclusions and Future Works

8.1. Summary and conclusions

The research in this thesis has been dedicated to enabling the field monitoring of the building overheating at a city scale for the assessment of the current buildings and to developing a regional climate model that can generate the weather data for urban scale building overheating studies.

During the building selection process, a building prescreening, building information survey and on-site visits to the building candidates are conducted. With the building information collected with these steps, 6 school buildings and 5 hospital buildings are finally selected from the building database of 200 hospitals and 396 schools for the field monitoring. The weather stations are installed on the roof of these buildings and indoor temperature and humidity sensors are installed in selected rooms at different floors and different orientations of the buildings. The field monitoring data are collected for the year 2020. The data have been used for quantitative analysis and comparison of the real overheating conditions between these buildings and rooms. Multiple overheating criteria based on the thermal indices of air temperature (T), Humidex (H), Heat Index (HI), Wet-Bulb Globe Temperature (WBGT), Summer Simmer Index (SSI), Discomfort Index (DI), and Standard Effective Temperature (SET), are calculated and compared to identify their potential connections and discrepancies in between. Major findings and contributions can be summarized as follows:

- The school buildings from the two school boards in Montreal, SB1 and SB2, have a severe overheating problem and they cannot achieve the requirements from Building Bulletin 101 and European Standard EN 16798-2019. The school building from SB3 has much better condition than the buildings from the other two school boards due to the night purge through the mechanical system in the classrooms. In general, those school buildings with overheating problems may have limited ventilation, an orientation with longer exposure to the solar radiation and larger area of roofs, windows, and external walls with few external shadings from the trees and other tall buildings adjacent to the building.

- For hospital buildings, the thermal conditions in the different rooms can be more varied than in school buildings due to the diverse room functions. Through the analysis of the measured data, three rooms in CH-B are found to have a severe overheating problem, while three other rooms few overheating problems. The room with air conditioners may have

significantly different diurnal patterns on the indoor thermal dynamics, which is highly affected by the operation of the air conditioners. In general, those rooms with overheating problems in the hospital buildings may have limited access to the air conditioner and mechanical ventilation, and they do not have sufficient fresh air or cooling air supply to the corridor and hall regions of the building.

- Through a correlation analysis of the mean and maximum values of the different thermal indices together with the relative humidity, it is found that the thermal indices have a negative correlation to relative humidity. The mean values of the thermal indices still achieved a high degree of concordance, while less concordance can be found between the maximum values.

- The overheating hours calculated by the assessment thresholds of the different thermal indices are found quite different from each other, while the criteria with similar simulation results can be clustered together through a correlation analysis. The overheating evaluated by a threshold of a high level has lower concordance than a low or medium level threshold.

To develop the high-resolution regional climate model, the urban canopy models to reproduce the urban effect in climate and the importance of the land cover are first compared and validated with the multiple weather gauges in the study area. Then simulations using the confirmed models are completed at two different spatial resolutions, 1 km and 25 km, for the representative of the convection effect, resolved regional climate model (convection-permitting model, CPM) and the traditional coarse resolution regional climate models (RCMs), respectively. The added benefits of the CPM in city-scale overheating assessment have been compared with the RCM using the evaluation of their accuracy in the reproduction of the near-surface climate variables, the difference of the simulated weather distribution over the city, and the changes in the indoor overheating condition simulated at the representative grids of the different resolution results. To further justify the necessity to preserve the urban effects in the climate dataset, the urban heat island effect in the evaluated two cities, the effect of the spatial variation of climate conditions on the building simulation are evaluated by building simulations at more selected representative locations. Major findings and contributions can be summarized as follows:

- It was found that compared to the simple BULK model and the outdated WRF default land cover data, the more advanced multilayer UCM in the WRF model, and the use of a more accurate description of urban land cover results in a more accurate description of near-

133

surface wind speed, precipitation, and relative humidity, while the precipitation is found to be very sensitive to the use of advanced urban parameterization scheme, and the more accurate depiction of urban areas in the model.

- Through the comparison between the CPM and RCM, it can be found that using the coarse resolution RCM underpredicts urban external mean air temperatures by up to 2 ºC in the cities and the maximum air temperatures are underpredicted by up to 3 ºC. The number of overheating hours could be underpredicted by up to 200 hours, which is half the number of overheating hours predicted from the high-resolution CPM. The indoor overheating is also underestimated using the coarse resolution RCM data, at least 70% of hours over the time of analysis are predicted with lower temperatures from simulations.

- The effect of the spatial distribution of the urban climate on building overheating is also justified. The mean indoor operative temperature difference can achieve 1.8°C in Montreal and 1.6°C in Ottawa over the five months between the locations in the city, and the difference of the overheating hours can be 829 hours in both cities. This also leads to the difference in the occurrence and duration of the overheating.

- The high-resolution climate dataset can also preserve the spatial variation of not only air temperature but also other climate variables, e.g., wind speed and wind direction, that may also affect the results in building simulation greatly.

8.2. Limitations and future works

Since the two major tasks covered in this study, the field monitoring, and the regional climate modelling, are both extremely time-consuming with the given resources, the data been used in this thesis is very limited. The limitations of the current works and some potential future works to be extended are summarized in the following:

- The field monitoring dataset collected in 2020 is very limited. It is worthwhile to carry out a complete overheating assessment and the comparison of the thermal criteria by using the field monitoring dataset for the whole summer.

- In addition to the field monitoring data, I have also collected the building drawings from the building managers of the selected buildings. The real building models can therefore be created with these resources. The overheating in these buildings under future climate

scenarios and the possible mitigation strategies can be evaluated through the building simulation of these building models.

- Although some equivalencies can be found between the different thresholds of the different thermal indices, the discrepancy between the thermal indices also suggests a more in-depth study is needed to evaluate the actual risk through the human body response (e.g., loss of water and human body core temperature variation) to the thermal environment. Therefore, a bio-heat model is needed to evaluate these variables quantitatively as a potential future work.

- The high-resolution WRF simulated climate data generated for the year 2018 can be used for a long-term urban climate analysis since the previous studies where the model is evaluated over one or two weeks. The synergistic interactions of the urban heat island effect and the occurrence of heatwaves should be explored by discussed through a comparison between days with and without a heatwave event.

- Downscaling the GCM datasets to a much finer resolution and preserving the location-specific climate details for an urban city would be critical elements for generating building simulation weather files. In the next study, a SYnthesized Representative Urban-effect Preserved (SYRUP) dataset is proposed for evaluating building energy performance, which can highly reduce the number of simulation cases for building energy modelling.

- The impact of using the high-resolution urban effect preserved climate data on building overheating mentioned in this study should be extended to other aspects of building-related studies, e.g. hygrothermal performance of building envelope, building energy performance. The urban climate pattern and its impacts on buildings should be also investigated by extending the current model for future scenarios.

References

Abdi, H., 2008. Kendall Rank Correlation Coefficient. Concise Encycl. Stat. 278–281. https://doi.org/10.1007/978-0-387-32833-1_211

ACGIH, Tlv., 2010. Threshold limit values for chemical substances and physical agents and biological exposure indices, in: USA: American Conference of Governmental Industrial Hygienists. pp. 200–219.

Administration, O.S. and H., 2014. Using the heat index: A guide for employers.

American College of Sports Medicine, 1984. Prevention of thermal injuries during distance running. Med. Sci. Sport. Exerc. 16, iv–xiv.

Amoako-Attah, J., B-Jahromi, A., 2016. The impact of different weather files on London detached residential building performance-deterministic, uncertainty, and sensitivity analysis on CIBSE TM48 and CIBSE TM49 future weather variables using CIBSE TM52 as overheating criteria. Sustain. 8. https://doi.org/10.3390/su8111194

Argüeso, D., Evan, J.P., Fita, L., Borman, K.J., 2014. Temperature response to future urbanization and climate change. Clim. Dyn. 42, 2183–2199. https://doi.org/10.1007/s00382-013-1789-6

Armstrong, B.G., Chalabi, Z., Fenn, B., Hajat, S., Kovats, S., Milojevic, A., Wilkinson, P., 2010. Association of mortality with high temperatures in a temperate climate: England and Wales. J. Epidemiol. Community Health 65, 340–345. https://doi.org/10.1136/jech.2009.093161

Armstrong, L.E., Casa, D.J., Millard-Stafford, M., Moran, D.S., Pyne, S.W., Roberts, W.O., 2007. Exertional heat illness during training and competition. Med. Sci. Sport. Exerc. 39, 556–572.

ASHRAE-55, 2017. Thermal environmental conditions for human occupancy. ANSI/ASHRAE Stand. - 55 7, 6.

Australian Bureau of Meteorology, 2021. Thermal Comfort observations.

Ban, N., Schmidli, J., Schär, C., 2014. Evaluation of the convection-resolving regional climate modeling approach in decade-long simulations. J. Geophys. Res. Atmos. 119, 7889–7907.

Barlage, M., Tewari, M., Chen, F., Miguez-Macho, G., Yang, Z.L., Niu, G.Y., 2015. The effect of groundwater interaction in North American regional climate simulations with WRF/Noah-MP. Clim. Change 129, 485–498. https://doi.org/10.1007/s10584-014-1308-8

Barrett, P., Davies, F., Zhang, Y., Barrett, L., 2015. The impact of classroom design on pupils' learning: Final results of a holistic, multi-level analysis. Build. Environ. 89, 118–133. https://doi.org/10.1016/j.buildenv.2015.02.013

Bartholmes, J., Todini, E., 2005. Coupling meteorological and hydrological models for flood forecasting. Hydrol. Earth Syst. Sci. Discuss. 9, 333–346.

Bassil, K.L., Cole, D.C., 2010. Effectiveness of public health interventions in reducing morbidity and mortality during heat episodes: A structured review. Int. J. Environ. Res. Public Health

7, 991–1001. https://doi.org/10.3390/ijerph7030991

Beizaee, A., Lomas, K.J., Firth, S.K., 2013. National survey of summertime temperatures and overheating risk in English homes. Build. Environ. 65, 1–17. https://doi.org/10.1016/j.buildenv.2013.03.011

Belcher, S.E., Hacker, J.N., Powell, D.S., 2005. Constructing design weather data for future climates. Build. Serv. Eng. Res. Technol. 26, 49–61. https://doi.org/10.1191/0143624405bt112oa

Berardi, U., Jafarpur, P., 2020. Assessing the impact of climate change on building heating and cooling energy demand in Canada. Renew. Sustain. Energy Rev. 121, 109681. https://doi.org/10.1016/j.rser.2019.109681

Bhati, S., Mohan, M., 2016. WRF model evaluation for the urban heat island assessment under varying land use/land cover and reference site conditions. Theor. Appl. Climatol. 126, 385–400. https://doi.org/10.1007/s00704-015-1589-5

Bohnenstengel, S.I., Evans, S., Clark, P.A., Belcher, S.E., 2011. Simulations of the London urban heat island. Q. J. R. Meteorol. Soc. 137, 1625–1640. https://doi.org/10.1002/qj.855

Bravais, A., 1844. Analyse mathématique sur les probabilités des erreurs de situation d'un point. Impr. Royale.

BS EN 16798, 2019. Energy Performance of Buildings—Ventilation for Buildings—Part 1: Indoor Environmental Input Parameters for Design and Assessment of Energy Performance of Buildings Addressing Indoor Air Quality, CEN.

Campbell, S., Remenyi, T.A., White, C.J., Johnston, F.H., 2018. Heatwave and health impact research: A global review. Heal. Place 53, 210–218. https://doi.org/10.1016/j.healthplace.2018.08.017

Cannistraro, G., Cannistraro, M., Restivo, R., 2014. A Smart Thermo-hygrometric Global Index for the Evaluation of Particularly Critical Urban Areas Quality: the City of Messina Chosen as a Case Study. Smart Sci. 2, 29–35. https://doi.org/10.1080/23080477.2014.11665601

Caya, D., Laprise, R., 1999. A semi-implicit semi-Lagrangian regional climate model: The Canadian RCM. Mon. Weather Rev. 127, 341–362. https://doi.org/10.1175/1520-0493(1999)127<0341:asislr>2.0.co;2

Chan, S.C., Kendon, E.J., Fowler, H.J., Blenkinsop, S., Ferro, C.A.T., Stephenson, D.B., 2013. Does increasing the spatial resolution of a regional climate model improve the simulated daily precipitation? Clim. Dyn. 41, 1475–1495.

Chen, D., 2019. Overheating in residential buildings: Challenges and opportunities. Indoor Built Environ. 28, 1303–1306. https://doi.org/10.1177/1420326X19871717

Chen, F., Dudhia, J., 2001a. Coupling an advanced land surface-hydrology model with the Penn-State-NCAR MM5 modeling system. Part I : Model Implementation and Sensitivity. Mon. Weather Rev. 129, 569–585.

Chen, F., Dudhia, J., 2001b. Coupling an Advanced Land Surface – Hydrology Model with the Penn State – NCAR MM5 Modeling System . Part II : Preliminary Model Validation. Mon. Weather Rev. 129, 587–604.

Chen, F., Kusaka, H., Bornstein, R., Ching, J., Grimmond, C.S.B., Grossman-Clarke, S., Loridan, T., Manning, K.W., Martilli, A., Miao, S., Sailor, D., Salamanca, F.P., Taha, H., Tewari, M., Wang, X., Wyszogrodzki, A.A., Zhang, C., 2011. The integrated WRF/urban modelling system: Development, evaluation, and applications to urban environmental problems. Int. J. Climatol. 31, 273–288. https://doi.org/10.1002/joc.2158

Chen, F., Yang, X., Zhu, W., 2014. WRF simulations of urban heat island under hot-weather synoptic conditions: The case study of Hangzhou City, China. Atmos. Res. 138, 364–377. https://doi.org/10.1016/j.atmosres.2013.12.005

Chen, G., Zhao, L., Mochida, A., 2016. Urban Heat Island simulations in Guangzhou, China, using the coupled WRF/UCM model with a land use map extracted from remote sensing data. Sustain. 8. https://doi.org/10.3390/su8070628

Chew, L.W., Liu, X., Li, X.X., Norford, L.K., 2021. Interaction between heat wave and urban heat island: A case study in a tropical coastal city, Singapore. Atmos. Res. 247, 105134. https://doi.org/10.1016/j.atmosres.2020.105134

Ciancio, V., Falasca, S., Golasi, I., Curci, G., Coppi, M., Salata, F., 2018. Influence of input climatic data on simulations of annual energy needs of a building: Energyplus and WRF modeling for a case study in Rome (Italy). Energies 11. https://doi.org/10.3390/en11102835

CIBSE, 2017. Design methodology for the assessment of overheating risk in homes. Tech. Memo. 59. https://doi.org/CIBSE TM59: 2017

CIBSE, 2014. Design Summer Years for London. Tech. Memo. 49 1–29.

CIBSE, 2013. The limits of thermal comfort : avoiding overheating in European buildings, CIBSE TM52. https://doi.org/10.1017/CBO9781107415324.004

CIBSE, 2011. Environmental design CIBSE: Guide A.

CIBSE, G.J., 2002. Weather, solar and illuminance data. Chart. Inst. Build. Serv. Eng.

Clarke, J.A., Yaneske, P.P., Pinney, A.A., 1990. The harmonisation of thermal properties of building materials. BRE, UK 87.

Cloke, H.L., Pappenberger, F., 2009. Ensemble flood forecasting: A review. J. Hydrol. 375, 613–626.

Crawley, D.B., Lawrie, L.K., 2015. Rethinking the tmy: Is the "typical" meteorological year best for building performance simulation?, in: 14th International Conference of IBPSA - Building Simulation 2015, BS 2015, Conference Proceedings. pp. 2655–2662.

Cui, Y.Y., De Foy, B., 2012. Seasonal variations of the urban heat island at the surface and the near-surface and reductions due to urban vegetation in Mexico City. J. Appl. Meteorol.

Climatol. 51, 855–868. https://doi.org/10.1175/JAMC-D-11-0104.1

Curry, C.L., Tencer, B., Whan, K., Weaver, A.J., Giguère, M., Wiebe, E., 2016. Searching for Added Value in Simulating Climate Extremes with a High-Resolution Regional Climate Model over Western Canada. Atmos. - Ocean 54, 364–384. https://doi.org/10.1080/07055900.2016.1158146

Dee, D.P., Uppala, S.M., Simmons, A.J., Berrisford, P., Poli, P., Kobayashi, S., Andrae, U., Balmaseda, M.A., Balsamo, G., Bauer, d P., 2011. The ERA-Interim reanalysis: Configuration and performance of the data assimilation system. Q. J. R. Meteorol. Soc. 137, 553–597.

Demanuele, C., Mavrogianni, A., Davies, M., Kolokotroni, M., Rajapaksha, I., 2012. Using localised weather files to assess overheating in naturally ventilated offices within London's urban heat island. Build. Serv. Eng. Res. Technol. 33, 351–369. https://doi.org/10.1177/0143624411416064

Department for Education Schools and Families (DfES), 2006. Building Bulletin 101 Ventilation of School Buildings.

Department of Health, 2007a. Heating and ventilation systems Health Technical Memorandum 03-01: Specialised ventilation for healthcare premises. Part B: Operational management and performance verification, Department of Health.

Department of Health, 2007b. Heating and ventilation systems. Health Technical Memorandum 03-01: Specialised ventilation for healthcare premises. Part A: Design and validation., Department of Health.

Di Luca, A., de Elía, R., Laprise, R., 2015. Challenges in the quest for added value of regional climate dynamical downscaling. Curr. Clim. Chang. Reports 1, 10–21.

DiNardi, S.R., 2003. The occupational environment: its evaluation, control, and management. AIHA Press (American Industrial Hygiene Association) Fairfax, VA.

Direction régionale de santé publique de Montréal, 2018. Canicule : Juillet 2018 - Montréal, Bilan préliminaire. Montréal, Québec.

DOD, 2003. Technical bulletin: heat stress control and heat casualty management. TB MED 507/AFPAM 48-152 (I)., Washington, DC: Departments of the U.S. Army, Navy, and Air Force.

Doherty, T., Arens, E.A., 1988. Evaluation of the physiological bases of thermal comfort models. ASHRAE Trans. 94.

Du, H., Underwood, C.P., Edge, J.S., 2012. Generating design reference years from the UKCP09 projections and their application to future air-conditioning loads. Build. Serv. Eng. Res. Technol. 33, 63–79. https://doi.org/10.1177/0143624411431775

Duan, S., Luo, Z., Yang, X., Li, Y., 2019. The impact of building operations on urban heat/cool islands under urban densification: A comparison between naturally-ventilated and air-

conditioned buildings. Appl. Energy 235, 129–138. https://doi.org/10.1016/j.apenergy.2018.10.108

Dudhia, J., 1989. Numerical study of convection observed during the winter monsoon experiment using a mesoscale two-dimensional model. J. Atmos. Sci. 46, 3077–3107.

Eames, M., Kershaw, T., Coley, D., 2012. The appropriate spatial resolution of future weather files for building simulation. J. Build. Perform. Simul. 5, 347–358. https://doi.org/10.1080/19401493.2011.608133

Eames, M.E., 2016. An update of the UK's design summer years: Probabilistic design summer years for enhanced overheating risk analysis in building design. Build. Serv. Eng. Res. Technol. 37, 503–522. https://doi.org/10.1177/0143624416631131

ECCC, 2021. Historical weather data, Canada.

ECCC, 2019. Canada's top 10 weather stories of 2018. [WWW Document]. URL https://www.canada.ca/en/environment-climate-change/services/top-ten-weather-stories/2018.html#toc1

Ek, M.B., Mitchell, K.E., Lin, Y., Rogers, E., Grunmann, P., Koren, V., Gayno, G., Tarpley, J.D., 2003. Implementation of Noah land surface model advances in the National Centers for Environmental Prediction operational mesoscale Eta model. J. Geophys. Res. 108, 8851. https://doi.org/10.1029/2002JD003296

Environment and Climate Change Canada, 2021. Glossary - Climate - Environment and Climate Change Canada [WWW Document]. climate.weather.gc.ca. URL https://climate.weather.gc.ca/glossary_e.html

Erler, A.R., Peltier, W.R., 2016. Projected changes in precipitation extremes for western Canada based on high-resolution regional climate simulations. J. Clim. 29, 8841–8863. https://doi.org/10.1175/JCLI-D-15-0530.1

Ferrari, D., Lee, T., 2008. Beyond TMY : Climate Data for Specific Applications, in: Proceedings 3rd International Solar Energy Society Conference–Asia Pacific Region (ISES-AP-08), Citeseer; 2008. pp. 1–12.

Flores-Larsen, S., Filippín, C., 2021. Energy efficiency, thermal resilience, and health during extreme heat events in low-income housing in Argentina. Energy Build. 231, 110576. https://doi.org/10.1016/j.enbuild.2020.110576

Foley, A.M., Leahy, P.G., Marvuglia, A., McKeogh, E.J., 2012. Current methods and advances in forecasting of wind power generation. Renew. energy 37, 1–8.

Fosser, G., Khodayar, S., Berg, P., 2015. Benefit of convection permitting climate model simulations in the representation of convective precipitation. Clim. Dyn. 44, 45–60.

Friedman, M., 1937. The Use of Ranks to Avoid the Assumption of Normality Implicit in the Analysis of Variance. J. Am. Stat. Assoc. 32, 675–701. https://doi.org/10.1080/01621459.1937.10503522

Gagge, A.P., Fobelets, A.P., Berglund, L., 1986. A standard predictive Index of human reponse to thermal enviroment. Trans. Soc. Heating, Refrig. Air-Conditioning Eng. 92, 709–731.

Gaur, A., Lacasse, M., Armstrong, M., 2019. Climate Data to Undertake Hygrothermal and Whole Building Simulations Under Projected Climate Change Influences for 11 Canadian Cities. Data 4, 72. https://doi.org/10.3390/data4020072

Gaur, A., Lacasse, M., Armstrong, M., Lu, H., Shu, C., Fields, A., Palou, F.S., Zhang, Y., 2021. Effects of using different urban parametrization schemes and land-cover datasets on the accuracy of WRF model over the City of Ottawa. Urban Clim. 35, 100737. https://doi.org/10.1016/j.uclim.2020.100737

Georgescu, M., Moustaoui, M., Mahalov, A., Dudhia, J., 2013. Summer-time climate impacts of projected megapolitan expansion in Arizona. Nat. Clim. Chang. 3, 37–41. https://doi.org/10.1038/nclimate1656

Giles, B.D., Balafoutis, C., Maheras, P., 1990. Too hot for comfort: The heatwaves in Greece in 1987 and 1988. Int. J. Biometeorol. 34, 98–104. https://doi.org/10.1007/BF01093455

Giorgi, F., 2019. Thirty Years of Regional Climate Modeling: Where Are We and Where Are We Going next? J. Geophys. Res. Atmos. 124, 5696–5723. https://doi.org/10.1029/2018JD030094

Giorgi, F., Gutowski Jr, W.J., 2015. Regional dynamical downscaling and the CORDEX initiative. Annu. Rev. Environ. Resour. 40, 467–490.

Giscience, A., April, R.S., Xian, G., Shi, H., Auch, R., Gallo, K., Zhou, Q., Wu, Z., Xian, G., Shi, H., Auch, R., Gallo, K., Zhou, Q., Wu, Z., 2021. The effects of urban land cover dynamics on urban heat Island intensity and temporal trends. GIScience Remote Sens. 00, 1–15. https://doi.org/10.1080/15481603.2021.1903282

Göndöcs, J., Breuer, H., Pongrácz, R., Bartholy, J., 2017. Urban heat island mesoscale modelling study for the Budapest agglomeration area using the WRF model. Urban Clim. 21, 66–86. https://doi.org/10.1016/j.uclim.2017.05.005

Gracik, S., Heidarinejad, M., Liu, J., Srebric, J., 2015. Effect of urban neighborhoods on the performance of building cooling systems. Build. Environ. 90, 15–29. https://doi.org/10.1016/j.buildenv.2015.02.037

Grossman-Clarke, S., Zehnder, J.A., Loridan, T., Grimmond, C.S.B., 2010. Contribution of land use changes to near-surface air temperatures during recent summer extreme heat events in the Phoenix metropolitan area. J. Appl. Meteorol. Climatol. 49, 1649–1664. https://doi.org/10.1175/2010JAMC2362.1

Guan, L., 2009. Preparation of future weather data to study the impact of climate change on buildings. Build. Environ. 44, 793–800. https://doi.org/10.1016/j.buildenv.2008.05.021

Guo, S., Yan, D., Hong, T., Xiao, C., Cui, Y., 2019. A novel approach for selecting typical hot-year (THY) weather data. Appl. Energy 242, 1634–1648. https://doi.org/10.1016/j.apenergy.2019.03.065

Gupta, R., Barnfield, L., Gregg, M., 2017. Overheating in care settings: magnitude, causes, preparedness and remedies. Build. Res. Inf. 45, 83–101. https://doi.org/10.1080/09613218.2016.1227923

Hahmann, A.N., Vincent, C.L., Peña, A., Lange, J., Hasager, C.B., 2015. Wind climate estimation using WRF model output: Method and model sensitivities over the sea. Int. J. Climatol. 35, 3422–3439. https://doi.org/10.1002/joc.4217

Han, W., Li, Z., Wu, F., Zhang, Y., Guo, J., Su, T., Cribb, M., Fan, J., Chen, T., Wei, J., Lee, S.S., 2020. The mechanisms and seasonal differences of the impact of aerosols on daytime surface urban heat island effect. Atmos. Chem. Phys. 20, 6479–6493. https://doi.org/10.5194/acp-20-6479-2020

Havenith, G., Fiala, D., 2016. Thermal indices and thermophysiological modeling for heat stress. Compr. Physiol. 6, 255–302. https://doi.org/10.1002/cphy.c140051

Herrera, M., Natarajan, S., Coley, D.A., Kershaw, T., Ramallo-González, A.P., Eames, M., Fosas, D., Wood, M., 2017. A review of current and future weather data for building simulation. Build. Serv. Eng. Res. Technol. 38, 602–627. https://doi.org/10.1177/0143624417705937

Hohenegger, C., Brockhaus, P., Schar, C., 2008. Towards climate simulations at cloud-resolving scales. Meteorol. Zeitschrift 17, 383–394.

Holmes, S.H., Phillips, T., Wilson, A., 2016. Overheating and passive habitability: Indoor health and heat indices. Build. Res. Inf. 44, 1–19. https://doi.org/10.1080/09613218.2015.1033875

Hong, S.Y., Dudhia, J., Chen, S.H., 2004. A revised approach to ice microphysical processes for the bulk parameterization of clouds and precipitation. Mon. Weather Rev. 132, 103–120. https://doi.org/10.1175/1520-0493(2004)132<0103:ARATIM>2.0.CO;2

Hwang, R.L., Lin, T.P., Lin, F.Y., 2020. Evaluation and mapping of building overheating risk and air conditioning use due to the urban heat island effect. J. Build. Eng. 32, 101726. https://doi.org/10.1016/j.jobe.2020.101726

Imran, H.M., Kala, J., Ng, A.W.M., Muthukumaran, S., 2018. Effectiveness of green and cool roofs in mitigating urban heat island effects during a heatwave event in the city of Melbourne in southeast Australia. J. Clean. Prod. 197, 393–405. https://doi.org/10.1016/j.jclepro.2018.06.179

International Standard Organization, 2004. ISO 7933:2004 Ergonomics of the thermal environment analytical determination and interpretation of heat stress using calculation of the predicted heat strain.

IOM, 2011. Climate Change, the Indoor Environment, and Health. National Academies Press, Washington, D.C. https://doi.org/10.17226/13115

IPCC, 2018. Special Report: Global Warming of 1.5 °C. https://doi.org/10.1016/j.oneear.2019.10.025

IPCC, 2014a. Climate Change 2014: Synthesis Report. Geneva, Switzerland.

https://doi.org/10.1016/S0022-0248(00)00575-3

IPCC, 2014b. Climate Change 2014: Synthesis Report. Contribution of Working Groups I-III to the Fifth Assessment Report of the IPCC, IPCC. https://doi.org/10.1016/S0022-0248(00)00575-3

IPCC, 2013. Summary for policymakers, in: Climate Change 2014: Impacts, Adaptation, and Vulnerability. Part A: Global and Sectoral Aspects. Contribution of Working Group II to the Fifth Assessment Report of the Intergovernmental Panel on Climate Change. p. 33. https://doi.org/10.1017/CBO9781107415324

ISO 7243, 2017. Ergonomics of the thermal environment — Assessment of heat stress using the WBGT (wet bulb globe. Int. Stand. 2017.

Jacklitsch, B., Williams, W., Musolin, K., Coca, A., Kim, J.-H., Turner, N., 2016. Criteria for a Recommended Standard Occupational Exposure to Heat and Hot Environment. US Dep. Heal. Hum. Serv. Publication 2016-106.

Jacklitsch, Brenda, Williams, W.J., Musolin, K., Coca, A., Kim, J.-H., Turner, N., 2016. NIOSH criteria for a recommended standard: occupational exposure to heat and hot environments. Dep Heal. Hum Serv Cent Dis Control Prev Natl Inst Occup Saf Heal. DHHS NIOSH Publ 106, 192.

Jain, R., Luo, X., Sever, G., Hong, T., Catlett, C., 2020. Representation and evolution of urban weather boundary conditions in downtown Chicago. J. Build. Perform. Simul. 13, 182–194. https://doi.org/10.1080/19401493.2018.1534275

Jandaghian, Z., Touchaei, A.G., Akbari, H., 2018. Sensitivity analysis of physical parameterizations in WRF for urban climate simulations and heat island mitigation in Montreal. Urban Clim. 24, 577–599. https://doi.org/10.1016/j.uclim.2017.10.004

Janjić, Z.I., 1994. The Step-Mountain Eta Coordinate Model: Further Developments of the Convection, Viscous Sublayer, and Turbulence Closure Schemes. Mon. Weather Rev. 53, 927–945. https://doi.org/https://doi.org/10.1175/1520-0493(1994)122<0927:TSMECM>2.0.CO;2

Jenkins, D.P., Peacock, A.D., Banfill, P.F.G., 2009. Will future low-carbon schools in the UK have an overheating problem? Build. Environ. 44, 490–501. https://doi.org/10.1016/j.buildenv.2008.04.012

Jentsch, M.F., Eames, M.E., Levermore, G.J., 2015. Generating near-extreme Summer Reference Years for building performance simulation. Build. Serv. Eng. Res. Technol. 36, 701–721. https://doi.org/10.1177/0143624415587476

Jentsch, M.F., Levermore, G.J., Parkinson, J.B., Eames, M.E., 2014. Limitations of the CIBSE design summer year approach for delivering representative near-extreme summer weather conditions. Build. Serv. Eng. Res. Technol. 35, 155–169. https://doi.org/10.1177/0143624413478436

Ji, L., Laouadi, A., Shu, C., Wang, L., Lacasse, M.A., 2021. Evaluation and improvement of the

thermoregulatory system for the two-node bioheat model. Energy Build. 249, 111235. https://doi.org/10.1016/j.enbuild.2021.111235

Jones, P., Jones, P., Harpham, C., Harpham, C., Kilsby, C., Kilsby, C., Glenis, V., Glenis, V., Burton, a, Burton, a, 2009. Projections of future daily climate for the UK from the Weather Generator. Weather 44.

Kain, J.S., 2004. The Kain–Fritsch Convective Parameterization: An Update. J. Appl. Meteorol. 43, 170–181.

Kang, H.-Q., Zhu, B., Zhu, T., Sun, J.-L., Ou, J.-J., 2014. Impact of Megacity Shanghai on the Urban Heat-Island Effects over the Downstream City Kunshan. Boundary-Layer Meteorol. 152, 411–426. https://doi.org/10.1007/s10546-014-9927-1

Kendall, M.G., 1948. Rank correlation methods.

Kendall, M.G., 1938. A New Measure of Rank Correlation. Biometrika 30, 81. https://doi.org/10.2307/2332226

Klein Rosenthal, J., Kinney, P.L., Metzger, K.B., 2014. Intra-urban vulnerability to heat-related mortality in New York City, 1997-2006. Heal. Place 30, 45–60. https://doi.org/10.1016/j.healthplace.2014.07.014

Kleissl, J., 2013. Solar energy forecasting and resource assessment. Academic Press.

Kolokotroni, M., Davies, M., Croxford, B., Bhuiyan, S., Mavrogianni, A., 2010. A validated methodology for the prediction of heating and cooling energy demand for buildings within the Urban Heat Island: Case-study of London. Sol. Energy 84, 2246–2255. https://doi.org/10.1016/j.solener.2010.08.002

Kolokotroni, M., Giannitsaris, I., Watkins, R., 2006. The effect of the London urban heat island on building summer cooling demand and night ventilation strategies. Sol. Energy 80, 383–392. https://doi.org/10.1016/j.solener.2005.03.010

Kolokotroni, M., Giridharan, R., 2008. Urban heat island intensity in London: An investigation of the impact of physical characteristics on changes in outdoor air temperature during summer. Sol. Energy 82, 986–998. https://doi.org/10.1016/j.solener.2008.05.004

Kolokotroni, M., Ren, X., Davies, M., Mavrogianni, A., 2012. London's urban heat island: Impact on current and future energy consumption in office buildings. Energy Build. 47, 302–311. https://doi.org/10.1016/j.enbuild.2011.12.019

Kolokotroni, M., Zhang, Y., Giridharan, R., 2009. Heating and cooling degree day prediction within the London urban heat island area. Build. Serv. Eng. Res. Technol. 30, 183–202. https://doi.org/10.1177/0143624409104733

Krayenhoff, E.S., Moustaoui, M., Broadbent, A.M., Gupta, V., Georgescu, M., 2018. Diurnal interaction between urban expansion, climate change and adaptation in US cities. Nat. Clim. Chang. 8, 1097–1103.

Kruskal, W.H., 1958. Ordinal measures of association. J. Am. Stat. Assoc. 53, 814–861.

Laframboise, K., 2018. Heat wave blamed for 53 deaths in Montreal [WWW Document]. Glob. News.

Lamothe, F., Roy, M., Racine-Hamel, S.-É., 2019. Enquête épidémiologique - Vague de chaleur à l'été 2018 à Montréal. Montréal, Québec. https://doi.org/9782550840206

Langhans, W., Schmidli, J., Fuhrer, O., Bieri, S., Schär, C., 2013. Long-term simulations of thermally driven flows and orographic convection at convection-parameterizing and cloud-resolving resolutions. J. Appl. Meteorol. Climatol. 52, 1490–1510.

Laouadi, A., Bartko, M., Lacasse, M.A., 2020a. A new methodology of evaluation of overheating in buildings. Energy Build. 226, 110360. https://doi.org/10.1016/j.enbuild.2020.110360

Laouadi, A., Gaur, A., Lacasse, M.A., Bartko, M., Armstrong, M., 2020b. Development of reference summer weather years for analysis of overheating risk in buildings. J. Build. Perform. Simul. 13, 301–319. https://doi.org/10.1080/19401493.2020.1727954

Lazurca, L.G., Mihaila, D., Bistricean, P. lonel, 2016. Spatial and temporal relevance of some bioclimatic indexes for the study of the bioclimate of Moldova (west of the Prut river) Spatial and temporal relevance of some bioclimatic indexes for the study of the bioclimate of Moldova (west of the Prut river. https://doi.org/10.4316/GEOREVIEW.2016.26.1.365

Leroyer, S., Bélair, S., Husain, S.Z., Mailhot, J., 2014. Subkilometer numerical weather prediction in an urban coastal area: A case study over the Vancouver metropolitan area. J. Appl. Meteorol. Climatol. 53, 1433–1453. https://doi.org/10.1175/JAMC-D-13-0202.1

Leroyer, S., Bélair, S., Mailhot, J., Strachan, I.B., 2011. Microscale numerical prediction over Montreal with the Canadian external urban modeling system. J. Appl. Meteorol. Climatol. 50, 2410–2428. https://doi.org/10.1175/JAMC-D-11-013.1

Leroyer, S., Bélair, S., Spacek, L., Gultepe, I., 2018. Modelling of radiation-based thermal stress indicators for urban numerical weather prediction. Urban Clim. 25, 64–81. https://doi.org/10.1016/j.uclim.2018.05.003

Li, D., Bou-Zeid, E., 2013. Synergistic interactions between urban heat islands and heat waves: The impact in cities is larger than the sum of its parts. J. Appl. Meteorol. Climatol. 52, 2051–2064. https://doi.org/10.1175/JAMC-D-13-02.1

Li, D., Bou-Zeid, E., Oppenheimer, M., 2014. The effectiveness of cool and green roofs as urban heat island mitigation strategies. Environ. Res. Lett. 9. https://doi.org/10.1088/1748-9326/9/5/055002

Li, H., Wolter, M., Wang, X., Sodoudi, S., 2018. Impact of land cover data on the simulation of urban heat island for Berlin using WRF coupled with bulk approach of Noah-LSM. Theor. Appl. Climatol. 134, 67–81. https://doi.org/10.1007/s00704-017-2253-z

Li, H., Zhou, Y., Wang, X., Zhou, X., Zhang, H., Sodoudi, S., 2019. Quantifying urban heat island intensity and its physical mechanism using WRF/UCM. Sci. Total Environ. 650, 3110–3119.

https://doi.org/10.1016/j.scitotenv.2018.10.025

Li, X.-X., Norford, L.K., 2016. Evaluation of cool roof and vegetations in mitigating urban heat island in a tropical city, Singapore. Urban Clim. 16, 59–74. https://doi.org/10.1016/j.uclim.2015.12.002

List of heat waves [WWW Document], 2020. URL https://en.wikipedia.org/wiki/List_of_heat_waves

Liu, C., Kershaw, T., Eames, M.E., Coley, D.A., 2016. Future probabilistic hot summer years for overheating risk assessments. Build. Environ. 105, 56–68. https://doi.org/10.1016/j.buildenv.2016.05.028

Liu, C., Kershaw, T., Fosas, D., Ramallo Gonzalez, A.P., Natarajan, S., Coley, D.A., 2017. High resolution mapping of overheating and mortality risk. Build. Environ. 122, 1–14. https://doi.org/10.1016/j.buildenv.2017.05.028

Liu, Y., Chen, F., Warner, T., Basara, J., 2006. Verification of a Mesoscale Data-Assimilation and Forecasting System for the Oklahoma City Area during the Joint Urban 2003 Field Project. J. Appl. Meteorol. Climatol. 45, 912–929.

Lomas, K.J., Giridharan, R., 2012. Thermal comfort standards, measured internal temperatures and thermal resilience to climate change of free-running buildings: A case-study of hospital wards. Build. Environ. 55, 57–72. https://doi.org/10.1016/j.buildenv.2011.12.006

Lomas, K.J., Porritt, S.M., 2017. Overheating in buildings: lessons from research. Build. Res. Inf. 45, 1–18. https://doi.org/10.1080/09613218.2017.1256136

Loughnan, M., Carroll, M., Tapper, N.J., 2015. The relationship between housing and heat wave resilience in older people. Int. J. Biometeorol. 59, 1291–1298. https://doi.org/10.1007/s00484-014-0939-9

Lucas-Picher, P., Laprise, R., Winger, K., 2017. Evidence of added value in North American regional climate model hindcast simulations using ever-increasing horizontal resolutions. Clim. Dyn. 48, 2611–2633. https://doi.org/10.1007/s00382-016-3227-z

Luo, X., Vahmani, P., Hong, T., Jones, A., 2020. City-scale building anthropogenic heating during heat waves. Atmosphere (Basel). 11. https://doi.org/10.3390/atmos11111206

Macintyre, H.L., Heaviside, C., Taylor, J., Picetti, R., Symonds, P., Cai, X.M., Vardoulakis, S., 2018. Assessing urban population vulnerability and environmental risks across an urban area during heatwaves – Implications for health protection. Sci. Total Environ. 610–611, 678–690. https://doi.org/10.1016/j.scitotenv.2017.08.062

Mahoney, K., Alexander, M., Scott, J.D., Barsugli, J., 2013. High-resolution downscaled simulations of warm-season extreme precipitation events in the Colorado Front Range under past and future climates. J. Clim. 26, 8671–8689.

Mahoney, K., Alexander, M.A., Thompson, G., Barsugli, J.J., Scott, J.D., 2012. Changes in hail and flood risk in high-resolution simulations over Colorado's mountains. Nat. Clim. Chang.

2, 125–131.

Martilli, A., Clappier, A., Rotach, M.W., 2002. An urban surface exchange parameterisation for mesoscale models. Boundary-Layer Meteorol. 104, 261–304.

Martynov, A., Laprise, R., Sushama, L., Winger, K., Šeparović, L., Dugas, B., 2013. Reanalysis-driven climate simulation over CORDEX North America domain using the Canadian Regional Climate Model, version 5: model performance evaluation. Clim. Dyn. 41, 2973–3005.

Masterton, J.M., Richardson, F.A., 1979. Humidex: a method of quantifying human discomfort due to excessive heat and humidity. Environment Canada, Atmospheric Environment.

Matzarakis, A., Mayer, H., 1991. The Extreme Heat Wave in Athens in July 1987 from the Point of View of Human Biometeorology. Atmos. Environ. 25.

Mavrogianni, A., Davies, M., Taylor, J., Chalabi, Z., Biddulph, P., Oikonomou, E., Das, P., Jones, B., 2014. The impact of occupancy patterns, occupant-controlled ventilation and shading on indoor overheating risk in domestic environments. Build. Environ. 78, 183–198. https://doi.org/10.1016/j.buildenv.2014.04.008

Mavrogianni, A., Davies, M., Wilkinson, P., Pathan, A., 2010. London housing and climate change: Impact on comfort and health - preliminary results of a summer overheating study. Open House Int.

Mavrogianni, A., Pathan, A., Oikonomou, E., Biddulph, P., Symonds, P., Davies, M., 2017. Inhabitant actions and summer overheating risk in London dwellings. Build. Res. Inf. 45, 119–142. https://doi.org/10.1080/09613218.2016.1208431

Mayer, S., Maule, C.F., Sobolowski, S., Christensen, O.B., Sørup, H.J.D., Sunyer, M.A., Arnbjerg-Nielsen, K., Barstad, I., 2015. Identifying added value in high-resolution climate simulations over Scandinavia. Tellus, Ser. A Dyn. Meteorol. Oceanogr. 67, 1–18. https://doi.org/10.3402/tellusa.v67.24941

McCarthy, M.P., Harpham, C., Goodess, C.M., Jones, P.D., 2012. Simulating climate change in UK cities using a regional climate model, HadRM3. Int. J. Climatol. 32, 1875–1888. https://doi.org/10.1002/joc.2402

McGill, G., Sharpe, T., Robertson, L., Gupta, R., Mawditt, I., 2017. Meta-analysis of indoor temperatures in new-build housing. Build. Res. Inf. 45, 19–39. https://doi.org/10.1080/09613218.2016.1226610

Meehl, G.A., Tebaldi, C., 2004. More intense, more frequent, and longer lasting heat waves in the 21st century. Science (80-.). 305, 994–997. https://doi.org/10.1126/science.1098704

Mesinger, F., DiMego, G., Kalnay, E., Mitchell, K., Shafran, P.C., Ebisuzaki, W., Jovic, D., Woolen, J., Rogers, E., Berbery, E.H., 2006. North American regional reanalysis. Bulletin of the American Meteorological Society. Am. Meteorol. Soc. 87, 343–360.

Miao, S., Chen, F., LeMone, M.A., Tewari, M., Li, Q., Wang, Y., 2009. An observational and

modeling study of characteristics of urban heat island and boundary layer structures in Beijing. J. Appl. Meteorol. Climatol. 48, 484–501. https://doi.org/10.1175/2008JAMC1909.1

Mlawer, E.J., Taubman, J., Brown, P.D., Iacono, M.J., Clough, S.A., 1997. Radiative transfer for inhomogeneous atmospheres: RRTM, a validated correlated-k model for the longwave 102.

Moazami, A., Nik, V.M., Carlucci, S., Geving, S., 2019. Impacts of future weather data typology on building energy performance – Investigating long-term patterns of climate change and extreme weather conditions. Appl. Energy 238, 696–720. https://doi.org/10.1016/j.apenergy.2019.01.085

Moffett, K.B., Makido, Y., Shandas, V., 2019. Urban-rural surface temperature deviation and intra-urban variations contained by an urban growth boundary. Remote Sens. 11. https://doi.org/10.3390/rs11222683

Mohamed, S., Rodrigues, L., Omer, S., Calautit, J., 2021. Overheating and indoor air quality in primary schools in the UK. Energy Build. 250, 111291. https://doi.org/10.1016/j.enbuild.2021.111291

Mölg, T., Kaser, G., 2011. A new approach to resolving climate-cryosphere relations: Downscaling climate dynamics to glacier-scale mass and energy balance without statistical scale linking. J. Geophys. Res. Atmos. 116.

Montazami, A., Nicol, F., 2013. Overheating in schools: Comparing existing and new guidelines. Build. Res. Inf. 41, 317–329. https://doi.org/10.1080/09613218.2013.770716

Morini, E., Touchaei, A.G., Castellani, B., Rossi, F., Cotana, F., 2016. The impact of albedo increase to mitigate the urban heat island in Terni (Italy) using the WRF model. Sustain. 8. https://doi.org/10.3390/su8100999

Murage, P., Kovats, S., Sarran, C., Taylor, J., McInnes, R., Hajat, S., 2020. What individual and neighbourhood-level factors increase the risk of heat-related mortality? A case-crossover study of over 185,000 deaths in London using high-resolution climate datasets. Environ. Int. 134, 105292. https://doi.org/10.1016/j.envint.2019.105292

Musco, F., Appiotti, F., Bianchi, I., Fontana, M.D., Gissi, E., Lucertini, G., Magni, F., Maragno, D., 2016. Planning and climate change: Concepts, approaches, design, Counteracting Urban Heat Island Effects in a Global Climate Change Scenario. https://doi.org/10.1007/978-3-319-10425-6

Mylona, A., 2019. Assessing and mitigating overheating in buildings. Build. Serv. Eng. Res. Technol. 40, 385–388. https://doi.org/10.1177/0143624419851442

Mylona, A., 2012. The use of UKCP09 to produce weather files for building simulation. Build. Serv. Eng. Res. Technol. 33, 51–62. https://doi.org/10.1177/0143624411428951

Narowski, P., Janicki, M., Heim, D., 2013. Comparison of Untypical Meteorological Years (UMY) and their influence on building energy performance simulations, in: Proceedings of BS2013: 13th Conference of International Building Performance Simulation Association, Chambéry, France, August 26-28. pp. 1414–1421.

National Centers for Environmental Prediction, National Weather Service, NOAA, U.S. Department of Commerce, 2005. NCEP North American Regional Reanalysis (NARR).

National Research Council of Canada, 2017. National Energy Code of Canada for Buildings 2017.

National Research Council of Canada, 2015. National Building Code of Canada.

National Weather Service, 2021. What is the heat index?

Nazarian, N., Fan, J., Sin, T., Norford, L., Kleissl, J., 2017. Predicting outdoor thermal comfort in urban environments: A 3D numerical model for standard effective temperature. Urban Clim. 20, 251–267. https://doi.org/10.1016/j.uclim.2017.04.011

Nik, V.M., 2016. Making energy simulation easier for future climate - Synthesizing typical and extreme weather data sets out of regional climate models (RCMs). Appl. Energy 177, 204–226. https://doi.org/10.1016/j.apenergy.2016.05.107

Niu, G.Y., Yang, Z.L., Mitchell, K.E., Chen, F., Ek, M.B., Barlage, M., Kumar, A., Manning, K., Niyogi, D., Rosero, E., Tewari, M., Xia, Y., 2011. The community Noah land surface model with multiparameterization options (Noah-MP): 1. Model description and evaluation with local-scale measurements. J. Geophys. Res. Atmos. 116, 1–19. https://doi.org/10.1029/2010JD015139

North American Land Change Monitoring System (NALCMS) dataset, 2015 [WWW Document], 2015.

Occupational Safety and Health Administration, 2011. Protecting workers from heat illness. OSHA-NIOSH Infosheet. URL= http//www. cdc. gov/niosh/docs/2011-174/pdfs/2011-174. pdf (accessed Oct. 21, 2012).

Oikonomou, E., Davies, M., Mavrogianni, A., Biddulph, P., Wilkinson, P., Kolokotroni, M., 2012. Modelling the relative importance of the urban heat island and the thermal quality of dwellings for overheating in London. Build. Environ. 57, 223–238. https://doi.org/10.1016/j.buildenv.2012.04.002

Oke, T.R., 2006. Instruments and observing methods: Report No. 81: initial guidance to obtain representative meteorological observations at urban sites. World Meteorol. Organ. WMO/TD 51.

Oke, T.R., 1982. The energetic basis of the urban heat island (Symons Memorial Lecture, 20 May 1980). Q. Journal, R. Meteorol. Soc. 108, 1–24.

Oke, T.R., 1981. Canyon geometry and the nocturnal urban heat island: comparison of scale model and field observations. J. Climatol. 1, 237–254.

Ooka, R., Minami, Y., Sakoi, T., Tsuzuki, K., Rijal, H.B., 2010. Improvement of sweating model in 2-Node Model and its application to thermal safety for hot environments. Build. Environ. 45, 1565–1573.

Otto, F.E.L., Massey, N., Van Oldenborgh, G.J., Jones, R.G., Allen, M.R., 2012. Reconciling two

approaches to attribution of the 2010 Russian heat wave. Geophys. Res. Lett. 39, 1–5. https://doi.org/10.1029/2011GL050422

Palou, F.S., Mahalov, A., 2019. Summer-and wintertime variations of the surface and near-surface urban heat island in a semiarid environment. Weather Forecast. 34, 1849–1865. https://doi.org/10.1175/WAF-D-19-0054.1

Parekh, A., 2012. Representative Housing Thermal Archetypes for Energy Analysis Models. Ottawa, ON, Canada.

Parsons, K., 2007. Human thermal environments: the effects of hot, moderate, and cold environments on human health, comfort and performance. CRC press.

Patania, F., Gagliano, A., Nocera, F., Galesi, A., 2015. Analysis of the thermal comfort of passengers inside the public transports of Catania city.

Paul, S., Ghosh, S., Mathew, M., Devanand, A., Karmakar, S., Niyogi, D., 2018. Increased Spatial Variability and Intensification of Extreme Monsoon Rainfall due to Urbanization. Sci. Rep. 8. https://doi.org/10.1038/s41598-018-22322-9

Pepi, J.W., 1987. The summer simmer index. Weatherwise 40, 143–145.

Pepi, J.W., Maynard, M.A., 2000. The New Summer Simmer Index-A Comfort Index For The New Millennium, in: International Audience at the 80th Annual Meeting of the AMS: 11 January 2000; Long Beach, California.

Perry, M., Hollis, D., 2005a. The generation of monthly gridded datasets for a range of climatic variables over the UK. Int. J. Climatol. 25, 1041–1054. https://doi.org/10.1002/joc.1161

Perry, M., Hollis, D., 2005b. The development of a new set of long-term climate averages for the UK. Int. J. Climatol. 25, 1023–1039. https://doi.org/10.1002/joc.1160

PHI, 2016. Criteria for the Passive House, EnerPHit and PHI Low Energy Building Standard. Passiv. House Inst. 1–27.

Poupkou, A., Nastos, P., Melas, D., Zerefos, C., 2011. Climatology of discomfort index and air quality index in a large urban mediterranean agglomeration. Water. Air. Soil Pollut. 222, 163–183. https://doi.org/10.1007/s11270-011-0814-9

Prein, A F, Gobiet, A., Suklitsch, M., Truhetz, H., Awan, N.K., Keuler, K., Georgievski, G., 2013. Added value of convection permitting seasonal simulations. Clim. Dyn. 41, 2655–2677.

Prein, Andreas F, Holland, G.J., Rasmussen, R.M., Done, J., Ikeda, K., Clark, M.P., Liu, C.H., 2013. Importance of regional climate model grid spacing for the simulation of heavy precipitation in the Colorado headwaters. J. Clim. 26, 4848–4857.

Prein, A.F., Langhans, W., Fosser, G., Ferrone, A., Ban, N., Goergen, K., Keller, M., Tölle, M., Gutjahr, O., Feser, F., Brisson, E., Kollet, S., Schmidli, J., Van Lipzig, N.P.M., Leung, R., 2015. A review on regional convection-permitting climate modeling: Demonstrations, prospects, and challenges. Rev. Geophys. 53, 323–361.

https://doi.org/10.1002/2014RG000475

Pyrgou, A., Castaldo, V.L., Pisello, A.L., Cotana, F., Santamouris, M., 2017. Differentiating responses of weather files and local climate change to explain variations in building thermal-energy performance simulations. Sol. Energy 153, 224–237. https://doi.org/10.1016/j.solener.2017.05.040

Qiu, L., Im, E.-S., Hur, J., Shim, K.-M., 2020. Added value of very high resolution climate simulations over South Korea using WRF modeling system. Clim. Dyn. 54, 173–189.

Quinn, A., Tamerius, J.D., Perzanowski, M., Jacobson, J.S., Goldstein, I., Acosta, L., Shaman, J., 2014. Predicting indoor heat exposure risk during extreme heat events. Sci. Total Environ. 490, 686–693. https://doi.org/10.1016/j.scitotenv.2014.05.039

Rasmussen, R., Ikeda, K., Liu, C., Gochis, D., Clark, M., Dai, A., Gutmann, E., Dudhia, J., Chen, F., Barlage, M., 2014. Climate change impacts on the water balance of the Colorado headwaters: High-resolution regional climate model simulations. J. Hydrometeorol. 15, 1091–1116.

Rasul, A., Balzter, H., Smith, C., 2016. Diurnal and seasonal variation of surface Urban Cool and Heat Islands in the semi-arid city of Erbil, Iraq. Climate 4. https://doi.org/10.3390/cli4030042

Robine, J.M., Cheung, S.L.K., Le Roy, S., Van Oyen, H., Griffiths, C., Michel, J.P., Herrmann, F.R., 2008. Death toll exceeded 70,000 in Europe during the summer of 2003. Comptes Rendus - Biol. 331, 171–178. https://doi.org/10.1016/j.crvi.2007.12.001

Robinson, P.J., 2011. On the definition of a heat wave. J. Appl. Meteorol. 2, 201–215. https://doi.org/10.5802/ambp.31

Rothfusz, L.P., Headquarters, N.W.S.S.R., 1990. The heat index equation (or, more than you ever wanted to know about heat index). Fort Worth, Texas Natl. Ocean. Atmos. Adm. Natl. Weather Serv. Off. Meteorol. 9023.

Saha, S., Moorthi, S., Pan, H.-L., Wu, X., Wang, J., Nadiga, S., Tripp, P., Kistler, R., Woollen, J., Behringer, D., 2010. The NCEP climate forecast system reanalysis. Bull. Am. Meteorol. Soc. 91, 1015–1058.

Salamanca, F., Krpo, A., Martilli, A., Clappier, A., 2010. A new building energy model coupled with an urban canopy parameterization for urban climate simulations-part I. formulation, verification, and sensitivity analysis of the model. Theor. Appl. Climatol. 99, 331–344. https://doi.org/10.1007/s00704-009-0142-9

Salamanca, F., Martilli, A., 2010. A new Building Energy Model coupled with an Urban Canopy Parameterization for urban climate simulations-part II. Validation with one dimension off-line simulations. Theor. Appl. Climatol. 99, 345–356. https://doi.org/10.1007/s00704-009-0143-8

Salamanca, F., Martilli, A., Tewari, M., Chen, F., 2011. A study of the urban boundary layer using different urban parameterizations and high-resolution urban canopy parameters with WRF. J. Appl. Meteorol. Climatol. 50, 1107–1128. https://doi.org/10.1175/2010JAMC2538.1

Salamanca, F., Zhang, Y., Barlage, M., Chen, F., Mahalov, A., Miao, S., 2018. Evaluation of the WRF-Urban Modeling System Coupled to Noah and Noah-MP Land Surface Models Over a Semiarid Urban Environment. J. Geophys. Res. Atmos. 2387–2408. https://doi.org/10.1002/2018JD028377

Santamouris, M., Cartalis, C., Synnefa, A., 2015. Local urban warming , possible impacts and a resilience plan to climate change for the historical center of Athens , Greece. Sustain. Cities Soc. 19, 281–291. https://doi.org/10.1016/j.scs.2015.02.001

Santamouris, M., Kolokotsa, D., 2015. On the impact of urban overheating and extreme climatic conditions on housing, energy, comfort and environmental quality of vulnerable population in Europe. Energy Build. 98, 125–133. https://doi.org/10.1016/j.enbuild.2014.08.050

Schär, C., Jendritzky, G., 2004. Hot news from summer 2003. Nature 432, 559–560. https://doi.org/10.1038/432559a

Schubert, S., Grossman-Clarke, S., 2013. The Influence of green areas and roof albedos on air temperatures during Extreme Heat Events in Berlin, Germany. Meteorol. ZEITSCHRIFT 22, 131–143. https://doi.org/10.1127/0941-2948/2013/0393

Šeparović, L., Alexandru, A., Laprise, R., Martynov, A., Sushama, L., Winger, K., Tete, K., Valin, M., 2013. Present climate and climate change over North America as simulated by the fifth-generation Canadian regional climate model. Clim. Dyn. 41, 3167–3201.

Sharma, A., Conry, P., Fernando, H.J.S., Hamlet, A.F., Hellmann, J.J., Chen, F., 2016. Green and cool roofs to mitigate urban heat island effects in the Chicago metropolitan area: Evaluation with a regional climate model. Environ. Res. Lett. 11. https://doi.org/10.1088/1748-9326/11/6/064004

Siami, L., Ramadhani, A., 2019. Climatology of Discomfort Index for Decade in Bandar Lampung, Indonesia. KnE Soc. Sci. 2019, 460–469. https://doi.org/10.18502/kss.v3i21.4987

Skamarock, W.C., Klemp, J.B., Dudhia, J., Gill, D.O., Liu, Z., Berner, J., Wang, W., Powers, J.G., Duda, M.G., Barker, D.M., Huang, X.-Y., 2019. A Description of the Advanced Research WRF Model Version 4. Boulder, Colorado, USA.

Souch, C., Grimmond, C.S.B., 2004. Applied climatology: "Heat waves." Prog. Phys. Geogr. 28, 599–606. https://doi.org/10.1191/0309133304pp428pr

Spearman, C., 1904. The Proof and Measurement of Association between Two Things. Am. J. Psychol. 15, 72–101.

Sun, K., Specian, M., Hong, T., 2020. Nexus of thermal resilience and energy efficiency in buildings: A case study of a nursing home. Build. Environ. 177. https://doi.org/10.1016/j.buildenv.2020.106842

Symonds, P., Taylor, J., Mavrogianni, A., Davies, M., Shrubsole, C., Hamilton, I., Chalabi, Z., 2017. Overheating in English dwellings: comparing modelled and monitored large-scale datasets. Build. Res. Inf. 45, 195–208. https://doi.org/10.1080/09613218.2016.1224675

Taha, H., 2008. Meso-urban meteorological and photochemical modeling of heat island mitigation. Atmos. Environ. 42, 8795–8809.

Taylor, J., Davies, M., Mavrogianni, A., Chalabi, Z., Biddulph, P., Oikonomou, E., Das, P., Jones, B., 2014. The relative importance of input weather data for indoor overheating risk assessment in dwellings. Build. Environ. 76, 81–91. https://doi.org/10.1016/j.buildenv.2014.03.010

Taylor, J., Wilkinson, P., Davies, M., Armstrong, B., Chalabi, Z., Mavrogianni, A., Symonds, P., Oikonomou, E., Bohnenstengel, S.I., 2015. Mapping the effects of urban heat island, housing, and age on excess heat-related mortality in London. Urban Clim. 14, 517–528. https://doi.org/10.1016/j.uclim.2015.08.001

Taylor, J., Wilkinson, P., Picetti, R., Symonds, P., Heaviside, C., Macintyre, H.L., Davies, M., Mavrogianni, A., Hutchinson, E., 2018. Comparison of built environment adaptations to heat exposure and mortality during hot weather, West Midlands region, UK. Environ. Int. 111, 287–294. https://doi.org/10.1016/j.envint.2017.11.005

The Institut national de santé publique du Québec, 2018. Îlots de chaleur/fraicheur urbains et température de surface [WWW Document]. INSPQ. URL https://www.donneesquebec.ca/recherche/fr/dataset/ilots-de-chaleur-fraicheur-urbains-et-temperature-de- surface.

Theeuwes, N.E., Steeneveld, G.J., Ronda, R.J., Rotach, M.W., Holtslag, A.A.M., 2015. Cool city mornings by urban heat. Environ. Res. Lett. 10. https://doi.org/10.1088/1748-9326/10/11/114022

Thom, E.C., 1959. The Discomfort Index. Weatherwise 12, 57–61. https://doi.org/10.1080/00431672.1959.9926960

Tölle, M.H., Gutjahr, O., Busch, G., Thiele, J.C., 2014. Increasing bioenergy production on arable land: Does the regional and local climate respond? Germany as a case study. J. Geophys. Res. Atmos. 119, 2711–2724.

Touchaei, A.G., Wang, Y., 2015. Characterizing urban heat island in Montreal (Canada) - Effect of urban morphology. Sustain. Cities Soc. 19, 395–402. https://doi.org/10.1016/j.scs.2015.03.005

Touchie, M.F., Tzekova, E.S., Siegel, J.A., Purcell, B., Morier, J., 2016. Evaluating summertime overheating in multi-unit residential buildings using surveys and in-suite monitoring. Therm. Perform. Exter. Envel. Whole Build. 2016-Decem, 135–151.

U.S. Department of Energy's, Building Technologies Office, 2020. EnergyPlus 2020.

Uejio, C.K., Wilhelmi, O. V, Golden, J.S., Mills, D.M., Gulino, S.P., Samenow, J.P., 2011. Intra-urban societal vulnerability to extreme heat: The role of heat exposure and the built environment, socioeconomics, and neighborhood stability. Heal. Place 17, 498–507. https://doi.org/10.1016/j.healthplace.2010.12.005

United Nations, Department of Economic and Social Affairs, Population Division, -, 2019. World

Urbanization Prospects: The 2018 Revision (ST/ESA/SER.A/420), Demographic Research. New York: United Nations. https://doi.org/10.4054/demres.2005.12.9

van Loenhout, J.A.F., le Grand, A., Duijm, F., Greven, F., Vink, N.M., Hoek, G., Zuurbier, M., 2016. The effect of high indoor temperatures on self-perceived health of elderly persons. Environ. Res. 146, 27–34. https://doi.org/10.1016/j.envres.2015.12.012

Van Weverberg, K., De Ridder, K., Van Rompaey, A., 2008. Modeling the contribution of the Brussels heat island to a long temperature time series. J. Appl. Meteorol. Climatol. 47, 976–990.

Vogel, J., Afshari, A., 2020. Comparison of Urban Heat Island Intensity Estimation Methods Using Urbanized WRF in Berlin, Germany. Atmosphere (Basel). 11. https://doi.org/10.3390/atmos11121338

Wang, J., Huang, B., Fu, D., Atkinson, P.M., Zhang, X., 2016. Response of urban heat island to future urban expansion over the Beijing-Tianjin-Hebei metropolitan area. Appl. Geogr. 70, 26–36. https://doi.org/10.1016/j.apgeog.2016.02.010

Watkins, R., Palmer, J., Kolokotroni, M., Littlefair, P., 2002. The London heat island: Results from summertime monitoring. Build. Serv. Eng. Res. Technol. 23, 97–106. https://doi.org/10.1191/0143624402bt031oa

World Meteorological Organization, 2016. Guidelines on the Defintion and Monitoring of Extreme Weather and Climate Events, Task Team on the Definition of Extreme Weather and Climate Events. https://doi.org/10.1109/CSCI.2015.171

World Meteorological Organization (WMO), World Health Organization (WHO), 2015. Heatwaves and Health: Guidance on Warning-System Development.

Wouters, H., Ridder, K. De, Demuzere, M., Lauwaet, D., Van Lipzig, N.P.M., 2013. The diurnal evolution of the urban heat island of Paris: a model-based case study during Summer 2006. Atmos. Chem. Phys. 13, 8525–8541.

Xu, Z., Cheng, J., Hu, W., Tong, S., 2018. Heatwave and health events: A systematic evaluation of different temperature indicators, heatwave intensities and durations. Sci. Total Environ. 630, 679–689. https://doi.org/10.1016/j.scitotenv.2018.02.268

Xue, M., Droegemeier, K.K., Wong, V., 2000. The Advanced Regional Prediction System (ARPS)–A multi-scale nonhydrostatic atmospheric simulation and prediction model. Part I: Model dynamics and verification. Meteorol. Atmos. Phys. 75, 161–193.

Xue, M., Droegemeier, K.K., Wong, V., Shapiro, A., Brewster, K., Carr, F., Weber, D., Liu, Y., Wang, D., 2001. The Advanced Regional Prediction System (ARPS)–A multi-scale nonhydrostatic atmospheric simulation and prediction tool. Part II: Model physics and applications. Meteorol. Atmos. Phys. 76, 143–165.

Yang, X., Li, Y., Luo, Z., Chan, P.W., 2017. The urban cool island phenomenon in a high-rise high-density city and its mechanisms. Int. J. Climatol. 37, 890–904. https://doi.org/10.1002/joc.4747

Yang, Z.L., Niu, G.Y., Mitchell, K.E., Chen, F., Ek, M.B., Barlage, M., Longuevergne, L., Manning, K., Niyogi, D., Tewari, M., Xia, Y., 2011. The community Noah land surface model with multiparameterization options (Noah-MP): 2. Evaluation over global river basins. J. Geophys. Res. Atmos. 116, 1–16. https://doi.org/10.1029/2010JD015140

Yao, R., Wang, L., Huang, X., Gong, W., Xia, X., 2019. Greening in Rural Areas Increases the Surface Urban Heat Island Intensity. Geophys. Res. Lett. 46, 2204–2212. https://doi.org/10.1029/2018GL081816

Zero Carbon Hub, 2015a. Overheating in homes: the big picture.

Zero Carbon Hub, 2015b. Assessing overheating risk, Zero Carbon Hub.

Zero Carbon Hub, 2015c. Defining overheating 21. https://doi.org/http://www.zerocarbonhub.org/sites/default/files/resources/reports/ZCH-OverheatingEvidenceReview-Definitions.pdf

Zhang, N., Zhu, L., Zhu, Y., 2011. Urban heat island and boundary layer structures under hot weather synoptic conditions: A case study of Suzhou City, China. Adv. Atmos. Sci. 28, 855–865. https://doi.org/10.1007/s00376-010-0040-1

Zhang, S., Lin, Z., 2020. Standard effective temperature based adaptive-rational thermal comfort model. Appl. Energy 264, 114723. https://doi.org/10.1016/j.apenergy.2020.114723

Zhou, B., Rybski, D., Kropp, J.P., 2017. The role of city size and urban form in the surface urban heat island. Sci. Rep. 7, 1–9. https://doi.org/10.1038/s41598-017-04242-2

Zhou, D., Zhao, S., Liu, S., Zhang, L., Zhu, C., 2014. Surface urban heat island in China's 32 major cities: Spatial patterns and drivers. Remote Sens. Environ. 152, 51–61. https://doi.org/10.1016/j.rse.2014.05.017

Appendix A Building information survey forms

Building Information Survey
(Building type: Schools and Educational Facilities)

The purpose of this survey is to provide information for a research program cooperated by Environment Canada, Health Canada, National Research Council of Canada and Concordia University. The research program aims to assess the overheating risks of buildings housing vulnerable people, such as patients, children, and senior people, and provide mitigation strategies to reduce the overheating risks.

The information gathered in this survey will be only held by the four research organizations mentioned above and will be only used for research and educational purpose.

Your participation in this survey is voluntary, while your cooperation will be highly appreciated since every of your response will be a contribution to protecting Canadians' health against climate change.

1. General information

School board name		Phone number of the resource person for the project	
School board address			
Building name		BICS code	
Building address			
Year of construction	(MM/YYYY)	Year of renovation if applicable and specify type of renovation if any	(MM/YYYY)
Total number of floors		Total building floor area (the sum of each floor)	
Total number of rooms		Total number of students	
Total number of staffs		Summer vacation	From (DD/MM) To (DD/MM)

2. Building performance and occupants' behaviors

2.1 Are there any complaints about overheating problem in this building: YES ☐ NO ☐

If yes, please specify the time of year and location that overheating occurred

Time of year: _____ (MM/YYYY)

Location: Floor number _____ Orientation _____ Room number _____

Could you please provide the school plan?

2.2 What types of activities do students do in rooms when there is overheating problem?

2.3 Have any students or staffs in the building ever had the symptoms caused by overheating such as heat stroke, dizziness, excessive sweating, distraction, etc.? YES ☐ NO ☐

2.4 Maximum number of students in each classroom:

2.5 What electrical devices are used in a typical classroom? (For example, projectors, computers).

And what electrical devices are used in rooms with overheating issue, if any?

Page 1 of 2

156

3 HVAC system

3.1 Is there air conditioning in each room? YES ☐ NO ☐
If yes, when was the air conditioning system installed? _____ (MM/YYYY).
Is there thermostat control installed for the air conditioning in each room? YES ☐ NO ☐
The air conditioning system is **centralized** ☐ or **unitary** (e.g., window type)
Is it possible to provide the HVAC system specifications? YES ☐ NO ☐
Is it possible for us to visit the school and have access to the air-conditioning system? YES ☐ NO ☐
If there is no air conditioning system, what measures do you take to cool down the room in the summertime?

3.2 How well the air conditioning system work in the summer?
Very good ☐   Good ☐   Fair ☐   Poor ☐   Very poor ☐   Depends on the location of the room ☐
The temperature set point in rooms with air conditioner: _____ ℃.

3.3 Are there any fans in each room? YES ☐ NO ☐

3.4 Are there any dehumidifiers in each room (or a centralized system)? YES ☐ NO ☐

4. Building envelope

4.1 The ratio between the window area and the wall area:
Less than 10% ☐   10-20% ☐   20-30% ☐   30-40% ☐   40-50% ☐   More than 50% ☐

4.2 Are the windows in each room openable? YES ☐ NO ☐
If yes, can it be opened **partially** ☐ or **fully** ☐?
And how often the window is open in the summer? (Infrequently: once a month. Frequently: once a day)
Never ☐   Infrequently ☐   Occasionally ☐   Frequently ☐

4.3 The type of shading structure over windows:
External overhang ☐   Internal blinds ☐   None ☐   Other types (please specify) _____ .

Are the windows shaded in the summer by trees or other buildings? YES ☐ NO ☐

If yes, on which facades? (please indicate on the building drawings)

4.4 Type of windows (choose all applicable):   Single glazing ☐   Double glazing ☐   Triple glazing ☐

4.5 Type of building structure:
Wood ☐   Concrete ☐   Steel ☐   Other types (please specify) _____ .

4.6 What is the type of cladding?
Brick veneer ☐   Solid brick ☐   Wood cladding ☐   Vinyl ☐   Precast concrete ☐   Metal panel ☐
Curtain wall ☐   Don't know ☐   Other types (please specify) _____ .

4.7 What is the color of the facade? _____ .

Thank you for your participation. Please provide the contact of the person who completed the form:
Name:
Title:
Phone
Email:

Page 2 of 2

157

Building Information Survey
(Building type: Hospital and Social Service)

The purpose of this survey is to provide information for a research program cooperated by Environment Canada, Health Canada, National Research Council of Canada and Concordia University. The research program aims to assess the overheating risks of buildings housing vulnerable people, such as patients, children, and senior people, and provide mitigation strategies to reduce the overheating risks.

The information gathered in this survey will be only held by the four research organizations mentioned above and will be only used for research and educational purpose.

Your participation in this survey is voluntary, while your cooperation will be highly appreciated since every of your response will be a contribution to protecting Canadians' health against climate change.

1. General information

Institution name		Phone number	
Address			
Year of construction	(MM/YYYY)	Year of renovation and specify what type of renovation, if any	(MM/YYYY)
Total number of floors		Total building floor area (the sum of each floor)	
Total number of rooms		Total number of occupants (including patients and staffs)	

2. Building performance and occupants' behaviors

2.1 Are there any complaints about overheating problem in this building: YES ☐   NO ☐
If yes, please specify the time of year and location that overheating occurred
Time of year: _____ (MM/YYYY)
Location: Floor number _____   Orientation _____   Room number _____
Could you please provide the hospital plan?

2.2 What type of room has overheating problems?
Ward☐   Consulting room☐   Dining room☐   Other types (please specify) _____ .

2.3 Have any patients in the building ever had the symptoms caused by overheating such as heat stroke, dizziness, excessive sweating, distraction, etc.?   YES ☐   NO ☐

2.4 Maximum number of patients in each ward:

2.5 What electrical devices are used in a typical ward? (For example, medical instruments).

And what electrical devices are used in rooms with overheating issue, if any?

Page 1 of 2

158

3 HVAC system

3.1 Is there air conditioning in each room?   YES ☐   NO ☐
If yes, when was the air conditioning system installed? _____ (MM/YYYY).
Is there thermostat control installed for the air conditioning system in each room?   YES ☐   NO ☐
The air conditioning system is **centralized** ☐ or **unitary** ☐ (e.g. windows type)
Is it possible for you to provide the HVAC system specification?   YES ☐   NO ☐
Is it possible for us to visit the hospital and have access to the air conditioning system?   YES ☐   NO ☐
If there is no air conditioning system, what measures do you take to cool down the room in the summertime?

3.2 How well the air conditioning system work in the summer?
Very good ☐   Good ☐   Fair ☐   Poor ☐   Very poor ☐   Depends on the location of the room ☐
The temperature set point in rooms with air conditioner: _____ ℃.

3.3 Are there any fans in each room?   YES ☐   NO ☐

3.4 Are there any dehumidifiers in each room?   YES ☐   NO ☐

4. Building envelope

4.1 The ratio between the window area and the wall area:
Less than 10% ☐   10-20% ☐   20-30% ☐   30-40% ☐   40-50% ☐   More than 50% ☐

4.2 Are the windows in each room openable?   YES ☐   NO ☐
If yes, can it be opened **partially** ☐ or **fully** ☐?
And how often is the window opened in summer? (Infrequently: once a month. Frequently: once a day)
Never ☐   Infrequently ☐   Occasionally ☐   Frequently ☐

4.3 The type of shading structure over windows:
External overhang ☐   Internal blinds ☐   None ☐   Other types (please specify) _____ .
Are the windows shaded in summer by trees or by other buildings?   YES ☐   NO ☐
If yes, on which façade? (Please indicate in the building drawings)

4.4 Type of windows (choose all applicable):   Single glazing ☐   Double glazing ☐   Triple glazing ☐

4.5 Type of building structure:
Wood-frame ☐   Concrete ☐   Steel ☐   Other types (please specify) _____ .

4.6 What is the type of cladding?
Brick veneer ☐   Solid brick ☐   Wood cladding ☐   Vinyl ☐   Precast concrete ☐   Metal panel ☐
Curtain wall ☐   Other types (please specify) _____   Don't know ☐.

4.7 What is the color of the facade? _____ .

Thank you for your participation. Please provide your contacts:
Name:
Title:
Phone
Email:

Building Information Survey
(Building type: Residential social housing buildings-- for the building)

The purpose of this survey is to provide information for a research program cooperated by Environment Canada, Health Canada, National Research Council of Canada and Concordia University. The research program aims to assess the overheating risks of buildings housing vulnerable people, such as patients, children, and senior people, and provide mitigation strategies to reduce the overheating risks.

The information gathered in this survey will be only held by the four research organizations mentioned above and will be only used for research and educational purpose.

Your participation in this survey is voluntary, while your cooperation will be highly appreciated since every of your response will be a contribution to protecting Canadians' health against climate change.

1. General information

Building name		Phone number of the resource person for this building	
Building address			
Year of construction	(MM/YYYY)	Year of renovation if applicable and specify type of renovation if any	(MM/YYYY)
Total number of floors		Total building floor area	
Total number of units		Total number of residents in the building	

2. Building performance and occupants' behaviors

2.1 Are there any complaints about overheating problem in this building: YES ☐ NO ☐

If yes, please specify the time of year and location that overheating occurred

Time of year: _____ (MM/YYYY)

Location: Floor number _____ Orientation _____ Unit number _____

Could you please provide the building plan?

2.2 What types of activities do occupants do in units when there is overheating problem?

2.3 Have any occupants in the building ever had the symptoms caused by overheating such as heat stroke, dizziness, excessive sweating, distraction, etc.? YES ☐ NO ☐

2.4 Maximum number of occupants in each unit:

2.5 What electrical devices are used in a typical unit? (For example, TVs, computers).

And what electrical devices are used in units with overheating issue, if any?

3 HVAC system

3.1 Is there air conditioning in each unit? YES ☐ NO ☐

If yes, when was the air conditioning system installed? _____ (MM/YYYY).

Is there thermostat control installed for the air conditioning in each room (bedroom and living room)?
YES ☐ NO ☐

The air conditioning system is **centralized** ☐ or **unitary** (e.g., window type)

Page 1 of 2

160

Is it possible to provide the HVAC system specifications? YES ☐ NO ☐
Is it possible for us to access to the air-conditioning system and machine room? YES ☐ NO ☐
If there is no air conditioning system, what measures do you take to cool down the units in the summertime?

3.2 How well the air conditioning system work in the summer?
Very good ☐   Good ☐   Fair ☐   Poor ☐   Very poor ☐   Depends on the location of the room ☐
The temperature set point in rooms with air conditioner: _____ ℃.

3.3 Are there any fans in each unit? YES ☐ NO ☐

3.4 Are there any dehumidifiers in each unit (or a centralized system)? YES ☐ NO ☐

4. Building envelope
4.1 The ratio between the window area and the wall area:
Less than 10% ☐   10-20% ☐   20-30% ☐   30-40% ☐   40-50% ☐   More than 50% ☐

4.2 Are the windows in each unit and each room (bedroom, living room) openable? YES ☐ NO ☐
If yes, can it be opened **partially** ☐ or **fully** ☐?
And how often the window is open in the summer? (Infrequently: once a month. Frequently: once a day)
Never ☐   Infrequently ☐   Occasionally ☐   Frequently ☐

4.3 The type of shading structure over windows:
External overhang ☐   Internal blinds ☐   None ☐   Other types (please specify) _____.

Are the windows shaded in the summer by trees or other buildings? YES ☐ NO ☐

If yes, on which facades? (please indicate on the building drawings)

4.4 Type of windows (choose all applicable):   Single glazing ☐   Double glazing ☐   Triple glazing ☐

4.5 Type of building structure:
Wood ☐   Concrete ☐   Steel ☐   Other types (please specify) _____.

4.6 What is the type of cladding?
Brick veneer ☐   Solid brick ☐   Wood cladding ☐   Vinyl ☐   Precast concrete ☐   Metal panel ☐
Curtain wall ☐   Don't know ☐   Other types (please specify) _____.

4.7 What is the color of the façade and roof? _____.

Thank you for your participation. Please provide the contact of the person who completed the form:
Name:
Title:
Phone
Email:

Building Information Survey
(Building type: Residential social housing buildings--for each unit)

The purpose of this survey is to provide information for a research program cooperated by Environment Canada, Health Canada, National Research Council of Canada and Concordia University. The research program aims to assess the overheating risks of buildings housing vulnerable people, such as patients, children, and senior people, and provide mitigation strategies to reduce the overheating risks.

The information gathered in this survey will be only held by the four research organizations mentioned above and will be only used for research and educational purpose.

Your participation in this survey is voluntary, while your cooperation will be highly appreciated since every of your response will be a contribution to protecting Canadians' health against climate change.

1. General information of the unit

Room No.		Floor number	
How many rooms ____	Bedroom _____ Living room_____ Dining room_____	Rough estimation of the unit area_____ and area of each room:	Bedroom _____ Living room_____ Dining room_____
Orientation of the rooms	Bedroom _____ Living room_____ Dining room_____	Total number of occupants _____ Living alone/couple/family	>60 elder people ____ <14 young kids _____ Adults _____
Air conditioning Yes /No			

2. Building performance and occupants' behaviors

2.1 Do you feel hot during summer when you are at home: YES ☐   NO ☐
If yes, please specify the time of year and location that overheating occurred
Time of year: _____ (MM/YYYY)
Location: Bedroom_____ Living room _____ Dining room_____ Other _____

2.2 (Schedule) How many people at home during
Weekday (Monday - Friday)_____   Daytime _____ ;Nighttime _____ ;
Weekend (Saturday and Sunday)_____   Daytime _____ ;Nighttime _____ ;
work time during weekdays or weekends (e.g. 9:00am – 5:00pm):

2.3 Is there any residents/family member in this unit ever had the symptoms caused by overheating such as heat stroke, dizziness, excessive sweating, distraction, etc.?   YES ☐   NO ☐

2.4 What electrical devices are used in the unit? (For example, TVs, refrigerator, microwave).
For example, some of them may have TVs in both living room and bedroom.

3 HVAC system

3.1 Is there air conditioning in living room_____ bedroom_____
If yes, when was the air conditioning system installed? _____ (MM/YYYY).
Is there thermostat control installed for the air conditioning in each room?   YES ☐   NO ☐
The temperature set point in rooms with air conditioner: _____ ℃.

3.2 Type of air conditioning in each room (e.g., window type) ____

cooling air supply method_____
Take a photo for the brand of air conditioner and the unit specifications.

3.3 If there is no air conditioning, what measures do you take to cool down the room in the summertime?
Are there any fans in each room?   YES ▢   NO ▢
Are there any dehumidifiers in each room (or a centralized system)?   YES ▢   NO ▢

3.4 How well the air conditioning system work in the summer?
Very good ▢   Good ▢   Fair ▢   Poor ▢   Very poor ▢   Depends on the location of the room ▢

3.4 (Heating) Type of heating equipment:
electric baseboard heater___ centralized heating____ air conditioner_____

4. Building envelope
4.1 Window-wall-ratio of each room:
Bedroom _____
Living room_____
Dining room_____
Are the windows shaded in the summer by trees or other buildings?   YES ▢   NO ▢

4.2 Are the windows in each room openable?   YES ▢   NO ▢
If yes, can it be opened **partially** ▢ or **fully** ▢?
And how often the window is open in the summer? (Infrequently: once a month. Frequently: once a day)
Never ▢   Infrequently ▢   Occasionally ▢   Frequently ▢

4.3 Type of windows (choose all applicable):   Single glazing ▢   Double glazing ▢   Triple glazing ▢

4.4 The type of shading structure over windows:
External overhang ▢   Internal blinds ▢   None ▢   Other types (please specify) _____.

4.5 Type of building structure:
Wood ▢   Concrete ▢   Steel ▢   Other types (please specify) _____.

4.6 What is the type of cladding?
Brick veneer ▢   Solid brick ▢   Wood cladding ▢   Vinyl ▢   Precast concrete ▢   Metal panel ▢
Curtain wall ▢   Don't know ▢   Other types (please specify) _____.

4.7 What is the color of the internal walls? _____.

Thank you for your participation. Please provide the contact of the tenant in this unit/apartment:

Name:
Title:
Phone
Email:

Appendix B Building site-visit procedure and checklist

Assessment and Mitigation of Summertime Overheating Conditions in Vulnerable Buildings of Urban Agglomerations

Site visiting procedure and checklist of documents

Building name: _____

Date: _____   Visitors: _____

1. Preparation of tools and materials

What we need to do before the site visit:

1	Print out the **survey forms** for both the managers and the tenants	
2	Print out the **project invitation letter** to explain the project to the participants	
3	Print out a table to record the sensor **locations and serial numbers** for later management	
4	Tools to investigate the buildings/rooms: **tape measure, thermal camera**	
5	Bring the indoor sensors and the project introduction page to present for the building manager/tenants	
6	Gifts/bonus to incent the participants we visited (if necessary)	

2. Procedure (to-do-list)

What we need to do and ask them during the visit:

1	Log the **time** we visit each of the buildings and rooms so that we can easily identify the corresponding weather conditions later.	
2	Check on the **surroundings** of the buildings from outside and take photos.	
3	Visit the **public space** of the building, e. g. the activity room, dining rooms, corridor, and lobby, and take photos.	
4	Visit the **typical floor/rooms/units** and take photos if possible.	
5	Visit **the roof and the mechanical room** and take photos.	
6	Finish the survey forms by asking the questions to the building manager and occupants/tenants and fill them out by ourselves. (To confirm the information obtained from the collected survey forms)	
7	**Interview the occupants** in the buildings, record their comments about their thermal feeling in the building during the summer. (**Overheating complaints** or not?)	
8	Let the building manager and the tenants know the frequency and purpose of accessing different areas, the features of our sensors and how to contact us.	
9	Take the **infra-red thermal image** in the rooms of different conditions for comparison.	
10	Take the **infra-red thermal image** from the outside of the building to compare the temperatures of the walls facing different orientations.	
11	**Install the sensors and record the location** of the sensors by taking photos and measuring the distance to walls.	

3. Checklist

The outcome of the site visiting. What shall we obtain from the site visit?

1	The plan of the building and typical units	
2	The elevation of the building	
3	The HVAC system diagram	
4	Photos and thermal images	
5	Completed survey forms	
6	Critical dimensions of the building/room by on-site measurement	
7	Location of the sensors (photos and dimensions)	

Page 1 of 1

Appendix C Building selection request form for residential buildings

Criteria for Residential Building Selections

Please help to reduce the scope of building selection according to the first two major criteria and please provide the information of the buildings as much as possible (as listed in the additional criteria).
Later, we will investigate the given information and finally identify the buildings.

No.	Items	Criteria for buildings selection	Notes
1	Type of ventilation and heating system	No air conditioning access in the summer	No cooling in the summer
2	Address	Rosemont-La Petite-Patrie Mercier-Hochelaga-Maisonneuve Ville-Marie LaSalle Montreal-Nord Lachine Verdun Villeray-Saint-Michel-Parc-Extention	8 Boroughs with high heat-related death occurrence in previous years. These boroughs have relatively higher urban heat island intensity among the 19 boroughs in Montreal city.
		The following are **additional criteria** for selecting buildings for field monitoring	
3	Construction date	The majority should be old (before 1970), but we still need one/two newer ones for comparison.	The construction year should be as representative as possible
4	Date of renovation	Please specify the type of renovation, if any	
5	Occupants	people live alone, seniors	Highly vulnerable groups of people.
6	Type of exterior claddings	Brick veneer, wood siding, dark colour paints	The lower thermal mass of exterior cladding has a higher risk of summertime overheating. Dark colour has higher absorptivity and receives more solar radiation.
7	Windows	Window-to-wall ratio (WWR) higher than 30% (The ratio between the area of the window and the wall)	According to ASHRAE 90.1, the maximum WWR is 40%. Higher WWR (larger windows) results in higher solar heat gain.
8	Colour of roof	Dark colour paints	Dark colour has higher absorptivity and receives more solar radiation.
9	Occupant density	High-density dwellings Higher than 4 person/100 m^2	According to standard ASHRAE 62.1, the reference value for bedroom and living room is 10 person/100 m^2 According to standard NECB-2017, for long-term care and multi-unit residential buildings, the occupant density should be 4 person/100 m^2

And could you please provide the information as follows if possible?

1. Do you have single-family houses in your database?
2. The percentage of buildings without air-conditioning in your database.
3. The range of the building age for those with air-conditioning.
4. Do you have any buildings with building envelope retrofits? And could you please provide the age of those buildings and whether they have air-conditioned or not?

Page 1 of 1

Appendix D Summary of the site visited buildings

Table D-1 Summary of school building information survey

School	Const. Year	Flo.	Surrounding environment			Envelope					
			Open Area	Park	Plants[1]	Window		Bldg. Str.	Cladding	Roof Color	Façade Color
						WWR	Type				
SB1-A	1930	3	SE-I	No	S, W-2, N-3	40%-50%	SGDW-HS	Con.	Bri.v, S.bri.	White	Red-brown
SB1-B	1955	2	N, S-I	No	W-1	>50%	SGDW-HS	Terr.	Bri.v	Grey	Brown
SB1-C	1970s, 2017	2	S-I	W	W, E-2	10%-20%	DGSW-DA	Con.	Bri.v	White	Red-brown
SB1-D	1954	2	SW, E, S -I	N	No	40%-50%	SGDW-HS	Con.	Bri.v	Grey	Red-brown
SB1-E	1920	4	W, E-I	No	N-3	40%-50%	DGSW-DA	Con.	Bri.v	Grey	Red-brown
SB1-F	1930	3	W, E, S-I	No	N-2	20%-30%	DGSW-DA SGDW-HS	Con.	Bri.v	Grey	Red-brown
SB1-G	1927, 2018	3	N-I	No	S-1	40%-50%	DGSW-HS	Con.	Bri.v, S.bri.	Grey	Light brown
SB1-H	1966	2	N, S, E-I, E-G	W	W-2	30%-40%	DGSW-DA	Con.	Acrylic, Stone	Grey	White
SB2-A	1951, 1990s, 2014	2	E-I	No	No	40%-50%	DGSW-HS	W, Con.	S.bri.	Grey	Red-brown
SB2-B	1916, 1950s	4	S-I	No	No	20%-30%	DGSW-HS	W, Con.	S.bri.	Grey	Red-brown
SB2-C	1930, 1992	4	S-I	No	W-2	20%-30%	DGSW-HS	W, Con.	S.bri.	White	Brown Red-brown
SB2-E	1953, 1990s	2	N, S-I	No	W-2	40%-50%	SGDW-HS	W, Con.	S.bri.	Grey	Light brown

SB2-D	1958, 1990s	2	E-I	No	W, S- 2	40%-50%	DGSW-HS	W, Con.	S.bri.	Grey	Light brown
SB2-F	1957	2	SE - I, G	No	N-2	40%-50%	DGSW-HS	W, Con.	S.bri.	Grey	Red-brown
SB3-A	1966	1	S, E, N, W-G S, E-I	No	No	10%-20%	SGDW-HS	N/A	Bri.v	Grey	White Red-brown

N= north; S= south; E= east; W= west; NE= northeast; NW=norhtwest; SE=southeast; SW=southwest; I=impervious; G=green; SGDW=single glazing double window; DGSW=double glazing single window; HS=horizontal slider;VS=vertical slider; DA=dual action; W=wood; Con.=Concrete; Bri.v=brick veneer; S.bri.=solid brick.

1. The orientation and height of plants, e.g. N-3 denotes that there are plants on the north side of the building with a height equivalent to 5 floors

Table D-2 Summary of hospital building information survey

Hospital	Const. Year	Flo.	Surrounding environment				Envelope					
			Open Area	Park	Plants 1	High Bldg.	Window		Bldg. Str.	Cladding	Roof Color	Façade Color
							WWR	Type				
CHSLD-A	1984	6	No	No	No	No	30%-40%	DGSW-C	Concrete	Solid brick	White	Red-brown
CHSLD-B	1980	6	SE-I	No	NW-5, NE-3	NW	10%-20%	DGSW-HS	Concrete	Solid brick	White	Red-brown
CHSLD-C	1959	3	NW-I	No	N-3	No	30%-40%	DGSW-DA	N/A	Brick veneer	Grey	Brown
CHSLD-D	1992	4	NE-G	No	NW, SE-4	No	30%-40%	SGDW-HS	Steel	Brick veneer	White	Red-brown
CHSLD-E	1960	3	No	No	SW, NE-3	NW SE	30%-40%	DGSW-C	Concrete	Solid brick	White	Red brown
CH-A	1939	10	No	No	NE-2 SW-3	No	40%-50%	DGSW-DA	N/A	Metal, Vinyl	White	White Light brown
CH-B	1959	8	NW-I	SW	No	No	30%-40%	DGSW-DA	N/A	Brick veneer	White	Red-brown
CH-C	1906	7	SW-I SE-I	SW SE	S-3	No	20%-30%	DGSW-DA	N/A	Terracotta Brick veneer	White Green	Red-brown
CH-D	1957	7	NW-I SE-G	No	No	No	40%-50%	SGDW-VS	Concrete	Solid brick	Brown	Tan
CH-E	1954	19	NE-I	W	S-5	No	40%-50%	DGSW-DA	Concrete	Solid brick	Grey	Red-brown
CH-F	1980	4	NE-I	NW	SW-4	No	30%-40%	DGSW-DA	Concrete	Solid brick	Grey	Light brown
CR-A	1950s 1960s 2018	3	SE-I	No	NW-4	No	20%-30%	SGDW-VS	N/A	Brick veneer	Grey	White Light green

N= north; S= south; E= east; W= west; NE= northeast; NW= norhtwest; SE=southeast; SW= southwest; I= impervious; G=green; SGDW=single glazing double window; DGSW= double glazing single window; HS=horizontal slider;VS= vertical slider; DA= dual action; C= casement.

1. The orientation and height of plants, e.g. N-3 denotes that there are plants on the north side of the building with a height equivalent to 5 floors

Appendix E The monitored buildings and selected rooms
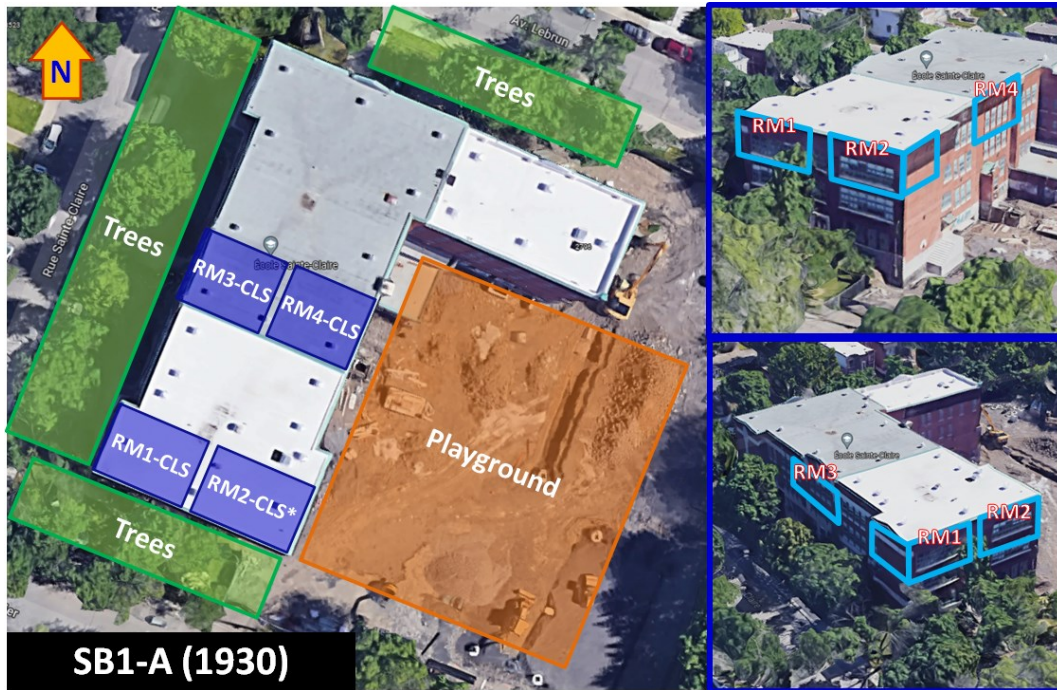
Figure E-1 The surroundings and outlook of the building SB1-A and the monitored rooms
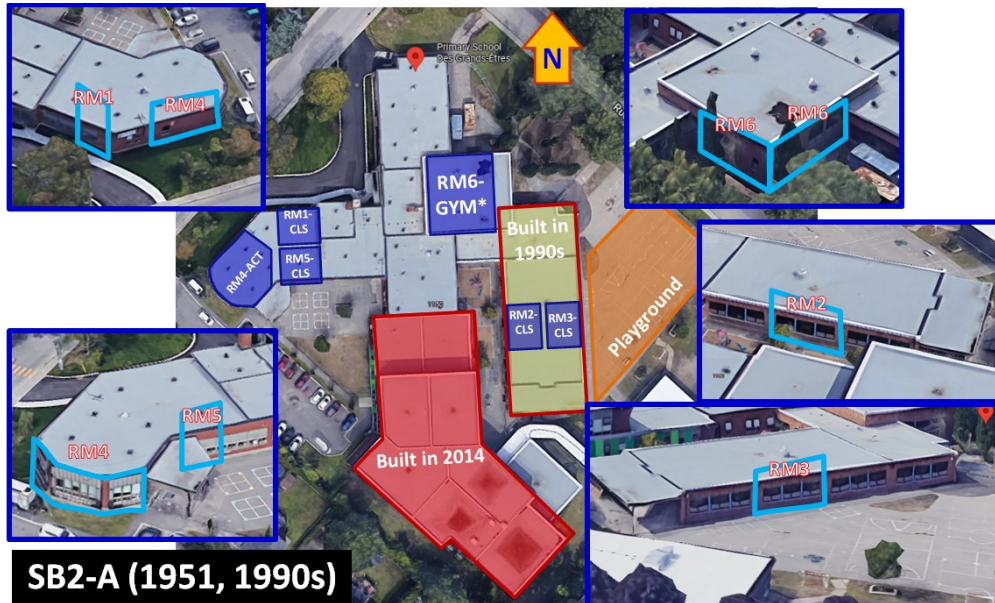
Figure E-2 The surroundings and outlook of the building SB2-A and the monitored rooms

Figure E-3 The surroundings and outlook of the building SB2-D and the monitored rooms

Figure E-4 The surroundings and outlook of the building SB3-A and the monitored rooms
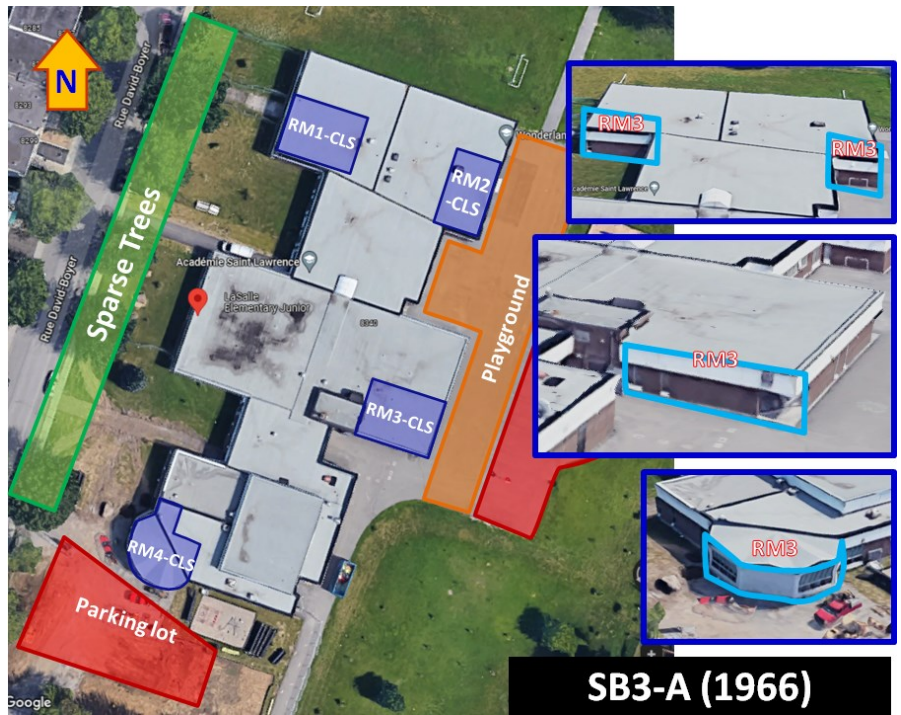
Figure E-5 The surroundings and outlook of the building SB3-A and the monitored rooms
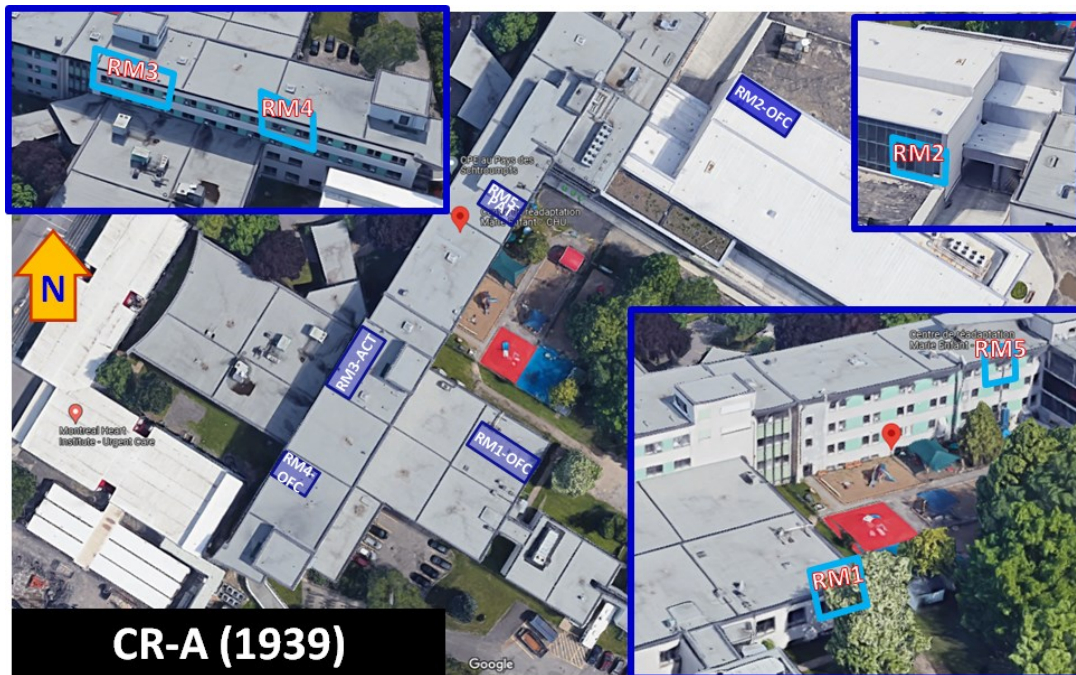
Figure E-6 The surroundings and outlook of the building CR-A and the monitored rooms

Appendix F The weather conditions of 2020 summer
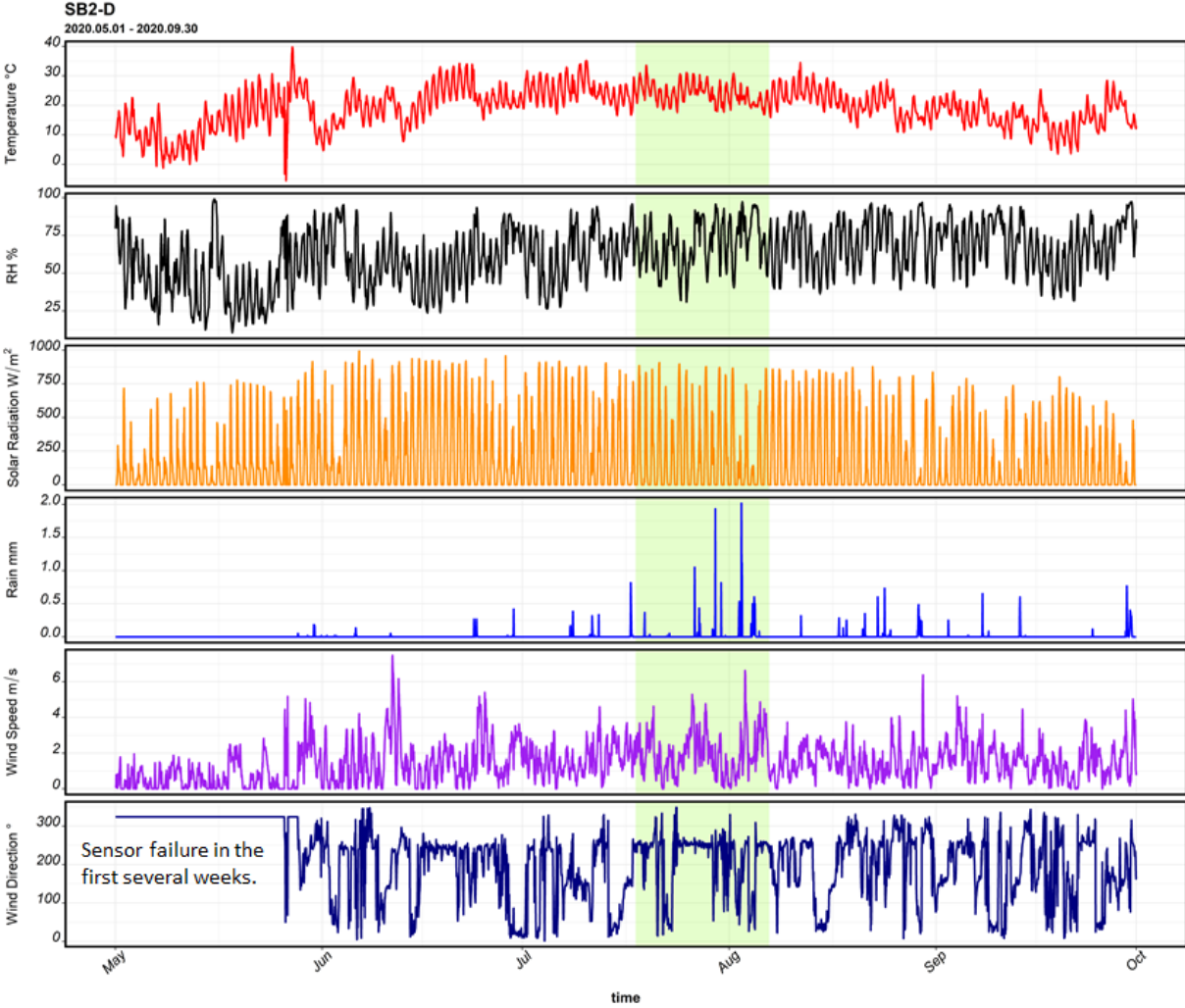
Figure F-1 Weather condition monitored at the building SB2-D from May 01, 2020, to September 30, 2020. The timeframe shaded in green is evaluated in this study.
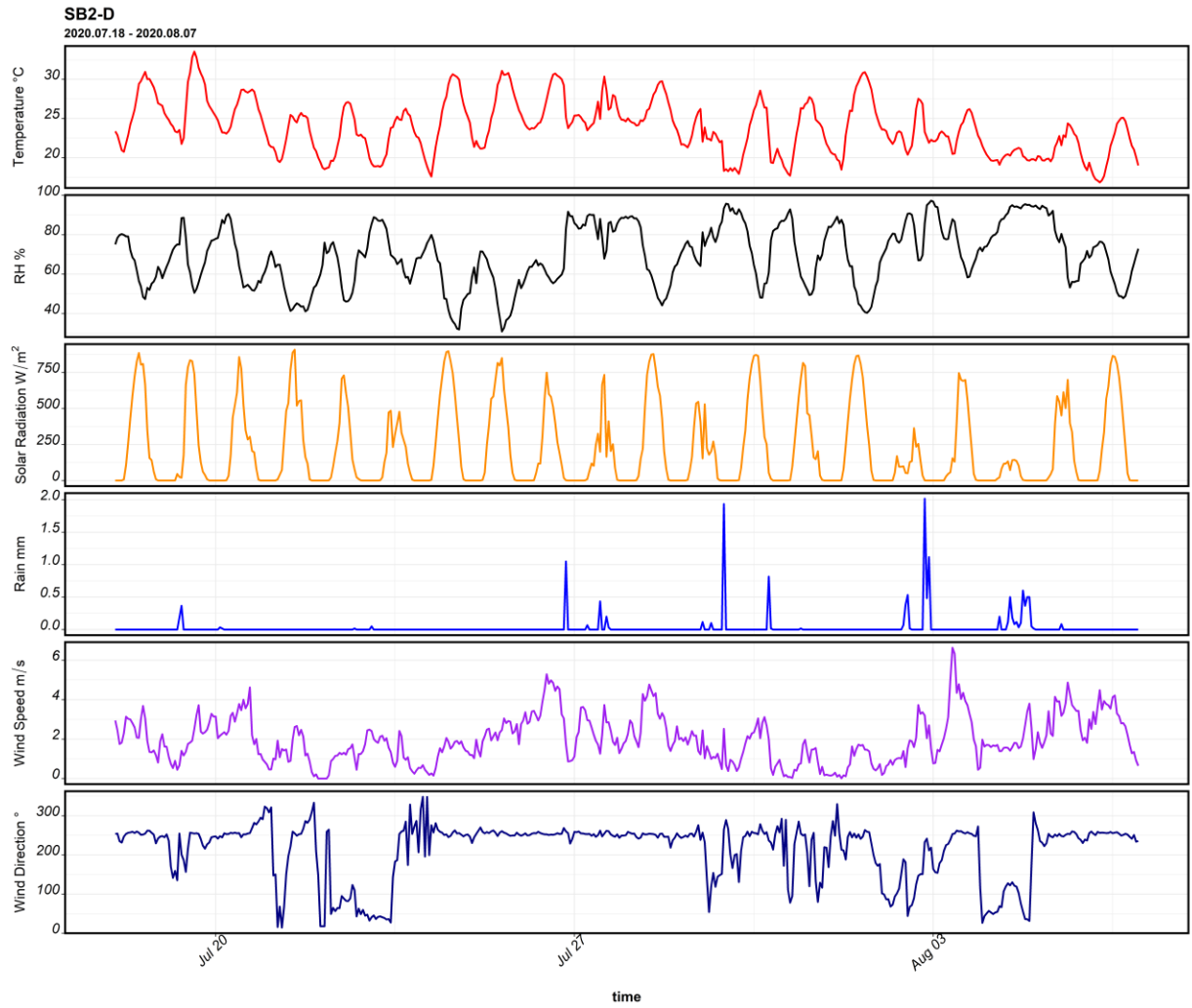
Figure F-2 Weather condition monitored at the building SB2-D from July 18, 2020 to August 07, 2020.

Appendix G Measured indoor temperature and relative humidity
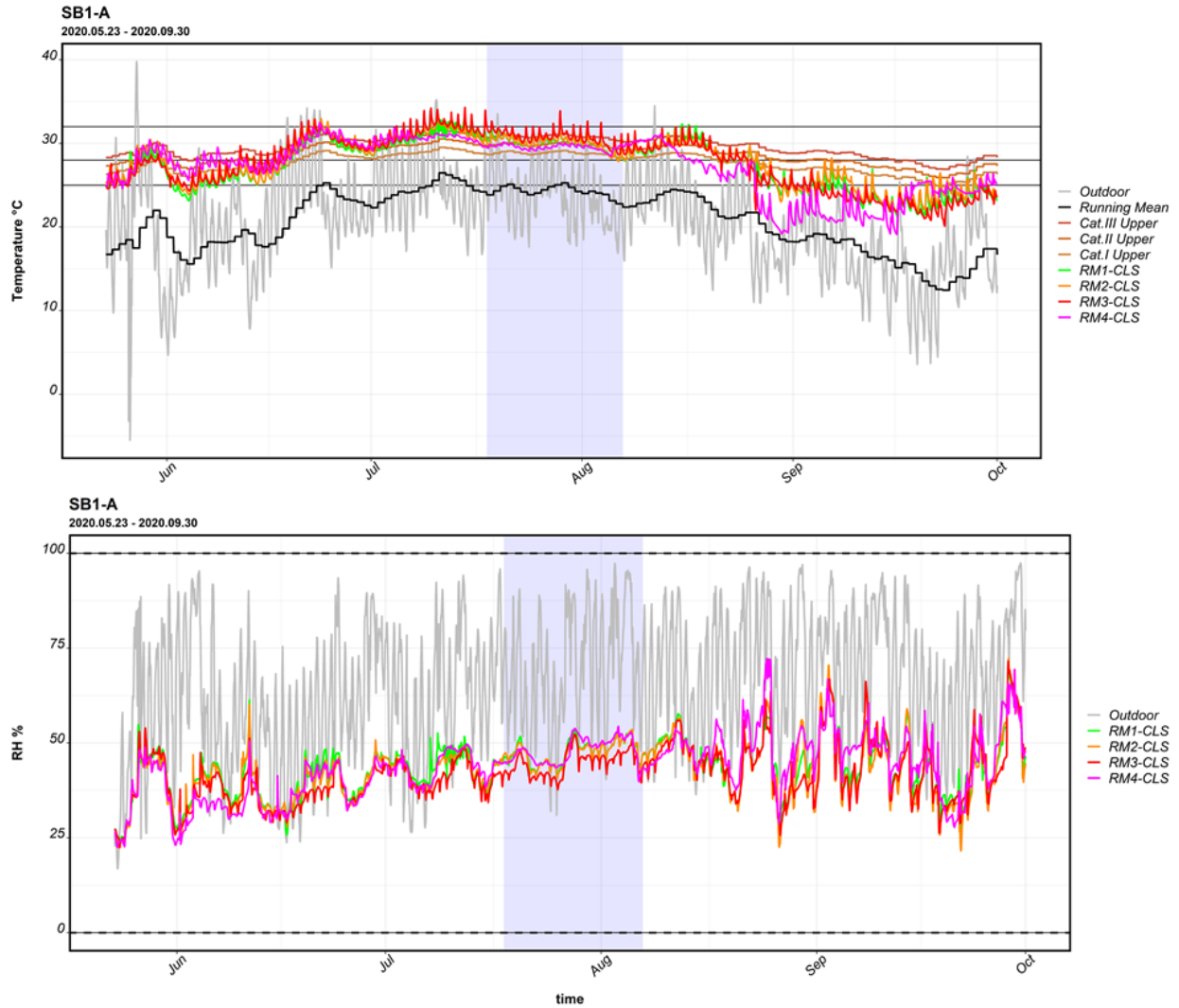
Figure G-1 Hourly indoor and outdoor temperature and relative humidity monitored at building SB1-A
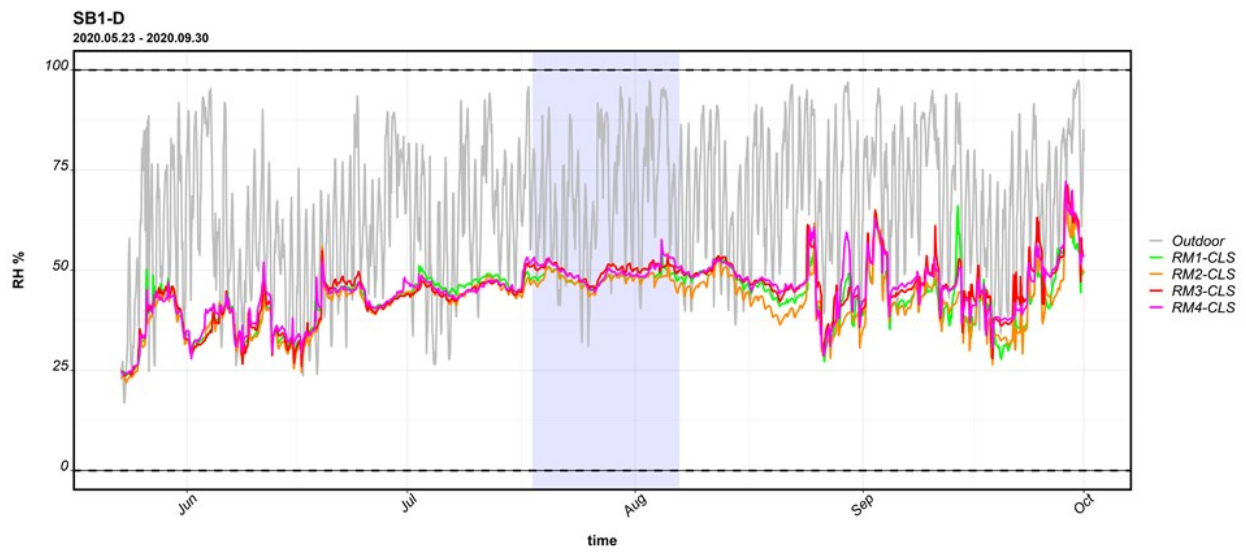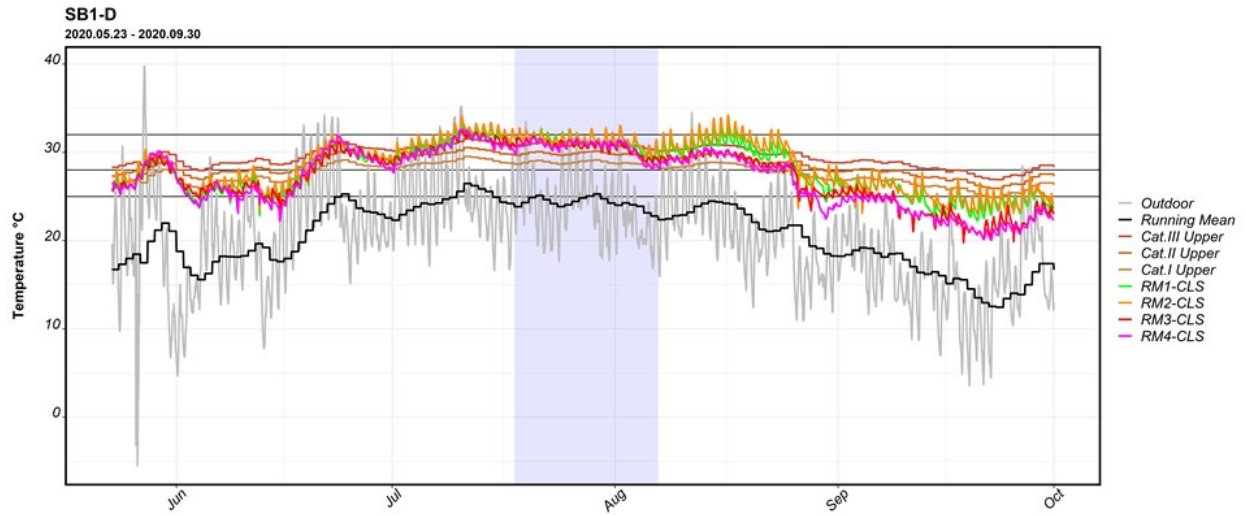
Figure G-2 Hourly indoor and outdoor temperature and relative humidity monitored at building

SB1-D
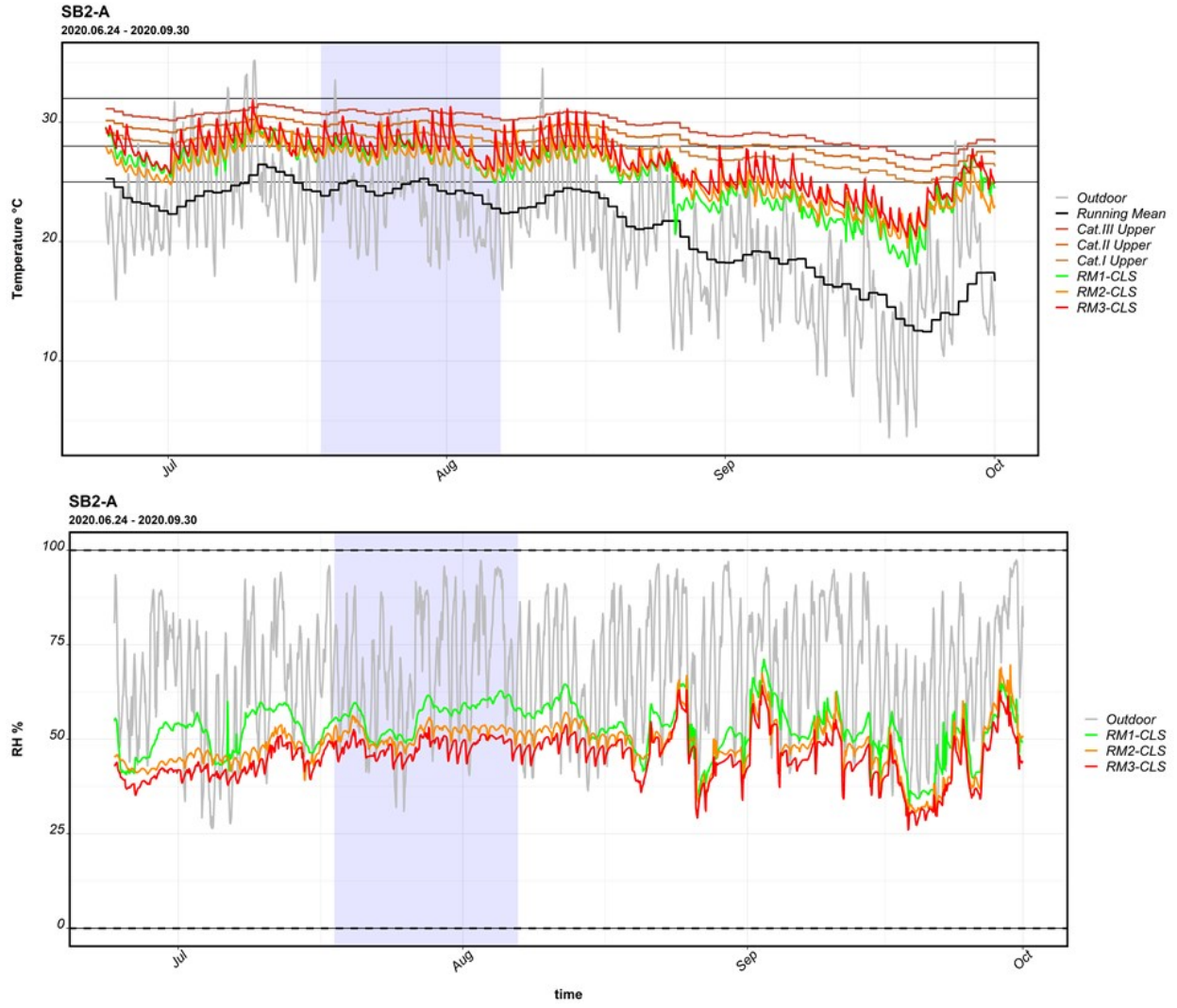
Figure G-3 Hourly indoor and outdoor temperature and relative humidity monitored at building SB2-A
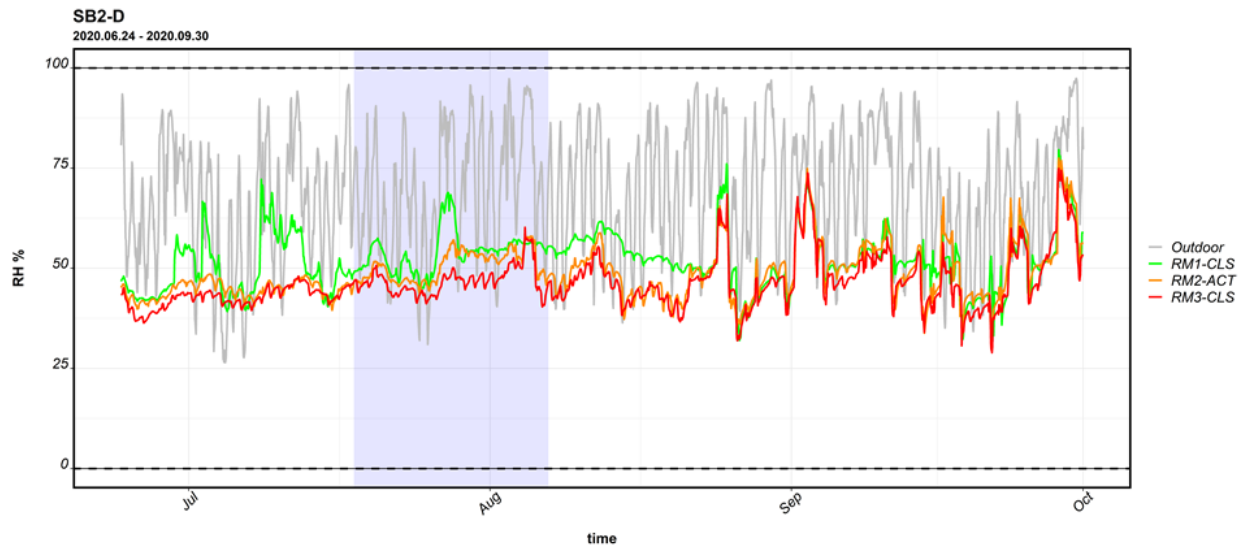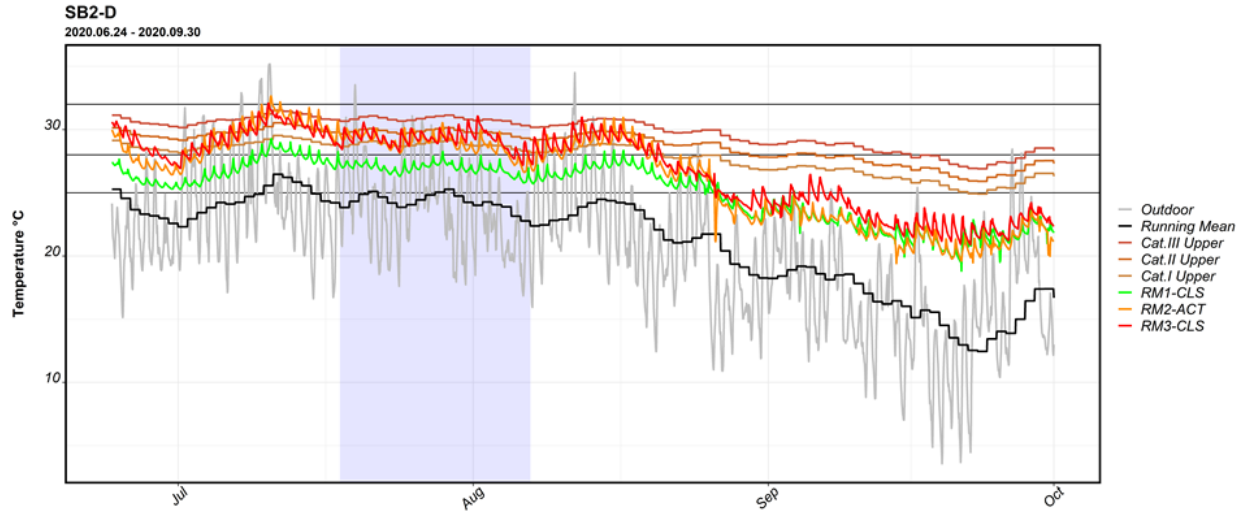
Figure G-4 Hourly indoor and outdoor temperature and relative humidity monitored at building

SB2-D
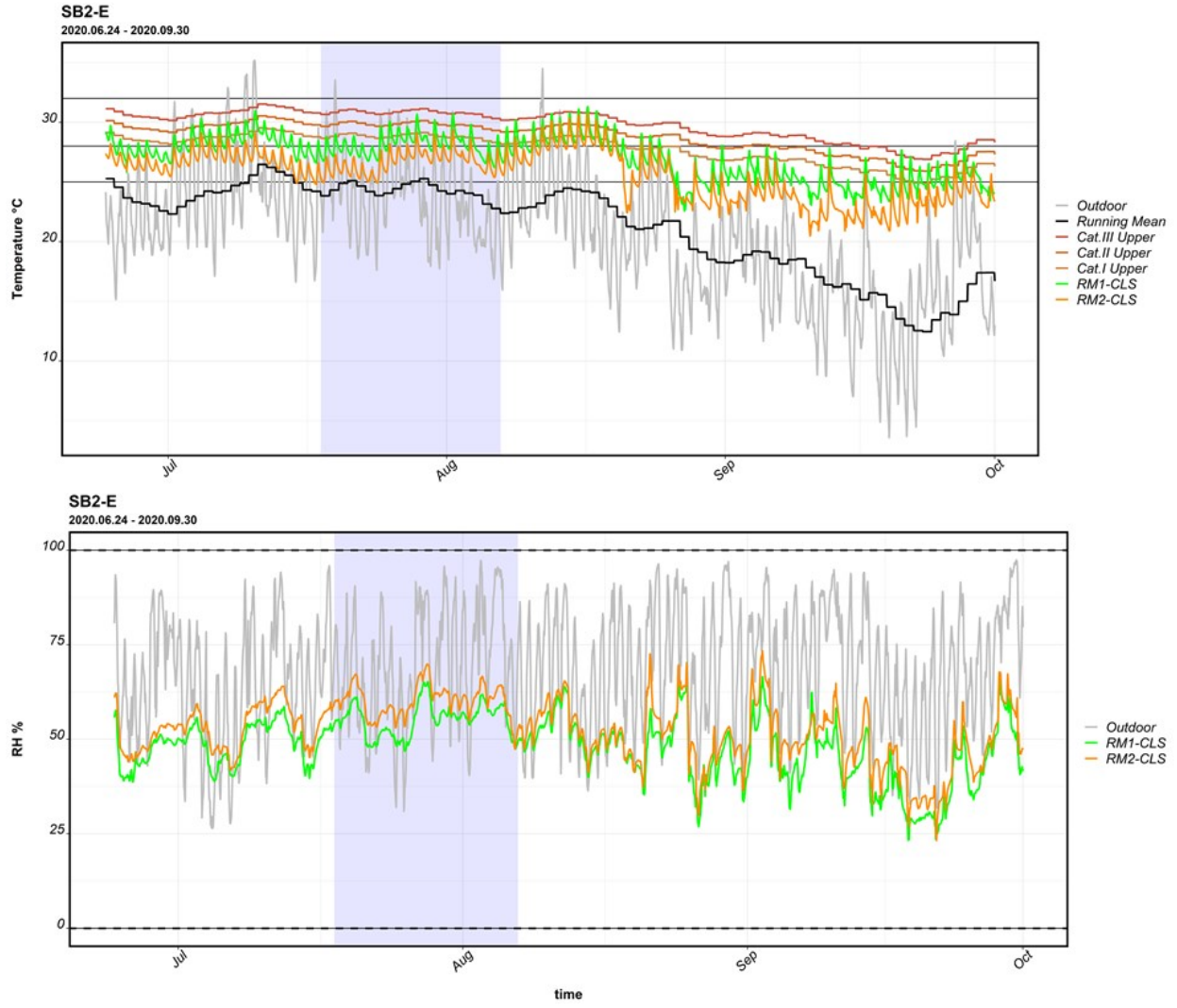
Figure G-5 Hourly indoor and outdoor temperature and relative humidity monitored at building

SB2-E
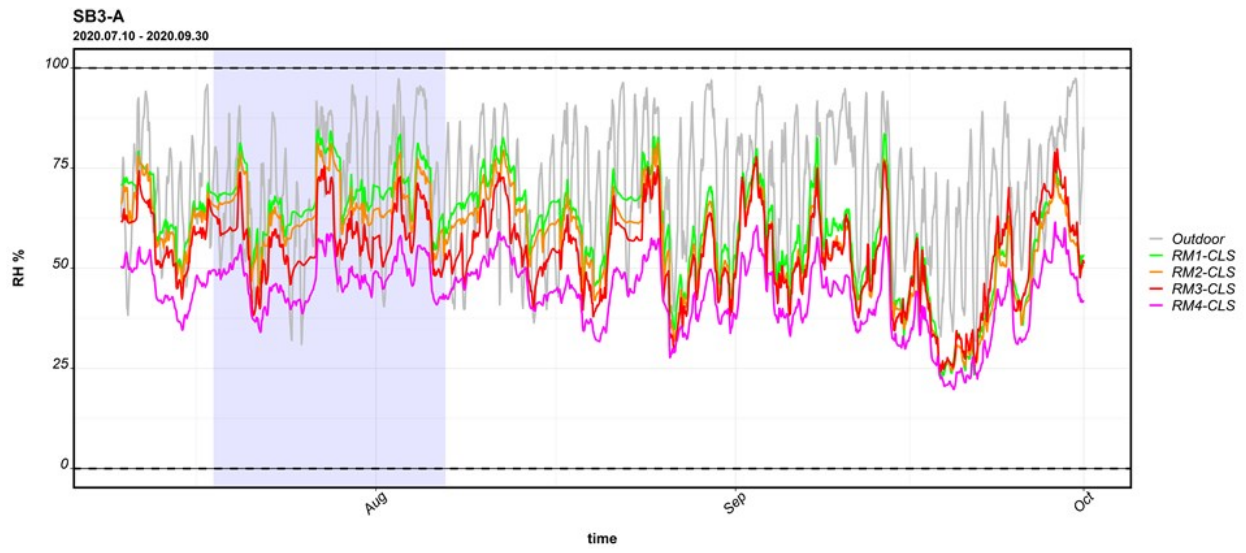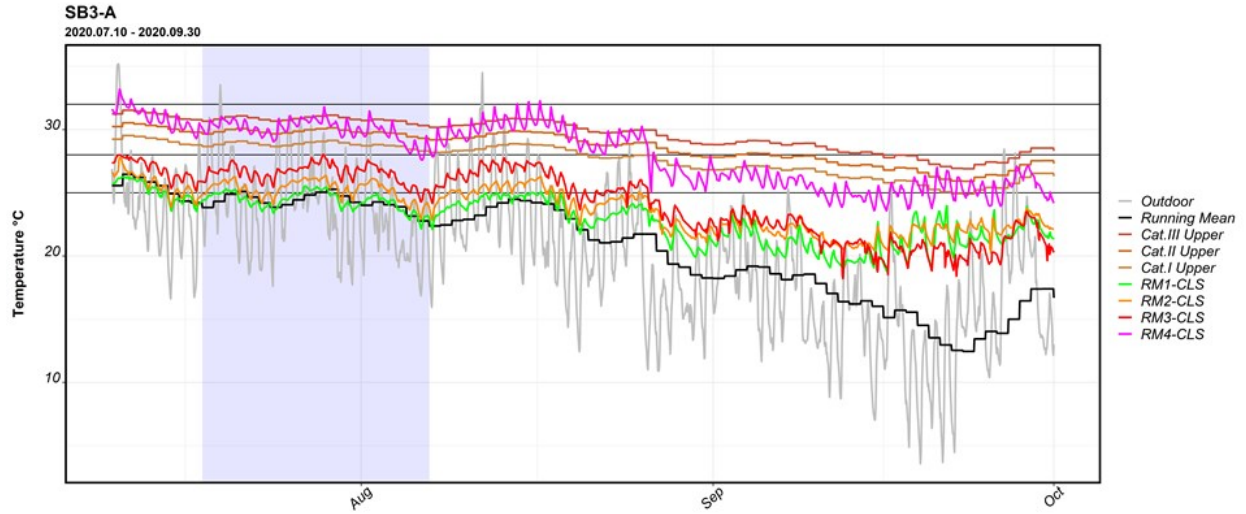
Figure G-6 Hourly indoor and outdoor temperature and relative humidity monitored at building
SB3-A
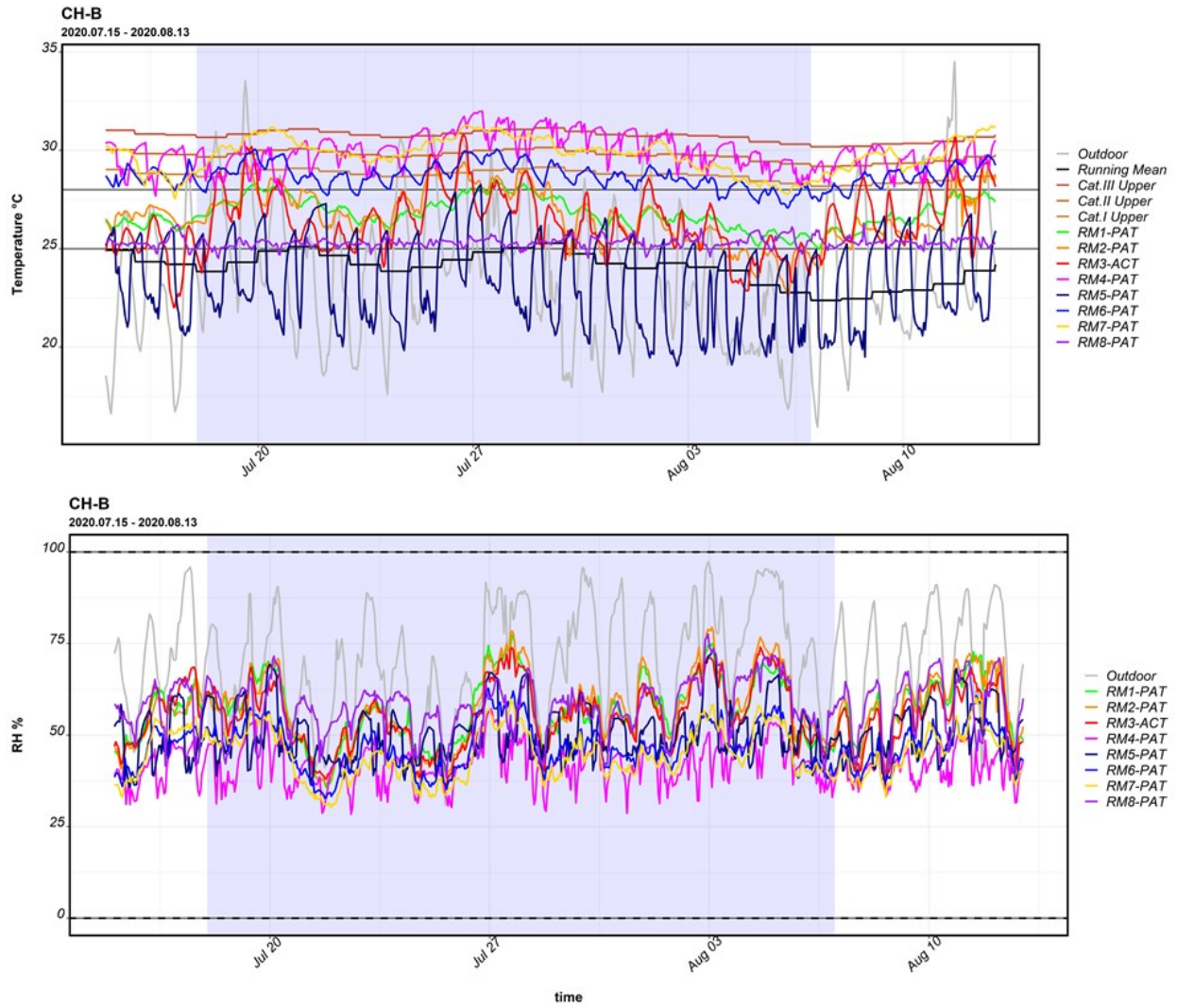
Figure G-7 Hourly indoor and outdoor temperature and relative humidity monitored at building

CH-B
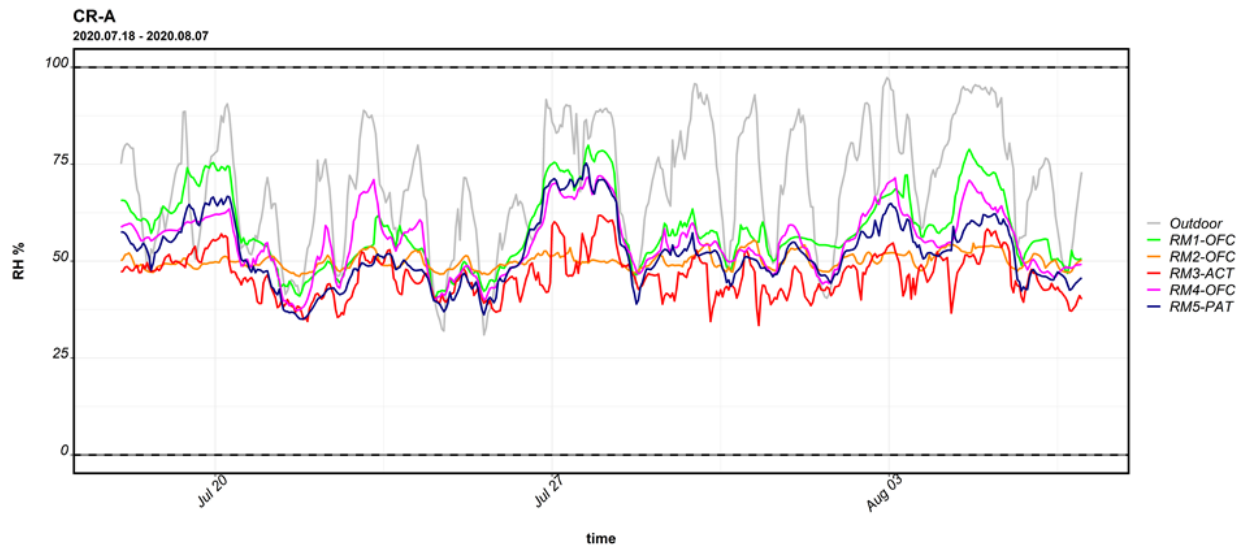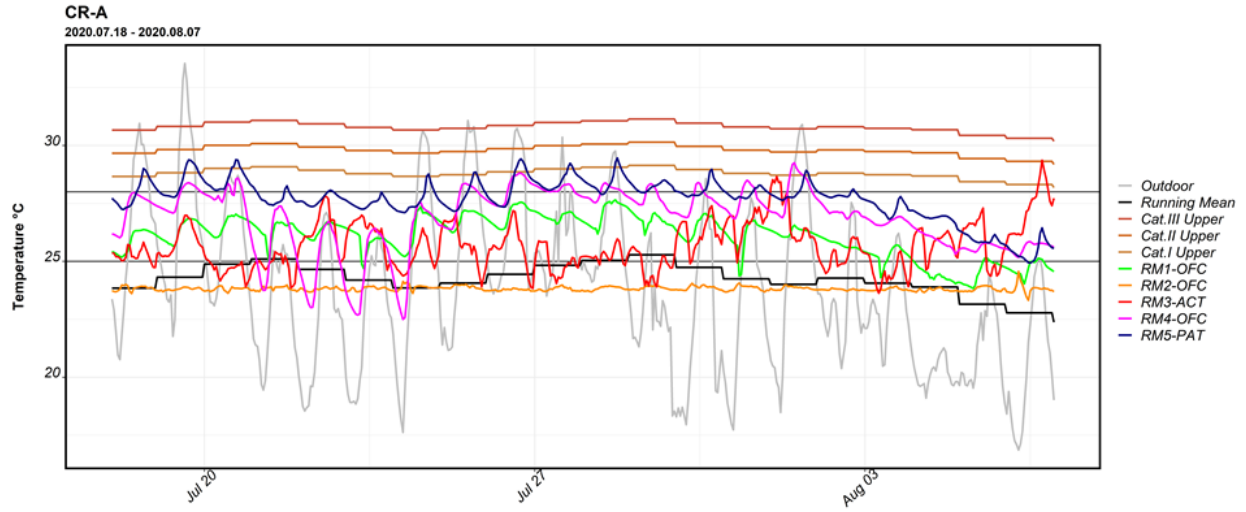
Figure G-8 Hourly indoor and outdoor temperature and relative humidity monitored at building CR-A

Appendix H Overheating hours calculated by thermal indices
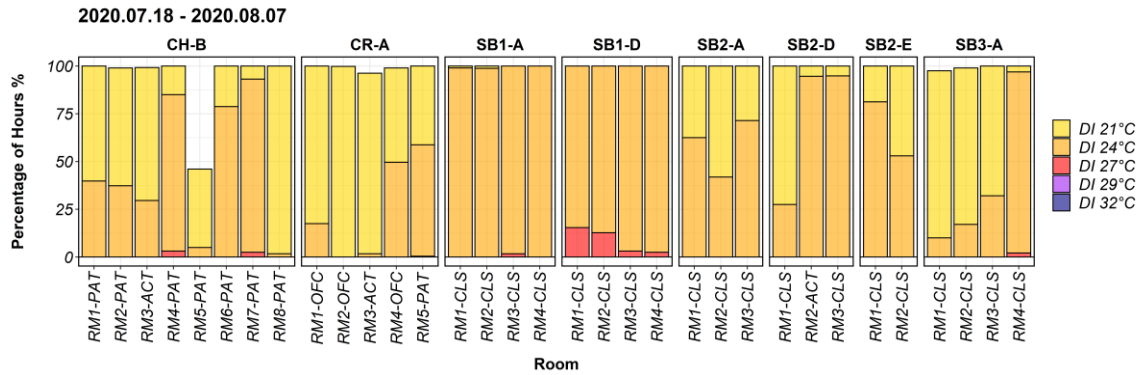
Figure H-1 Percentage of overheating hours in different buildings and rooms evaluated by Discomfort Index (DI) criteria during TF-5
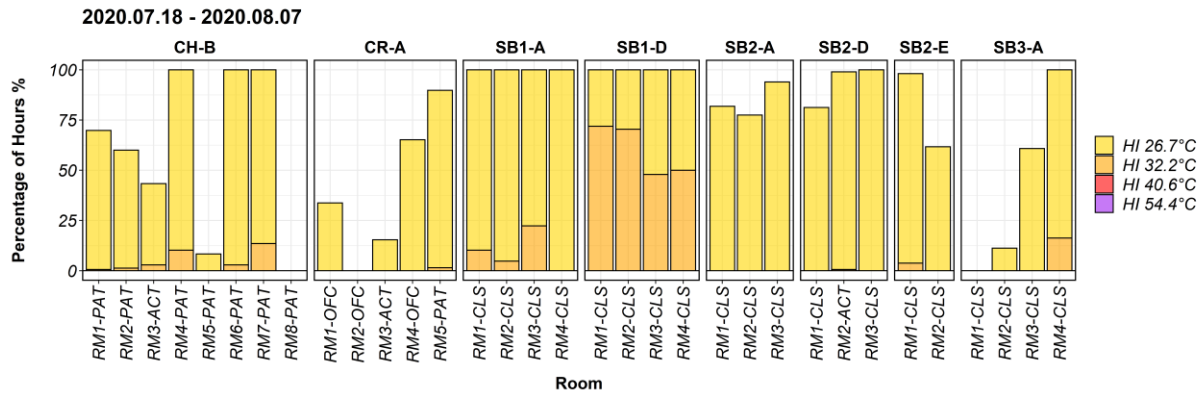
Figure H-2 Percentage of overheating hours in different buildings and rooms evaluated by Heat Index (HI) criteria during TF-5
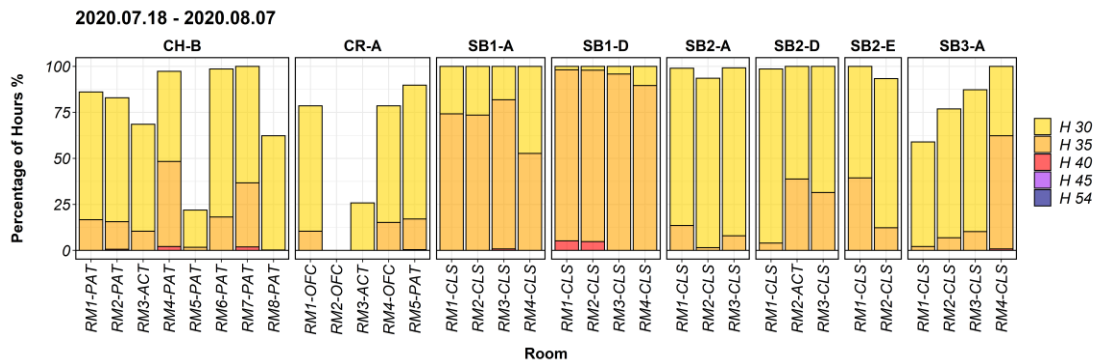
Figure H-3 Percentage of overheating hours in different buildings and rooms evaluated by Humidex (H) criteria during TF-5
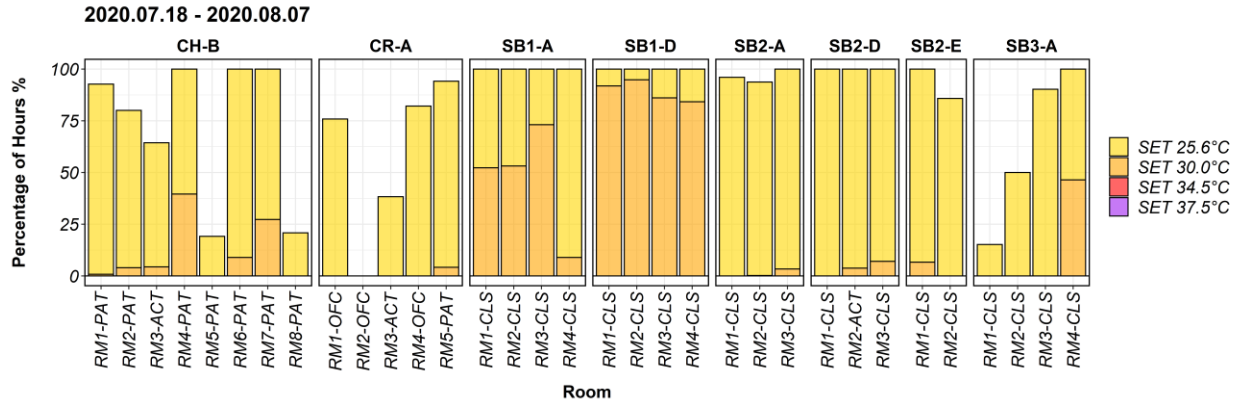
Figure H-4 Percentage of overheating hours in different buildings and rooms evaluated by Standard Effective Temperature (SET) criteria during TF-5
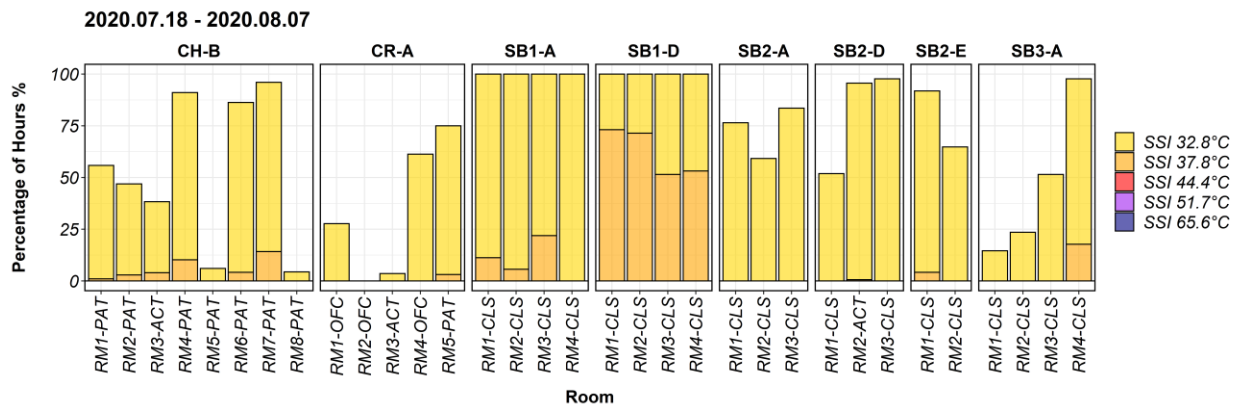
Figure H-5 Percentage of overheating hours in different buildings and rooms evaluated by Summer Simmer Index (SSI) criteria during TF-5
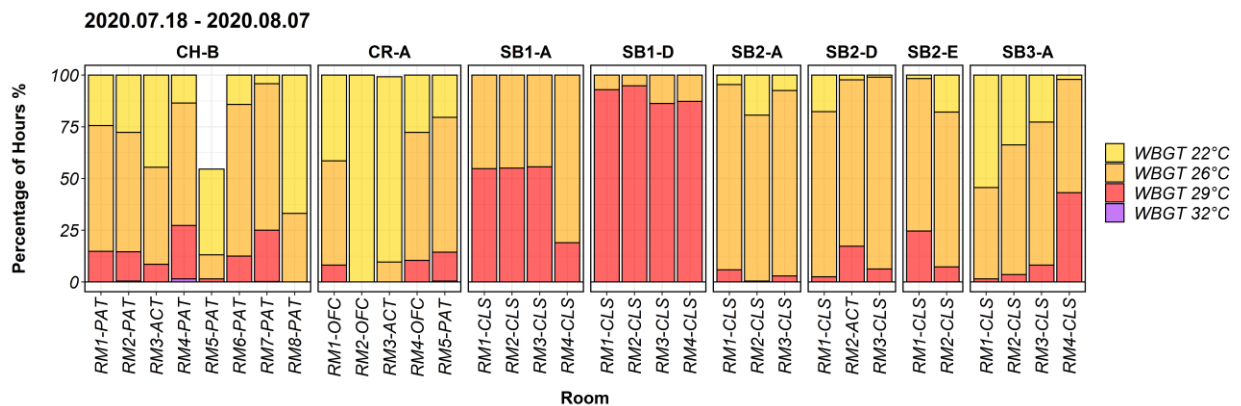
Figure H-6 Percentage of overheating hours in different buildings and rooms evaluated by Wet-Bulb Globe Temperature (WBGT) criteria during TF-5

Appendix I Boxplot of the thermal indices
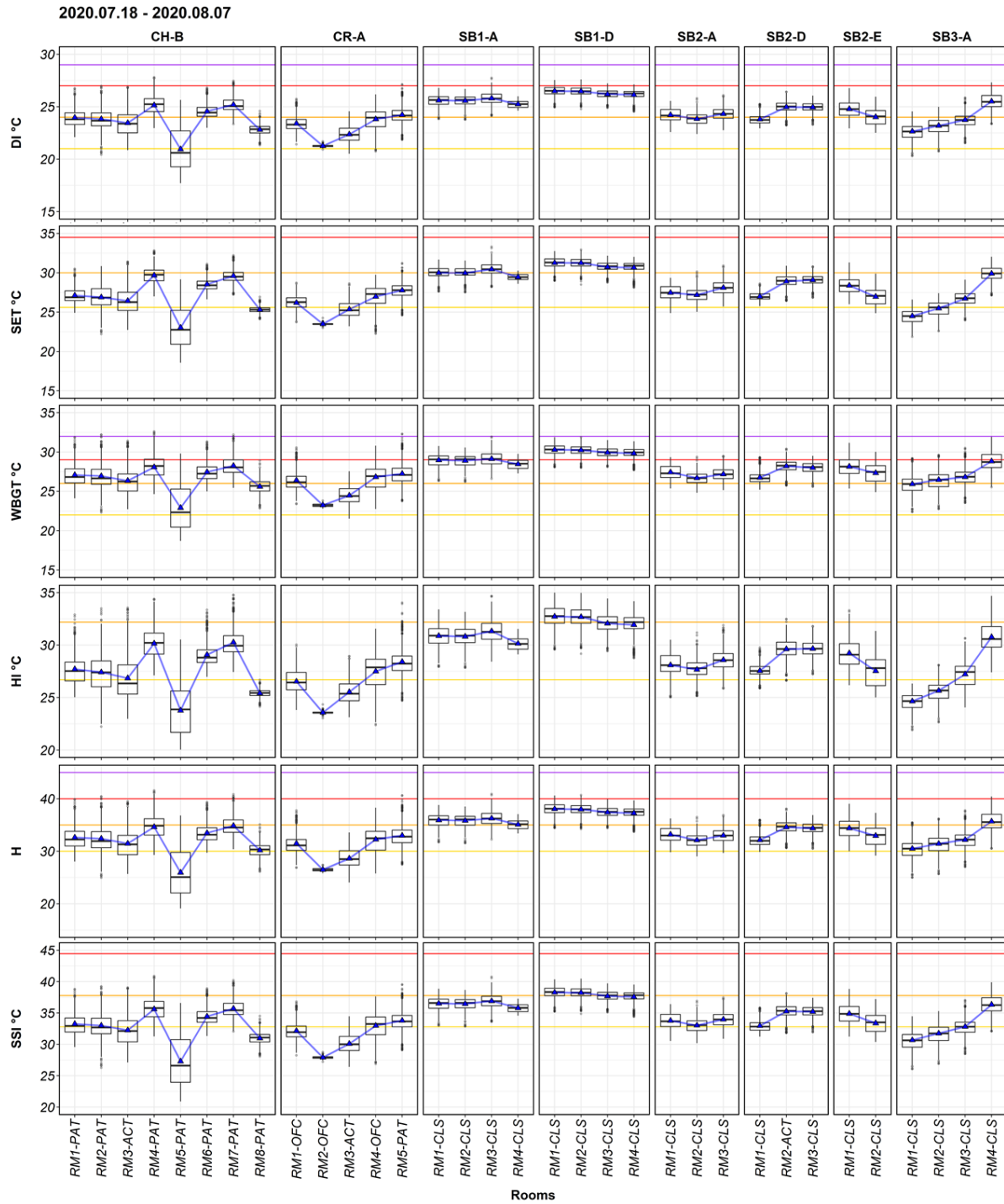
Figure I-1 Boxplot of the thermal indices in the monitored rooms

Appendix J Steps to run WRF model on clusters

The simulation in this study needs to use 5 programs in WRF Preprocessing System (WPS) and weather research and forecast (WRF) packages, namely, geogrid.exe, ungird.exe, metgrid.exe, real.exe and wrf.exe. The WPS package contains the geogrid.exe, ungird.exe, metgrid.exe. The role of these 3 programs is,

1) The geogrid.exe ingests the external static geographical data to generate the domain files for the simulation.

2) The ungrib.exe ingests the external gridded meteorological data to generate intermediate format files.

3) The metgrid.exe uses the intermediate format files generated by ungrib.exe as inputs to horizontally interpolate the meteorological data in the domain defined by the domain files generated by geogrid.exe and generate the preprocessing output files.

The WRF package contains the other two programs, real.exe, and wrf.exe:

1) The real.exe uses the output files from WPS to do the vertical interpolation for the domains as initialization and generate the WRF simulation input files.

2) The wrf.exe uses the output of real.exe and the WPS to do the calculation with the multiple physical models and creates the outputs for the simulation results.

Each program may need the output of the prior one as the input, therefore, to complete a simulation, these 5 programs need to be run one by one. Apart from the necessary input and outputs files to run the simulations, some parameters in the configuration files need to be adjusted for each simulation to well define the problem. Two of the most important configuration files are the namelist.wps file for the 3 programs in WPS, and namelist.input file for the programs in WRF.

Table J-1 Files to run the programs in WPS and WRF

Programs	Input file	Configuration file	Output file
geogrid.exe	External downloaded **static geographical data**	namelist.wps GEOGRID.TBL	domain files ***geo_em.d0N.nc***
ungird.exe	External downloaded	namelist.wps Vtable	intermediate format files

	gridded meteorological data		*(e.g. FILE:YY-MM-DD_HH)*
metgrid.exe	*geo_em.d0N.nc* *FILE:YY-MM-DD_HH*	namelist.wps	WPS output files *met_em.d0N.YYYY-MM-DD_HH:mm:ss.nc*
real.exe	*met_em.d0N.YYYY-MM-DD_HH:mm:ss.nc*	namelist.input	Input files: *wrfinput_d0N* *wrfbdy_d01*
wrf.exe	*wrfinput_d0N* *wrfbdy_d01* *met_em.d0N.YYYY-MM-DD_HH:mm:ss.nc*	namelist.input URBPARA.TBL	Simulation results: *wrfout_d0N_YYYY-MM-DD_HH:mm:ss* And restart files: *wrfrst_d0N_YYYY-MM-DD_HH:mm:ss*

To assist a fast hand on the simulation of WRF, the procedure to run the programs is listed in the following tables. As is mentioned, the programs in the WPS should be run before those in the WRF to get the input files for real.exe and wrf.exe. Take the simulation with the NCEP North American Regional Reanalysis (NARR) data as an example, the simulation procedure is detailed as below.

Table J-2 Procedure of preprocessing with WPS

Step 1	Download the static geographical datasets to a directory on the clusters: **"/home/<USER>/work/wrf/WPS_GEOG/geog"**
Step 2	Download the meteorological data in GRIB format to a directory on the clusters: **"/home/<USER>/work/wrf/AWIP/Files/"**
Step 3	**cd ~work/wrf/WPS**
Step 4	Edit the namelist.wps file for different simulation times, simulation resolutions, locations, and domain sizes: **vi namelist.wps** define the path to the static geographical files under the &geogrid panel:

	geog_data_path = '/home/\<USER\>/work/wrf/WPS_GEOG/geog', define the ungrib.exe output file prefix under the &ungrid panel: **prefix = 'FILE',** define the metgrid.exe input file prefix under the &metgrid panel: **fg_name = 'FILE'**
Step 5	Link a proper GEOGRID.TBL file for the geogrid.exe file **ln -s geogrid/GEOGRID.TBL.ARW geogrid/GEOGRID.TBL**
Step 6	run geogrid.exe under WPS directory with the command: **./geogrid.exe &> geogrid.log** Then the ***domain files geo_em.d0N.nc*** for each nesting level N can be obtained.
Step 7	Link the downloaded GRIB files to the current directory using the shell script link_grib.csh. **./link_grib.csh ../AWIP/Files/merged_AWIP32***
Step 8	Link a proper Vtable file for the ungrid.exe file **ln -s ungrib/Variable_Tables/Vtable.AWIP Vtable**
Step 9	run ungrib.exe under WPS directory with the command: **./ungrib.exe &> ungrib.log** Then the ***intermediate format files (e.g. FILE:YY-MM-DD_HH)*** files can be obtained.
Step 10	run metgrid.exe under WPS directory with the command: **./metgrid.exe &> metgrid.log** Then the ***WPS output files met_em.d0N.YYYY-MM-DD_HH:mm:ss.nc*** can be generated

After the preprocessing process, the meteorological files (met_em*.nc) can be obtained, then we can proceed with the WRF steps in Table J-3, and find the results of the simulation in the WRF output files ***wrfout_d0N_YYYY-MM-DD_HH:mm:ss***.

Table J-3 Procedure for WRF simulation

Step 1	**cd ~work/wrf/wrf-3.9.1.1_centos7/run/**
Step 2	Link the meteorological files generated by the metgrid.exe to the current directory: **ln -s ../../WPS_new/met_em* .**
Step 3	Edit the namelist.input file with proper configurations. Some parameters like the resolution, simulation time, location information should be identical with those in the namelist.wps setup. The parameter "**num_metgrid_levels**" should be consistent with the number in the met_em* files: 30 for NARR, and 27 for GCM. Make sure the item, **"input_from_file = .true.,. true.,. true.,".**
Step 4	Configure the URBPARAM.TBL file with the proper parameters in the run directory.
Step 5	Run the real.exe and wrf.exe together by submitting a job file: **cd ..** **jobsub wrf_smdmpar.job** The wrf input files *wrfinput_d0N*, and *wrfbdy_d01* will be generated by real.exe. And the wrf output files *wrfout_d0N_YYYY-MM-DD_HH:mm:ss* and restart files *wrfrst_d0N_YYYY-MM-DD_HH:mm:ss* will be generated by wrf.exe
Step 6	Then check the job status by: **jobst -u <USER>**

Appendix K Validation results at different weather stations
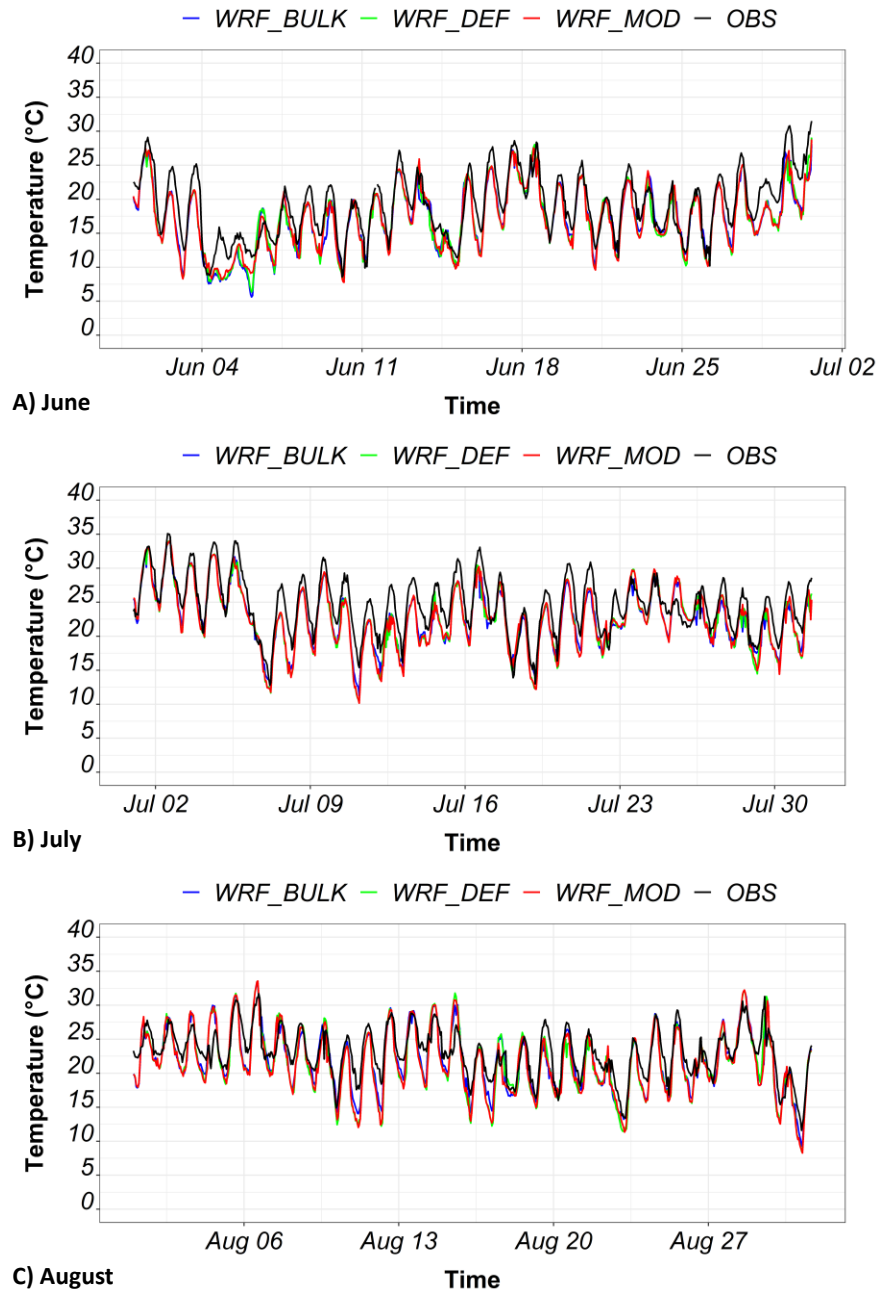
Figure K-1 Time series of observed (black) and WRF modelled 2-m air temperature at the Pierre Elliott Trudeau weather station in A) June, B) July, and C) August
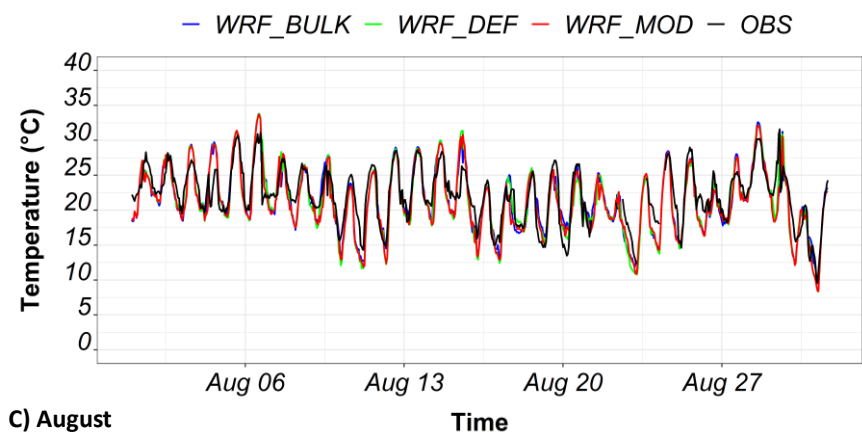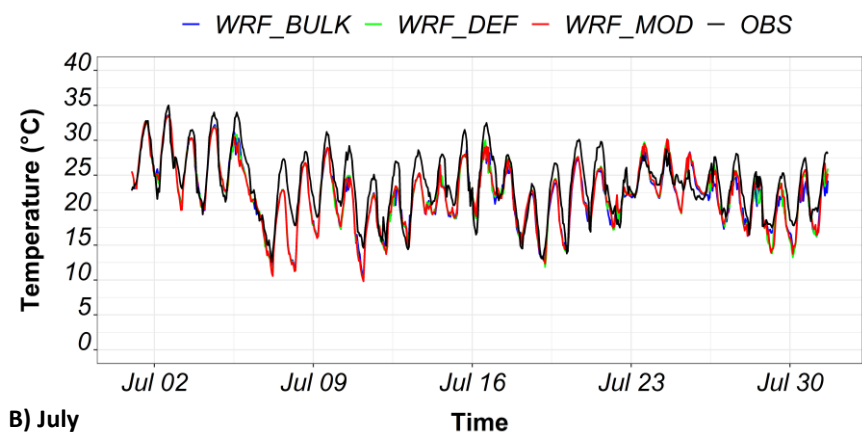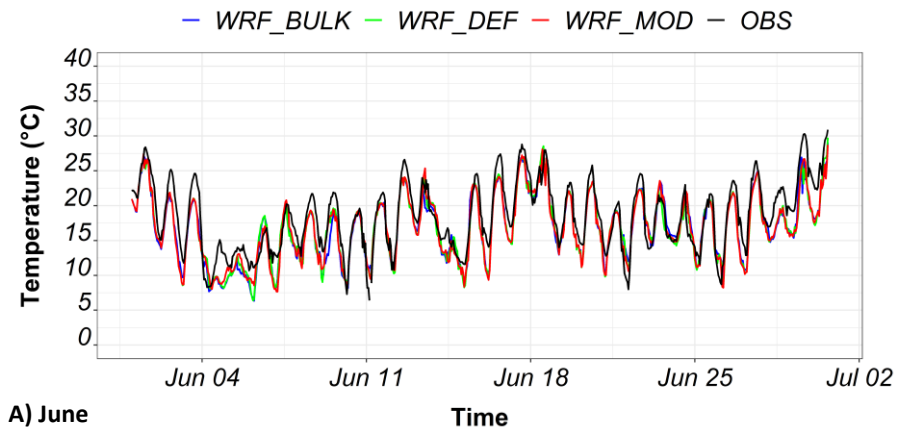
Figure K-2 Time series of observed (black) and WRF modelled 2-m air temperature at the Ste-anne-de-bellevue weather station in A) June, B) July, and C) August
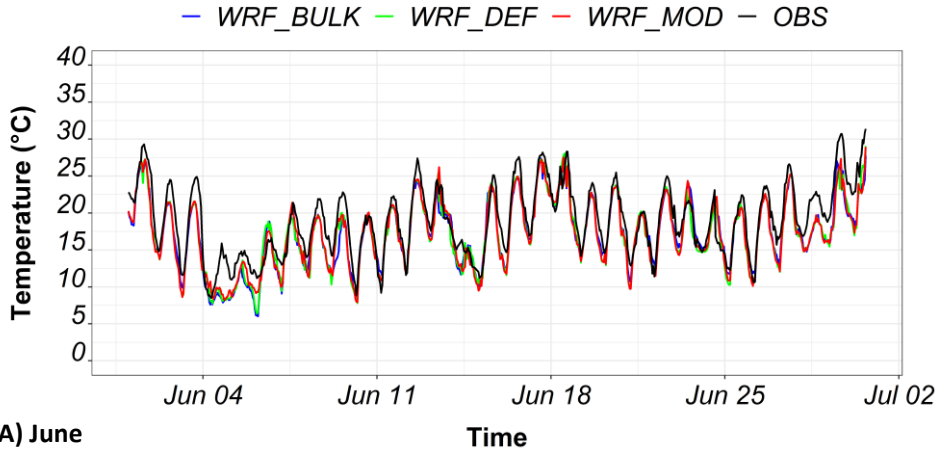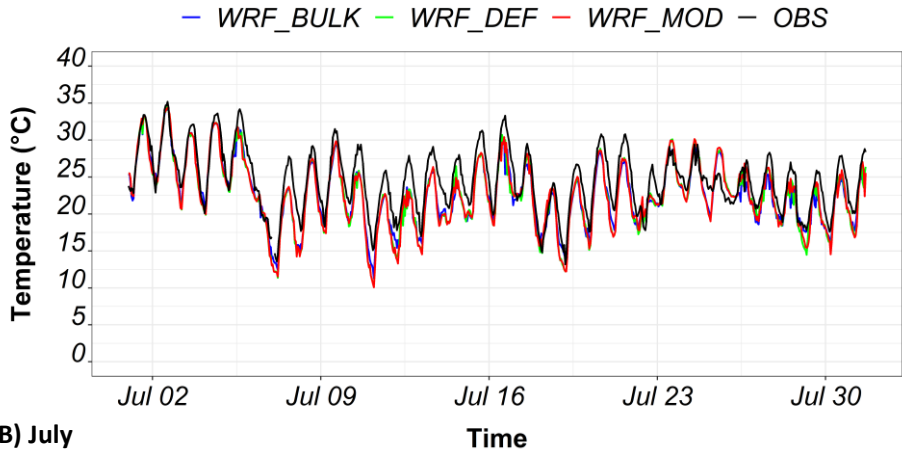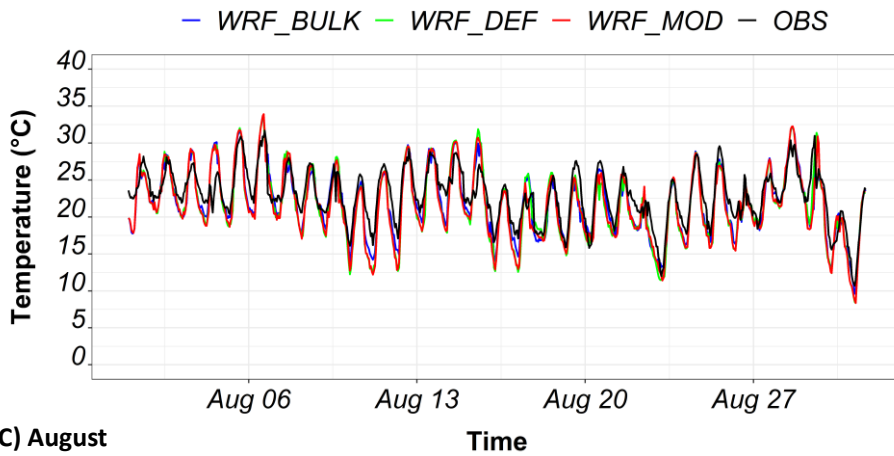
Figure K-3 Time series of observed (black) and WRF modeled 2-m air temperature at the
International Airport weather station in A) June, B) July, and C) August
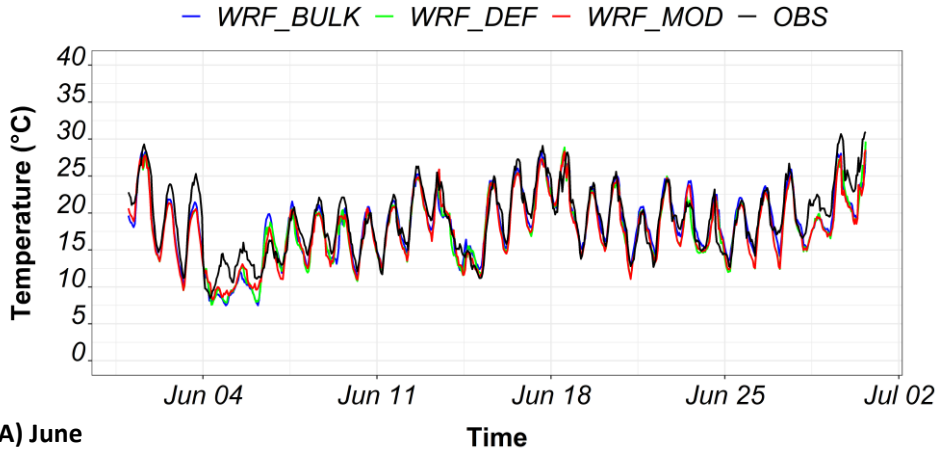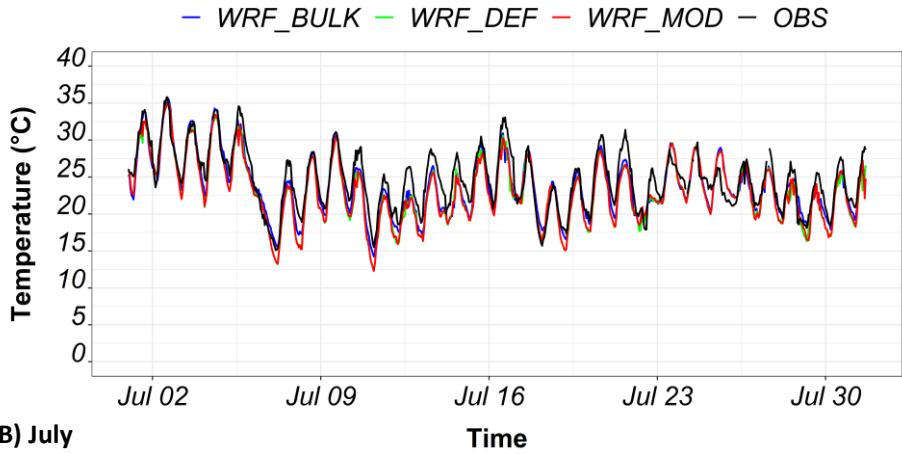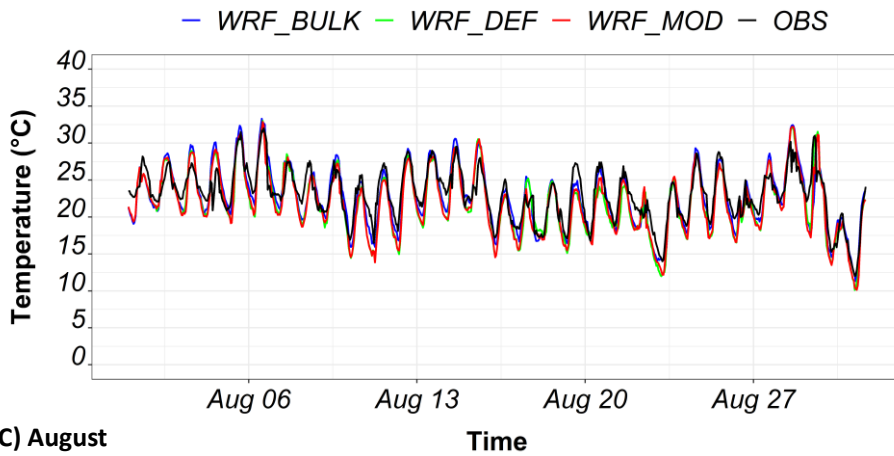
Figure K-4 Time series of observed (black) and WRF modeled 2-m air temperature at the Mc-Tavish weather station in A) June, B) July, and C) August
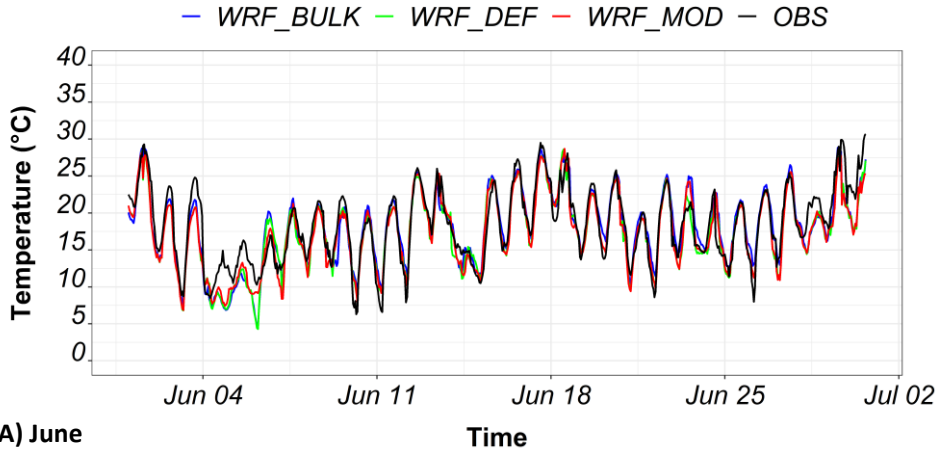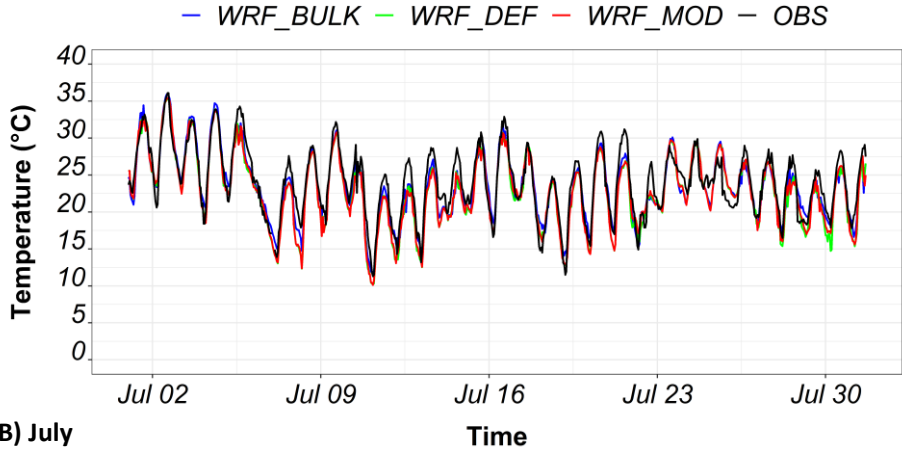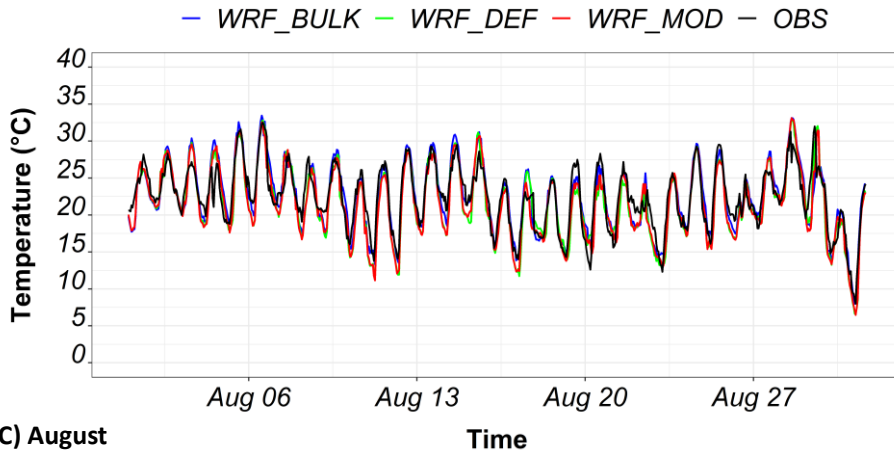
Figure K-5 Time series of observed (black) and WRF modeled 2-m air temperature at the St-Hubert weather station in A) June, B) July, and C) August
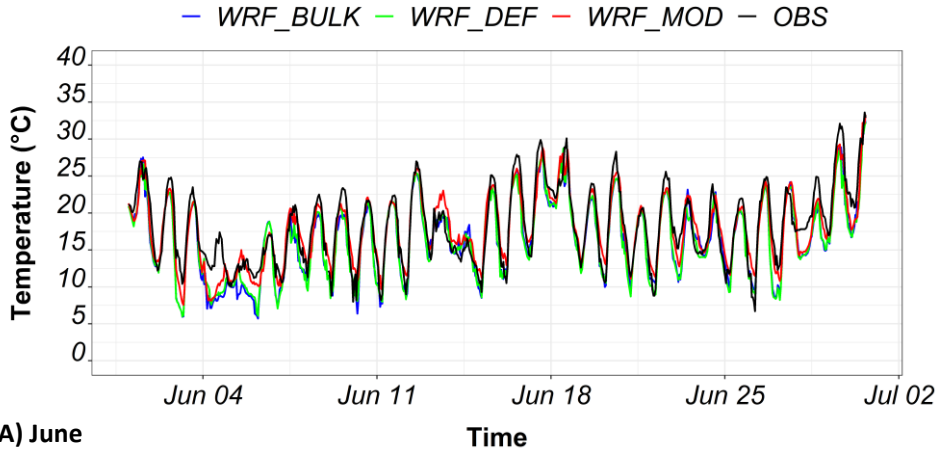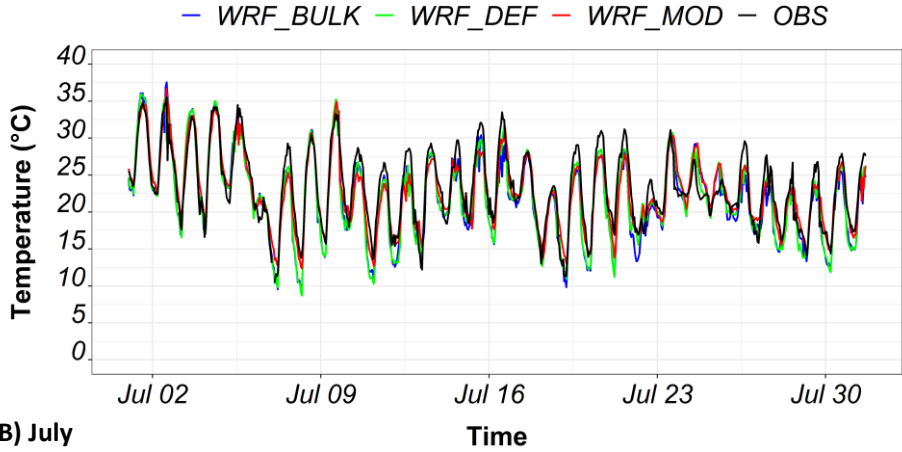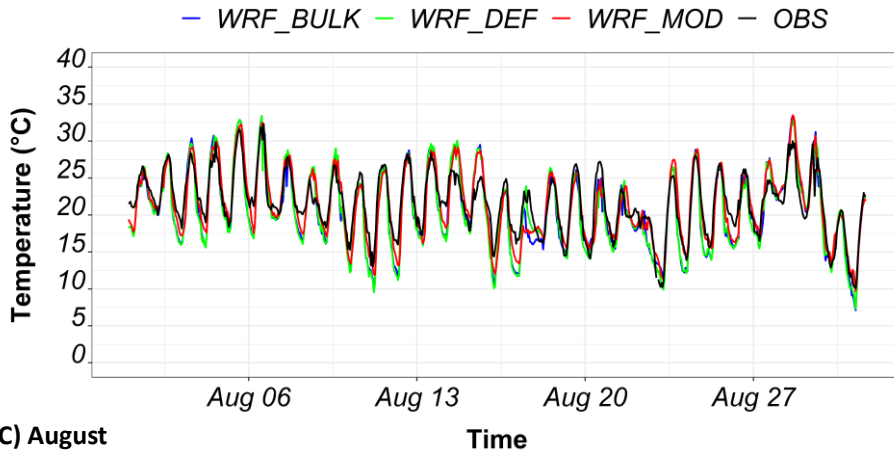
Figure K-6 Time series of observed (black) and WRF modeled 2-m air temperature at the Ottawa-Airport weather station in A) June, B) July, and C) August
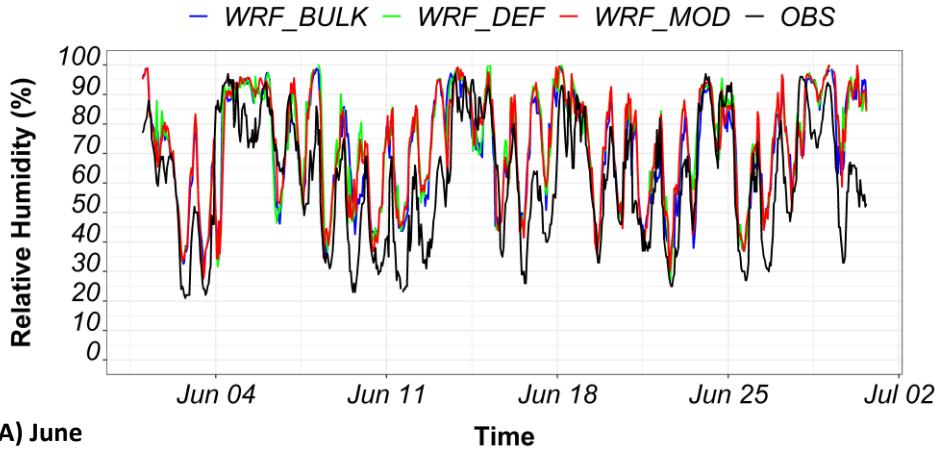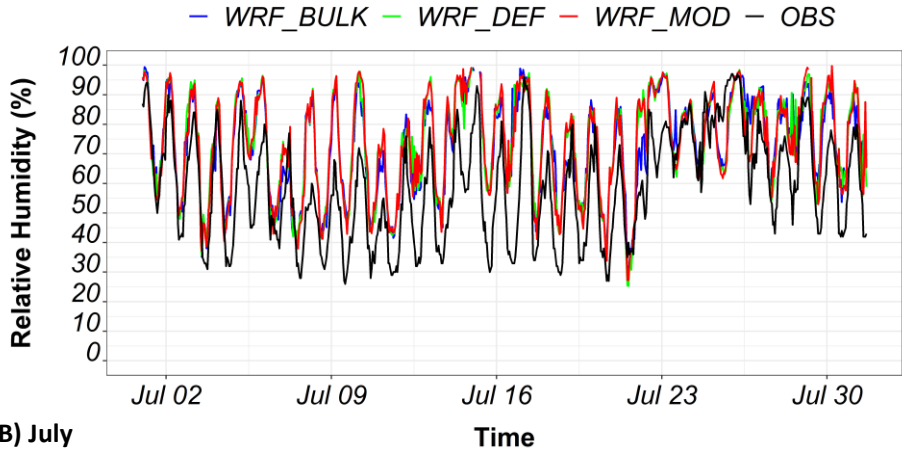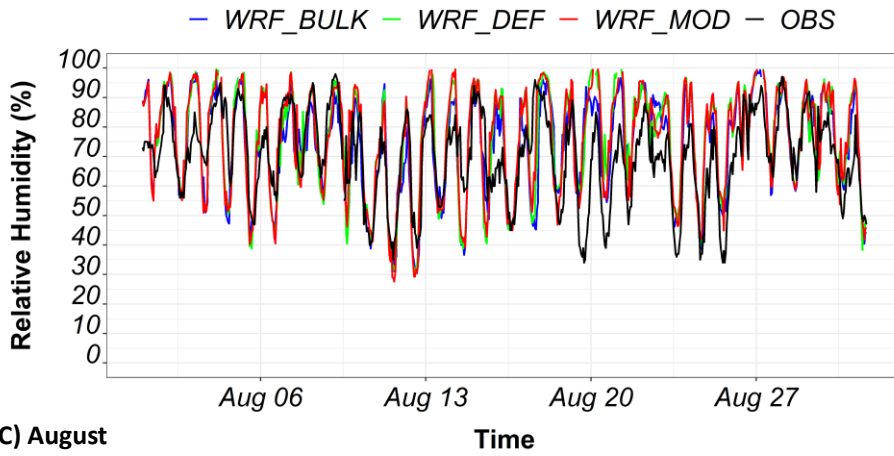
Figure K-7 Time series of observed (black) and WRF modelled near field relative humidity at the Pierre Elliott Trudeau weather station in A) June, B) July, and C) August
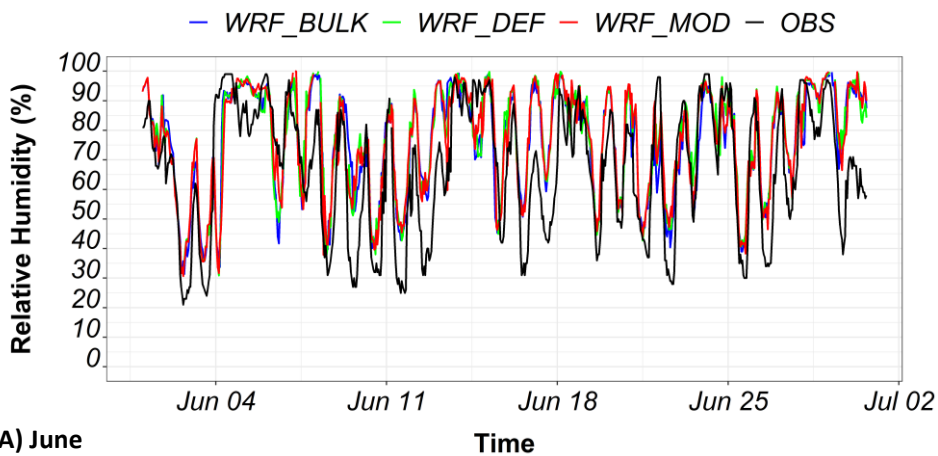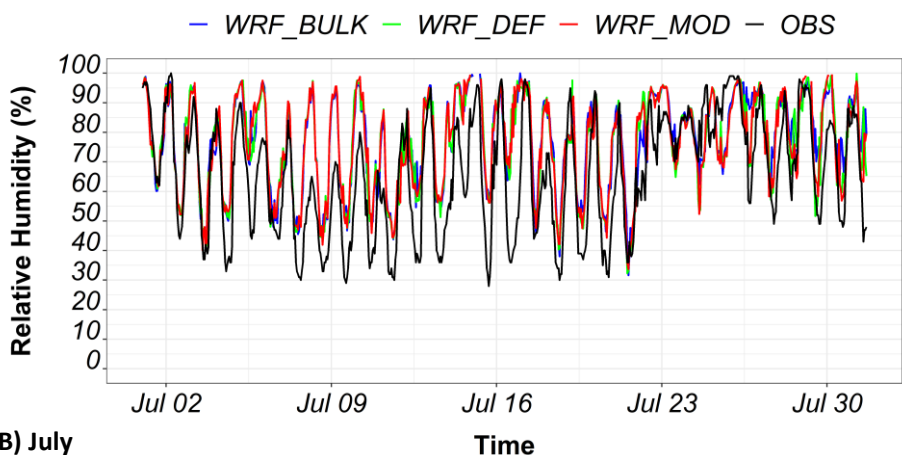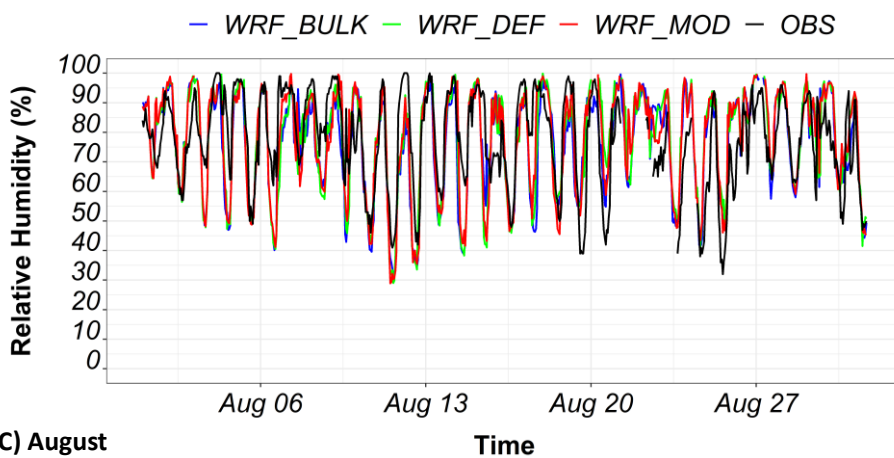
Figure K-8 Time series of observed (black) and WRF modeled near field relative humidity at the Ste-anne-de-bellevue weather station in A) June, B) July, and C) August
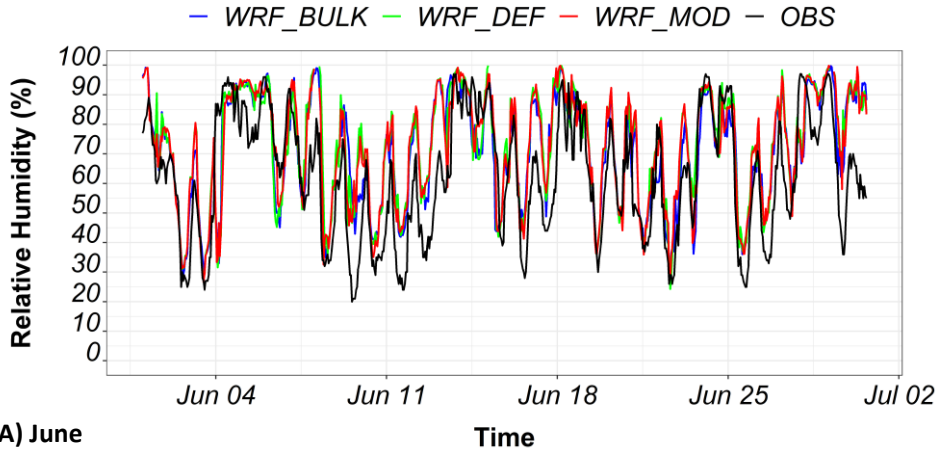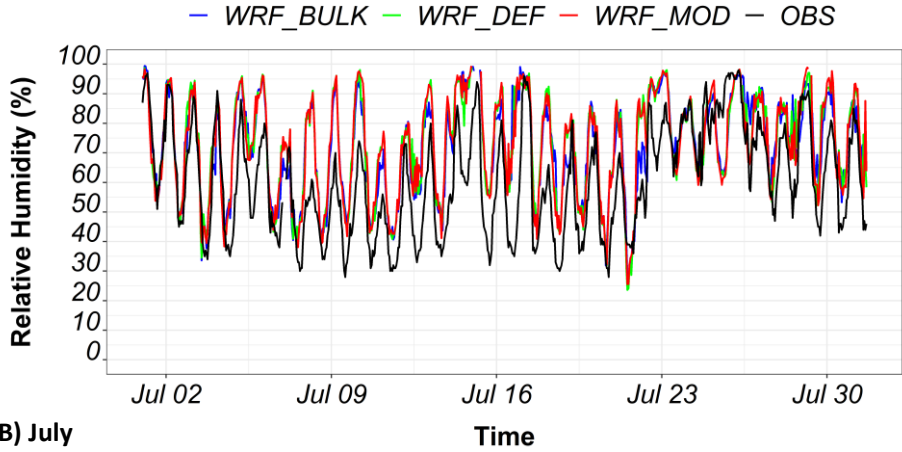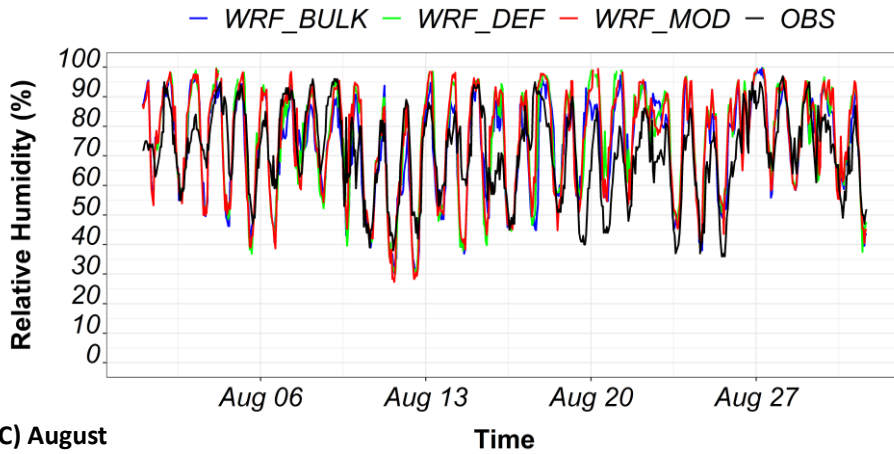
Figure K-9 Time series of observed (black) and WRF modeled near field relative humidity at the International Airport weather station in A) June, B) July, and C) August
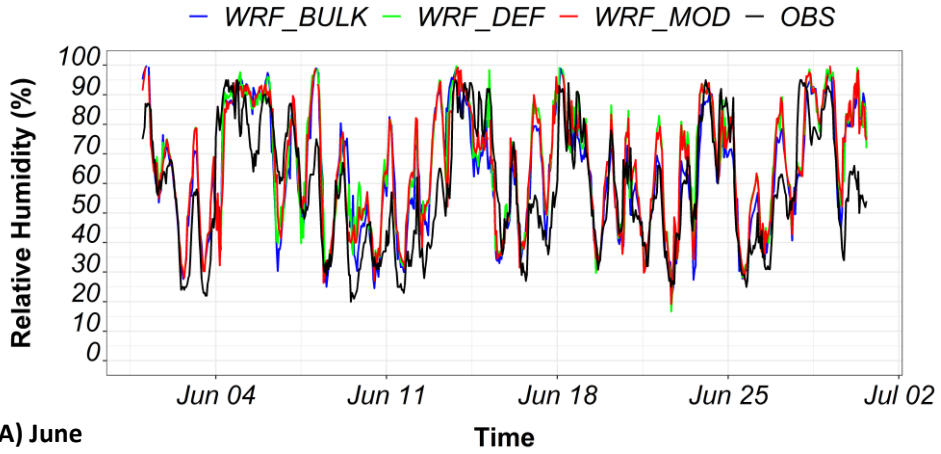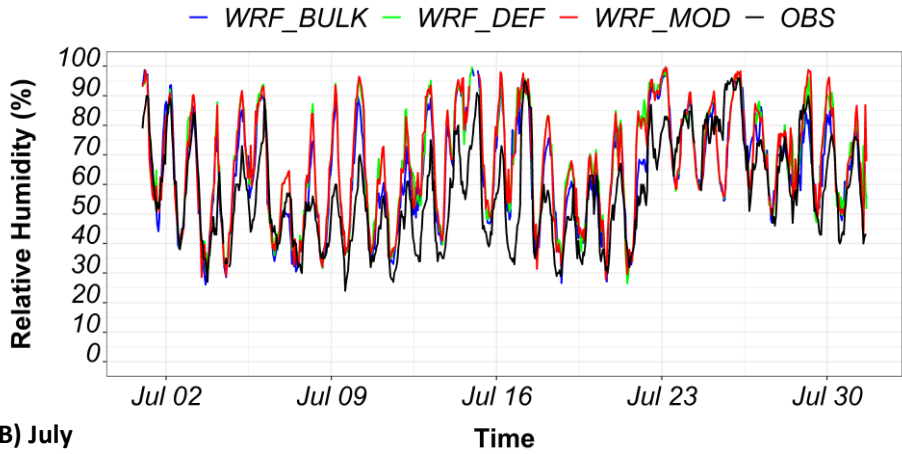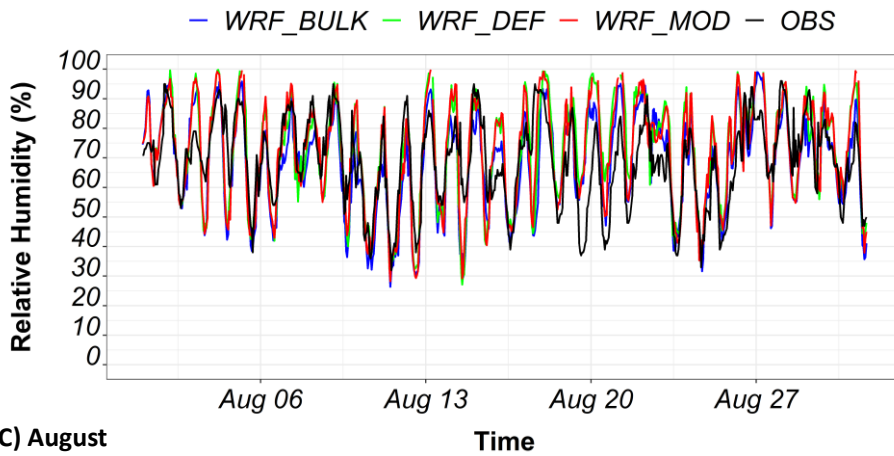
Figure K-10 Time series of observed (black) and WRF modeled near field relative humidity at the Mc-Tavish weather station in A) June, B) July, and C) August
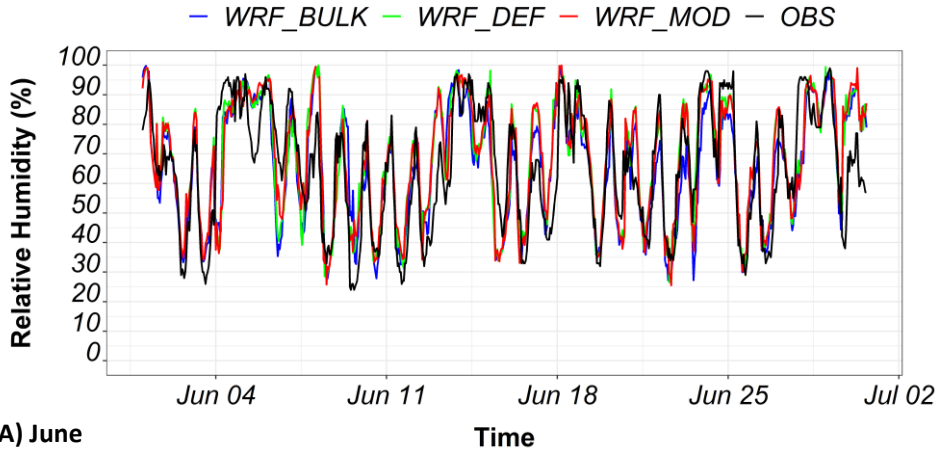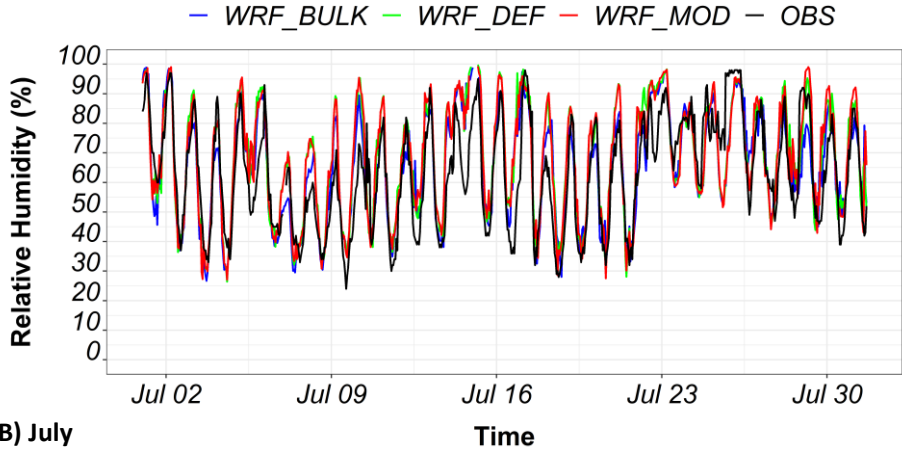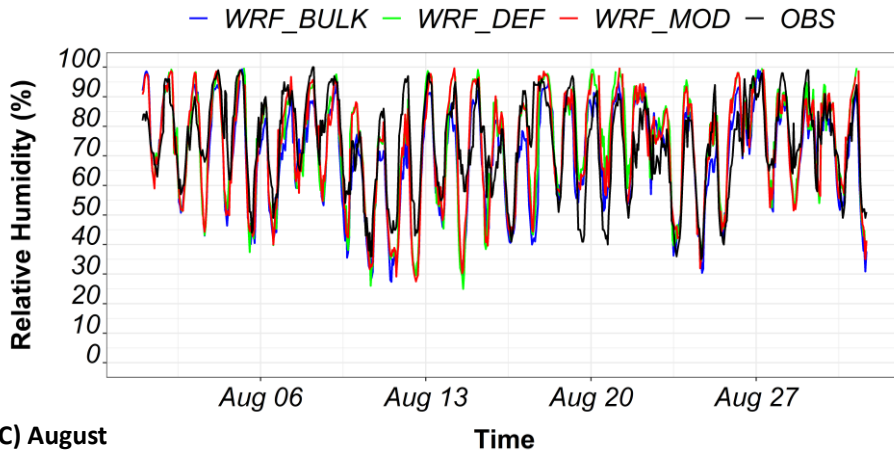
Figure K-11 Time series of observed (black) and WRF modeled near field relative humidity at the St-Hubert weather station in A) June, B) July, and C) August
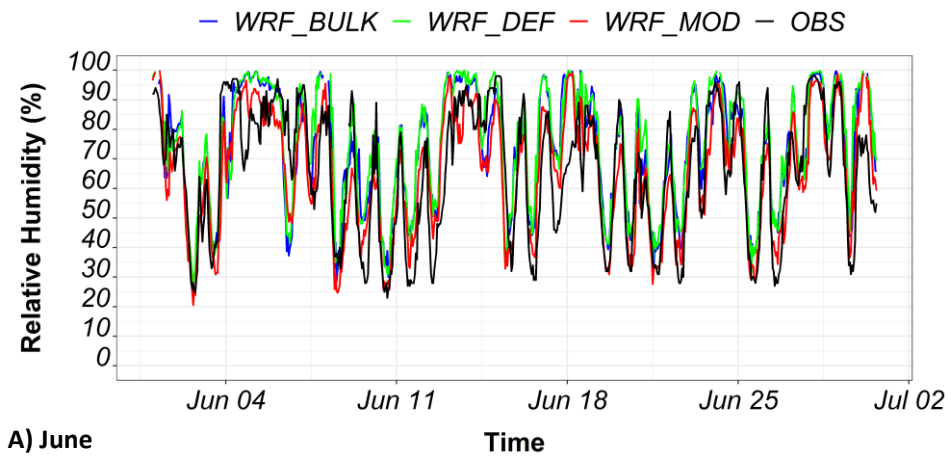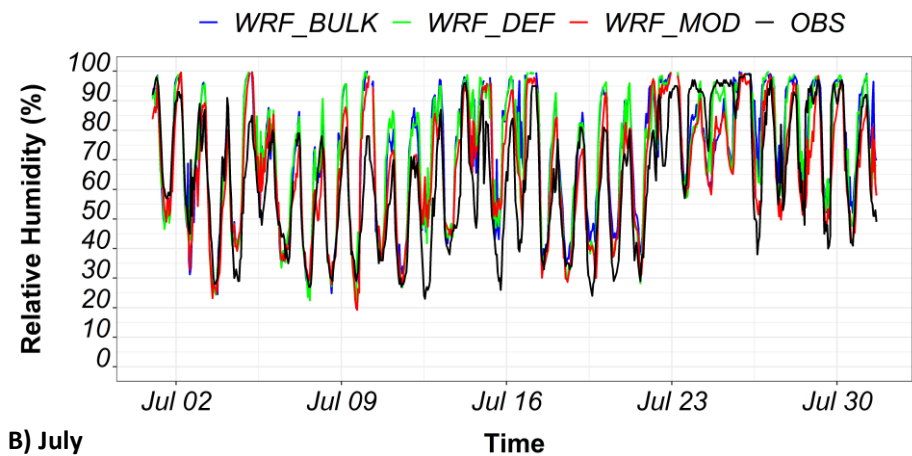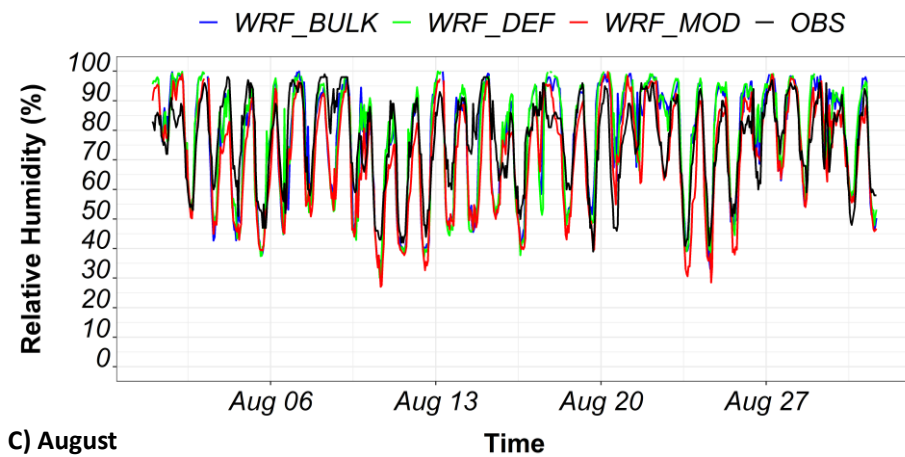
Figure K-12 Time series of observed (black) and WRF modeled near field relative humidity at
the Ottawa-Airport weather station in A) June, B) July, and C) August
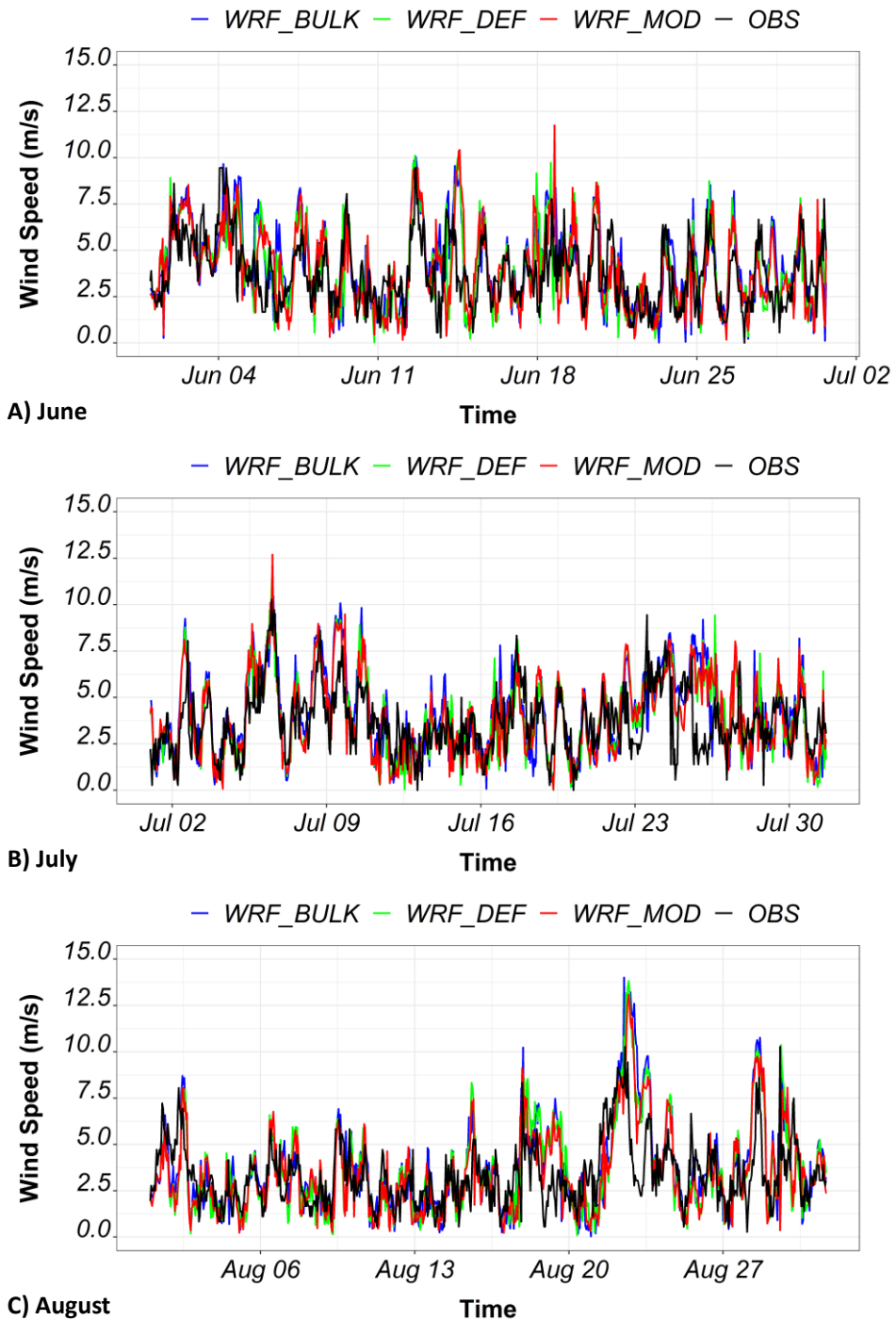
Figure K-13 Time series of observed (black) and WRF modelled 10-m wind speed at the Pierre Elliott Trudeau weather station in A) June, B) July, and C) August
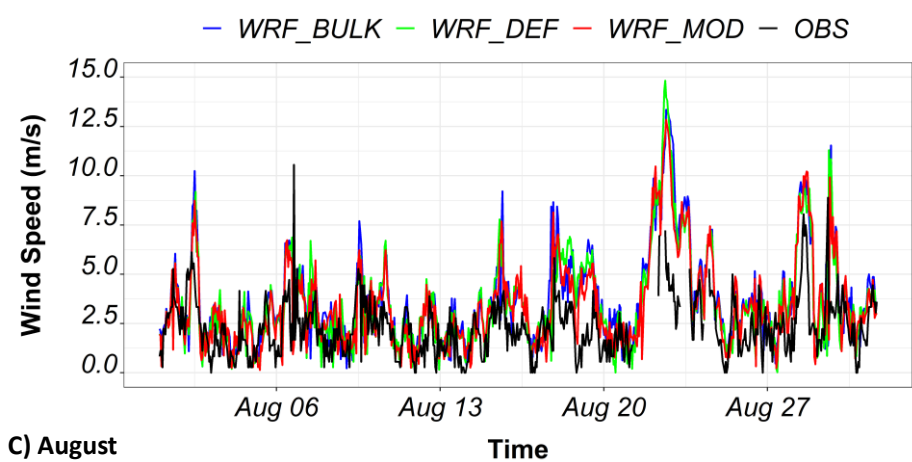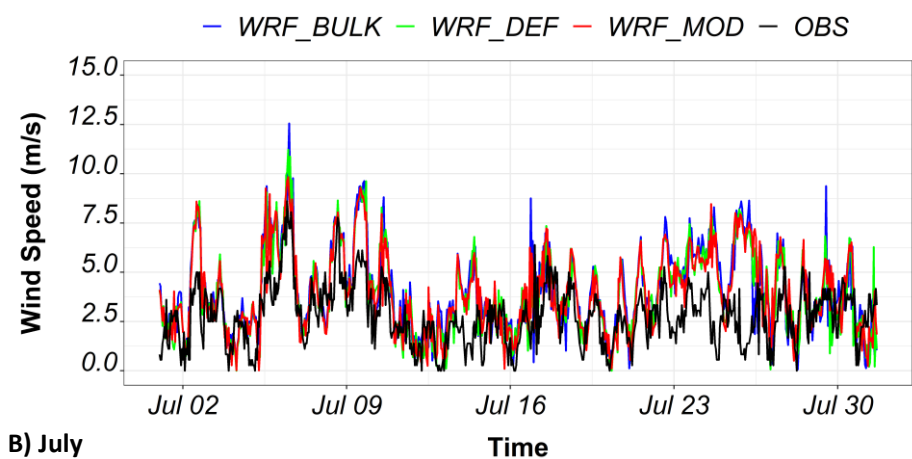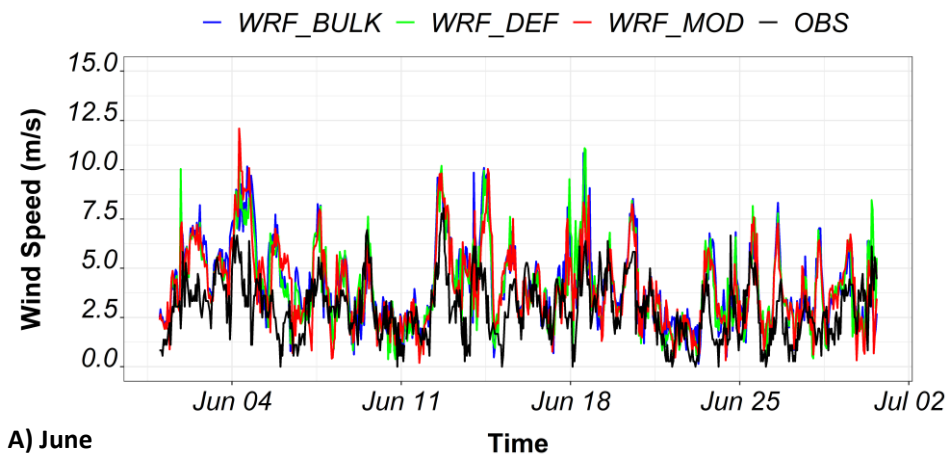
Figure K-14 Time series of observed (black) and WRF modeled 10-m wind speed at the Ste-anne-de-bellevue weather station in A) June, B) July, and C) August
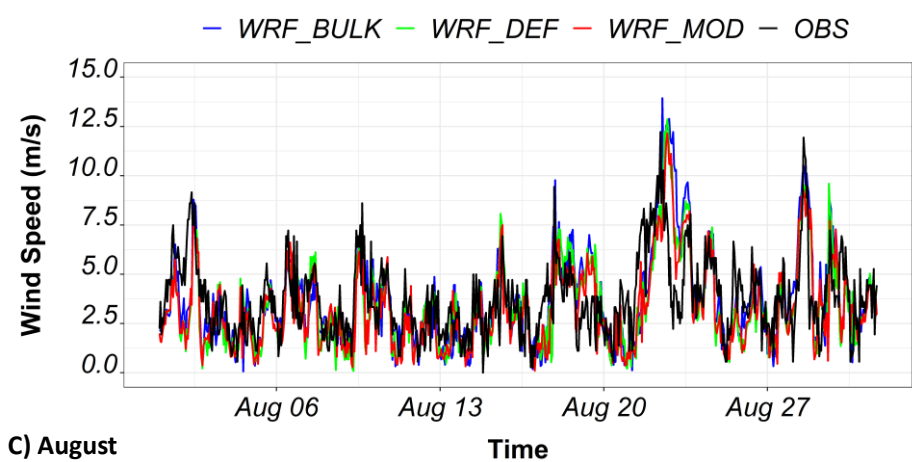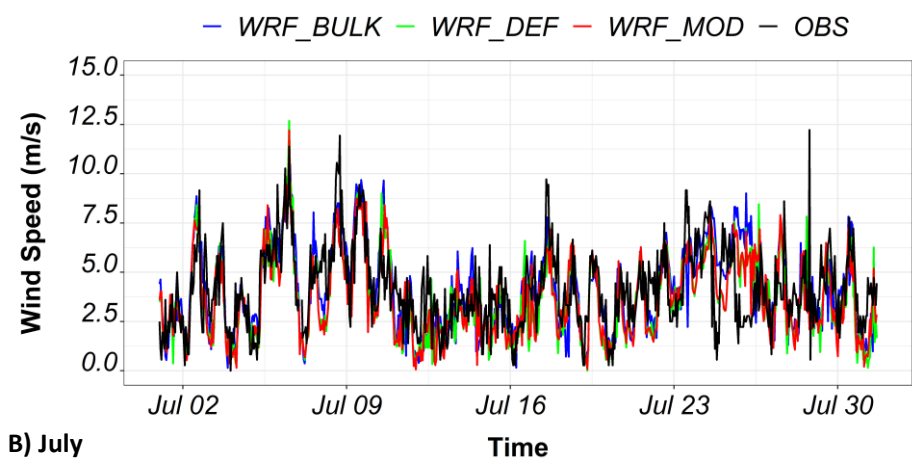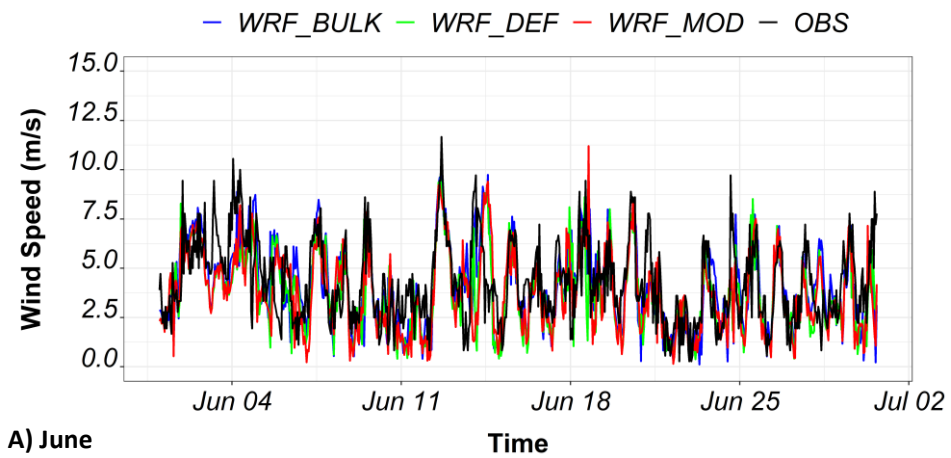
Figure K-15 Time series of observed (black) and WRF modeled 10-m wind speed at the International Airport weather station in A) June, B) July, and C) August
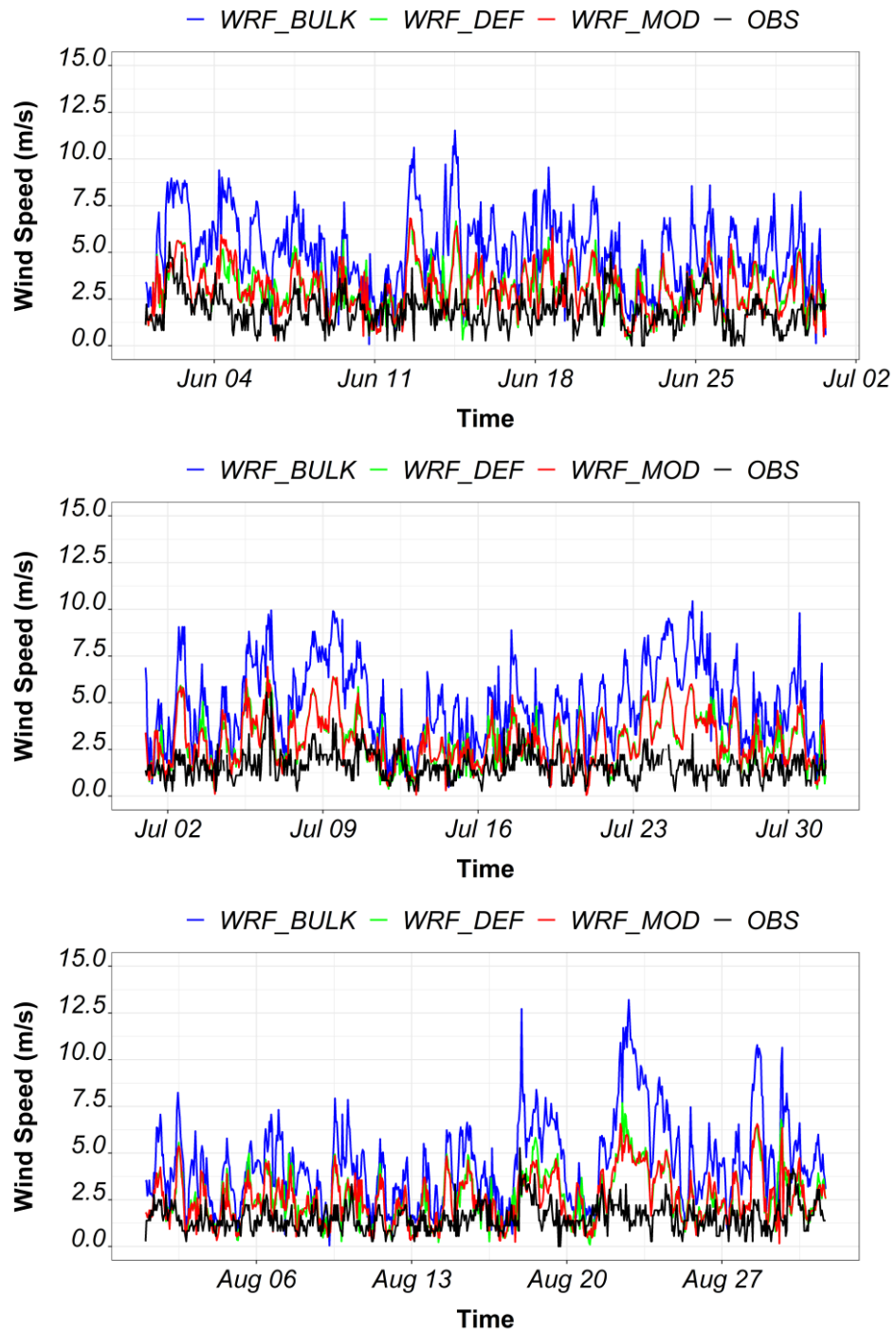
Figure K-16 Time series of observed (black) and WRF modeled 10-m wind speed at the Mc-Tavish weather station in A) June, B) July, and C) August
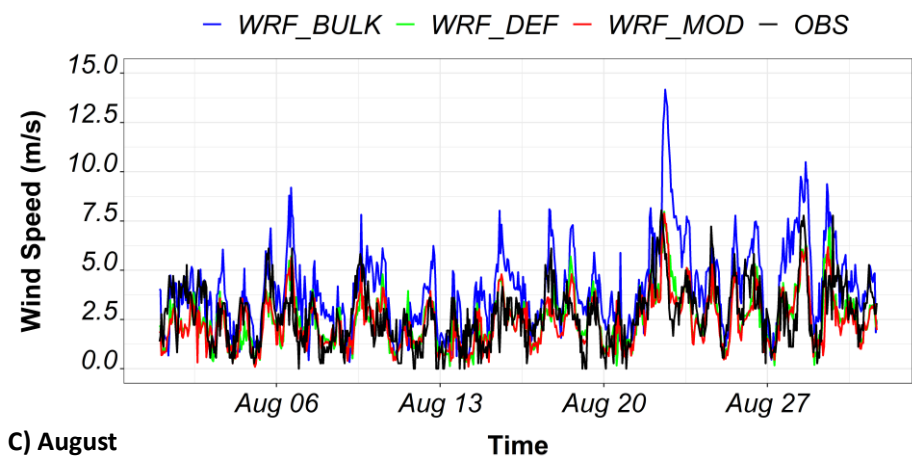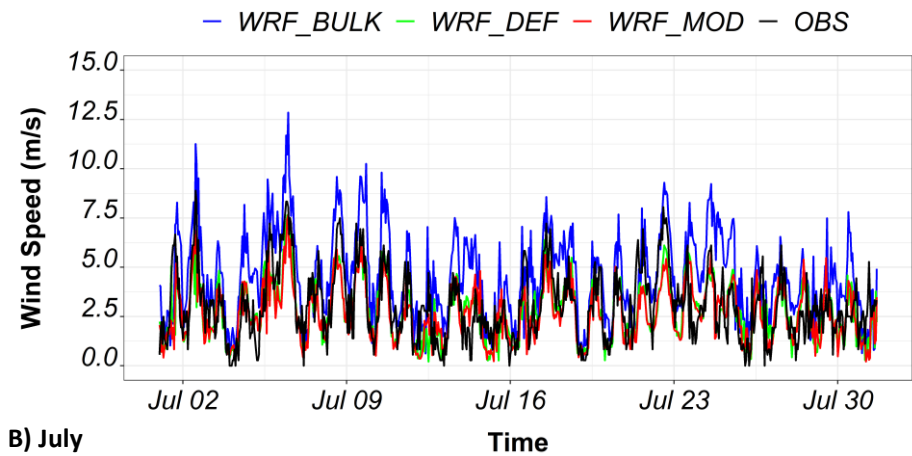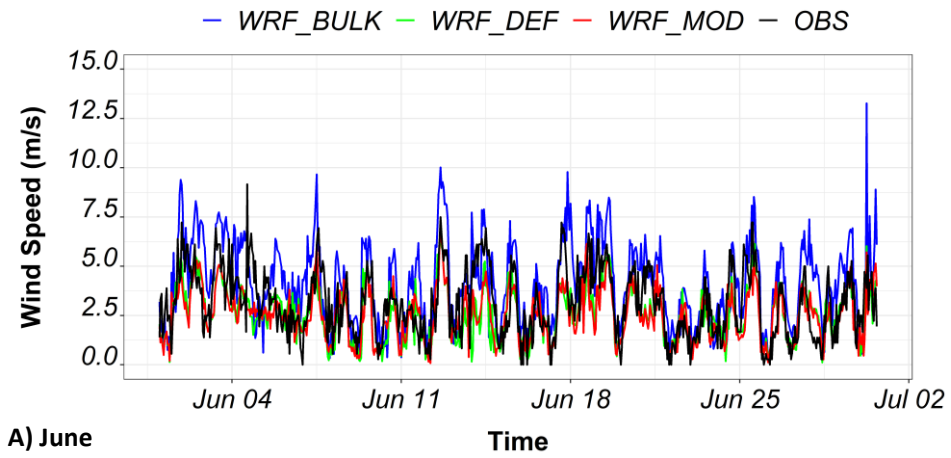
Figure K-17 Time series of observed (black) and WRF modeled 10-m wind speed at the St-Hubert weather station in A) June, B) July, and C) August
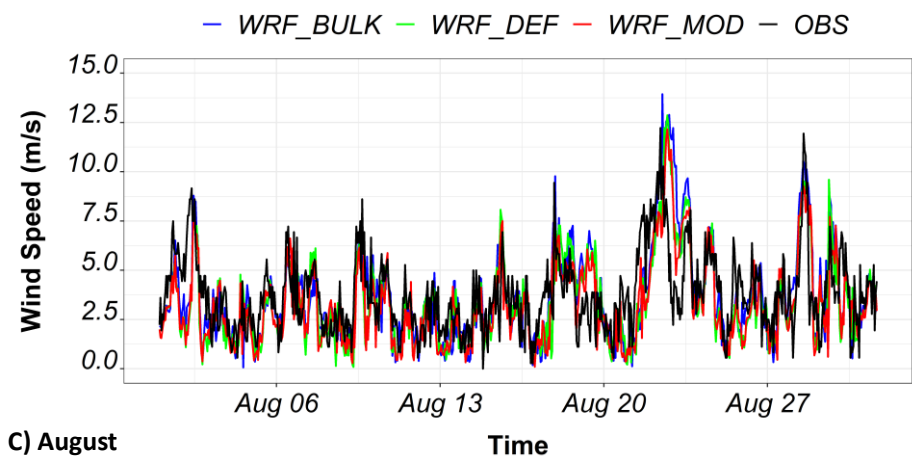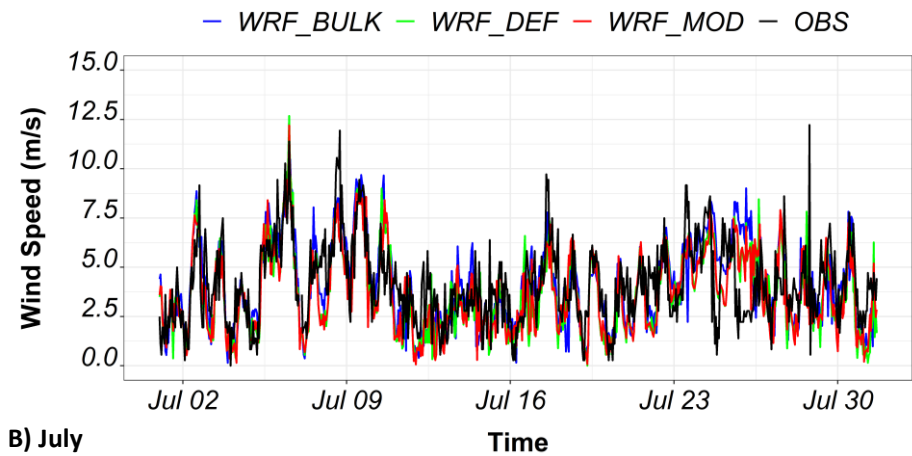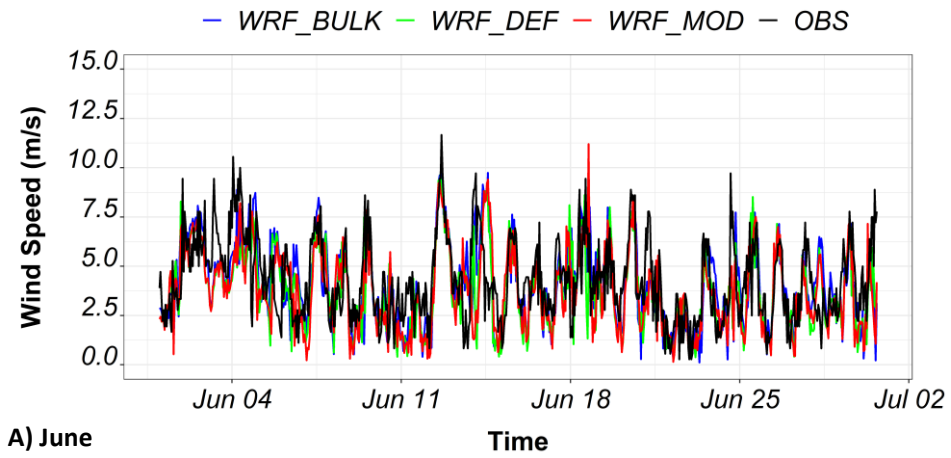
Figure K-18 Time series of observed (black) and WRF modeled 10-m wind speed at the Ottawa-Airport weather station in A) June, B) July, and C) August
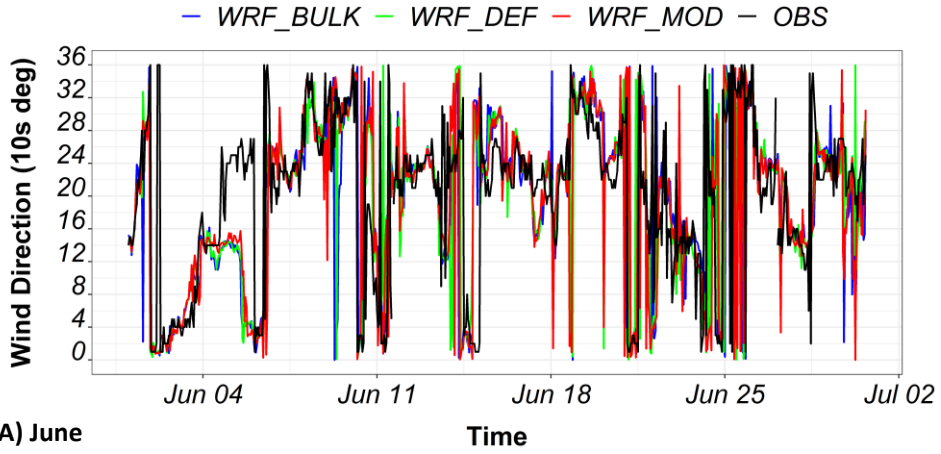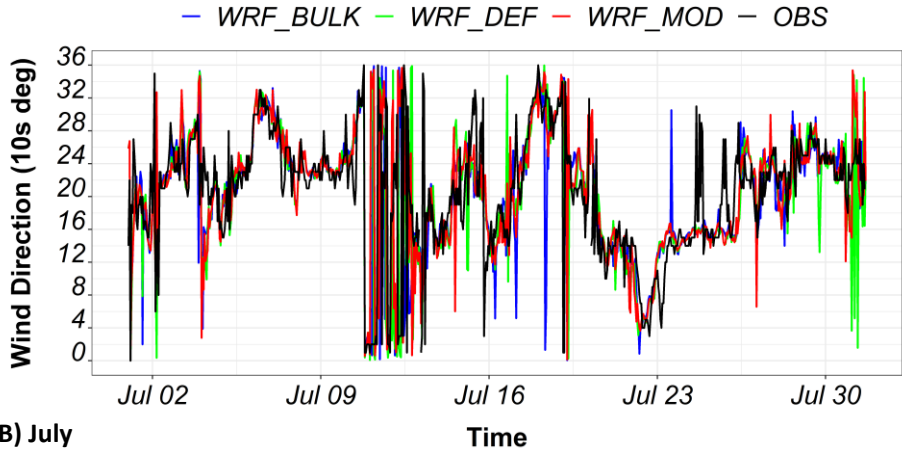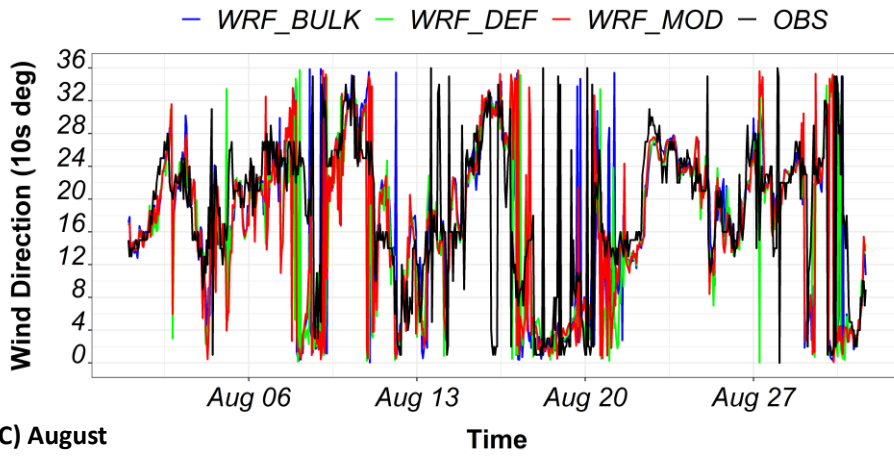
Figure K-19 Time series of observed (black) and WRF modelled 10-m wind direction at the Pierre Elliott Trudeau weather station in A) June, B) July, and C) August
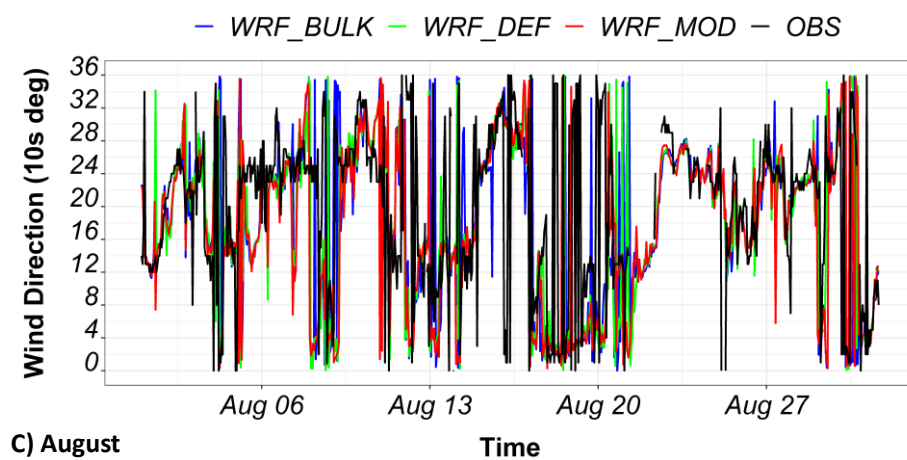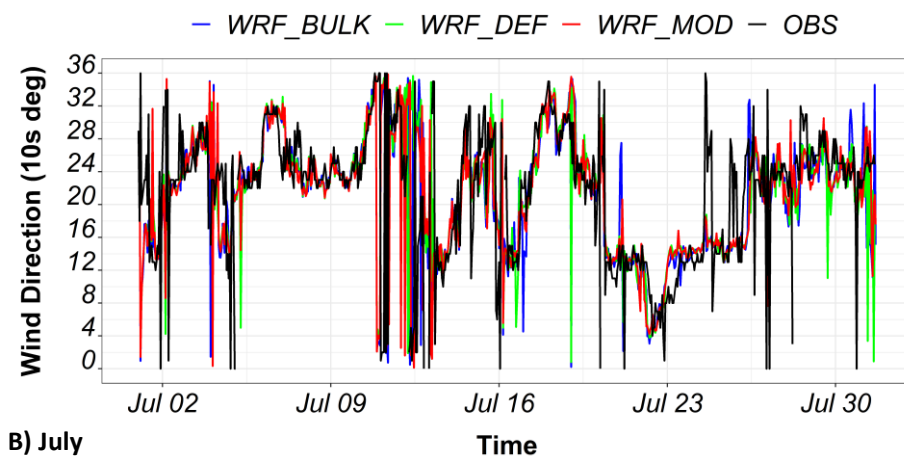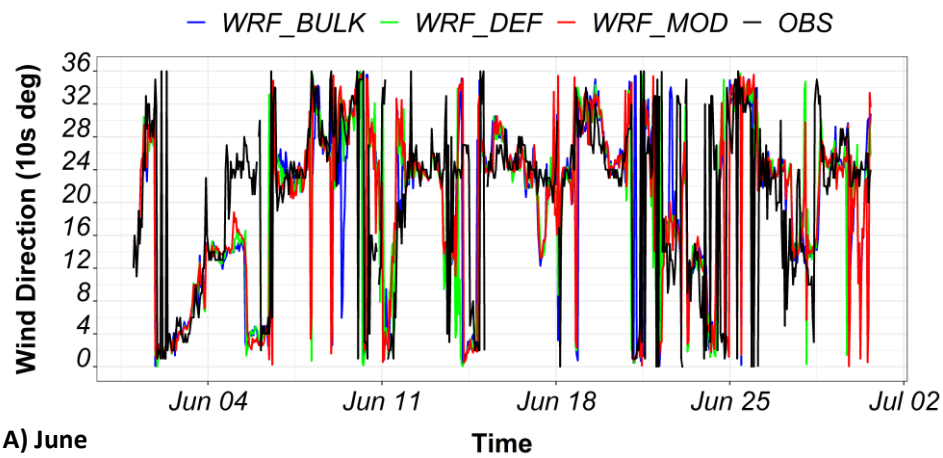
Figure K-20 Time series of observed (black) and WRF modeled 10-m wind direction at the Ste-anne-de-bellevue weather station in A) June, B) July, and C) August
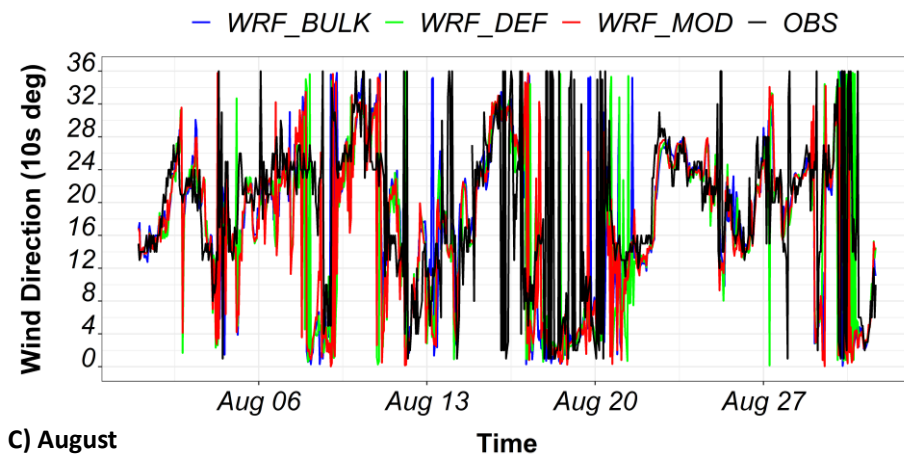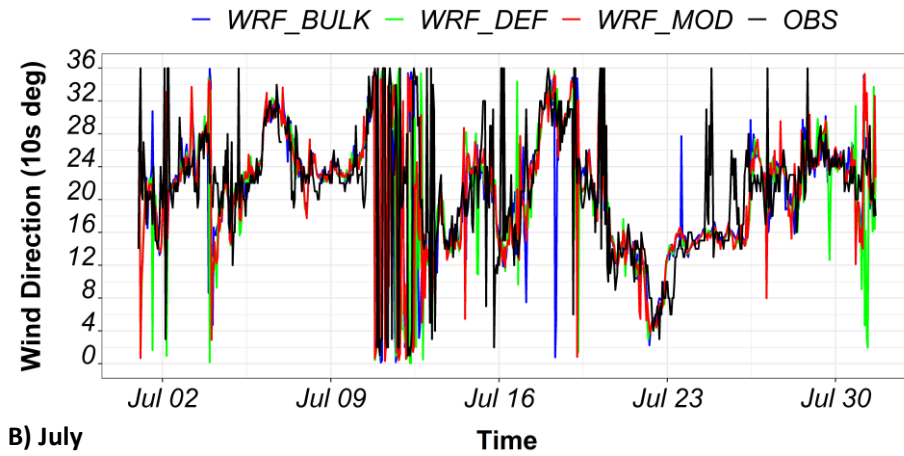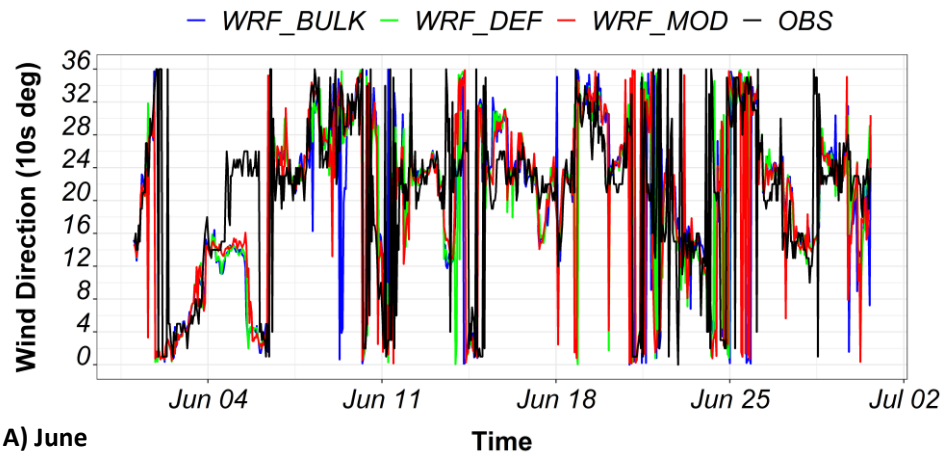
Figure K-21 Time series of observed (black) and WRF modeled 10-m wind direction at the International Airport weather station in A) June, B) July, and C) August
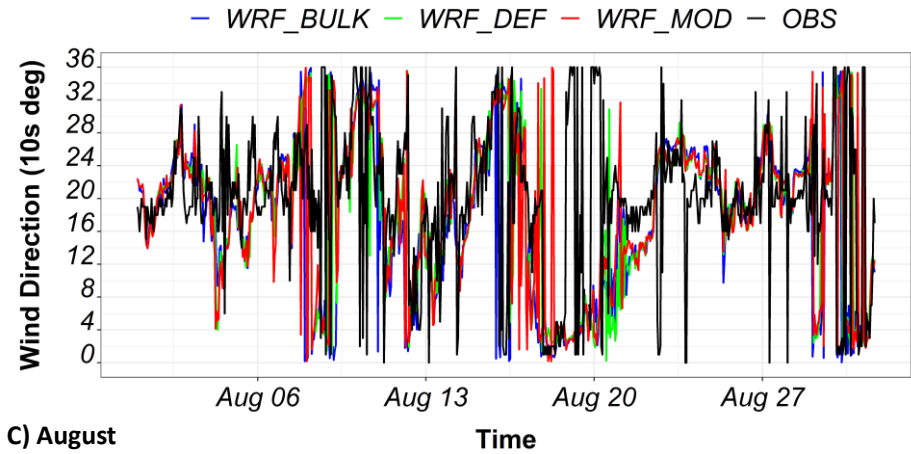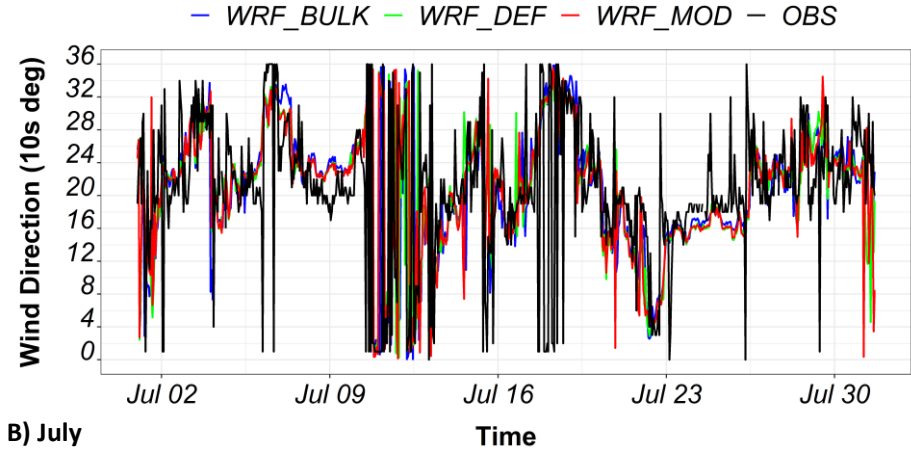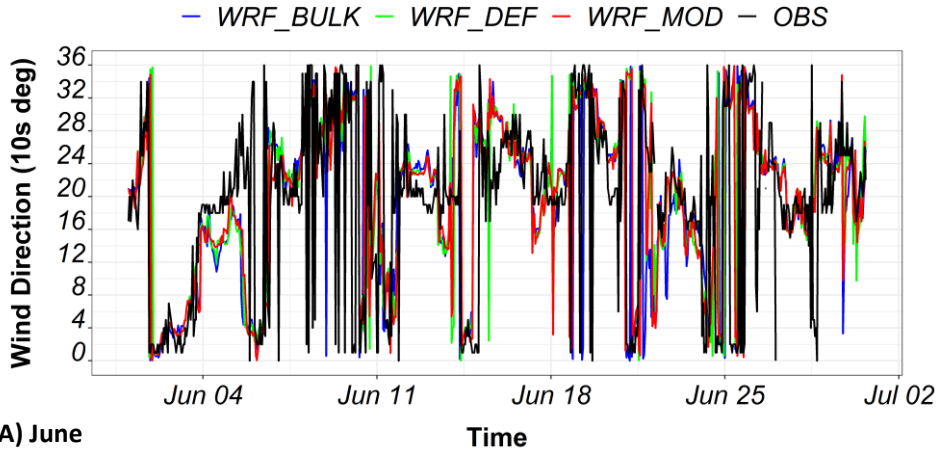
Figure K-22 Time series of observed (black) and WRF modeled 10-m wind direction at the Mc-Tavish weather station in A) June, B) July, and C) August
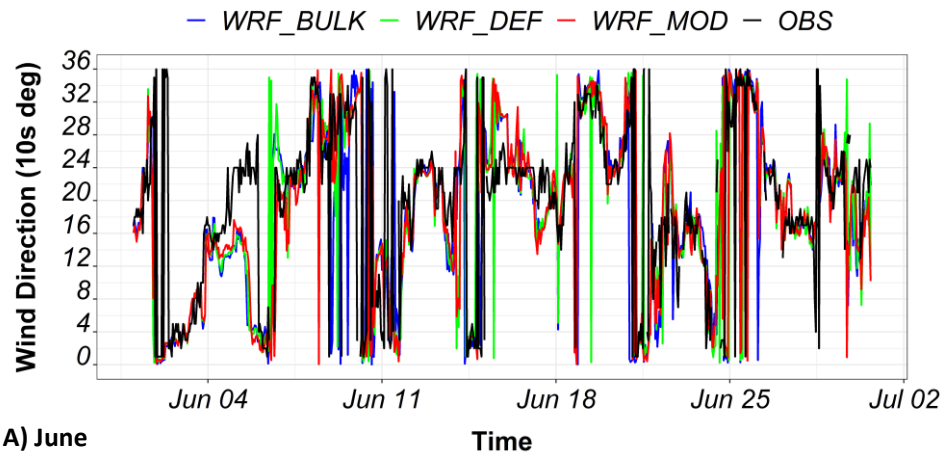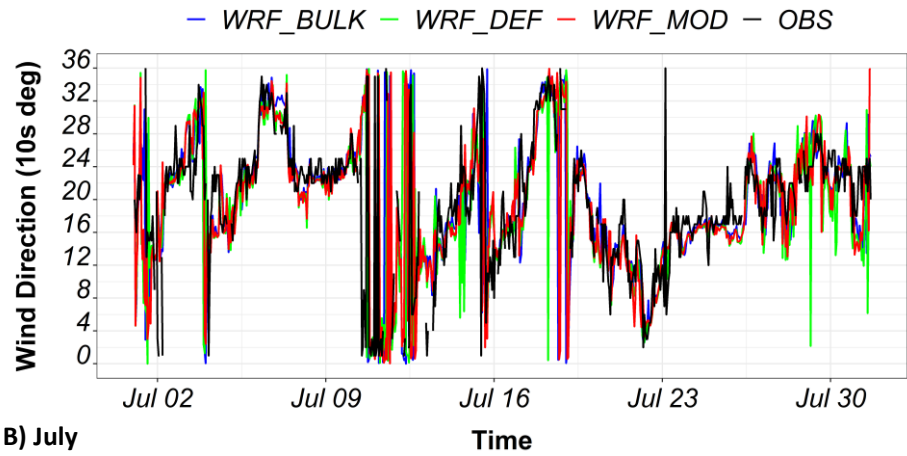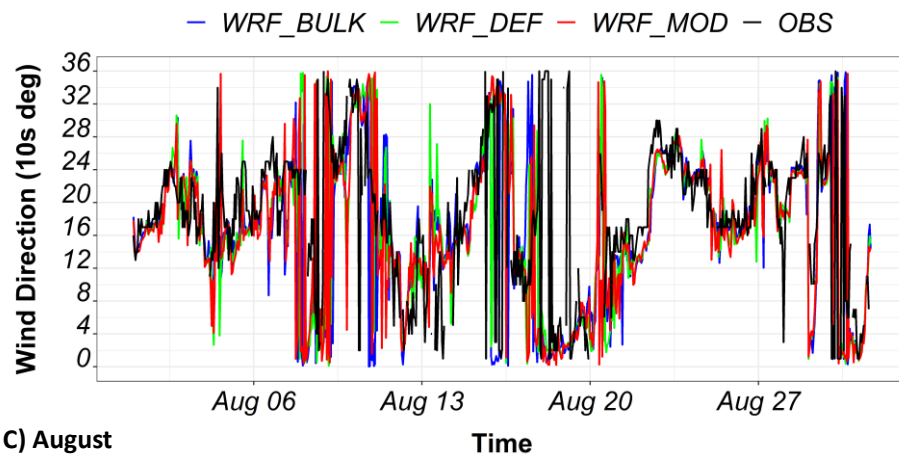
Figure K-23 Time series of observed (black) and WRF modeled 10-m wind direction at the St-Hubert weather station in A) June, B) July, and C) August
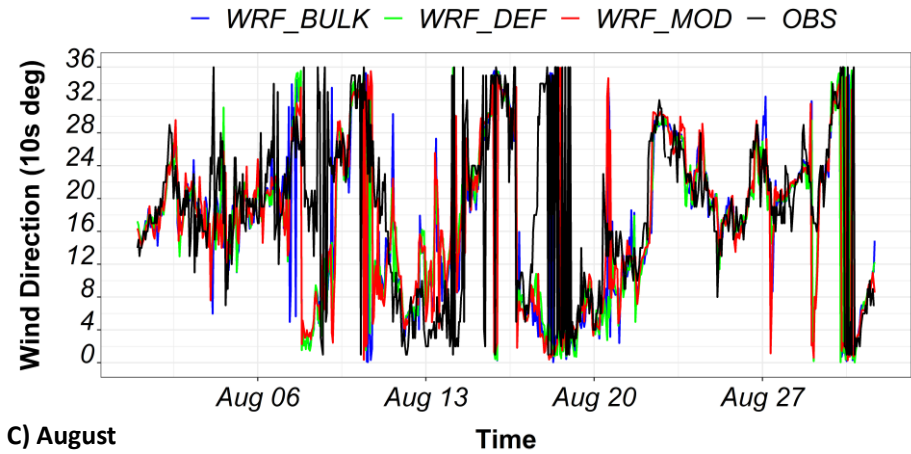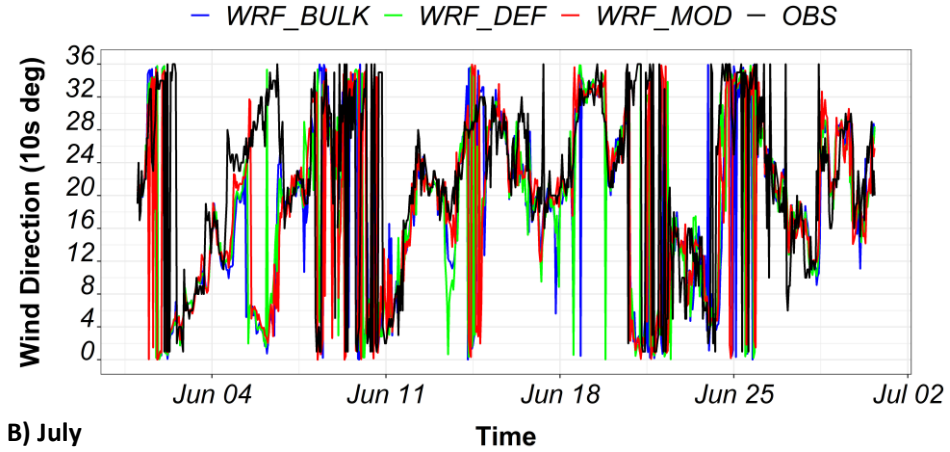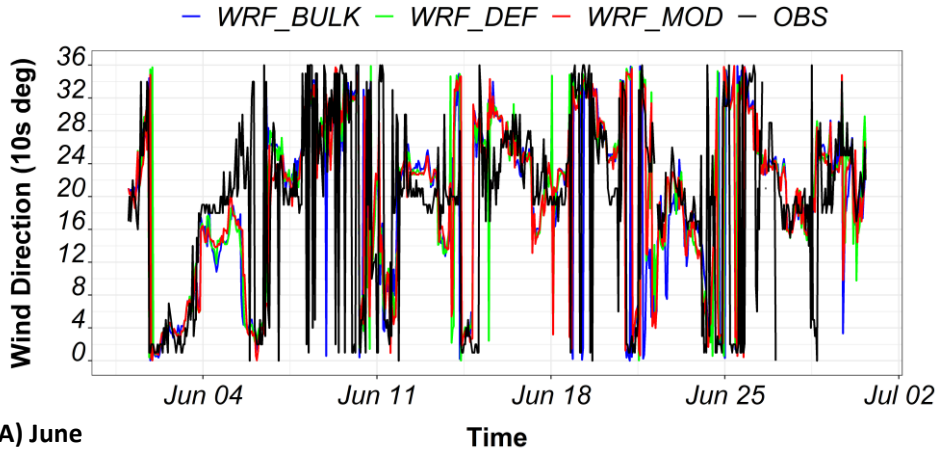
Figure K-24 Time series of observed (black) and WRF modeled 10-m wind direction at the Ottawa-Airport weather station in A) June, B) July, and C) August
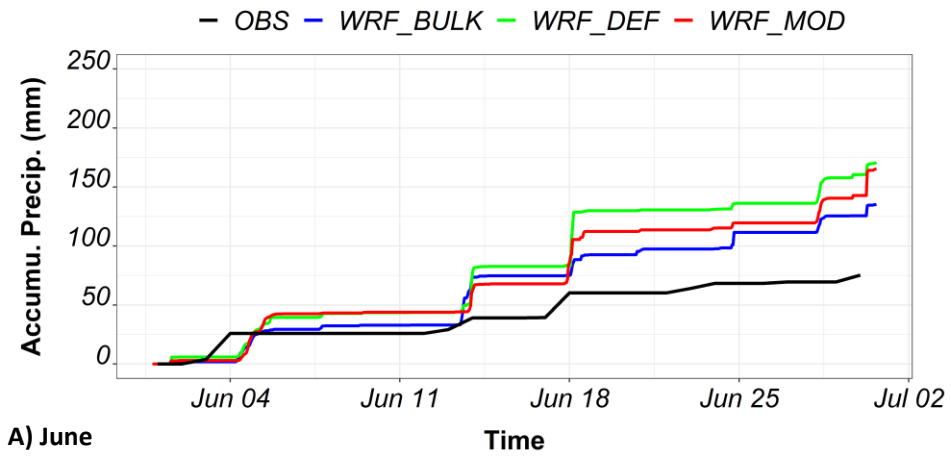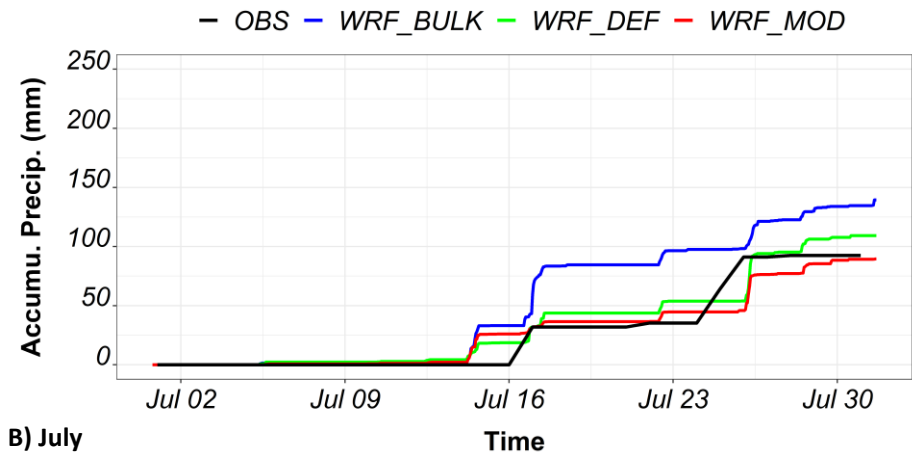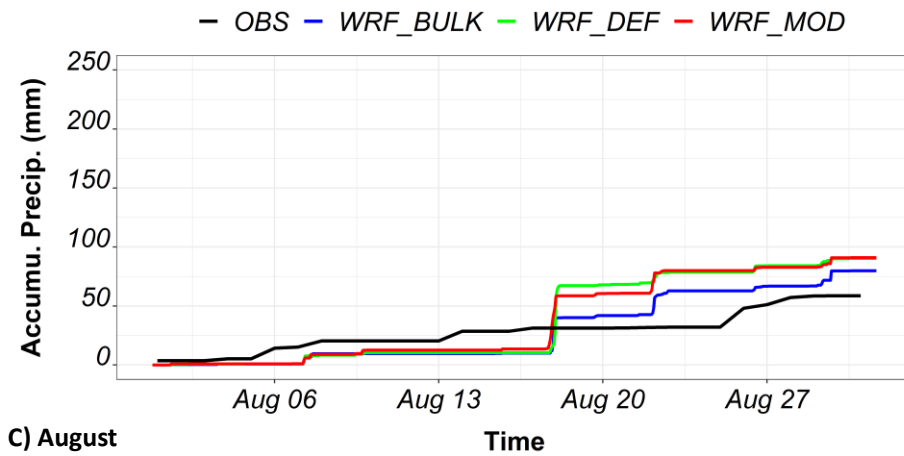
Figure K-25 Time series of observed (black) and WRF modelled accumulated precipitation at the Pierre Elliott Trudeau weather station in A) June, B) July, and C) August
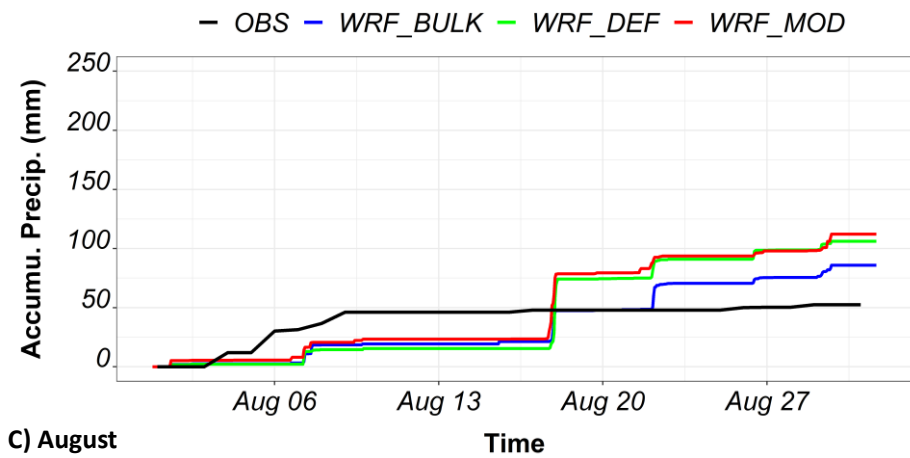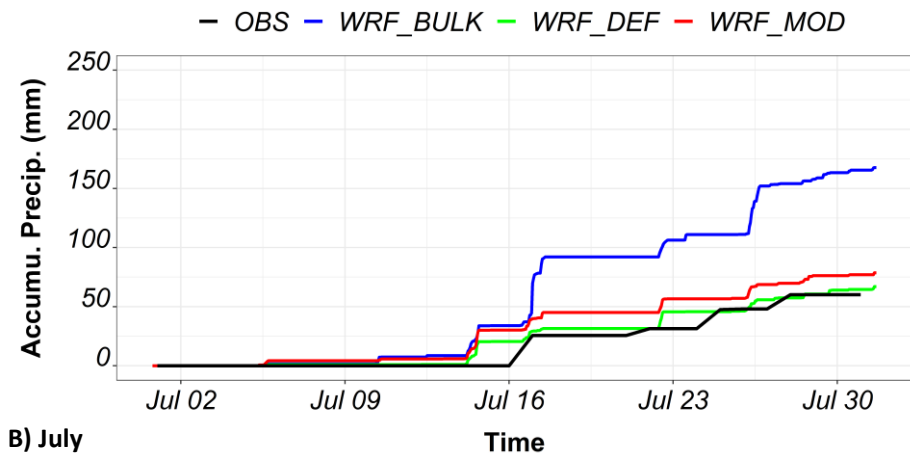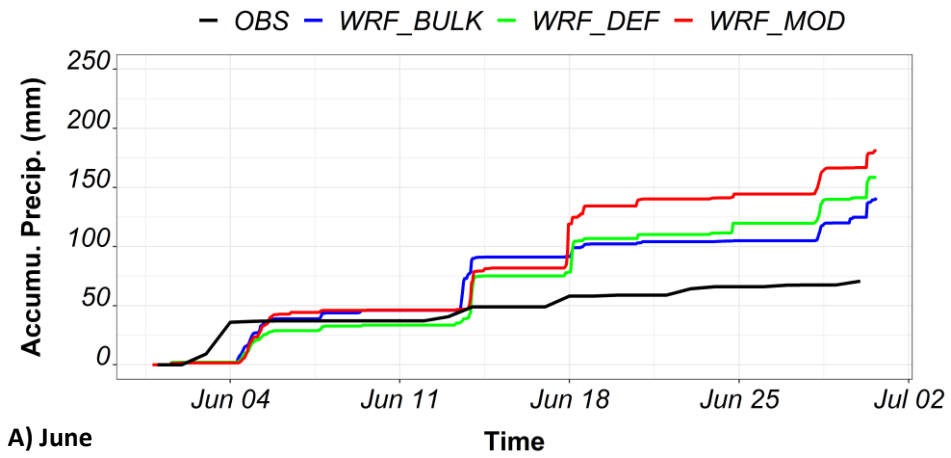
Figure K-26 Time series of observed (black) and WRF modeled accumulated precipitation at the Ste-anne-de-bellevue weather station in A) June, B) July, and C) August

215
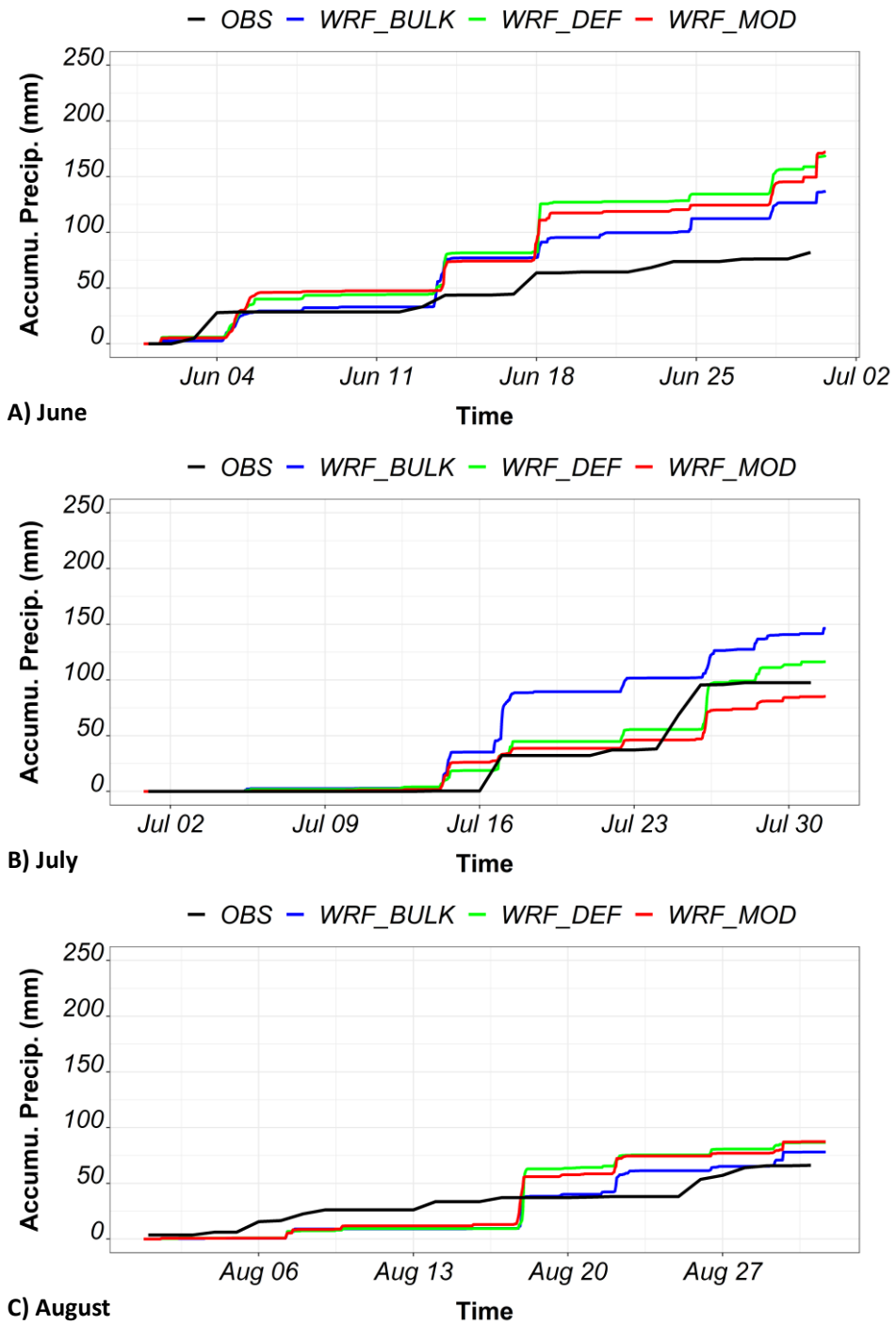
Figure K-27 Time series of observed (black) and WRF modeled accumulated precipitation at the International Airport weather station in A) June, B) July, and C) August
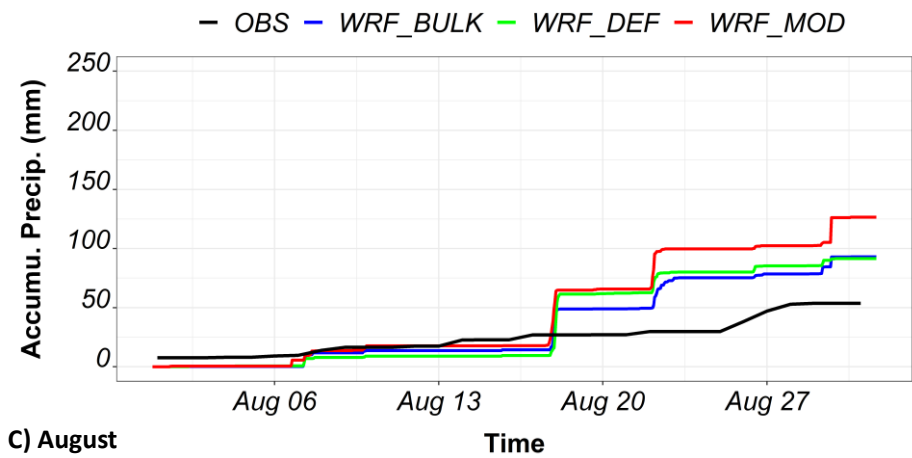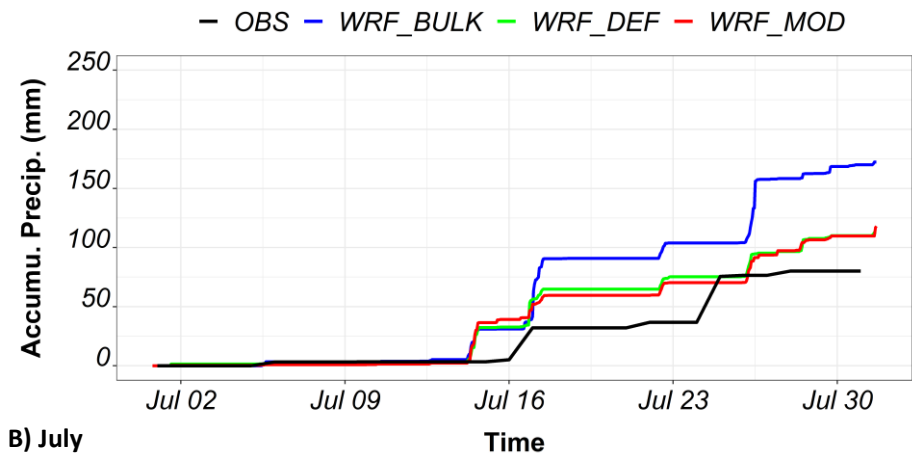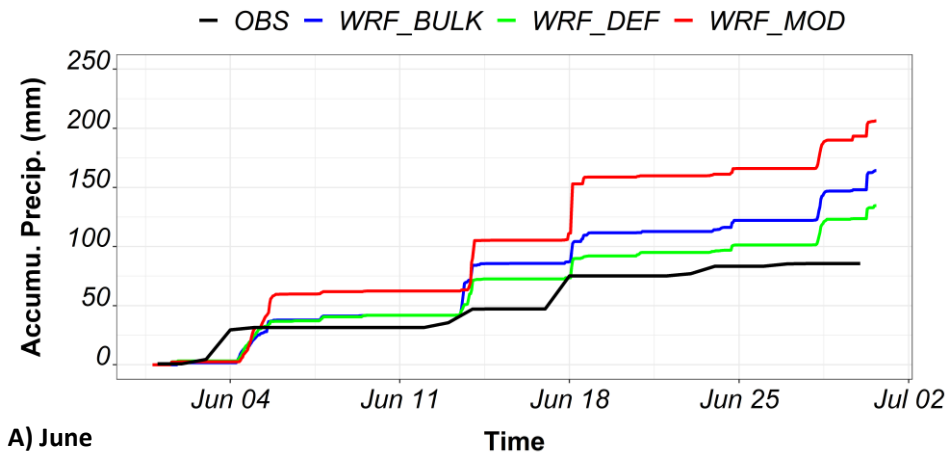
Figure K-28 Time series of observed (black) and WRF modeled accumulated precipitation at the Mc-Tavish weather station in A) June, B) July, and C) August
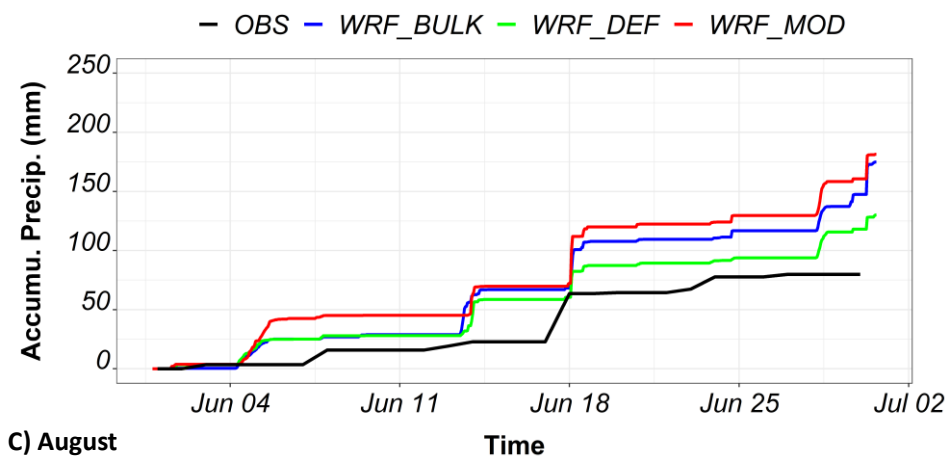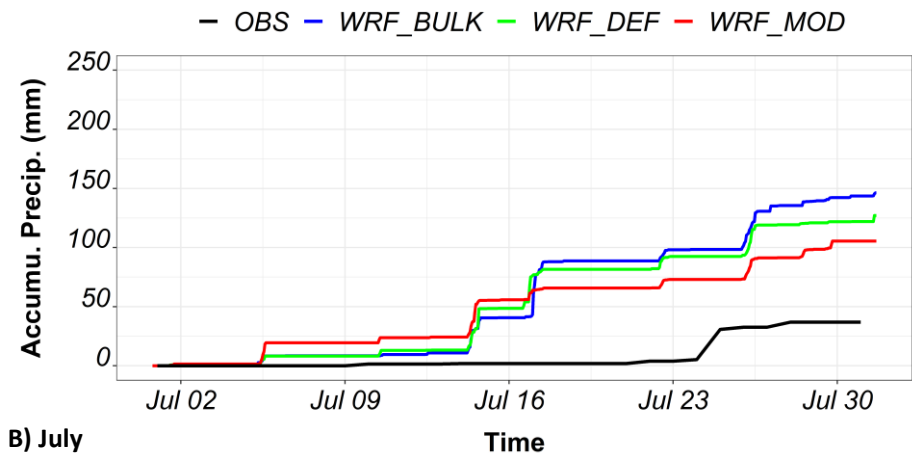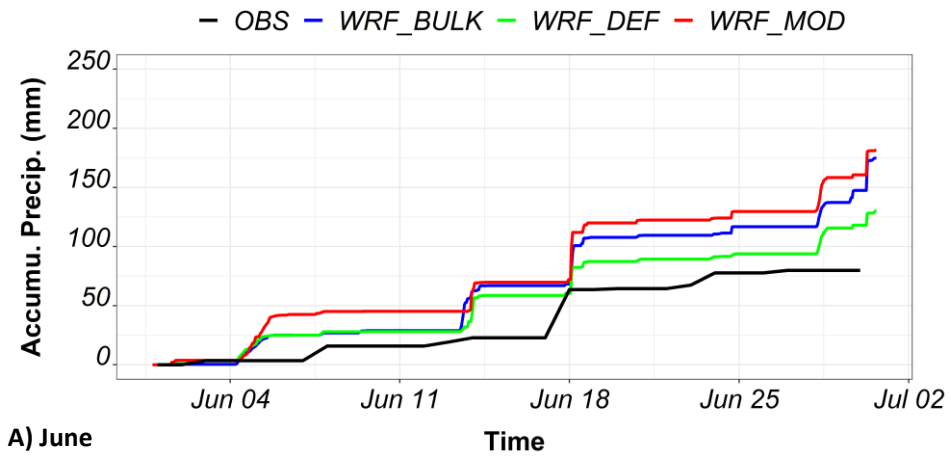
Figure K-29 Time series of observed (black) and WRF modeled accumulated precipitation at the St-Hubert weather station in A) June, B) July, and C) August
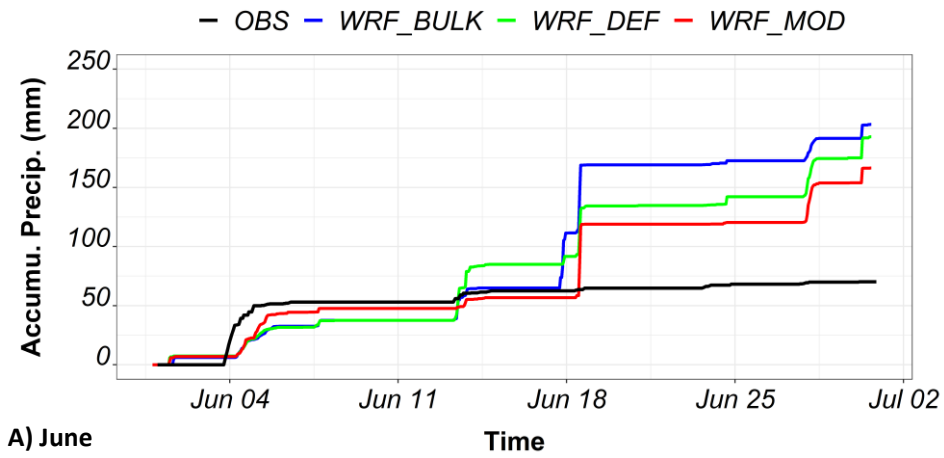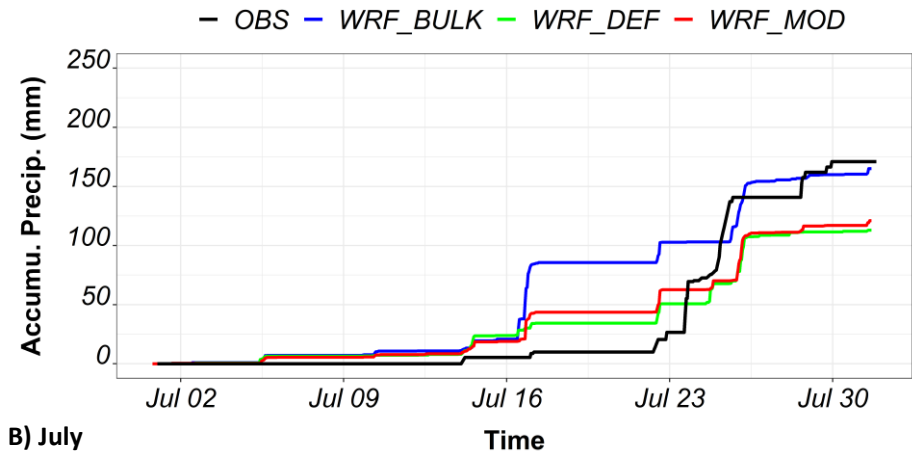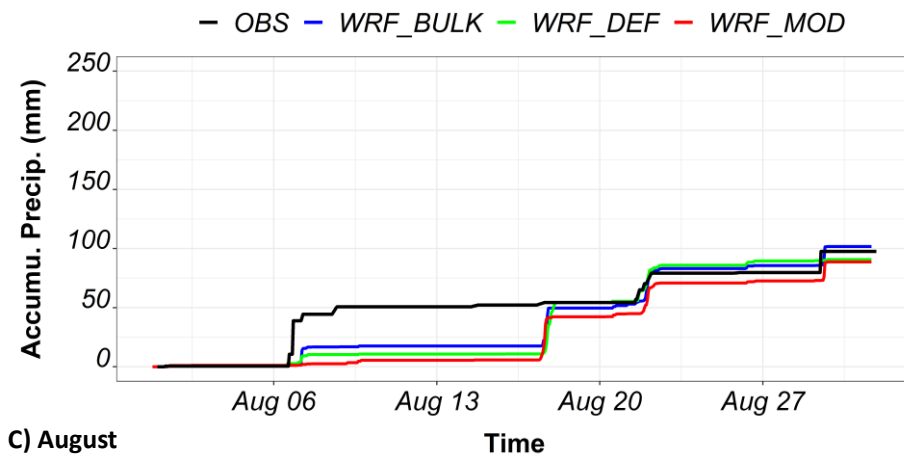
Figure K-30 Time series of observed (black) and WRF modeled accumulated precipitation at the Ottawa-Airport weather station in A) June, B) July, and C) August